SOURCE IMAGING IN DRUG RESISTANT EPILEPSY - CURRENT EVIDENCE AND PRACTICE

EDITED BY: Sándor Beniczky and Eugen Trinka
PUBLISHED IN: Frontiers in Neurology

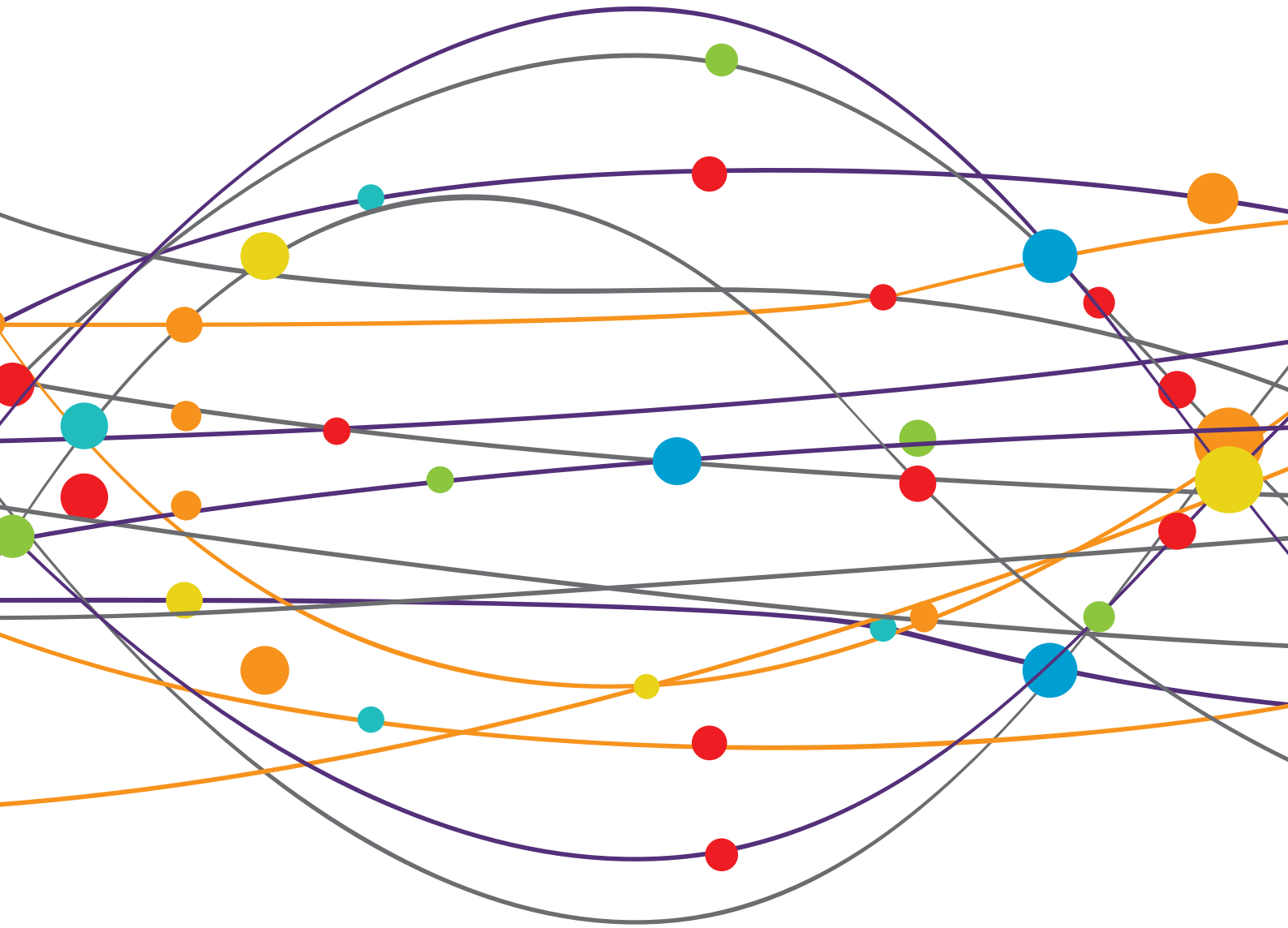

frontiers Research Topics

ISSN 1664-8714
ISBN 978-2-88963-673-0
DOI 10.3389/978-2-88963-673-0

About Frontiers

Frontiers is more than just an open-access publisher of scholarly articles: it is a pioneering approach to the world of academia, radically improving the way scholarly research is managed. The grand vision of Frontiers is a world where all people have an equal opportunity to seek, share and generate knowledge. Frontiers provides immediate and permanent online open access to all its publications, but this alone is not enough to realize our grand goals.

Frontiers Journal Series

The Frontiers Journal Series is a multi-tier and interdisciplinary set of open-access, online journals, promising a paradigm shift from the current review, selection and dissemination processes in academic publishing. All Frontiers journals are driven by researchers for researchers; therefore, they constitute a service to the scholarly community. At the same time, the Frontiers Journal Series operates on a revolutionary invention, the tiered publishing system, initially addressing specific communities of scholars, and gradually climbing up to broader public understanding, thus serving the interests of the lay society, too.

Dedication to Quality

Each Frontiers article is a landmark of the highest quality, thanks to genuinely collaborative interactions between authors and review editors, who include some of the world's best academicians. Research must be certified by peers before entering a stream of knowledge that may eventually reach the public - and shape society; therefore, Frontiers only applies the most rigorous and unbiased reviews.
Frontiers revolutionizes research publishing by freely delivering the most outstanding research, evaluated with no bias from both the academic and social point of view. By applying the most advanced information technologies, Frontiers is catapulting scholarly publishing into a new generation.

What are Frontiers Research Topics?

Frontiers Research Topics are very popular trademarks of the Frontiers Journals Series: they are collections of at least ten articles, all centered on a particular subject. With their unique mix of varied contributions from Original Research to Review Articles, Frontiers Research Topics unify the most influential researchers, the latest key findings and historical advances in a hot research area! Find out more on how to host your own Frontiers Research Topic or contribute to one as an author by contacting the Frontiers Editorial Office: researchtopics@frontiersin.org

SOURCE IMAGING IN DRUG RESISTANT EPILEPSY - CURRENT EVIDENCE AND PRACTICE

Topic Editors:
Sándor Beniczky, Danish Epilepsy Centre and Aarhus University Hospital, Denmark
Eugen Trinka, Paracelsus Medical University, Austria

Citation: Beniczky, S., Trinka, E., eds. (2020). Source Imaging in Drug Resistant Epilepsy - Current Evidence and Practice. Lausanne: Frontiers Media SA.
doi: 10.3389/978-2-88963-673-0

Table of Contents

frontiers in Neurology

EDITORIAL
published: 11 February 2020
doi: 10.3389/fneur.2020.00056

Editorial: Source Imaging in Drug Resistant Epilepsy - Current Evidence and Practice

Sándor Beniczky[1,2,3]* *and Eugen Trinka*[4,5]

[1] Department of Clinical Neurophysiology, Danish Epilepsy Centre, Dianalund, Denmark, [2] Department of Clinical Neurophysiology, Aarhus University Hospital, Aarhus, Denmark, [3] Department of Clinical Medicine, Aarhus University, Aarhus, Denmark, [4] Department of Neurology, Christian Doppler Clinic, Paracelsus Medical University, Salzburg, Austria, [5] Center for Cognitive Neuroscience, Salzburg, Austria

Keywords: EEG, epilepsy, ictal, interictal, MEG, presurgical evaluation, source imaging, source analysis

Editorial on the Research Topic

Source Imaging in Drug Resistant Epilepsy - Current Evidence and Practice

Localizing the source of electroencephalography (EEG) and magnetoencephalography (MEG) signals has been the objective of extensive research in the last decades. Imaging the source of epileptiform activity in the brain is especially important for patients with drug-resistant focal epilepsy, since it provides clinically useful information for planning the surgical therapy.

For long time, source imaging (SI) has been considered an experimental technique. A recent survey published by the E-PILEPSY consortium, comprising 25 European centers, showed that less than half of the centers used these methods for presurgical evaluation (1). There are multiple possible causes for the under-utilization of this method. Many clinicians are skeptical about SI because they are not aware of the evidence provided by numerous clinical trials. Often, clinicians doing presurgical evaluation lack the expertise in advanced signal analysis.

To address this problem and to facilitate clinical implementation of SI in the presurgical evaluation of patients with drug-resistant focal epilepsy, in this special issue (eCollection) of Frontiers in Neurology, we present a series of papers that provide evidence for the accuracy of SI, explain the technical background in a language accessible for clinicians and emphasize the advantages and the limitations of this method.

Sharma et al. present the results of a large meta-analysis of EEG and MEG SI, based on data from 1,152 operated patients. They found that these methods have high sensitivity (up to 90%) and diagnostic odds ratio (up to 7.9).

Scherg et al. explain the basic principles of EEG signal generation, and how to take the EEG recorded from scalp sensors back into the brain. They describe a novel method of visualizing the signals in the source space, by using the power of multiple discrete sources.

The practical review by Michel and Brunet explains these different steps in SI. The authors illustrate the process of SI, in a comprehensive analysis pipeline using a stand-alone freely available academic software.

OPEN ACCESS

Edited and reviewed by:
Jan Kassubek,
University of Ulm, Germany

***Correspondence:**
Sándor Beniczky
sbz@filadelfia.dk

Specialty section:
This article was submitted to Applied Neuroimaging, a section of the journal Frontiers in Neurology

Received: *24 November 2019*
Accepted: *15 January 2020*
Published: *11 February 2020*

Citation:
Beniczky S and Trinka E (2020) Editorial: Source Imaging in Drug Resistant Epilepsy - Current Evidence and Practice. Front. Neurol. 11:56. doi: 10.3389/fneur.2020.00056

Carrette and Stefan review the current practice for using magnetic SI of focal interictal and ictal epileptic activity during the presurgical evaluation of drug resistant patients.

Besides localization of the epileptic focus (what needs to be resected), in presurgical evaluation it is important to localize the eloquent cortex (what must not be resected). Kreidenhuber et al. provide a general overview of MEG and high-density EEG based methods of functional cortical mapping.

van Mierlo et al. describe the potential of EEG and MEG source connectivity to provide an intuitive view of the epileptic activity in the brain, that help localizing the seizure onset zone and the irritative zone.

High-frequency oscillations (HFOs) are promising biomarker of the epileptic focus. Most of the evidence is still based on invasive recordings; nevertheless, there is increasing expertise with recording HFOs non-invasively. Thomschewski et al. review the current literature on this topic, with emphasis on findings and technical considerations regarding their localization.

SI is an important tool in the presurgical evaluation of patients with drug-resistant focal epilepsy. It provides non-redundant, clinically useful information. The papers in this special issue (eCollection) of Frontiers in Neurology summarize the published evidence on the accuracy of various SI methods. The papers in this eCollection help the readers to integrate this method into their presurgical workup, but in the same time, they emphasize the current limitations of SI and propose further development of the methods, especially for automatizing the analysis and extending the method to imaging of connectivity changes in these patients.

AUTHOR CONTRIBUTIONS

SB drafted the manuscript. All authors contributed to editing the manuscript.

FUNDING

This study was supported a grant from Henry and Karla Hansen Foundation.

ACKNOWLEDGMENTS

We would like to express our gratitude to the authors of all the papers included into this collection.

REFERENCES

1. Mouthaan BE, Rados M, Barsi P, Boon P, Carmichael DW, Carrette E, et al. Current use of imaging and electromagnetic source localization procedures in epilepsy surgery centers across Europe. *Epilepsia*. (2016) 57:770–6. doi: 10.1111/epi.13347

Conflict of Interest: The authors declare that the research was conducted in the absence of any commercial or financial relationships that could be construed as a potential conflict of interest.

frontiers in Neurology

REVIEW
published: 12 February 2019
doi: 10.3389/fneur.2019.00094

Localization of the Epileptogenic Zone Using High Frequency Oscillations

Aljoscha Thomschewski[1,2], *Ana-Sofía Hincapié*[3] *and Birgit Frauscher*[3]*

[1] Department of Neurology, Christian Doppler Medical Center, Paracelsus Medical University, Salzburg, Austria, [2] Department of Psychology, Paris-Lodron University of Salzburg, Salzburg, Austria, [3] Montreal Neurological Institute and Hospital, McGill University, Montreal, QC, Canada

For patients with drug-resistant focal epilepsy, surgery is the therapy of choice in order to achieve seizure freedom. Epilepsy surgery foremost requires the identification of the epileptogenic zone (EZ), defined as the brain area indispensable for seizure generation. The current gold standard for identification of the EZ is the seizure-onset zone (SOZ). The fact, however that surgical outcomes are unfavorable in 40–50% of well-selected patients, suggests that the SOZ is a suboptimal biomarker of the EZ, and that new biomarkers resulting in better postsurgical outcomes are needed. Research of recent years suggested that high-frequency oscillations (HFOs) are a promising biomarker of the EZ, with a potential to improve surgical success in patients with drug-resistant epilepsy without the need to record seizures. Nonetheless, in order to establish HFOs as a clinical biomarker, the following issues need to be addressed. First, evidence on HFOs as a clinically relevant biomarker stems predominantly from retrospective assessments with visual marking, leading to problems of reproducibility and reliability. Prospective assessments of the use of HFOs for surgery planning using automatic detection of HFOs are needed in order to determine their clinical value. Second, disentangling physiologic from pathologic HFOs is still an unsolved issue. Considering the appearance and the topographic location of presumed physiologic HFOs could be immanent for the interpretation of HFO findings in a clinical context. Third, recording HFOs non-invasively via scalp electroencephalography (EEG) and magnetoencephalography (MEG) is highly desirable, as it would provide us with the possibility to translate the use of HFOs to the scalp in a large number of patients. This article reviews the literature regarding these three issues. The first part of the article focuses on the clinical value of invasively recorded HFOs in localizing the EZ, the detection of HFOs, as well as their separation from physiologic HFOs. The second part of the article focuses on the current state of the literature regarding non-invasively recorded HFOs with emphasis on findings and technical considerations regarding their localization.

Keywords: high-frequency oscillations, epilepsy, EEG, MEG, source localization

OPEN ACCESS

Edited by:
Sandor Beniczky,
Aarhus University Hospital, Denmark

Reviewed by:
Firas Fahoum,
Tel Aviv Sourasky Medical Center, Israel
Pál Gunnar Larsson,
Oslo University Hospital, Norway

***Correspondence:**
Birgit Frauscher
birgit.frauscher@mcgill.ca

Specialty section:
This article was submitted to Applied Neuroimaging, a section of the journal Frontiers in Neurology

Received: *08 November 2018*
Accepted: *23 January 2019*
Published: *12 February 2019*

Citation:
Thomschewski A, Hincapié A-S and Frauscher B (2019) Localization of the Epileptogenic Zone Using High Frequency Oscillations. Front. Neurol. 10:94. doi: 10.3389/fneur.2019.00094

1. INTRODUCTION

Despite more than 30 antiepileptic medication available on the market (1, 2), about 30–40% of patients treated for epilepsy continue to have seizures (3). For these patients with drug-resistant focal epilepsy, surgery constitutes the most promising treatment option in order to achieve seizure freedom (4–6). The success of surgical interventions foremost depends on the localization of the epileptogenic zone (EZ), defined as the area of brain responsible for seizure generation (7). However, identifying this brain region is challenging, as all available diagnostic tools are not able to directly measure the EZ. Only *post-hoc*, after surgery, and when seizure freedom is achieved, we are able to conclude that the EZ had been within the resected area (7). Consequently, results from multiple modalities are considered in order to indirectly infer the location of the EZ. The current gold standard for identification of the EZ is the seizure-onset zone (SOZ). The fact, however that surgical outcomes are unfavorable in 40–50% of well-selected patients (8), suggests that the SOZ is a suboptimal biomarker of the EZ, and that new biomarkers resulting in better postsurgical outcomes are needed.

High frequency oscillations (HFOs) have been proposed as a promising biomarker of the EZ (9–15). HFOs are spontaneous events occurring in electroencephalography (EEG) or magnetoencephalography (MEG) signals, defined as at least four oscillations with frequencies higher than 80 Hz, which distinctively stand out from the background signal (16). HFOs are divided into three subgroups: ripples (80–250 Hz), fast ripples (250–500 Hz), and very-fast ripples with frequencies exceeding even 500 Hz (17–20). Regarding epilepsy, studies suggested that a resection of brain tissue generating high rates of HFOs may lead to good post-surgical outcome (e.g., 21–23). The possible value of HFOs recorded interictally is of special interest, as this does not require to record seizures, a process which is not only time and resource consuming, but also bearing the risk of complications due to secondary generalization after lowering the patients' antiepileptic drugs. This notion of interictal HFOs as a possible biomarker for the EZ has tipped the scale to further pursue their investigation.

To establish HFOs as clinical biomarker for epilepsy, three main issues still need to be tackled. First, evidence on HFOs as a clinically relevant biomarker stems predominantly from retrospective assessments with visual marking of HFOs, leading to problems of reproducibility and reliability (24, 25). Second, there are also physiologic, non-epileptic HFOs and their existence poses a challenge, as disentangling them from clinically relevant pathologic HFOs still is an unsolved issue with considerable influence on HFO research (26–30). Such a distinction is crucial to further investigate the clinical value of HFOs in predicting outcome after epilepsy surgery. Third, most findings on HFO research stem from invasive intracranial EEG (iEEG) obtained from patients with drug-resistant epilepsy, as part of their presurgical evaluation (e.g., 17, 31–34). Recording HFOs non-invasively via scalp EEG and MEG is highly desirable, as it would provide us with the possibility to translate the use of HFOs to the scalp in a large number of patients, and to extend its application from presurgical evaluation to monitoring of disease activity and predicting seizure occurrence in vulnerable patient populations. However, accurately recording HFOs on the scalp is problematic, regarding artifacts mimicking HFOs (35–38), and a low signal-to-noise ratio (39). Moreover, localizing the sources of HFOs obtained on the scalp is challenging.

In the first part, this review considers findings from iEEG recordings, assessing the value of HFOs for the localization of the EZ. Furthermore, technical issues regarding HFO detection, and findings regarding the appearance and location of physiologic HFOs are presented. The normative values of invasively-recorded HFOs are also discussed. In the second part, this article focuses on findings of pathologic HFOs recorded non-invasively, and discusses technical considerations regarding localization of HFOs.

2. HIGH-FREQUENCY OSCILLATIONS IN THE INTRACRANIAL EEG

Invasive EEG recordings performed in the context of presurgical epilepsy evaluation in people with drug-resistant epilepsy provide us with excellent data to investigate high frequencies in the EEG, as they have a high signal-to-noise ratio and are less prone to artifacts in comparison to non-invasive recording techniques. Although these results are limited to this special population, many studies point to a prognostic value of HFOs in predicting the EZ (10–15, 22, 23).

Another limitation is the difficulty to perform prospective studies within this population. A recently updated Cochrane review by Gloss et al. (40) investigated the clinical value of HFOs regarding decision making in epilepsy surgery. They identified only two prospective studies and concluded that there is not enough evidence so far to allow for any reliable conclusions regarding the clinical value of HFOs as a marker for the EZ. Despite this somewhat disillusioning result, general evidence points to a potential clinical value as outlined in detail by Frauscher et al. (16). In this section, we will (i) discuss the studies that support the identification of HFOs as biomarker of the EZ, (ii) present the few prospective trials that have been reported or that are currently being conducted, and (iii) review important aspects for the detection of HFOs. Lastly, we will (iv) review means to distinguish physiologic from pathologic HFOs and discuss normative values of HFOs.

2.1. HFOs as Biomarker of the EZ: Evidence From Retrospective Studies

In a meta-analysis, Höller et al. (41) investigated whether patients in whom high HFO generating areas had been resected presented a better post-surgical seizure outcome in comparison to patients in whom those areas had not been resected. They found significant effects for resected areas that either presented a high number of ripples or fast ripples. However, effect sizes were small and only eleven studies fulfilled their selection criteria (41). Since then, several studies investigated the predictive value of HFOs, showing that the resection of areas with high rates of both ictal (42–45), as well as interictal HFOs resulted in a favorable surgical outcome (46–50). Better results regarding the outcome

prediction were reported for very-fast ripples than for ripples and fast ripples (19, 20), which was attributed to the possibility that very-fast ripples might be less prone to being mimicked by physiologic activity or artifacts (19). However, it was also noted that very-fast ripples have not been detected in all subjects, making it only useful for a subgroup of patients (20).

Importantly, it has been suggested, that pre-surgically assessed HFO rates might not be key in predicting seizure outcome, but that high rates recorded after resection might be an indicator of seizure reoccurrence (50–54), suggesting the importance to disconnect HFO generating networks (53). Accordingly, Weiss et al. (55) found that areas with fast ripples occurring on spikes that were not resected during epilepsy surgery were linked to a poor surgical outcome. This might also explain the high specificities occasionally reported by some studies (42, 50, 52, 56). Fedele et al. (56) for instance, reported on 20 patients with mesial temporal lobe or extratemporal lobe epilepsy who underwent resective surgery. Using a prospectively trained automated HFO detector, the authors evaluated the accuracy of HFOs in post-surgical outcome prediction, and reported a specificity of 100% in predicting surgical success by combining ripples and fast ripples as a biomarker.

Noteworthy, just this year (57) reported on results from three tertiary epilepsy referral centers, in which surgical outcome was correlated and predicted by the ratio of interictal HFO removal. They found significant correlations between the resection of high rates of ripples and fast ripples with surgical outcome. However, individual analysis suggested that HFO assessment was only associated with good surgical outcome in two thirds of their patients (57). Concordantly, also Roehri et al. (58) reported that HFOs are not better in predicting epileptogenic regions on an individual level than spikes. These discrepancies and concerns further stress the need for prospective trials.

2.2. HFOs as Biomarker of the EZ: Prospective Studies

Höller et al. (41), searched pubmed in February 2015 and found two prospective trials. Conducting another search using the pubmed database with the terms "High frequency oscillation," we found 1,055 publications since 2015 (search conducted on August 22nd, 2018). Screening these articles, we could identify one additional publication on a prospective trial. Two further trials are currently being conducted, and thus are registered in trial databases (see **Table 1**). For this review, we considered trials only to be prospective, if they entailed that findings on HFOs were taken into consideration for surgical decision making.

Regarding the published results, Ramachandran Nair et al. (62) reported on five children suffering from focal-onset epileptic spasms. All five children received invasive video EEG monitoring using subdural grid electrodes and resective surgery afterwards. Surgical decision was based on the findings of ictal HFOs among other criteria. After surgical resection including the HFO generating areas, all children yielded a reduction in seizure frequency or were seizure-free (see **Table 1** for more details). In a second study, six children with neocortical epilepsy and unifocal seizure onsets who underwent resective surgery were investigated (61). Decisions regarding resection area and resection boundaries were based on the SOZ and on ictal HFO findings in subdural invasive recordings. Findings revealed a positive seizure outcome of Engel class I or II in five out of six children. Just recently, Leung et al. (60) reported on a cohort of epilepsy patients who received iEEG recordings, from which ictal HFOs were analyzed either visually or automatically using a wavelet-transform-based analysis approach. In comparison with a previous cohort of patients where no HFO analysis was performed, the authors reported an increase of patients eligible for resective surgery from 70 to 76.5% following wavelet-transformed HFO analysis and 75% following visual HFO analysis. Accordingly, the rate of good surgical outcome increased from 57 to 71.4% and 75%.

Regarding the ongoing studies, there are currently two large trials conducted which aim at prospectively assessing the clinical value of HFO analyses for surgical decision making. The recently started SPREAD trial is a multi-center study including several hospitals in France, where the clinical value of certain biomarkers for surgical decision making in patients with focal cortical dysplasia will be evaluated (59). The investigators plan to recruit up to 240 patients and one biomarker of interest will be the interictal HFO distribution obtained by invasive stereo-EEG recordings. The second study will assess the value of interictal HFOs for delineating the EZ in intraoperative electrocorticography (63). Surgery tailored by HFOs and surgery tailored by interictal spikes will be compared with respect to surgical outcome.

What becomes apparent upon reviewing the literature is that despite notable findings suggesting that HFOs might provide us with a valuable biomarker for epileptogenicity, there are also concerns regarding their reliability as a marker (50, 51, 53, 57). This stresses the need for prospective multi-center trials enabling clinicians to quantify a potential value. In the context of this need, it becomes important to answer the question on how we can best and least time consuming assess HFOs and how we can separate epileptic from non-epileptic physiologic HFOs.

2.3. Detection of HFOs

Various groups have reviewed the technical aspects of HFO detection (see e.g., 39, 64, 65). The detection of HFOs is a challenging task, mainly due to their usual low signal-to-noise ratio, their association with other epileptic activity, and the still open questions regarding their nature and definition. We can summarize the process of detecting HFOs in three steps: recording of the signals, HFO detection, and HFO validation. Here we will summarize the approaches and practical technical guidelines to execute them. When recording, we need to consider appropriate temporal and spatial sampling of the signals. For an appropriate temporal sampling, we need a recording system that allows to record at least three times the highest frequency of interest, with a low noise level for high frequencies (39, 65, 66). Regarding spatial sampling, the literature suggests that clinical SEEG electrodes are a very good option, thanks to their robust HFO measurements (65, 67–70), their safety surgical record (65, 71), and their sampling scale, which represents a good compromise between micro and macro-scales (17, 39, 65, 68, 72).

TABLE 1 | Prospective HFO studies.

References	Patient population	Age range	*N*	iEEG method-ology	HFO measure-ment	Primary outcome	Secondary outcome(s)	Outcome
Hirsch and Scholly (59)	Drug-resistant focal epilepsy (3 groups: FCD type I, FCD type II, non-pathologic)	>3	240	Stereotactic EEG	Interictal HFOs	Percentage of seizure-free patients 12 months after surgery	Types of seizure-onset patterns; duration of epilepsy; topographic distribution of structures (i) with high epileptogenicity, (ii) with maximal interictal HFO rates, (iii) showing interictal/preictal functional connectivity alterations	Recruiting
Leung et al. (60)	Drug-resistant epilepsy	Mean = 34	34	Subdural grids/strips	Ictal HFOs	Eligibility and favorable outcome after surgery	Comparison between visual and automated HFO analysis and to a cohort of patients without HFO analysis at all	increase in eligibility by 5–6.5% and good surgical outcome by 17–18%
Modur et al. (61)	Neocortical epilepsy and focal seizures	19–32	6	Subdural grids/strips	Visually detected ictal HFOs	Seizure outcome (at least 20 months post-surgery)	Temporal and spatial HFO characteristics; concordance with common EEG markers	Engel I: $n = 3$; II: $n = 2$; III: $n = 1$
Ramachandran Nair et al. (62)	Neocortical epilepsy and epileptic spasms	4–14	5	Subdural grids	Ictal ripples	Seizure outcome (at least 1 year post-surgery)	Concordance of HFOs with other clinical markers	seizure free: $n = 3$; 90% reduction: $n = 1$; 50–75% reduction: $n = 1$
van't Klooster (63)	Drug-resistant focal epilepsy	All ages	78	ECoG	Visually detected interictal HFOs	Post-operative outcome after 1 year, HFO- vs. spike-tailored surgery	Volume of resected tissue, neurologic deficits, surgical duration, complications, cognition, QoL	Recruiting

iEEG, intracranial EEG; HFOs, high-frequency oscillations; ECoG, intraoperative electrocorticography; QoL, quality of life

HFO detection has greatly benefitted from the development of automated detectors (see 64, for a 2016 review) (30, 54, 73–76). It is well-known that visual HFO detection is very time-consuming, and the reliability of this procedure has been questioned on several occasions (16). Just recently, Spring et al. (25) investigated the interrater reliability of visual HFO detection in iEEG recordings. Even though the experts were presented with an automatically detected set of possible HFOs, the evaluation agreement for these events was poor with a mean Cohen's Kappa of 0.4. Furthermore, it was shown that HFO rates for given recording channels vary over time, leading to inconsistent sources (77). Automatic detectors help to minimize the time required for HFO detection and to reduce the bias induced by human raters.

Many detectors work by first bandpass filtering the signal around the frequencies of interest (i.e., the ones of ripples or fast ripples). Many of them use forward and backward filtering to eliminate phase distortion (24, 78–81), and use Finite Impulse Response (FIR) filters that in comparison to Infinite Impulse Response (IIR) filters have less tendency to oscillate and have linear phase properties (64, 67). Their general aim is to differentiate the HFO events from the background activity (39). When working with existing detectors, it is important to consider that the design of automatic detectors is based on a definition of HFO, which is not yet standardized in the field. A common definition is that of events with at least four oscillations in a frequency range from 80 to 500 Hz that "distinctively" stand out from the background signal. This definition, however, lacks precision, and thus various groups applied different ways to interpret and implement it (82).

Furthermore, the detectors are optimized for the data-set for which they were designed. Therefore, to obtain good results when working with an existing detector, it is advisable to train and validate it on a data-set with similar characteristics to the one of interest (39, 81). The quality of the detections can also be affected by muscle activity, as it can contaminate the signal resulting in increased power in the HFO frequencies of interest (39, 69, 83, 84). This latter is less of a problem in iEEG. Another important aspect to consider is that the filtering process itself can produce spurious oscillations, and can therefore contaminate the data (64, 79). For example, filtering of sharp EEG events, including spikes, can result in filtering effects mimicking HFOs (39, 70, 79). To minimize the contamination introduced by the filtering process, Navarrete et al. (64) and Bénar et al. (79) give a series of recommendations to choose an adequate configuration to minimize filter distortions and to handle these artifacts, when detecting HFOs, accordingly. For clinical purposes though, Burnos et al. (85) showed that both spike-related and non-related HFOs are likewise markers of epileptogenicity.

To minimize the number of true undetected HFOs (false negatives), a typical approach is to set the automatic detector to work with high sensitivity and low specificity (24, 38, 86, 87). Given the low specificity, the next step is the validation of the automatic detections by an expert reviewer to discard false positive detections. Zijlmans et al. (65) give practical guidelines on the visual identification process for reviewers. As different reviewers might have different definitions of HFOs and training, this is a highly subjective step. A common approach to account for inter-reviewer reliability is to consider more than one reviewer, checking for consistency in the markings (24, 38, 86, 87). Nonetheless, to account for the lack of reproducibility and possible bias that comes from relying on the selection performed by an expert, there is a need for standardized automated detection strategies and the definition of a gold standard for detection (25, 39, 64, 65).

2.4. Physiologic vs. Pathologic HFOs

The fact that HFOs are not only pathologic in nature but also occur under physiological conditions is a further challenge when assessing the validity of HFOs as a marker for epilepsy. Distinguishing pathologic from physiologic HFOs might increase the specificity of that marker. This requires defining HFOs to be considered either being physiologic or pathologic. For instance, continuous high frequency activity in the background EEG has been suggested to reflect physiologic activity distinctive for certain brain regions, such as the hippocampus or the occipital lobe (88). Concordantly HFOs have been considered to reflect epileptic activity when observed on a flat background, and not when they are embedded in an oscillatory background (13). Just recently, Liu et al. (89) reported on a morphological difference between HFOs obtained in patients with epilepsy and healthy controls, associating stereotypical HFOs with a high degree of waveform similarity to the SOZ of patients and HFOs appearing within random waveforms to functional regions.

In addition, HFOs couple with interictal epileptiform discharges (IEDs), such as spikes, can be considered to reflect epileptic activity as there is a clear association with pathology, and indeed, they have been shown to be more specific for the SOZ than independent HFO events (90). Furthermore, it has been suggested that the physiologic nature pertains mainly to ripples and that fast ripples mostly represent epileptic activity in these areas (31, 89, 91, 92). In this context, very-fast ripples might even more exclusively reflect epilepsy-related activity, making them a very promising candidate for clinical use, when present (18–20).

There is also the possibility to identify HFOs as being physiologic by associating them with certain physiologic processes. There are, for example, certain physiologic HFOs linked to specific cognitive processes that can be observed in special conditions or can be even evoked by tasks or stimuli. The different types of physiologic HFOs are presented in **Table 2**. Noteworthy, in this review article we focus on oscillations with frequencies above 80 Hz only. A more detailed description of the gamma band oscillations and their role for cognitive processes are provided in a comprehensive review by Lachaux et al. (117).

Distinguishing Physiologic From Pathologic HFOs

In 2013, Matsumoto et al. (118) reported on the possibility to distinguish somatosensory associated HFOs from epileptic HFOs in patients with intracranial EEG recordings. They evoked somatosensory HFOs by asking patients to press digits on a keyboard, and compared the detected events to spontaneously occurring HFOs. Pathologic HFOs were found to have lower mean frequencies but longer durations when compared to physiologically evoked events. Automated classification revealed

TABLE 2 | Different types of physiologic HFOs.

Type	Localization	Relevant findings
Memory-related HFOs	Hippocampus, parahippocampus, entorhinal cortex	Spontaneously and bilaterally occurring (17, 31, 68, 78); coupled with neocortical sleep spindles (93–95); occurrence rate correlates with memory performance (96–98)
Motor-related HFOs	Motor cortex, subthalamic regions	Occur over motor areas (77, 99); highly localized and movement specific (100); associated to symptoms in Parkinson's disease and tremors (101–104)
Somatosensory HFOs	Somatosensory cortex, thalamic regions	Overly the P20 and N20 components of SEPs (105–107); HFOs overlying the ascending N20 phase, possibly reflect presynaptic action potentials and are linked to arousal and critical stimuli detection (108–110); HFOs overlying the descending N20 phase may reflect bursts of inhibitory interneurons (111, 112)
Visually evoked HFOs	Occipital lobe, visual cortex	Spontaneously occurring (90, 92); possibly related to processing of visual stimuli (113–115); evokable by visual stimuli (116)

SEPs, somatosensory evoked potentials.

high sensitivity and specificity in classifying pathologic HFOs. Evoked physiologic HFOs detected on electrodes within the SOZ also differed from evoked HFOs recorded from other sites and appeared to be more similar to epileptic HFOs. Comparable results have been obtained for HFOs that can be evoked by visual stimulation (116), yielding also higher frequencies and shorter durations in comparison to epileptic HFOs (118).

A recent study by Bruder et al. (119) could further show that certain features are marginally different between memory-related ripples that appear linked to sleep spindles and supposedly epileptic ripples. Spindle-linked ripples seem to be shorter and appear to have lower amplitudes (119). In addition, both spindles and physiologic HFO activity were found to be increased during the "up-state" and decreased during the "down-state" of slow oscillations during deep sleep (26, 120). Accordingly, epileptic HFOs have been shown to appear increasingly during the "down-state" or the transition to it (121). Implementing these findings into the process of detecting HFOs and classifying iEEG channels according to epileptic or non-epileptic brain regions, von Ellenrieder et al. (122) showed enhanced classification performance after considering the different coupling to slow waves.

Besides memory-related HFOs, the study of Nonoda et al. (123) indicates that HFOs recorded over somatosensory and visual cortices that seem to reflect physiologic processes are also linked to slow waves (123). In comparison to epileptic HFOs, which were found to couple with slow waves at 3Hz, these physiologic ripples were further found to couple with even slower waves at 1 Hz during sleep in a study by (116). Similar to the results presented in the study by von Ellenrieder et al. (122) also Nonoda et al. (123) found that considering the different types of slow-wave coupled HFOs and interpreting the seemingly pathologic HFO rates only, significantly increased the prediction accuracy for the SOZ.

In addition to slow wave phases, sleep stages have also been found to modulate the occurrence of HFOs. HFOs in general are considered to appear most frequently and most widespread during NREM sleep, whilst being the least frequent and most focal during REM sleep (124–127). However, there seems to be a difference between physiologic and pathologic HFOs with respect to the sleep stages. In contrast to pathologic HFOs, physiologic HFOs appear predominantly during phasic REM sleep (128) and seem to increase in rate over night during REM sleep (127). von Ellenrieder et al. (127) further found pathologic ripples and fast ripples to decrease with increased duration of sleep. Therefore, for clinical HFO evaluation, the authors suggested to analyze the night's first NREM sleep. Interestingly, it was also shown that the occurrence of pathologic HFOs in close proximity to the EZ might be less suppressed during REM sleep (126).

Although the possibility to evoke physiologic HFOs presents an exciting way to study these phenomena in more detail and to investigate possible differences to epileptic HFOs, considering the different appearance rates during certain sleep stages seems more profitable at this point. Importantly it has also been acknowledged that there are great variations and overlap in appearance and rates of physiologic HFOs with regard to the topographic location, suggesting that establishing normative values for these various appearance rates might improve the use of HFOs for clinical purposes even further (129).

Normative Value of HFOs

The ability of HFOs as a biomarker for the EZ might be improved by correcting HFO rates according to their topographic localization. As mentioned before, rates of ripples vary substantially across different brain regions. A multicenter project aiming at developing normative values of iEEG activity (see 130) investigated this question by carefully selecting iEEG channels showing normal physiologic EEG activity defined as (i) absence of interictal activity during the recording period, (ii) exclusion of a significant slow wave anomaly, and (iii) being outside of lesional tissue as assessed with MRI. In a subproject of this atlas of normative iEEG activity, normative rates of HFOs (ripples and fast ripples) were assessed (131). A total of 1,171 bipolar channels with normal physiologic activity from 71 patients were analyzed. Note is made that rates of ripples varied substantially across the different regions analyzed, with rates of up to 30/min in primary eloquent cortical areas. The mean 95th percentile was 9.6/min. The highest 95th percentile rates were recorded in the occipital cortex, the medial and basal temporal region, the transverse temporal gyrus and planum temporale, the pre- and postcentral gyri, and the medial parietal lobe (see **Figure 1**).

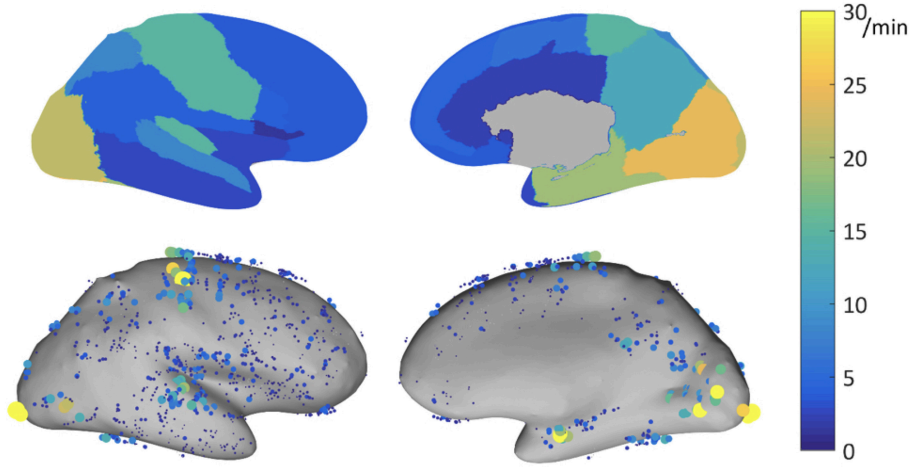

FIGURE 1 | Physiologic ripple rate results for bipolar channels recorded with DIXI electrodes, represented on the inflated cortex. **Top**: 95th percentile of the physiologic ripple rate per brain region. **Bottom**: rate of the individual channels, each dot represents a channel, the size and color indicates its ripple rate (**left**: lateral view, **right**: medial view). Source: Frauscher et al. (131) with permission from Wiley.

The mean rate of fast ripples was very low with 0.038/min. Only 5% of channels had a rate of at least 0.2/min. This multicenter atlas is the first to provide region-specific normative values for physiologic HFOs in a common stereotactic space. It demonstrated that physiologic ripples are particularly frequent in eloquent cortical areas. In contrast, physiologic fast ripples are very rare, even in eloquent cortical areas, which makes them a better candidate for defining the EZ, when present. This atlas is an open resource available for augmentation and consultation on the web (http://mni-open-ieegatlas.research.mcgill.ca).

3. HFOS OBTAINED FROM NON-INVASIVE RECORDINGS

In the previous sections we have reviewed findings regarding invasively obtained HFOs and the possible value for presurgical evaluation in epilepsy. However, the ultimate goal for a new biomarker of epileptogenicity would be to record it non-invasively, thus sparing patients the invasive procedure of electrode implantation. Furthermore, non-invasive recordings are of interest, as they enable us to study HFOs in larger populations and not only for pre-surgical evaluation, but also for drug and disease monitoring, or even for the assessment of epileptogenic potentials after brain injury. In this section, we will present findings of ictal and interictal HFOs obtained from both EEG and MEG. Finally, we will emphasize findings regarding source localization of HFOs and review important technical considerations.

3.1. HFOs on the Scalp EEG

Similar to research of iEEG in the context of epilepsy, high frequencies were first investigated in the ictal state in scalp EEG recordings (132, 133). Furthermore, high frequency activity, that is frequency band power ranging above 80 Hz, rather than single HFO events, were studied first. For instance, in 2004 Kobayashi et al. (132), reported on high gamma activity of up to 100 Hz recorded during epileptic spasms in children with West-Syndrome. Comparable findings were obtained for the onset of tonic seizures in children with Lennox-Gastaut syndrome (133). Iwatani et al. (134) could show a few years later that sources of HFOs recorded at spasm onset in children with West-Syndrome spatially corresponded with cortical lesions determined by neuroimaging. A chronological list of scalp EEG studies investigating high frequency activity and later HFO events is given in **Table 3**.

Regarding the investigation of interictal HFOs, the first study using scalp EEG was published in 2010 by Kobayashi et al. (135). They recorded children with epilepsy and continuous spike-waves during sleep and found ripples co-occurring with epileptic spikes. In concordance with these results, the Montreal group reported for the first time an association between interictal ripples and epileptic spikes recorded non-invasively in adult patients (38). Since then several studies addressed the relationship between HFOs and IEDs (88, 137, 140, 142, 144, 147). In this context, Melani et al. (88) reported that ripple rates seem to relate to the rates of IEDs. van Klink et al. (147) further showed that ripples preceded IEDs, suggesting an interrelation between these phenomena, and excluding the possibility of these ripples to be artificially created due to filtering effects.

Importantly, when dealing with scalp EEG in the absence of iEEG findings, assessing the clinical value of HFOs with regard to the EZ becomes more difficult. In the absence of epilepsy surgery, the value of HFOs can only be assessed according to their localizing value of the SOZ or an epileptic lesion. As such, Andrade-Valenca et al. (38) investigated the localizing value of ripples for the scalp electrodes detecting the seizure onset. They found significantly more ripples on these electrodes yielding an 81% accuracy to identify the SOZ channels. Furthermore, ripples yielded a lower sensitivity but higher specificity than spikes in this context, a result that was also reported by Melani et al.

TABLE 3 | HFO investigation in epilepsy using scalp EEG.

References	Patient population	Age range	*N*	Measurement	Detection method	Application/finding
Kobayashi et al. (132)	West syndrome	3m-4y	11	Ictal HFA	Time-frequency plot	HFA during epileptic spasms and hypsarrhythmia
Kobayashi et al. (133)	Lennox-Gastaut syndrome	3y-29y	20	ictal HFA	Time-frequency plot	HFA during tonic seizure onset
Kobayashi et al. (135)	children with epilepsy and continuous spike-waves	6y-9y	10	Interictal ripples	Time-frequency plot and visual	Co-occurrence with spikes
Andrade-Valenca et al. (38)	Focal epilepsy	19y-63y	15	Interictal ripples	visual	Co-occurrence with spikes; SOZ localization accuracy for ripples 81%; lower sensitivity but higher specificity than spikes
Kobayashi et al. (136)	Childhood epilepsy with centrotemporal spikes and Panayiotopoulos syndrome	2y-9y	45	Interictal ripples	Time-frequency plot and visual	Co-occurrence with spikes; Negative correlation of HFO rates with time since last seizure
Iwatani et al. (134)	West syndrome	9m-14m	4	Ictal ripples	Time-frequency analysis and visual	HFO sources during epileptic spasms localized to lesion
Melani et al. (88)	Focal epilepsy	22y-68y	32	Interictal ripples	Visual	Ripple rates depend on spike rates; Localization of SOZ: lower sensitivity but higher specificity than spikes
Fahoum et al. (137)	Focal epilepsy	18y-43y	22	Interictal ripples	Visual	Greater thalamic BOLD changes during IEDs with high HFO rates
Lu et al. (138)	Focal epilepsy	25y-53y	5	Interictal HFA events	Visual and ICA	Association with SOZ and resection area
Zelmann et al. (139)	Epilepsy with FCD	17y-52y	11	Interictal ripples	Automated detection and visual confirmation	Proof-of-principle; SOZ identification
Chaitanya et al. (140)	Childhood/juvenile absence epilepsy	6y-10y	9	Interictal and ictal ripples	ICA, time-frequency analysis	Co-occurrence with spike-waves
Kobayashi et al. (141)	West-Syndrome	3m-9m	17	Interictal ripples	Time-frequency plot and visual	Pharmaco-response monitoring of adrenocorticotropic hormones
Toda et al. (142)	Early epileptic encephalopathy	0-17w	6	Interictal ripples	Time-frequency analysis	Co-occurrence with epileptic bursts during suppression-burst patterns
Papadelis et al. (143)	Epilepsy with encephalomalacia	11y-15y	2	Interictal ripples	Automated detection and visual confirmation	SOZ identification
Pizzo et al. (144)	Genetic generalized and focal epilepsy	21y-60y	17	Interictal ripples	Visual	Concordance between ripple-dominant hemisphere with clinical lateralization; differential diagnosis
Pizzo et al. (145)	Focal epilepsy	21y-59y	10	Interictal fast ripples	Visual	Proof-of-principle; concordance with SOZ
Qian et al. (146)	Childhood epilepsy with centrotemporal spikes	4y-11y	14	Interictal ripples	Visual	Ripple rates identified atypical forms; pharmaco-response monitoring of methylprednisolone
van Klink et al. (147)	Focal and multifocal epilepsy	18y-76y	31	Interictal ripples	Visual	Ripples preceded epileptic spikes
van Klink et al. (148)	Childhood epilepsy with centrotemporal spikes	3y-15y	22	Interictal ripples	Visual	Differentiation of atypical and self-limited forms; seizure prediction

(Continued)

TABLE 3 | Continued

References	Patient population	Age range	*N*	Measurement	Detection method	Application/finding
von Ellenrieder et al. (87)	Focal epilepsy	19y-68y	17	Interictal ripples	Automated detection and visual confirmation	Localization concordance with clinical data or resected area (65% sensitivity)
Cuello-Oderiz et al. (149)	Lesional epilepsy	18y-71y	58	Interictal ripples	Visual	HFO rates higher with superficial lesions compared to deep seated focus
Mooij et al. (150)	Different types of epilepsy	11m-14y	23	Interictal ripples	Visual	Proof-of-principle; comparison with controls
Gong et al. (151)	Epileptic encephalopathy with continuous spike-and-wave during sleep	4y-13y	21	Interictal ripples	Visual	Concordance with MRI abnormalities in patients with structural etiologies; pharmaco-response monitoring under methylprednisolone
van Klink et al. (152)	Focal epilepsy	3y-42y	9	Interictal ripples	Visual	Localization concordance with clinical data or resected area (sensitivity: 55.4%, specificity: 72.2%)
van Klink (153)	Focal epilepsy	8y-54y	30	Interictal ripples	Automated detection and visual confirmation	50% localization concordance with clinical data or resected area
Bernardo et al. (154)	Children with tuberous sclerosis simplex and healthy controls	2m-5y	11	Interictal fast ripples	visual and automated detection	proof-of-principle; occurrence comparison between pediatric patients and controls
Ikemoto et al. (155)	Childhood epilepsy with centrotemporal spikes	2y-9y	25	Interictal ripples and HFA	Time-frequency analysis and Visual	Ripple rates identified atypical forms
Kobayashi et al. (156)	Myoclonic epilepsy	5m-17y	21	Ictal HFA events	Time-frequency analysis and visual confirmation	Involvement of HFA in generation of myoclonic seizures
Kuhnke et al. (157)	Epilepsies of different etiologies	8y-52y	13	Interictal ripples	Visual	Comparison of high-density and conventional EEG; higher ripple rates and better concordance with SOZ for high-density EEG
Mooij et al. (158)	Different types of epilepsy	11m-8y	23	Interictal ripples	Visual	Co-occurrence with sleep specific transients; occurrence rate during sleep stages

m, month(s); y, year(s); w, week(s); HFA, high frequency activity; SOZ, seizure-onset zone; HFO, high frequency oscillations; BOLD, blood oxygen level-dependent; IEDs, interictal epileptiform discharges; ICA, independent component analysis; FCD, focal cortical dysplasia.

(88). In order to increase the possibility to detect ripples on the scalp, using a larger coverage with more electrodes seems to be promising. Kuhnke et al. (157) just recently reported that the usage of a high-density scalp EEG with 128 electrodes did not only yield an increased detection rate of ripples, but an increased correspondence with iEEG results. Though not using source-localization in a strict sense, they were able to co-localize ripples more accurately to iEEG electrodes within areas that had been resected when using 128 electrodes as compared to only using 20 electrodes, which often led to false localizations (157).

Cuello-Oderiz et al. (149) showed that interictal scalp HFOs are predominantly recorded in epilepsy patients with superficial lesions compared to deep-seated foci. In another study, scalp HFO dominant regions were found to be concordant with MRI abnormalities in patients with structural etiologies (151). Patients with focal epilepsy were further found to have greater thalamic BOLD changes during IEDs when yielding high rates of interictal scalp HFOs accompanying those discharges (137). The occurrence of ripples was therefore associated with a more pronounced pathology of cortical-thalamo-cortical networks.

In accordance with the findings of ripples reflecting epileptogenesis, a possible application is the prediction of seizure activity. In children with Rolandic spikes, ripples were shown to predict the occurrence of seizures, and their rates differed significantly between self-limited and atypical or symptomatic courses (148). A similar observation was made by Qian et al. (146) and 2 years later by Ikemoto et al. (155), reporting on interictal ripple rates identifying atypical forms in childhood epilepsy with centrotemporal spikes. Qian et al. (146) further found interictal ripples to sensitively monitor the response to pharmacological treatment with methylprednisolone. Sensitive treatment response assessments using scalp HFOs were also reported for children suffering from epileptic encephalopathy with continuous spike-and-wave during sleep treated with methylprednisolone (151), and for children with hypsarrhythmia in West syndrome being treated with adrenocorticotropic hormones (141).

Noteworthy, there is also one report of scalp HFOs obtained in non-epileptic children by Mooij et al. (150). The authors found ripples in subjects who did not present with seizures or any interictal epileptiform activity using a standard 10–20 montage (150). This result fosters the idea of using scalp EEG not only for clinical purposes but also as a possibility to study "pure physiologic" HFOs in healthy subjects. The same authors showed that these physiological ripples were coupled to sleep-specific oscillations in children (158). On another note, all but two studies on scalp HFOs reported on frequencies below 250 Hz only. Of course, technical issues arising when trying to detect ripples are magnified for the detection of fast ripples. This is exactly the observation made by Pizzo et al. (145). They showed that a detection of frequencies >250 Hz is possible, although it is difficult and fast ripples are far less observable in scalp EEG signals than ripples due to their smaller generators and the amplifier noise at frequencies above 200 Hz (145). Just recently, Bernardo et al. (154) reported on the possibility to detect fast ripples in children with tuberous sclerosis complex. They speculate, that a detection of oscillations above the ripple band may be more feasible in children, as the skull is thinner in a pediatric population, leading to a decreased signal attenuation (154). Use of a low-noise amplifier might be helpful to overcome this challenge (56, 159).

3.2. HFOs in MEG

Similar to EEG, MEG recordings have an excellent temporal resolution. While EEG records electric fields that are sensitive to both tangential and radial dipole sources, MEG records magnetic fields and is sensitive to tangential dipolar sources (160) and is more selective for activity arising from fissural cortices than the EEG (161). Magnetic fields are less prone to volume conduction effects than electric fields. Therefore, MEG presents some advantages over EEG to reconstruct the neural sources responsible for the activity recorded at the scalp, which is done by means of magnetic source imaging (MSI) techniques (162).

Hand in hand with the investigation of HFOs using scalp EEG, researchers started to investigate the possibility of using MEG as well (see **Table 4** for an overview). The early studies also focused on high frequency activity rather than on discrete events embedded within the MEG/EEG signals (163–165). However, Guggisberg et al. (163) showed that source localizing spike-locked beta/gamma MEG activity identified the surgically resected area in patients with a good post-surgical outcome, with an accuracy of 85%.

When applying strict criteria for HFOs as single events, as described by Zijlmans et al. (65), interictal MEG studies reported lower event rates than in EEG recordings (87, 173). van Klink et al. (173) for example reported to find ripples only in three out of 12 patients analyzing 15 min of interictal MEG recordings. The detection rate was significantly increased when considering virtual sensors created via beamforming as compared to sensors alone (173). Especially combining methods such as beamforming with automated HFO detection algorithms resulted in a high sensitivity for interictal MEG recordings (87, 174). However, visual supervision of the automatic detection results is necessary in order to reduce false positive detections (87, 174).

Along with interictal HFO analyses, ictal MEG activity is also a subject of active investigation. Using MSI, Miao et al. (167) showed that ictal HFOs were spatially more refined than spikes and reliably localized a propagative pattern during absence seizures in childhood absence epilepsy (167, 168). Velmurugan et al. (175) just recently demonstrated the benefit of MSI in a large sample of patients with drug-resistant focal epilepsy. They were able to localize the EZ using ictal HFOs concordantly with other modalities; surgery of this identified zone performed in six patients led to seizure freedom in all of these six patients. Interestingly and differently to scalp EEG research, very high frequency components of up to 1,000 Hz have been recorded using MEG. Also, these frequencies could be localized to areas associated with the SOZ (164, 166). Xiang et al. (170) later even reported on frequencies up to 2,000 Hz. However, these studies did not investigate distinctive electrophysiological events, but merely frequency components of the recorded signals.

As revealed by studies that investigated both MEG and EEG, there are ripples observable in one modality that remain unseen in the other and vice versa (87, 153). These studies show a

TABLE 4 | HFO investigation in epilepsy using MEG.

References	Patient population	Age range	N	Measurement	Detection method	Application/finding
Guggisberg et al. (163)	Focal epilepsy	17y-67y	27	Interictal HFA	Time-frequency analysis	HFA sources identified resection area in patients with good outcome with an accuracy of 85%
Xiang et al. (164)	Lesional epilepsy	6y-17y	30	Interictal VHFA	Time-frequency analysis	Association with SOZ and epileptic lesion, proof-of-principle
Rampp et al. (165)	Focal epilepsy	20y-50y	6	Interictal HFA	Time-frequency analysis	SOZ identification in 5/6 patients (compared to invasive recording)
Xiang et al. (166)	Focal epilepsy	6y-26y	4	Ictal and interictal VHFA	Time-frequency analysis	association with SOZ and epileptic lesion, proof-of-principle
Miao et al. (167)	Childhood absence epilepsy	5y-11y	10	Ictal ripples and fast ripples	Time-frequency analysis	Identification of SOZ using source localization; Fast ripple rates corresponded with seizure frequency
Miao et al. (168)	Childhood absence epilepsy	5y-12y	14	Ictal HFO	Time-frequency analysis	Identification of SOZ using source localization
Tenney et al. (169)	Childhood absence epilepsy	6y-12y	12	Ictal HF	Time-frequency analysis	Source localization
Xiang et al. (170)	Childhood absence epilepsy	6y-10y	10	Interictal VHFA	Time-frequency analysis	Proof-of-principle; comparison with controls
Nissen et al. (171)	Focal epilepsy	6y-29y	12	Interictal ripples	Visual	Concordance between HFO and spike sources
Papadelis et al. (143)	Epilepsy with encephalomalacia	11y-15y	2	Interictal ripples	Automated detection and visual confirmation	SOZ identification
Tang et al. (172)	Childhood absence epilepsy	5y-12y	12	Ictal and interictal VHFA	Time-frequency analysis	HFO source strength correlated with seizure severity
van Klink et al. (173)	Focal epilepsy	6y-29y	12	interictal HFO	Visual	Lateralization of irritative hemisphere
von Ellenrieder et al. (87)	Focal epilepsy	19y-68y	17	Interictal ripples	Automated detection and visual confirmation	Localization concordance with clinical data or resected area (47% sensitivity)
Migliorelli et al. (74)	Focal epilepsy	6y-22y	9	Interictal ripples	Automated detection	SOZ-lobe identification with a precision of 79%
van Klink et al. (174)	Focal epilepsy	4y-29y	25	Interictal ripples	Automated detection and visual confirmation	localization concordance with clinical data; concordance with resection area in 6/8 patients, 4 achieved a good outcome
van Klink (153)	Focal epilepsy	8y-54y	30	Interictal ripples	Automated detection and visual confirmation	75% localization concordance with clinical data or resected area
Velmurugan et al. (175)	Focal epilepsy	3y-44y	20	Ictal ripples	Time-frequency analysis and visual	Localization concordance with clinical data; concordance with resection area in 6/6 patients, all achieved seizure-freedom

m, month(s); y, year(s); HFA, high frequency activity; VHFA, very-fast high frequency activity; SOZ, seizure-onset zone; HFO, high frequency oscillations.

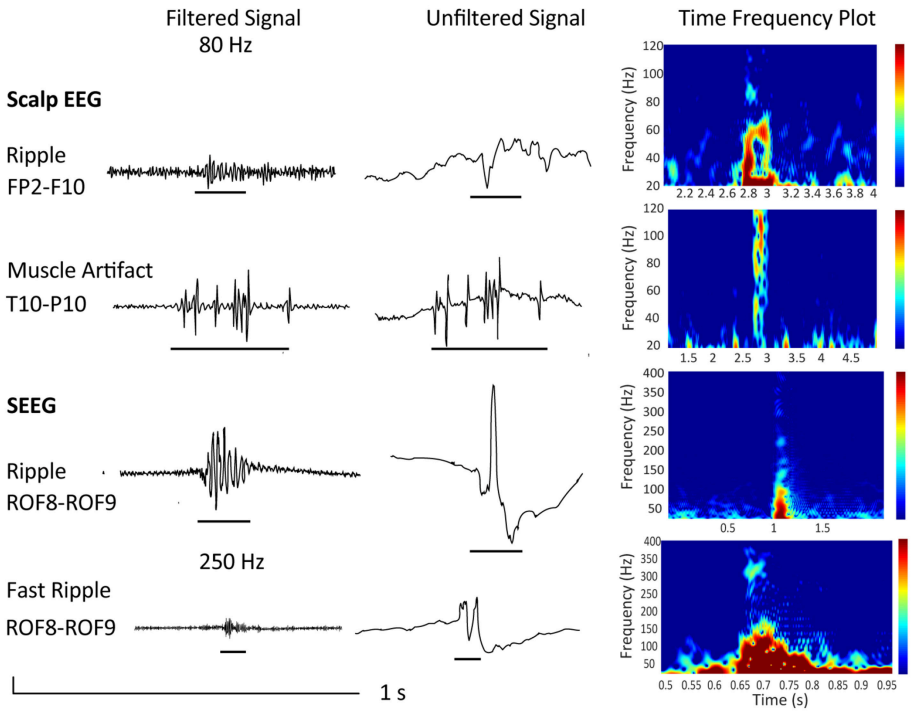

FIGURE 2 | Depicted are examples from a 34 year old female patient undergoing presurgical evaluation including stereo EEG recording at the Montreal Neurological Institute and Hospital. She presented with a MRI-negative drug-resistent epilepsy and a seizure semiology suggestive of a right frontal and possible orbitofrontal generator. Scalp EEG with 25 electrodes recorded at a sampling frequency of 600 Hz showed interictal and ictal changes over right frontotemporal electrodes. Implantation showed continuous spiking over the lateral orbitofrontal region (electrode ROF 8–9). The patient underwent resection and is now seizure-free (Engel class 1) since 8 years. Neuropathology confirmed FCD IIb. Shown are a true ripple over Fp2-F10 contrasted to a muscle artifact over T10-P10 as well as a ripple and fast ripple recorded invasively at electrode ROF. All examples are given as filtered EEG signals at 80 or 250 Hz respectively, unfiltered signals, and time frequency plots. Note the isolated blobs in case of "true" HFOs.

superior detection rate of ripples in scalp EEG. However, MEG ripple sources appeared to be more specific for the identification of epileptogenic tissue (87). Taking this into consideration, as well as the fact that source localization performance increases with the number of events, a combination of MEG and EEG might be very beneficial for both the detection and localization of interictal HFOs. Ultimately, such an endeavor is worthwhile compared to the expenditure that comes with invasive EEG monitoring and further diminishes sampling errors resulting from the restricted area investigated with intracranial electrodes.

3.3. Technical Issues and Obstacles of Non-invasive Recording of Scalp HFOs and Source Localization

Besides the challenges described for intracranial recording and detection of HFOs, there are other additional difficulties we need to face at the scalp level. Scalp recordings lack the excellent spatial resolution of intracranial recordings and therefore, we need to use mathematical algorithms called inverse solutions, to estimate where in the brain the signals are being generated. The whole head coverage with a high number of sensors of MEG and HD-EEG systems gives a global view of the brain activity, and a spatial sampling that is expected to facilitate the source localization procedure (compared to traditional EEG systems). Nonetheless, this high number of sensors represents a challenge for the visual detection and validation of HFOs given the amount of information needed to process. Thus, the HD-EEG and MEG HFO detection requires the implementation of automated detectors that allow to run the analysis in a suitable time frame. As in iEEG, a common approach is to use an automatic detector as a first step on the detection process, and then visually validate the detections (24, 38, 86, 87). An open question regarding the scalp spatial sampling is how many channels would be necessary to identify and localize MEG and scalp EEG HFOs.

Also, it is important to consider that artifacts produced by movement, muscle activity, and poor electrode contact have similar characteristics as HFO events (35–38). An example is given in **Figure 2**, which shows a "true" ripple obtained via scalp EEG and a muscle artifact, that, when filtered, mimics a ripple. Please note the difference in signal-to-noise ratio and the difference in duration in case of the muscle artifact. The figure also shows a ripple and fast ripple obtained using invasive stereo EEG for comparison. As the signal-to-noise ratio is more favorable in intracranial as compared to scalp EEG, and artifacts are more prominent in scalp as compared to iEEG, scalp EEG requires a very thorough differentiation to artifacts. As explained in section 2.4, it would be therefore advisable to

assess HFOs during NREM sleep, especially when analyzing scalp EEG recordings.

Although the scalp identification of HFOs is informative, for clinical purposes we are interested in the brain areas that give rise to this activity. Reconstructing these sources constitutes an inverse problem, which requires the use of mathematical algorithms called inverse solutions to address them. Various inverse solutions exist in the literature, which mainly differ from one another by the assumptions on the neuronal sources and on the noise. Knowledge of the characteristics of the sources is therefore highly helpful when designing and implementing the inverse solution for source reconstruction (176). When source-localizing HFOs, it is important to consider that they are oscillatory transients that are not necessarily mutually phase locked, and therefore can be removed, when applying methods on averaged trials and are associated with low signal-to-noise ratio (39). Currently, there are various Open Source Software solutions for the analysis of EEG and MEG signals that include implementations of different inverse models and tutorials where the reader can have a further introduction to this subject (i.e., 177–179).

Up to now HFO source reconstruction has only been performed using MEG. The most frequently used method for HFO source reconstruction are the beamformers (74, 167, 173–175, 180, 181). The beamformers use a set of spatial filters to scan the source space. The spatial filters are designed to pass the brain activity from a specified location while attenuating activity originating at other locations. Beamformers have been widely used in the neuroscience literature to reconstruct the activity of oscillatory sources at the HFOs frequencies of interest, and they have been shown to be robust to different levels of signal-to-noise ratio (182–187). A more recent method, especially suited to localize HFO events is based on the wavelet-based Maximum Entropy on the Mean method (wMEM; 188). The wMEM was designed to localize single-trial events of oscillatory transient cortical activity which is usually associated with low signal-to-noise ratio. wMEM has been proved to correctly localize HFOs events in realistic simulations (188) and has been used to localize HFOs detected at the scalp in MEG (87, 143).

4. CONCLUSION AND FUTURE DIRECTIONS

With the present article we aimed to provide a comprehensive overview of the current state of HFO research in epilepsy. There is an increasing body of evidence pointing toward the use of HFOs for delineating the EZ. However, there is still a lack of evidence derived from prospective clinical trials evaluating the clinical value of such a biomarker. Prospective trials are needed in order to assess the potential value of HFOs, especially as there are still concerns regarding the potential of HFOs as a reliable clinical marker (58). Therefore, it is indicated that conclusions of findings, especially with regard to surgical decision-making, need to be taken with caution.

Furthermore, the development and implementation of a framework for standardized HFO detection needs to be pursued, in order to reduce biases (16, 25) and make the analysis of HFOs useful in clinical routine. Therefore, automatic detectors need to be further investigated and existing algorithms need to be systematically evaluated in order to enable prolonged analysis of multiple recordings as well as the reliable detection of HFOs. The existence of physiologic HFOs in multiple areas of the brain is another obstacle that needs to be tackled. Identification of physiologic events is of special importance when it comes to source localization of HFOs as including them will obviously seriously alter the results. It awaits confirmation if normalizing HFO rates for the different brain regions as possible with the recent availability of an atlas on physiologic HFOs will indeed increase the specificity of pathologic HFOs.

Nonetheless, the increasing amount of findings suggesting also non-invasively obtained HFOs to be of use should fuel further research, as they give hope that localized sources of pathologic HFOs might improve guidance for resective surgery in the future and spare iEEG recordings. Novel markers such as very-fast ripples of up to 2,000 Hz (18–20), and more advanced analyses considering the network properties of HFOs (189–191) provide further exciting novel approaches for future research.

AUTHOR CONTRIBUTIONS

AT wrote the initial draft of the manuscript. A-SH provided the sections concerning technical issues and source localization. BF provided both figures, and the input with regard to the general content and structure of the manuscript. All authors together planned the manuscript, critically revised the initial draft and made final improvements prior to submission.

FUNDING

The presented research was funded by the Austrian Science Fund (FWF): KLI657-B31 and by the PMU-FFF: A-18/01/029-HL. BF's salary is supported by a salary award (Chercheur-boursier clinicien Junior2) 2018-2021 of the Fonds de la Recherche en Santé du Québec. A-SH was funded by the CIBC Post-Doctoral Fellowship in Brain Imaging from the Montreal Neurological Institute.

ACKNOWLEDGMENTS

The authors wish to thank Andreas M. Koupparis, MD Ph.D., postdoc at the Montreal Neurological Institute and Hospital, for his help in preparing the time frequency plots for **Figure 2**.

REFERENCES

1. Brodie MJ. Antiepileptic drug therapy the story so far. *Seizure* (2010) 19:650–5. doi: 10.1016/j.seizure.2010.10.027

2. Vossler DG, Weingarten M, Gidal BE, Committee AEST. Summary of Antiepileptic Drugs Available in the United States of America: working toward a world without Epilepsy. *Epilepsy Curr.* (2018) 18:1–26. doi: 10.5698/1535-7597.18.4s1.1

3. Kwan P, Sander J. The natural history of epilepsy: an epidemiological view. *J Neurol Neurosurg Psychiatry* (2004) 75:1376–81. doi: 10.1136/jnnp.2004.045690
4. Wieser HG, Blume WT, Fish D, Goldensohn E, Hufnagel A, King D, et al. Proposal for a new classification of outcome with respect to epileptic seizures following epilepsy surgery. *Epilepsia* (2001) 42:282–6. doi: 10.1046/j.1528-1157.2001.4220282.x
5. McIntosh AM, Kalnins RM, Mitchell LA, Fabinyi GC, Briellmann RS, Berkovic SF. Temporal lobectomy: long-term seizure outcome, late recurrence and risks for seizure recurrence. *Brain* (2004) 127:2018–30. doi: 10.1093/brain/awh221
6. Wellmer J, von der Groeben F, Klarmann U, Weber C, Elger CE, Urbach H, et al. Risks and benefits of invasive epilepsy surgery workup with implanted subdural and depth electrodes. *Epilepsia* (2012) 53:1322–32. doi: 10.1111/j.1528-1167.2012.03545.x
7. Rosenow F, Lüders H. Presurgical evaluation of epilepsy. *Brain* (2001) 124:1683–700. doi: 10.1093/brain/124.9.1683
8. Malmgren K, Edelvik A. Long-term outcomes of surgical treatment for epilepsy in adults with regard to seizures, antiepileptic drug treatment and employment. *Seizure* (2017) 44:217–24. doi: 10.1016/j.seizure.2016.10.015
9. Bragin A, Engel J Jr, Staba RJ. High-frequency oscillations in epileptic brain. *Curr Opin Neurol.* (2010) 23:151. doi: 10.1097/WCO.0b013e3283373ac8
10. Jacobs J, Staba R, Asano E, Otsubo H, Wu J, Zijlmans M, et al. High-frequency oscillations (HFOs) in clinical epilepsy. *Prog Neurobiol.* (2012) 98:302–15. doi: 10.1016/j.pneurobio.2012.03.001
11. Haegelen C, Perucca P, Châtillon CE, Andrade-Valença L, Zelmann R, Jacobs J, et al. High-frequency oscillations, extent of surgical resection, and surgical outcome in drug-resistant focal epilepsy. *Epilepsia* (2013) 54:848–57. doi: 10.1111/epi.12075
12. Cho JR, Koo DL, Joo EY, Seo DW, Hong SC, Jiruska P, et al. Resection of individually identified high-rate high-frequency oscillations region is associated with favorable outcome in neocortical epilepsy. *Epilepsia* (2014) 55:1872–83. doi: 10.1111/epi.12808
13. Kerber K, Dümpelmann M, Schelter B, Le Van P, Korinthenberg R, Schulze-Bonhage A, et al. Differentiation of specific ripple patterns helps to identify epileptogenic areas for surgical procedures. *Clin Neurophysiol.* (2014) 125:1339–45. doi: 10.1016/j.clinph.2013.11.030
14. Okanishi T, Akiyama T, Tanaka SI, Mayo E, Mitsutake A, Boelman C, et al. Interictal high frequency oscillations correlating with seizure outcome in patients with widespread epileptic networks in tuberous sclerosis complex. *Epilepsia* (2014) 55:1602–10. doi: 10.1111/epi.12761
15. Van Klink N, Van't Klooster M, Zelmann R, Leijten F, Ferrier C, Braun K, et al. High frequency oscillations in intra-operative electrocorticography before and after epilepsy surgery. *Clin Neurophysiol.* (2014) 125:2212–9. doi: 10.1016/j.clinph.2014.03.004
16. Frauscher B, Bartolomei F, Kobayashi K, Cimbalnik J, Klooster MA, Rampp S, et al. High-frequency oscillations: The state of clinical research. *Epilepsia* (2017) 58:1316–29. doi: 10.1111/epi.13829
17. Bragin A, Engel J, Wilson CL, Fried I, Buzsáki G. High-frequency oscillations in human brain. *Hippocampus* (1999) 9:137–42. doi: 10.1002/(SICI)1098-1063(1999)9:2<137::AID-HIPO5>3.0.CO;2-0
18. Usui N, Terada K, Baba K, Matsuda K, Nakamura F, Usui K, et al. Very high frequency oscillations (over 1000 Hz) in human epilepsy. *Clin Neurophysiol.* (2010) 121:1825–31. doi: 10.1016/j.clinph.2010.04.018
19. Usui N, Terada K, Baba K, Matsuda K, Usui K, Tottori T, et al. Significance of very-high-frequency oscillations (over 1,000 H z) in epilepsy. *Ann Neurol.* (2015) 78:295–302. doi: 10.1002/ana.24440
20. Brázdil M, Pail M, Halámek J, Plešinger F, Cimbálník J, Roman R, et al. Very high frequency oscillations: novel biomarkers of the epileptogenic zone. *Ann Neurol.* (2017) 82:299–310. doi: 10.1002/ana.25006
21. Jacobs J, Zijlmans M, Zelmann R, Chatillon CÉ, Hall J, Olivier A, et al. High-frequency electroencephalographic oscillations correlate with outcome of epilepsy surgery. *Ann Neurol.* (2010) 67:209–20. doi: 10.1002/ana.21847
22. Usui N, Terada K, Baba K, Matsuda K, Nakamura F, Usui K, et al. Clinical significance of ictal high frequency oscillations in medial temporal lobe epilepsy. *Clin Neurophysiol.* (2011) 122:1693–700. doi: 10.1016/j.clinph.2011.02.006
23. Fujiwara H, Greiner HM, Lee KH, Holland-Bouley KD, Seo JH, Arthur T, et al. Resection of ictal high-frequency oscillations leads to favorable surgical outcome in pediatric epilepsy. *Epilepsia* (2012) 53:1607–17. doi: 10.1111/j.1528-1167.2012.03629.x
24. Gardner AB, Worrell GA, Marsh E, Dlugos D, Litt B. Human and automated detection of high-frequency oscillations in clinical intracranial EEG recordings. *Clin Neurophysiol.* (2007) 118:1134–43. doi: 10.1016/j.clinph.2006.12.019
25. Spring AM, Pittman DJ, Aghakhani Y, Jirsch J, Pillay N, Bello-Espinosa LE, et al. Interrater reliability of visually evaluated high frequency oscillations. *Clin Neurophysiol.* (2017) 128:433–41. doi: 10.1016/j.clinph.2016.12.017
26. Engel J Jr, da Silva FL. High-frequency oscillations–where we are and where we need to go. *Prog. Neurobiol.* (2012) 98:316–18. doi: 10.1016/j.pneurobio.2012.02.001
27. Staba RJ. Normal and pathologic high-frequency oscillations. In: Noebels JL, Avoli M, Rogawski MA, Olsen RW, Delgado-Escueta AV, editors. *Jasper's Basic Mechanisms of the Epilepsies [Internet], 4th ed*. Bethesda, MD: National Center for Biotechnology Information (US) (2012). p. 202–12.
28. Kobayashi K, Akiyama T, Agari T, Sasaki T, Shibata T, Hanaoka Y, et al. Significance of High-frequency Electrical Brain Activity. *Acta Med Okayama.* (2017) 71:191–200. doi: 10.18926/AMO/55201
29. van't Klooster M, van Klink N, van Blooijs D, Ferrier C, Braun K, Leijten F, et al. Evoked versus spontaneous high frequency oscillations in the chronic electrocorticogram in focal epilepsy. *Clin Neurophysiol.* (2017) 128:858–66. doi: 10.1016/j.clinph.2017.01.017
30. Höller P, Trinka E, Höller Y. High-frequency oscillations in the scalp electroencephalogram: mission impossible without computational intelligence. *Comput Intell Neurosci.* (2018) 2018:1638097. doi: 10.1155/2018/1638097
31. Bragin A, Engel J, Wilson CL, Fried I, Mathern GW. Hippocampal and entorhinal cortex high-frequency oscillations (100–500 Hz) in human epileptic brain and in kainic acid-treated rats with chronic seizures. *Epilepsia* (1999) 40:127–37.
32. Akiyama T, Otsubo H, Ochi A, Ishiguro T, Kadokura G, RamachandranNair R, et al. Focal cortical high-frequency oscillations trigger epileptic spasms: confirmation by digital video subdural EEG. *Clin Neurophysiol.* (2005) 116:2819–25. doi: 10.1016/j.clinph.2005.08.029
33. Jirsch J, Urrestarazu E, LeVan P, Olivier A, Dubeau F, Gotman J. High-frequency oscillations during human focal seizures. *Brain* (2006) 129:1593–608. doi: 10.1093/brain/awl085
34. Urrestarazu E, Jirsch JD, LeVan P, Hall J. High-frequency intracerebral EEG activity (100–500 Hz) following interictal spikes. *Epilepsia* (2006) 47:1465–76. doi: 10.1111/j.1528-1167.2006.00618.x
35. Reva N, Aftanas L. The coincidence between late non-phase-locked gamma synchronization response and saccadic eye movements. *Int J Psychophysiol.* (2004) 51:215–22. doi: 10.1016/j.ijpsycho.2003.09.005
36. Yuval-Greenberg S, Tomer O, Keren AS, Nelken I, Deouell LY. Transient induced gamma-band response in EEG as a manifestation of miniature saccades. *Neuron* (2008) 58:429–41. doi: 10.1016/j.neuron.2008.03.027
37. Melloni L, Schwiedrzik CM, Wibral M, Rodriguez E, Singer W. Response to: Yuval-Greenberg et al., "Transient induced gamma-band response in EEG as a manifestation of miniature saccades." Neuron 58, 429–441. *Neuron* (2009) 62:8–10. doi: 10.1016/j.neuron.2009.04.002
38. Andrade-Valenca L, Dubeau F, Mari F, Zelmann R, Gotman J. Interictal scalp fast oscillations as a marker of the seizure onset zone. *Neurology* (2011) 77:524–31. doi: 10.1212/WNL.0b013e318228bee2
39. Worrell GA, Jerbi K, Kobayashi K, Lina JM, Zelmann R, Le Van Quyen M. Recording and analysis techniques for high-frequency oscillations. *Prog Neurobiol.* (2012) 98:265–78. doi: 10.1016/j.pneurobio.2012.02.006
40. Gloss D, Nevitt SJ, Staba R. The role of high-frequency oscillations in epilepsy surgery planning. *Cochrane Library* (2017). CD010235. doi: 10.1002/14651858.CD010235.pub2
41. Höller Y, Kutil R, Klaffenböck L, Thomschewski A, Höller PM, Bathke AC, et al. High-frequency oscillations in epilepsy and surgical outcome. A meta-analysis. *Front Hum Neurosci*. (2015) 9:574. doi: 10.3389/fnhum.2015.00574
42. Leung H, Zhu CX, Chan DT, Poon WS, Shi L, Mok VC, et al. Ictal high-frequency oscillations and hyperexcitability in refractory epilepsy. *Clin Neurophysiol.* (2015) 126:2049–57. doi: 10.1016/j.clinph.2015.01.009

43. Fujiwara H, Leach JL, Greiner HM, Holland-Bouley KD, Rose DF, Arthur T, et al. Resection of ictal high frequency oscillations is associated with favorable surgical outcome in pediatric drug resistant epilepsy secondary to tuberous sclerosis complex. *Epilepsy Res.* (2016) 126:90–7. doi: 10.1016/j.eplepsyres.2016.07.005
44. Liu C, Zhang R, Zhang G, Yu T, Tai J, Du W, et al. High frequency oscillations for lateralizing suspected bitemporal epilepsy. *Epilepsy Res.* (2016) 127:233–40. doi: 10.1016/j.eplepsyres.2016.09.006
45. Grinenko O, Li J, Mosher JC, Wang IZ, Bulacio JC, Gonzalez-Martinez J, et al. A fingerprint of the epileptogenic zone in human epilepsies. *Brain* (2018) 141:117–31. doi: 10.1093/brain/awx306
46. Iimura Y, Jones K, Hattori K, Okazawa Y, Noda A, Hoashi K, et al. Epileptogenic high-frequency oscillations skip the motor area in children with multilobar drug-resistant epilepsy. *Clin Neurophysiol.* (2017) 128:1197–205. doi: 10.1016/j.clinph.2017.03.031
47. Iimura Y, Jones K, Takada L, Shimizu I, Koyama M, Hattori K, et al. Strong coupling between slow oscillations and wide fast ripples in children with epileptic spasms: investigation of modulation index and occurrence rate. *Epilepsia* (2018) 59:544–54. doi: 10.1111/epi.13995
48. Pail M, Řehulka P, Cimbálník J, Doležalová I, Chrastina J, Brázdil M. Frequency-independent characteristics of high-frequency oscillations in epileptic and non-epileptic regions. *Clin Neurophysiol.* (2017) 128:106–14. doi: 10.1016/j.clinph.2016.10.011
49. Wang S, So NK, Jin B, Wang IZ, Bulacio JC, Enatsu R, et al. Interictal ripples nested in epileptiform discharge help to identify the epileptogenic zone in neocortical epilepsy. *Clin Neurophysiol.* (2017) 128:945–51. doi: 10.1016/j.clinph.2017.03.033
50. Cuello-Oderiz C, von Ellenrieder N, Sankhe R, Olivier A, Hall J, Dubeau F, et al. Value of ictal and interictal epileptiform discharges and high frequency oscillations for delineating the epileptogenic zone in patients with focal cortical dysplasia. *Clin Neurophysiol.* (2018) 129:1311–9. doi: 10.1016/j.clinph.2018.02.003
51. van't Klooster MA, Van Klink NE, Leijten FS, Zelmann R, Gebbink TA, Gosselaar PH, et al. Residual fast ripples in the intraoperative corticogram predict epilepsy surgery outcome. *Neurology* (2015) 85:120–8. doi: 10.1212/WNL.0000000000001727
52. Fedele T, van't Klooster M, Burnos S, Zweiphenning W, van Klink N, Leijten F, et al. Automatic detection of high frequency oscillations during epilepsy surgery predicts seizure outcome. *Clin Neurophysiol.* (2016) 127:3066–74. doi: 10.1016/j.clinph.2016.06.009
53. van't Klooster MA, van Klink NE, Zweiphenning WJ, Leijten FS, Zelmann R, Ferrier CH, et al. Tailoring epilepsy surgery with fast ripples in the intraoperative electrocorticogram. *Ann Neurol.* (2017) 81:664–76. doi: 10.1002/ana.24928
54. Ren GP, Yan JQ, Yu ZX, Wang D, Li XN, Mei SS, et al. Automated detector of high frequency oscillations in epilepsy based on maximum distributed peak points. *Int J Neural Syst.* (2017) 27:1750029. doi: 10.1142/S0129065717500290
55. Weiss SA, Berry B, Chervoneva I, Waldman Z, Guba J, Bower M, et al. Visually validated semi-automatic high-frequency oscillation detection aides the delineation of epileptogenic regions during intra-operative electrocorticography. *Clin Neurophysiol.* (2018) 129:2089–98. doi: 10.1016/j.clinph.2018.06.030
56. Fedele T, Ramantani G, Burnos S, Hilfiker P, Curio G, Grunwald T, et al. Prediction of seizure outcome improved by fast ripples detected in low-noise intraoperative corticogram. *Clin Neurophysiol.* (2017) 128:1220–6. doi: 10.1016/j.clinph.2017.03.038
57. Jacobs J, Wu JY, Perucca P, Zelmann R, Mader M, Dubeau F, et al. Removing high-frequency oscillations: a prospective multicenter study on seizure outcome. *Neurology* (2018) 91:e1040–52. doi: 10.1212/WNL.0000000000006158
58. Roehri N, Pizzo F, Lagarde S, Lambert I, Nica A, McGonigal A, et al. High-frequency oscillations are not better biomarkers of epileptogenic tissues than spikes. *Ann Neurol.* (2018) 83:84–97. doi: 10.1002/ana.25124
59. Hirsch E, Scholly J. *Study of Predictive Biomarkers for Rational Management of Drug-Resistant Epilepsy Associated With Focal Cortical Dysplasia (SPREAD).* Available online at: https://clinicaltrials.gov/ct2/show/NCT03321240?term=HFO&cond=Epilepsy&rank=4.
60. Leung H, Poon W, Kwan P, Lui C, Poon T, Chan E, et al. Ictal intracranial electroencephalography using wavelet analysis of high-frequency oscillations in Chinese patients with refractory epilepsy. *Hong Kong Med J.* (2018) 24(3 Suppl. 3) S21–3.
61. Modur PN, Zhang S, Vitaz TW. Ictal high-frequency oscillations in neocortical epilepsy: implications for seizure localization and surgical resection. *Epilepsia* (2011) 52:1792–801. doi: 10.1111/j.1528-1167.2011.03165.x
62. Ramachandran Nair R, Ochi A, Imai K, Benifla M, Akiyama T, Holowka S, et al. Epileptic spasms in older pediatric patients: MEG and ictal high-frequency oscillations suggest focal-onset seizures in a subset of epileptic spasms. *Epilepsy Res.* (2008) 78:216–24. doi: 10.1016/j.eplepsyres.2007.12.007
63. van't Klooster MA, Leijten FS, Huiskamp G, Ronner HE, Baayen JC, van Rijen PC, et al. High frequency oscillations in the intra-operative ECoG to guide epilepsy surgery ("The HFO Trial"): study protocol for a randomized controlled trial. *Trials* (2015) 16:422. doi: 10.1186/s13063-015-0932-6
64. Navarrete M, Pyrzowski J, Corlier J, Valderrama M, Le Van Quyen M. Automated detection of high-frequency oscillations in electrophysiological signals: methodological advances. *J Physiol Paris* (2016) 110:316–26. doi: 10.1016/j.jphysparis.2017.02.003
65. Zijlmans M, Worrell GA, Dümpelmann M, Stieglitz T, Barborica A, Heers M, et al. How to record high-frequency oscillations in epilepsy: a practical guideline. *Epilepsia* (2017) 58:1305–15. doi: 10.1111/epi.13814
66. Schomer DL, Da Silva FL. *Niedermeyer's Electroencephalography: Basic Principles, Clinical Applications, and Related Fields.* Philadelphia, PA: Lippincott Williams & Wilkins (2011).
67. Urrestarazu E, Chander R, Dubeau F, Gotman J. Interictal high-frequency oscillations (100–500 Hz) in the intracerebral EEG of epileptic patients. *Brain* (2007) 130:2354–66. doi: 10.1093/brain/awm149
68. Worrell GA, Gardner AB, Stead SM, Hu S, Goerss S, Cascino GJ, et al. High-frequency oscillations in human temporal lobe: simultaneous microwire and clinical macroelectrode recordings. *Brain* (2008) 131:928–37. doi: 10.1093/brain/awn006
69. Jerbi K, Freyermuth S, Dalal S, Kahane P, Bertrand O, Berthoz A, et al. Saccade related gamma-band activity in intracerebral EEG: dissociating neural from ocular muscle activity. *Brain Topogr.* (2009) 22:18–23. doi: 10.1007/s10548-009-0078-5
70. Amiri M, Lina JM, Pizzo F, Gotman J. High frequency oscillations and spikes: separating real HFOs from false oscillations. *Clin Neurophysiol.* (2016) 127:187–96. doi: 10.1016/j.clinph.2015.04.290
71. Cardinale F, Cossu M, Castana L, Casaceli G, Schiariti MP, Miserocchi A, et al. Stereoelectroencephalography: surgical methodology, safety, and stereotactic application accuracy in 500 procedures. *Neurosurgery* (2013) 72:353–66. doi: 10.1227/NEU.0b013e31827d1161
72. Schevon CA, Trevelyan A, Schroeder C, Goodman R, McKhann Jr G, Emerson R. Spatial characterization of interictal high frequency oscillations in epileptic neocortex. *Brain* (2009) 132:3047–59. doi: 10.1093/brain/awp222
73. Liu S, Sha Z, Sencer A, Aydoseli A, Bebek N, Abosch A, et al. Exploring the time–frequency content of high frequency oscillations for automated identification of seizure onset zone in epilepsy. *J Neural Eng.* (2016) 13:026026. doi: 10.1088/1741-2560/13/2/026026
74. Migliorelli C, Alonso JF, Romero S, Nowak R, Russi A, Mañanas MA. Automated detection of epileptic ripples in MEG using beamformer-based virtual sensors. *J. Neural Eng.* (2017) 14:046013. doi: 10.1088/1741-2552/aa684c
75. Quitadamo LR, Foley E, Mai R, De Palma L, Specchio N, Seri S. EPINETLAB: a software for seizure-onset zone identification from intracranial EEG signal in epilepsy. *Front Neuroinform.* (2018) 12:45. doi: 10.3389/fninf.2018.00045
76. Shimamoto S, Waldman ZJ, Orosz I, Song I, Bragin A, Fried I, et al. Utilization of independent component analysis for accurate pathological ripple detection in intracranial EEG recordings recorded extra-and intra-operatively. *Clin Neurophysiol.* (2018) 129:296–307. doi: 10.1016/j.clinph.2017.08.036
77. Gliske SV, Irwin ZT, Chestek C, Hegeman GL, Brinkmann B, Sagher O, et al. Variability in the location of high frequency oscillations during prolonged intracranial EEG recordings. *Nat Commun.* (2018) 9:2155. doi: 10.1038/s41467-018-04549-2

78. Staba RJ, Wilson CL, Bragin A, Fried I, Engel J Jr. Quantitative analysis of high-frequency oscillations (80–500 Hz) recorded in human epileptic hippocampus and entorhinal cortex. *J Neurophysiol.* (2002) 88:1743–52. doi: 10.1152/jn.2002.88.4.1743
79. Bénar CG, Chauvière L, Bartolomei F, Wendling F. Pitfalls of high-pass filtering for detecting epileptic oscillations: a technical note on "false" ripples. *Clin Neurophysiol.* (2010) 121:301–10. doi: 10.1016/j.clinph.2009.10.019
80. Blanco JA, Stead M, Krieger A, Viventi J, Marsh WR, Lee KH, et al. Unsupervised classification of high-frequency oscillations in human neocortical epilepsy and control patients. *J Neurophysiol.* (2010) 104:2900–12. doi: 10.1152/jn.01082.2009
81. Zelmann R, Mari F, Jacobs J, Zijlmans M, Dubeau F, Gotman J. A comparison between detectors of high frequency oscillations. *Clin Neurophysiol.* (2012) 123:106–16. doi: 10.1016/j.clinph.2011.06.006
82. Roehri N, Pizzo F, Bartolomei F, Wendling F, Bénar CG. What are the assets and weaknesses of HFO detectors? A benchmark framework based on realistic simulations. *PLoS ONE* (2017) 12:e0174702. doi: 10.1371/journal.pone.0174702
83. Otsubo H, Ochi A, Imai K, Akiyama T, Fujimoto A, Go C, et al. High-frequency oscillations of ictal muscle activity and epileptogenic discharges on intracranial EEG in a temporal lobe epilepsy patient. *Clin Neurophysiol.* (2008) 119:862–8. doi: 10.1016/j.clinph.2007.12.014
84. Kovach CK, Tsuchiya N, Kawasaki H, Oya H, Howard III MA, Adolphs R. Manifestation of ocular-muscle EMG contamination in human intracranial recordings. *Neuroimage* (2011) 54:213–33. doi: 10.1016/j.neuroimage.2010.08.002
85. Burnos S, Frauscher B, Zelmann R, Haegelen C, Sarnthein J, Gotman J. The morphology of high frequency oscillations (HFO) does not improve delineating the epileptogenic zone. *Clin Neurophysiol.* (2016) 127:2140–8. doi: 10.1016/j.clinph.2016.01.002
86. Zelmann R, Mari F, Jacobs J, Zijlmans M, Chander R, Gotman J. Automatic detector of high frequency oscillations for human recordings with macroelectrodes. In: *Engineering in Medicine and Biology Society (EMBC), 2010 Annual International Conference of the IEEE*. Buenos Aires: IEEE (2010). p. 2329–33.
87. von Ellenrieder N, Pellegrino G, Hedrich T, Gotman J, Lina JM, Grova C, et al. Detection and magnetic source imaging of fast oscillations (40–160 Hz) recorded with magnetoencephalography in focal epilepsy patients. *Brain Topogr.* (2016) 29:218–31. doi: 10.1007/s10548-016-0471-9
88. Melani F, Zelmann R, Mari F, Gotman J. Continuous high frequency activity: a peculiar SEEG pattern related to specific brain regions. *Clin Neurophysiol.* (2013) 124:1507–16. doi: 10.1016/j.clinph.2012.11.016
89. Liu S, Gurses C, Sha Z, Quach MM, Sencer A, Bebek N, et al. Stereotyped high-frequency oscillations discriminate seizure onset zones and critical functional cortex in focal epilepsy. *Brain* (2018) 141:713–30. doi: 10.1093/brain/awx374
90. Wang S, Wang IZ, Bulacio JC, Mosher JC, Gonzalez-Martinez J, Alexopoulos AV, et al. Ripple classification helps to localize the seizure-onset zone in neocortical epilepsy. *Epilepsia* (2013) 54:370–76. doi: 10.1111/j.1528-1167.2012.03721.x
91. Jefferys JG, de La Prida LM, Wendling F, Bragin A, Avoli M, Timofeev I, et al. Mechanisms of physiological and epileptic HFO generation. *Prog Neurobiol.* (2012) 98:250–64. doi: 10.1016/j.pneurobio.2012.02.005
92. Alkawadri R, Gaspard N, Goncharova II, Spencer DD, Gerrard JL, Zaveri H, et al. The spatial and signal characteristics of physiologic high frequency oscillations. *Epilepsia* (2014) 55:1986–95. doi: 10.1111/epi.12851
93. Clemens Z, Mölle M, Erőss L, Barsi P, Halász P, Born J. Temporal coupling of parahippocampal ripples, sleep spindles and slow oscillations in humans. *Brain.* (2007) 130:2868–78. doi: 10.1093/brain/awm146
94. Siapas AG, Wilson MA. Coordinated interactions between hippocampal ripples and cortical spindles during slow-wave sleep. *Neuron* (1998) 21:1123–8. doi: 10.1016/S0896-6273(00)80629-7
95. Sirota A, Csicsvari J, Buhl D, Buzsáki G. Communication between neocortex and hippocampus during sleep in rodents. *Proc Natl Acad Sci USA.* (2003) 100:2065–9. doi: 10.1073/pnas.0437938100
96. Axmacher N, Elger CE, Fell J. Ripples in the medial temporal lobe are relevant for human memory consolidation. *Brain* (2008) 131:1806–17. doi: 10.1093/brain/awn103
97. Kunii N, Kawai K, Kamada K, Ota T, Saito N. The significance of parahippocampal high gamma activity for memory preservation in surgical treatment of atypical temporal lobe epilepsy. *Epilepsia* (2014) 55:1594–601. doi: 10.1111/epi.12764
98. Pu Y, Cornwell BR, Cheyne D, Johnson BW. High-gamma activity in the human hippocampus and parahippocampus during inter-trial rest periods of a virtual navigation task. *Neuroimage* (2018) 178:92–103. doi: 10.1016/j.neuroimage.2018.05.029
99. Blanco JA, Stead M, Krieger A, Stacey W, Maus D, Marsh E, et al. Data mining neocortical high-frequency oscillations in epilepsy and controls. *Brain* (2011) 134:2948–59. doi: 10.1093/brain/awr212
100. Jiang T, Liu S, Pellizzer G, Aydoseli A, Karamursel S, Sabanci PA, et al. Characterization of hand clenching in human sensorimotor cortex using high-, and ultra-high frequency band modulations of electrocorticogram. *Front Neurosci.* (2018) 12:110. doi: 10.3389/fnins.2018.00110
101. Özkurt TE, Butz M, Homburger M, Elben S, Vesper J, Wojtecki L, et al. High frequency oscillations in the subthalamic nucleus: a neurophysiological marker of the motor state in Parkinson's disease. *Exp Neurol.* (2011) 229:324–31. doi: 10.1016/j.expneurol.2011.02.015
102. Hirschmann J, Butz M, Hartmann CJ, Hoogenboom N, Özkurt TE, Vesper J, et al. Parkinsonian rest tremor is associated with modulations of subthalamic high-frequency oscillations. *Movement Disord.* (2016) 31:1551–9. doi: 10.1002/mds.26663
103. Hirschmann J, Schoffelen J, Schnitzler A, Van Gerven M. Parkinsonian rest tremor can be detected accurately based on neuronal oscillations recorded from the subthalamic nucleus. *Clin Neurophysiol.* (2017) 128:2029–36. doi: 10.1016/j.clinph.2017.07.419
104. Schnitzler S, Hartmann CJ, Groiss SJ, Wojtecki L, Schnitzler A, Vesper J, et al. Occurrence of thalamic high frequency oscillations in patients with different tremor syndromes. *Clin Neurophysiol.* (2018) 129:959–66. doi: 10.1016/j.clinph.2018.01.073
105. Hashimoto I, Mashiko T, Imada T. Somatic evoked high-frequency magnetic oscillations reflect activity of inhibitory interneurons in the human somatosensory cortex. *Electroencephalogr Clin Neurophysiol.* (1996) 100:189–203. doi: 10.1016/0168-5597(95)00244-8
106. Ozaki I, Suzuki C, Yaegashi Y, Baba M, Matsunaga M, Hashimoto I. High frequency oscillations in early cortical somatosensory evoked potentials. *Electroencephalogr Clin Neurophysiol.* (1998) 108:536–42. doi: 10.1016/S0168-5597(98)00032-X
107. Haueisen J, Heuer T, Nowak H, Liepert J, Weiller C, Okada Y, et al. The influence of lorazepam on somatosensory-evoked fast frequency (600 Hz) activity in MEG. *Brain Res.* (2000) 874:10–4. doi: 10.1016/S0006-8993(00)02534-8
108. Curio G, Mackert BM, Burghoff M, Koetitz R, Abraham-Fuchs K, Härer W. Localization of evoked neuromagnetic 600 Hz activity in the cerebral somatosensory system. *Electroencephalogr Clin Neurophysiol.* (1994) 91:483–7. doi: 10.1016/0013-4694(94)90169-4
109. Restuccia D, Del Piero I, Martucci L, Zanini S. High-frequency oscillations after median-nerve stimulation do not undergo habituation: a new insight on their functional meaning? *Clin Neurophysiol.* (2011) 122:148–52. doi: 10.1016/j.clinph.2010.06.008
110. Restuccia D, Coppola G. Auditory stimulation enhances thalamic somatosensory high-frequency oscillations in healthy humans: a neurophysiological marker of cross-sensory sensitization? *Eur J Neurosci.* (2015) 41:1079–85. doi: 10.1111/ejn.12873
111. Ozaki I, Hashimoto I. Neural mechanisms of the ultrafast activities. *Clin EEG Neurosci.* (2005) 36:271–77. doi: 10.1177/155005940503600406
112. Ozaki I, Hashimoto I. Exploring the physiology and function of high-frequency oscillations (HFOs) from the somatosensory cortex. *Clin Neurophysiol.* (2011) 122:1908–23. doi: 10.1016/j.clinph.2011.05.023
113. Arieli A, Sterkin A, Grinvald A, Aertsen A. Dynamics of ongoing activity: explanation of the large variability in evoked cortical responses. *Science* (1996) 273:1868–71. doi: 10.1126/science.273.5283.1868
114. Kenet T, Bibitchkov D, Tsodyks M, Grinvald A, Arieli A. Spontaneously emerging cortical representations of visual attributes. *Nature* (2003) 425:954. doi: 10.1038/nature02078

115. Tsodyks M, Kenet T, Grinvald A, Arieli A. Linking spontaneous activity of single cortical neurons and the underlying functional architecture. *Science* (1999) 286:1943–6. doi: 10.1126/science.286.5446.1943
116. Nagasawa T, Juhász C, Rothermel R, Hoechstetter K, Sood S, Asano E. Spontaneous and visually driven high-frequency oscillations in the occipital cortex: intracranial recording in epileptic patients. *Hum Brain Mapp.* (2012) 33:569–83. doi: 10.1002/hbm.21233
117. Lachaux JP, Axmacher N, Mormann F, Halgren E, Crone NE. High-frequency neural activity and human cognition: past, present and possible future of intracranial EEG research. *Prog Neurobiol.* (2012) 98:279–301. doi: 10.1016/j.pneurobio.2012.06.008
118. Matsumoto A, Brinkmann BH, Matthew Stead S, Matsumoto J, Kucewicz MT, Marsh WR, et al. Pathological and physiological high-frequency oscillations in focal human epilepsy. *J Neurophysiol.* (2013) 110:1958–64. doi: 10.1152/jn.00341.2013
119. Bruder JC, Dümpelmann M, Piza DL, Mader M, Schulze-Bonhage A, Jacobs-Le Van J. Physiological ripples associated with sleep spindles differ in waveform morphology from epileptic ripples. *Int J Neural Syst.* (2017) 27:1750011. doi: 10.1142/S0129065717500113
120. Le Van Quyen M, Staba R, Bragin A, Dickson C, Valderrama M, Fried I, et al. Large-scale microelectrode recordings of high-frequency gamma oscillations in human cortex during sleep. *J Neurosci.* (2010) 30:7770–82. doi: 10.1523/JNEUROSCI.5049-09.2010
121. Frauscher B, von Ellenrieder N, Ferrari-Marinho T, Avoli M, Dubeau F, Gotman J. Facilitation of epileptic activity during sleep is mediated by high amplitude slow waves. *Brain* (2015) 138:1629–41. doi: 10.1093/brain/awv073
122. von Ellenrieder N, Frauscher B, Dubeau F, Gotman J. Interaction with slow waves during sleep improves discrimination of physiologic and pathologic high-frequency oscillations (80–500 Hz). *Epilepsia* (2016) 57:869–78. doi: 10.1111/epi.13380
123. Nonoda Y, Miyakoshi M, Ojeda A, Makeig S, Juhász C, Sood S, et al. Interictal high-frequency oscillations generated by seizure onset and eloquent areas may be differentially coupled with different slow waves. *Clin Neurophysiol.* (2016) 127:2489–99. doi: 10.1016/j.clinph.2016.03.022
124. Bagshaw AP, Jacobs J, LeVan P, Dubeau F, Gotman J. Effect of sleep stage on interictal high-frequency oscillations recorded from depth macroelectrodes in patients with focal epilepsy. *Epilepsia* (2009) 50:617–28. doi: 10.1111/j.1528-1167.2008.01784.x
125. Staba RJ, Wilson CL, Bragin A, Jhung D, Fried I, Engel J. High-frequency oscillations recorded in human medial temporal lobe during sleep. *Ann Neurol.* (2004) 56:108–15. doi: 10.1002/ana.20164
126. Sakuraba R, Iwasaki M, Okumura E, Jin K, Kakisaka Y, Kato K, et al. High frequency oscillations are less frequent but more specific to epileptogenicity during rapid eye movement sleep. *Clin Neurophysiol.* (2016) 127:179–86. doi: 10.1016/j.clinph.2015.05.019
127. von Ellenrieder N, Dubeau F, Gotman J, Frauscher B. Physiological and pathological high-frequency oscillations have distinct sleep-homeostatic properties. *Neuroimage Clin.* (2017) 14:566–73. doi: 10.1016/j.nicl.2017.02.018
128. Frauscher B, Ellenrieder N, Dubeau F, Gotman J. EEG desynchronization during phasic REM sleep suppresses interictal epileptic activity in humans. *Epilepsia* (2016) 57:879–88. doi: 10.1111/epi.13389
129. Guragain H, Cimbalnik J, Stead M, Groppe DM, Berry BM, Kremen V, et al. Spatial variation in high-frequency oscillation rates and amplitudes in intracranial EEG. *Neurology* (2018) 90:e639–46. doi: 10.1212/WNL.0000000000004998
130. Frauscher B, von Ellenrieder N, Zelmann R, Doležalová I, Minotti L, Olivier A, et al. Atlas of the normal intracranial electroencephalogram: neurophysiological awake activity in different cortical areas. *Brain* (2018) 141:1130–44. doi: 10.1093/brain/awy035
131. Frauscher B, von Ellenrieder N, Zelmann R, Rogers C, Nguyen DK, Kahane P, et al. High-frequency oscillations in the normal human brain. *Ann Neurol.* (2018) 84:374–85. doi: 10.1002/ana.25304
132. Kobayashi K, Oka M, Akiyama T, Inoue T, Abiru K, Ogino T, et al. Very fast rhythmic activity on scalp EEG associated with epileptic spasms. *Epilepsia* (2004) 45:488–96. doi: 10.1111/j.0013-9580.2004.45703.x
133. Kobayashi K, Inoue T, Watanabe Y, Oka M, Endoh F, Yoshinaga H, et al. Spectral analysis of EEG gamma rhythms associated with tonic seizures in Lennox–Gastaut syndrome. *Epilepsy Res.* (2009) 86:15–22. doi: 10.1016/j.eplepsyres.2009.03.011
134. Iwatani Y, Kagitani-Shimono K, Tominaga K, Okinaga T, Kishima H, Kato A, et al. Ictal high-frequency oscillations on scalp EEG recordings in symptomatic West syndrome. *Epilepsy Res.* (2012) 102:60–70. doi: 10.1016/j.eplepsyres.2012.04.020
135. Kobayashi K, Watanabe Y, Inoue T, Oka M, Yoshinaga H, Ohtsuka Y. Scalp-recorded high-frequency oscillations in childhood sleep-induced electrical status epilepticus. *Epilepsia* (2010) 51:2190–4. doi: 10.1111/j.1528-1167.2010.02565.x
136. Kobayashi K, Yoshinaga H, Toda Y, Inoue T, Oka M, Ohtsuka Y. High-frequency oscillations in idiopathic partial epilepsy of childhood. *Epilepsia* (2011) 52:1812–9. doi: 10.1111/j.1528-1167.2011.03169.x
137. Fahoum F, Melani F, Andrade-Valença L, Dubeau F, Gotman J. Epileptic scalp ripples are associated with corticothalamic BOLD changes. *Epilepsia* (2014) 55:1611–9. doi: 10.1111/epi.12760
138. Lu Y, Worrell GA, Zhang HC, Yang L, Brinkmann B, Nelson C, et al. Noninvasive imaging of the high frequency brain activity in focal epilepsy patients. *IEEE Trans Biomed Eng.* (2014) 61:1660–7. doi: 10.1109/TBME.2013.2297332
139. Zelmann R, Lina J, Schulze-Bonhage A, Gotman J, Jacobs J. Scalp EEG is not a blur: it can see high frequency oscillations although their generators are small. *Brain Topogr.* (2014) 27:683–704. doi: 10.1007/s10548-013-0321-y
140. Chaitanya G, Sinha S, Narayanan M, Satishchandra P. Scalp high frequency oscillations (HFOs) in absence epilepsy: an independent component analysis (ICA) based approach. *Epilepsy Res.* (2015) 115:133–40. doi: 10.1016/j.eplepsyres.2015.06.008
141. Kobayashi K, Akiyama T, Oka M, Endoh F, Yoshinaga H. A storm of fast (40–150Hz) oscillations during hypsarrhythmia in West syndrome. *Ann Neurol.* (2015) 77:58–67. doi: 10.1002/ana.24299
142. Toda Y, Kobayashi K, Hayashi Y, Inoue T, Oka M, Endo F, et al. High-frequency EEG activity in epileptic encephalopathy with suppression-burst. *Brain Dev.* (2015) 37:230–6. doi: 10.1016/j.braindev.2014.04.004
143. Papadelis C, Tamilia E, Stufflebeam S, Grant PE, Madsen JR, Pearl PL, et al. Interictal high frequency oscillations detected with simultaneous magnetoencephalography and electroencephalography as biomarker of pediatric epilepsy. *J Vis Exp.* (2016) 54883. doi: 10.3791/54883
144. Pizzo F, Ferrari-Marinho T, Amiri M, Frauscher B, Dubeau F, Gotman J. When spikes are symmetric, ripples are not: bilateral spike and wave above 80 Hz in focal and generalized epilepsy. *Clin Neurophysiol.* (2016) 127:1794–802. doi: 10.1016/j.clinph.2015.11.451
145. Pizzo F, Frauscher B, Ferrari-Marinho T, Amiri M, Dubeau F, Gotman J. Detectability of fast ripples (>250 Hz) on the scalp EEG: a proof-of-principle study with subdermal electrodes. *Brain Topogr.* (2016) 29:358–67. doi: 10.1007/s10548-016-0481-7
146. Qian P, Li H, Xue J, Yang Z. Scalp-recorded high-frequency oscillations in atypical benign partial epilepsy. *Clin Neurophysiol.* (2016) 127:3306–13. doi: 10.1016/j.clinph.2016.07.013
147. van Klink N, Frauscher B, Zijlmans M, Gotman J. Relationships between interictal epileptic spikes and ripples in surface EEG. *Clin Neurophysiol.* (2016) 127:143–9. doi: 10.1016/j.clinph.2015.04.059
148. van Klink NE, vanť Klooster MA, Leijten FS, Jacobs J, Braun KP, Zijlmans M. Ripples on rolandic spikes: a marker of epilepsy severity. *Epilepsia* (2016) 57:1179–89. doi: 10.1111/epi.13423
149. Cuello-Oderiz C, Ellenrieder N, Dubeau F, Gotman J. Influence of the location and type of epileptogenic lesion on scalp interictal epileptiform discharges and high-frequency oscillations. *Epilepsia* (2017) 58:2153–63. doi: 10.1111/epi.13922
150. Mooij AH, Raijmann RC, Jansen FE, Braun KP, Zijlmans M. Physiological ripples (±100 Hz) in spike-free scalp EEGs of children with and without epilepsy. *Brain Topogr.* (2017) 30:739–46. doi: 10.1007/s10548-017-0590-y
151. Gong P, Xue J, Qian P, Yang H, Liu X, Cai L, et al. Scalp-recorded high-frequency oscillations in childhood epileptic encephalopathy with continuous spike-and-wave during sleep with different etiologies. *Brain Dev.* (2018). 40:299–310. doi: 10.1016/j.braindev.2017.12.010
152. van Klink N, Mol A, Ferrier C, Hillebrand A, Huiskamp G, Zijlmans M. Beamforming applied to surface EEG improves ripple visibility. *Clin Neurophysiol.* (2018) 129:101–11. doi: 10.1016/j.clinph.2017.10.026

153. van Klink NE. *High Frequency Oscillations in Epilepsy: Towards Clinical Application*. Utrecht University (2018).
154. Bernardo D, Nariai H, Hussain SA, Sankar R, Salamon N, Krueger DA, et al. Visual and semi-automatic non-invasive detection of interictal fast ripples: A potential biomarker of epilepsy in children with tuberous sclerosis complex. *Clin Neurophysiol.* (2018) 129:1458–66. doi: 10.1016/j.clinph.2018.03.010
155. Ikemoto S, Hamano Si, Yokota S, Koichihara R, Hirata Y, Matsuura R. Enhancement and bilateral synchronization of ripples in atypical benign epilepsy of childhood with centrotemporal spikes. *Clin Neurophysiol.* (2018) 129:1920–5. doi: 10.1016/j.clinph.2018.06.023
156. Kobayashi K, Ohuchi Y, Shibata T, Hanaoka Y, Akiyama M, Oka M, et al. Detection of fast (40–150 Hz) oscillations from the ictal scalp EEG data of myoclonic seizures in pediatric patients. *Brain Dev.* (2018) 40:397–405. doi: 10.1016/j.braindev.2018.01.004
157. Kuhnke N, Schwind J, Dümpelmann M, Mader M, Schulze-Bonhage A, Jacobs J. High frequency oscillations in the ripple band (80–250 Hz) in scalp EEG: higher density of electrodes allows for better localization of the seizure onset zone. *Brain Topogr.* (2018) 31:1059–72. doi: 10.1007/s10548-018-0658-3
158. Mooij AH, Frauscher B, Goemans SA, Huiskamp GJ, Braun KP, Zijlmans M. Ripples in scalp EEGs of children: co-occurrence with sleep-specific transients and occurrence across sleep stages. *Sleep* (2018) 41:zsy169. doi: 10.1093/sleep/zsy169
159. Fedele T, Schönenberger C, Curio G, Serra C, Krayenbühl N, Sarnthein J. Intraoperative subdural low-noise EEG recording of the high frequency oscillation in the somatosensory evoked potential. *Clin Neurophysiol.* (2017) 128:1851–7. doi: 10.1016/j.clinph.2017.07.400
160. Ahlfors SP, Han J, Belliveau JW, Hämäläinen MS. Sensitivity of MEG and EEG to source orientation. *Brain Topogr.* (2010) 23:227–32. doi: 10.1007/s10548-010-0154-x
161. Hari R. Magnetoencephalography: methods and applications. In: Schomer DL, Lopes da Silva FH, editors. *Niedermeyer's Electroencephalography: Basic Principles, Clinical Applications and Related Fields, 6th ed.* Philadelphia, PA: Lippincott Williams & Wilkins (2011). p. 865–900.
162. Williamson SJ, Lü ZL, Karron D, Kaufman L. Advantages and limitations of magnetic source imaging. *Brain Topogr.* (1991) 4:169–80. doi: 10.1007/BF01132773
163. Guggisberg AG, Kirsch HE, Mantle MM, Barbaro NM, Nagarajan SS. Fast oscillations associated with interictal spikes localize the epileptogenic zone in patients with partial epilepsy. *Neuroimage* (2008) 39:661–8. doi: 10.1016/j.neuroimage.2007.09.036
164. Xiang J, Liu Y, Wang Y, Kirtman EG, Kotecha R, Chen Y, et al. Frequency and spatial characteristics of high-frequency neuromagnetic signals in childhood epilepsy. *Epilept Disord.* (2009) 11:113–25. doi: 10.1684/epd.2009.0253
165. Rampp S, Kaltenhäuser M, Weigel D, Buchfelder M, Blümcke I, Dörfler A, et al. MEG correlates of epileptic high gamma oscillations in invasive EEG. *Epilepsia* (2010) 51:1638–42. doi: 10.1111/j.1528-1167.2010.02579.x
166. Xiang J, Wang Y, Chen Y, Liu Y, Kotecha R, Huo X, et al. Noninvasive localization of epileptogenic zones with ictal high-frequency neuromagnetic signals: case report. *J Neurosurg Pediatr.* (2010) 5:113–22. doi: 10.3171/2009.8.PEDS09345
167. Miao A, Xiang J, Tang L, Ge H, Liu H, Wu T, et al. Using ictal high-frequency oscillations (80–500 Hz) to localize seizure onset zones in childhood absence epilepsy: a MEG study. *Neurosci Lett.* (2014) 566:21–6. doi: 10.1016/j.neulet.2014.02.038
168. Miao A, Tang L, Xiang J, Guan Q, Ge H, Liu H, et al. Dynamic magnetic source imaging of absence seizure initialization and propagation: a magnetoencephalography study. *Epilepsy Res.* (2014) 108:468–80. doi: 10.1016/j.eplepsyres.2014.01.006
169. Tenney JR, Fujiwara H, Horn PS, Vannest J, Xiang J, Glauser TA, et al. Low- and high-frequency oscillations reveal distinct absence seizure networks. *Ann Neurol.* (2014) 76:558–67. doi: 10.1002/ana.24231
170. Xiang J, Tenney JR, Korman AM, Leiken K, Rose DF, Harris E, et al. Quantification of interictal neuromagnetic activity in absence epilepsy with accumulated source imaging. *Brain Topogr.* (2015) 28:904–14. doi: 10.1007/s10548-014-0411-5
171. Nissen IA, van Klink NE, Zijlmans M, Stam CJ, Hillebrand A. Brain areas with epileptic high frequency oscillations are functionally isolated in MEG virtual electrode networks. *Clin Neurophysiol.* (2016) 127:2581–91. doi: 10.1016/j.clinph.2016.04.013
172. Tang L, Xiang J, Huang S, Miao A, Ge H, Liu H, et al. Neuromagnetic high-frequency oscillations correlate with seizure severity in absence epilepsy. *Clin Neurophysiol.* (2016) 127:1120–9. doi: 10.1016/j.clinph.2015.08.016
173. van Klink N, Hillebrand A, Zijlmans M. Identification of epileptic high frequency oscillations in the time domain by using MEG beamformer-based virtual sensors. *Clin Neurophysiol.* (2016) 127:197–208. doi: 10.1016/j.clinph.2015.06.008
174. van Klink N, van Rosmalen F, Nenonen J, Burnos S, Helle L, Taulu S, et al. Automatic detection and visualisation of MEG ripple scillations in epilepsy. *Neuroimage Clin.* (2017) 15:689–701. doi: 10.1016/j.nicl.2017.06.024
175. Velmurugan J, Nagarajan SS, Mariyappa N, Ravi SG, Thennarasu K, Mundlamuri RC, et al. Magnetoencephalographic imaging of ictal high-frequency oscillations (80-200 Hz) in pharmacologically resistant focal epilepsy. *Epilepsia* (2018) 59:190–202. doi: 10.1111/epi.13940
176. Hincapié AS, Kujala J, Mattout J, Pascarella A, Daligault S, Delpuech C, et al. The impact of MEG source reconstruction method on source-space connectivity estimation: a comparison between minimum-norm solution and beamforming. *Neuroimage* (2017) 156:29–42. doi: 10.1016/j.neuroimage.2017.04.038
177. Tadel F, Baillet S, Mosher JC, Pantazis D, Leahy RM. Brainstorm: a user-friendly application for MEG/EEG analysis. *Comput Intell Neurosci.* (2011) 2011:879716. doi: 10.1155/2011/879716
178. Oostenveld R, Fries P, Maris E, Schoffelen JM. FieldTrip: open source software for advanced analysis of MEG, EEG, and invasive electrophysiological data. *Comput Intell Neurosci.* (2011) 2011:156869. doi: 10.1155/2011/156869
179. Gramfort A, Luessi M, Larson E, Engemann DA, Strohmeier D, Brodbeck C, et al. MNE software for processing MEG and EEG data. *Neuroimage* (2014) 86:446–60. doi: 10.1016/j.neuroimage.2013.10.027
180. Leiken K, Xiang J, Zhang F, Shi J, Tang L, Liu H, et al. Magnetoencephalography detection of high-frequency oscillations in the developing brain. *Front Hum Neurosci.* (2014) 8:969. doi: 10.3389/fnhum.2014.00969
181. Xiang J, Luo Q, Kotecha R, Korman A, Zhang F, Luo H, et al. Accumulated source imaging of brain activity with both low and high-frequency neuromagnetic signals. *Front Neuroinform.* (2014) 8:57. doi: 10.3389/fninf.2014.00057
182. Van Veen BD, Van Drongelen W, Yuchtman M, Suzuki A. Localization of brain electrical activity via linearly constrained minimum variance spatial filtering. *IEEE Trans Biomed Eng.* (1997) 44:867–80. doi: 10.1109/10.623056
183. Baillet S, Mosher JC, Leahy RM. Electromagnetic brain mapping. *IEEE Signal Process Mag.* (2001) 18:14–30. doi: 10.1109/79.962275
184. Groß J, Kujala J, Hämäläinen M, Timmermann L, Schnitzler A, Salmelin R. Dynamic imaging of coherent sources: studying neural interactions in the human brain. *Proc Natl Acad Sci USA.* (2001) 98:694–9. doi: 10.1073/pnas.98.2.694
185. Darvas F, Pantazis D, Kucukaltun-Yildirim E, Leahy R. Mapping human brain function with MEG and EEG: methods and validation. *Neuroimage* (2004) 23:S289–99. doi: 10.1016/j.neuroimage.2004.07.014
186. Hadjipapas A, Hillebrand A, Holliday IE, Singh KD, Barnes GR. Assessing interactions of linear and nonlinear neuronal sources using MEG beamformers: a proof of concept. *Clin Neurophysiol.* (2005) 116:1300–13. doi: 10.1016/j.clinph.2005.01.014
187. Küçükaltun-Yildirim E, Pantazis D, Leahy R. Task-based comparison of inverse methods in magnetoencephalography. *IEEE Trans Biomed Eng.* (2006) 53:1783–93. doi: 10.1109/TBME.2006.873747
188. Lina JM, Chowdhury R, Lemay E, Kobayashi E, Grova C. Wavelet-based localization of oscillatory sources from magnetoencephalography data. *IEEE Trans Biomed Eng.* (2014) 61:2350–64. doi: 10.1109/TBME.2012.2189883
189. Cotic M, Zalay OC, Chinvarun Y, del Campo M, Carlen PL, Bardakjian BL. Mapping the coherence of ictal high frequency oscillations in

human extratemporal lobe epilepsy. *Epilepsia* (2015) 56:393–402. doi: 10.1111/epi.12918

190. Cotic M, Chinvarun Y, del Campo M, Carlen PL, Bardakjian BL. Spatial coherence profiles of ictal high-frequency oscillations correspond to those of interictal low-frequency oscillations in the ECoG of epileptic patients. *IEEE Trans Biomed Eng.* (2016) 63:76–85. doi: 10.1109/TBME.2014.2386791
191. Zweiphenning W, van't Klooster M, van Diessen E, van Klink N, Huiskamp G, Gebbink T, et al. High frequency oscillations and high frequency functional network characteristics in the intraoperative electrocorticogram in epilepsy. *Neuroimage Clin.* (2016) 12:928–39. doi: 10.1016/j.nicl.2016.09.014

Conflict of Interest Statement: The authors declare that the research was conducted in the absence of any commercial or financial relationships that could be construed as a potential conflict of interest.

frontiers in Neurology

REVIEW
published: 04 April 2019
doi: 10.3389/fneur.2019.00325

EEG Source Imaging: A Practical Review of the Analysis Steps

Christoph M. Michel[1,2]* *and Denis Brunet*[1,2]

[1] Department of Basic Neurosciences, University of Geneva, Geneva, Switzerland, [2] Center for Biomedical Imaging Lausanne-Geneva (CIBM), Geneva, Switzerland

The electroencephalogram (EEG) is one of the oldest technologies to measure neuronal activity of the human brain. It has its undisputed value in clinical diagnosis, particularly (but not exclusively) in the identification of epilepsy and sleep disorders and in the evaluation of dysfunctions in sensory transmission pathways. With the advancement of digital technologies, the analysis of EEG has moved from pure visual inspection of amplitude and frequency modulations over time to a comprehensive exploration of the temporal and spatial characteristics of the recorded signals. Today, EEG is accepted as a powerful tool to capture brain function with the unique advantage of measuring neuronal processes in the time frame in which these processes occur, namely in the sub-second range. However, it is generally stated that EEG suffers from a poor spatial resolution that makes it difficult to infer to the location of the brain areas generating the neuronal activity measured on the scalp. This statement has challenged a whole community of biomedical engineers to offer solutions to localize more precisely and more reliably the generators of the EEG activity. High-density EEG systems combined with precise information of the head anatomy and sophisticated source localization algorithms now exist that convert the EEG to a true neuroimaging modality. With these tools in hand and with the fact that EEG still remains versatile, inexpensive and portable, electrical neuroimaging has become a widely used technology to study the functions of the pathological and healthy human brain. However, several steps are needed to pass from the recording of the EEG to 3-dimensional images of neuronal activity. This review explains these different steps and illustrates them in a comprehensive analysis pipeline integrated in a stand-alone freely available academic software: Cartool. The information about how the different steps are performed in Cartool is only meant as a suggestion. Other EEG source imaging software may apply similar or different approaches to the different steps.

Keywords: EEG, pre-processing, source localization, head model, inverse model

OPEN ACCESS

Edited by:
Sandor Beniczky,
Aarhus University Hospital, Denmark

Reviewed by:
Bruno J. Weder,
University of Bern, Switzerland
Jurgis Strautmanis,
Riga Stradinš University, Latvia

***Correspondence:**
Christoph M. Michel
christoph.michel@unige.ch

Specialty section:
This article was submitted to Applied Neuroimaging, a section of the journal Frontiers in Neurology

Received: *05 January 2019*
Accepted: *15 March 2019*
Published: *04 April 2019*

Citation:
Michel CM and Brunet D (2019) EEG Source Imaging: A Practical Review of the Analysis Steps. Front. Neurol. 10:325. doi: 10.3389/fneur.2019.00325

INTRODUCTION

The electric potential differences between electrodes placed on distinct scalp positions is due to the propagation of current flow induced by synchronized post-synaptic potentials of pyramidal neurons in the head according to Poisson's equations (1). However, this propagation is not homogenous. The current flow is strongly attenuated by the skull due to its high resistivity. This attenuation has to be properly modeled when solving the so-called forward problem, i.e., determining the potential at each scalp electrode generated by a known source in the brain (2).

Since the thickness of the skull is not homogeneous across the head, it is highly recommended that the individual anatomical information derived from the MRI is used to determine the skull thickness and thus the local conductivity properties. Also, the shape of the head is not spherical and thus the distance of the electrodes to the center of the head is variable. The exact position of each electrode on the individual head should therefore be known. These properties (local skull thickness and 3D electrode position) are then incorporated in the lead field, which determines how the electric activity at a certain electrode is related to the activity of the different sources in the brain. The more precise and anatomically correct this lead field is determined, the more precise the source localization will be (3).

Once the proper head model has been built and the lead field is constructed, the second step consists in solving the inverse problem, i.e., determining the intracranial sources that generate a given EEG potential measurement on the scalp. This inverse problem is a fundamental challenge because a very large number of different source distributions can produce the same potential field on the scalp (4). Due to this non-uniqueness, a priori assumptions need to be incorporated (5). They can be purely mathematical or include neurophysiological, biophysical and anatomical knowledge about the distribution of neuronal activity in space and in time. It must be made very clear that no matter how sophisticated these assumptions and constraints are, the provided source solution remains an estimation that depends on how well-genuine sources conform to these assumptions (6). This holds for the EEG as well as for the MEG.

Localization of a limited number of equivalent dipoles is the most classical approach to solve the inverse problem (7). The a priori assumption in this solution is that only one or a few active areas in the brain generated the scalp potential field. Under this constraint, non-linear multidimensional optimization procedures allow to determine the dipole parameters that best explain the observed scalp potential measurements in a least-square sense (8, 9). The maximal number of dipoles that can be reliably localized depends on the number of scalp electrodes and is further limited by the non-linear complexity of the search algorithms with multiple sources (5). The number of dipoles can be increased by searching for the best solutions of dipoles with time-varying strength over a certain time period and by decoupling the linear and non-linear part of the estimation [BESA, (10), MUSIC, (11)]. It is important to be aware of the fact that if the number of dipoles is underestimated the source localization is biased by the missing dipoles. On the other hand, if too many dipoles are assumed, spurious sources will be introduced. Nevertheless, dipole source localization can produce reasonable results under some particular conditions (12), in particular in localizing the irritative zone in focal epilepsy (13–15) or the localization of primary sensory areas in evoked potentials, such as the sensorimotor cortex in surgical candidates (16). Dipole source localization is still widely used in the MEG community for these clinical applications (17).

Recent development in brain source imaging has offered more exciting options to localize brain sources from scalp EEG signals and have largely replaced the dipole source localization approach. These so-called distributed source localization methods do not make a priori assumption with respect to the number of dipoles. The most popular distributed source models currently used in the EEG community are modifications of a solution initially proposed by Hämäläinen and Ilmoniemi (18), called the Minimum Norm Solution (MN). The constraint introduced in this solution is that the current distribution over all solution points has minimum energy (minimizing the least-square error, i.e., the L2-norm) and that the forward solution of this distribution optimally explains the measured data. MN solutions are biased toward superficial sources because of their spatial vicinity to the sensors. Therefore, weighting parameters have been introduced to mitigate this bias, leading to the so-called weighted minimum norm (WMN) solutions (19–21). A variation of WMN is the low resolution electromagnetic tomography (LORETA) in which the norm of the second-order spatial derivative of the current source distribution is minimized to ensure spatial coherence and smoothness (22). This constraint has been justified by the physiological plausible assumption that activity in neighbored voxels are correlated. Another modification has been suggested by Grave de Peralta Menendez (23), called LAURA (Local AUtoRegressive Average). It incorporates the biophysical law that the strength of the source falls off with the inverse of the cubic distance for vector fields. LAURA integrates this law in terms of a local autoregressive average with coefficients depending on the distances between solution points. The general communality of all these linear inverse solutions is that they provide a distribution of the current density in the whole brain volume that is described as a 3D grid of discrete solution points. In each of these solution points, a current dipole with a certain orientation and strength is estimated. Usually, the space of these solution points is restricted to the gray matter (24). Several other linear and non-linear source localization algorithms have been described in the literature. This review focuses on the pre-processing steps that are needed for source localization and not on the characteristics of the different inverse solutions. For detailed discussions we refer to previous comprehensive review articles (3, 25–28).

In the following, we describe the different steps that are needed to get to these source localizations by illustrating them with the implementation in our freely available academic software package Cartool, a stand-alone program for the spatio-temporal analysis of EEG and evoked potentials (29), https://sites.google.com/site/cartoolcommunity/. The purpose of this concrete illustration is to explain in detail the points that are important to consider in each processing step and how they are implemented in Cartool. Several other powerful commercial or academic software packages for EEG source imaging exist that have implemented similar or alternative strategies. A comprehensive overview of different academic software applications can be found in a special issue of the Journal Computational Intelligence and Neuroscience (30), where programs such as BrainStorm (31), EEGLAB (32), FieldTrip (33), NUTMEG (34), SPM (35), and Cartool (29) are described. Widely used commercially available software packages for EEG/MEG source localization are BESA, Curry, GeoSource, and BrainVision Analyzer. **Table 1** gives a summary of some of the most often used software packages and the source localization methods that

TABLE 1 | Non-exhaustive list of academic and commercial software packages that offer EEG source localization tools.

Name	Website	Inverse models
ACADEMIC SOFTWARE PACKAGES		
Brainstorm	https://neuroimage.usc.edu/brainstorm	Dipole modeling, Beamformer, sLORETA, dSPM
Cartool	https://sites.google.com/site/cartoolcommunity/	Minimum Norm, LORETA, LAURA, Epifocus
EEGLab	https://sccn.ucsd.edu/eeglab/index.php	Dipole modeling
Fieldtrip	http://www.fieldtriptoolbox.org/	Dipole modeling, Beamformer, Minimum Norm
LORETA	http://www.uzh.ch/keyinst/loreta.htm	LORETA, sLORETA, eLORETA
MNE	https://martinos.org/mne/stable/index.html	MNE, dSPM, sLORETA, eLORETA
NUTMEG	https://www.nitrc.org/projects/nutmeg	Beamformer
SPM	https://www.fil.ion.ucl.ac.uk/spm/	dSMP
COMMERCIAL SOFTWARE PACKAGES		
BESA	http://www.besa.de/products/besa-research/besa-research-overview/	Dipole modeling, RAP-MUSIC, LORETA, sLORETA, LAURA, SSLOFO
brainvision analyzer	https://www.brainproducts.com/	LORETA
BrainVoyager	https://www.brainvoyager.com/	Beamformer, Minimum Norm, LORETA, LAURA
GeoSource	https://www.usa.philips.com/healthcare/solutions/neuro/neuro-research-applications	Minimum Norm, LORETA, sLORETA, LAURA
CURRY	https://compumedicsneuroscan.com/curry-source-reconstruction/	Dipole modeling, MUSIC, Beamformer, Minimum norm, sLORETA, eLORETA, SWARM

they implemented. Whatever software is used, it is crucial that the user is aware and informed about the implementation of the different processing steps. In view of recent efforts to setup best practice guidelines of reporting EEG/MEG studies (https://cobidasmeeg.wordpress.com/), having access to the information of how the steps are done in the different software packages and reporting this information in the publications is important to ensure reproducibility and replicability.

BASIC REQUIREMENTS

EEG Pre-processing

Raw EEG data are contaminated by artifacts from many non-physiological (power line, bad electrode contact, broken electrodes, etc.) and physiological (cardiac pulse, muscle activity, sweating, movement, etc.) sources. These artifacts have to be carefully identified and either removed or excluded from further analysis. This is a cumbersome work and should be done by visual inspection of the raw data by experienced electrophysiologists. However, with the increasing availability of public EEG databases and the desire to analyze large datasets, the need for and the usage of automatic artifact detection and removal software is on the rise. Blindly applying such programs is problematic, because the type of artifacts is manifold and can vary in different experimental conditions. It is therefore recommended that if automatic artifact detection and correction methods are used, they should still be followed up by visual inspection of the data (36). In the following we describe the pre-processing pipeline implemented in Cartool.

Temporal Filtering

Most studies first apply a temporal filter to the data in order to remove frequencies that are considered to be non-physiological and/or non-relevant for the study at hand. Since there is no consensus regarding the relevant frequency range and an increasing recognition of physiological relevance of frequencies below and above the conventional EEG frequencies [infraslow frequencies in resting state activity (37), high frequency oscillations in normal and pathological brains (38)], the range of the band-pass filter is driven by the study question. Resting-sate EEG is often filtered between 1–40 Hz, while evoked potential data usually considers broader frequency ranges (0.1–100 Hz). Filtering the data can have important effects on the time-courses and the phases of the data (39, 40), as well as on the localization of the waveforms' local extrema. This is of particular relevance in evoked potential studies, time-frequency analysis and connectivity measures. The exact characteristics of the filter that has been used should be described in the study report (36). In Cartool, we implemented a non-causal, Infinite Impulse Response (IIR) Butterworth filter of 2nd order, known for its optimally flat passband response, which limits the artificial introduction of new local maxima (41). Both Butterworth low- and high-pass filters have a−12 db/octave roll-off, and are computed linearly with forward and backward passes, which eliminates any phase shifts. This ensures that the local maxima will remain at their expected positions, irrespectively of their frequency content. In the specific case of Butterworth high-pass filtering, the D.C. value is explicitly removed beforehand, as very high baselines could cause IIR filters to become instable.

Down-Sampling

After filtering, it is often useful to down-sample the data as most of the frequencies higher than the low-pass cutting frequency should be gone. It can dramatically reduce the memory requirements for the subsequent processing, without losing any information. The Nyquist theorem would require down-sampling not lower than twice the highest remaining frequency. In practice, though, because the filters' cut-offs are never perfectly sharp, and in order to keep some additional time resolution, the final sampling frequency should be chosen to be about four

times the highest remaining frequency after low-pass filtering. In Cartool and for integer down-sampling ratios, down-sampling is done with a Cascaded Integrator-Comb (CIC) filter (42), which in practice is quite easy to compute in off-line applications. Other software packages, such as for example EEGLAB (32) apply antializing filters to reduce the sampling frequency.

Electrode Interpolation and ICA

In Cartool, data inspection is performed semi-automatically. The user scrolls through the data and the program detects and visualizes electrodes with amplitudes above a certain range. If the user decides that a given electrode is an outlier due to bad contact, this electrode is marked and ignored in the subsequent independent component analysis (ICA).

The ICA is used to detect and correct artifacts, particular eye movements, eye blinks and cardiac pulse artifacts (43). It is important that the time course of the ICA components that are considered to reflect one of these artifacts is inspected together with the raw EEG data and it is assured that they indeed spatially (topography) and temporally correlate with the appearance of these events. Once this is assured, the data are back-projected by excluding these components. At the time of publication, ICA is not fully implemented in Cartool. An often used software for artifact removal using ICA is EEGLAB (44).

After ICA correction, the bad electrodes detected in the first step are interpolated using a 3D or spherical spline algorithm (45). In order to do that, the 3-dimensional position of each electrode needs to be known (see section Determining the Solution Points in the Gray Matter.).

Spatial Filtering

The precursor of EEG source imaging is the scalp potential map (5). Therefore, visualizing and inspecting the quality of the topography of the maps is as important as the inspection of the waveforms. Even after interpolation of artifacted electrodes and removing irrelevant ICA components, transient events can corrupt a few electrodes for a short time period. They can be seen on the potential map displays as isolated "islands" within the local neighborhood. Such outlier electrodes will have dramatic effects on source localization as the steep gradients will lead to local maxima beneath the electrode [see Figure 4.7. in (46)].

Here we describe a spatial filter that we designed and implemented in Cartool. It is an instantaneous filter which removes local outliers by spatially smoothing the maps without losing its topographical characteristics.

The spatial filter is designed in the following way (see **Figure 1A**):

- For each electrode, the values of the 6 closest neighbors are determined, plus the central electrode value itself.
- The 7 data points are sorted.
- The minimal and maximal values are removed by dropping the first and last items of this list.
- The remaining 5 values are then averaged, with weights proportional to the inverse distance to the central electrode. The central electrode is given a weight of 1.

This is very similar to an Interquartile Mean (IQM), but cutting the Cumulated Density Function into 7 intervals instead of 4, so we technically have an Inter Septile Weighted Mean. For each electrode e:

$$SpatialFilter(e) = \left(\sum_{i=1}^{i=5} \frac{v_i}{d_i}\right) / \left(\sum_{i=1}^{i=5} \frac{1}{d_i}\right) \quad (1)$$

With v_i being the 5 remaining voltage values from the 6 nearest neighbors of electrode e, plus the central value, each being at distance d_i. An example of the effect of the spatial filter on the waveforms (**Figures 1B,C**), but more importantly on the topography, can be seen in **Figures 1D,E**.

Detecting Bad Epochs

Hopefully, at this stage the EEG data is clean enough for further processing. Still, transient artifacts may remain (muscle artifacts, sweating, remaining eye blinks, etc.) that none of the steps above successfully removed. It is therefore strongly recommended that the "cleaned" data are visually inspected and that bad epochs are marked. In Cartool, we have implemented a tool that helps to identify these bad epochs. It is based on a set of simple statistics on the tracks and then estimates how much each track deviates from its own individual baseline. The statistics is based on instantaneous values (absolute value, variance, skewness and kurtosis among electrodes at a given time point) and on short time periods by computing the cross-convolution, which is a convenient way to estimate the noise in a signal. All these outlier estimators are merged together to a single compound estimator and the highly suspicious time periods are highlighted. By visual inspection, the user can then decide whether these periods should be marked as "bad" or not. These bad epochs will be conveniently used in later processing, as many toolboxes of Cartool allow to skip them.

CONSTRUCTING THE HEAD MODEL

The head model is the model for which the EEG forward solution is calculated. The forward solution determines how much a given electrical source in the brain will impact each electrode on the scalp. It provides the lead field matrix from which the inverse problem will be solved. It is strongly recommended to use the individual MRI of the participant to construct the head model, particularly in clinical studies where the source localization is used to guide surgery as for example in epilepsy or in functional mapping of eloquent cortex. If this is not available, a template MRI can be used (for example the MNI brain), but the source localization will be less precise, as shown in Brodbeck et al. (47) in a large patient cohort. The MRI needs several pre-processing steps in order to get to a proper delineation of the gray matter in which the source activity is estimated, and to describe the different compartments of the head (skin, skull, CSF, brain) that have different conductivity parameters. Since the electric field that spreads from the sources to the scalp surface is attenuated by these compartments (particularly by the skull), a proper incorporation of the head shape and the conductivity parameters in the head model is essential for

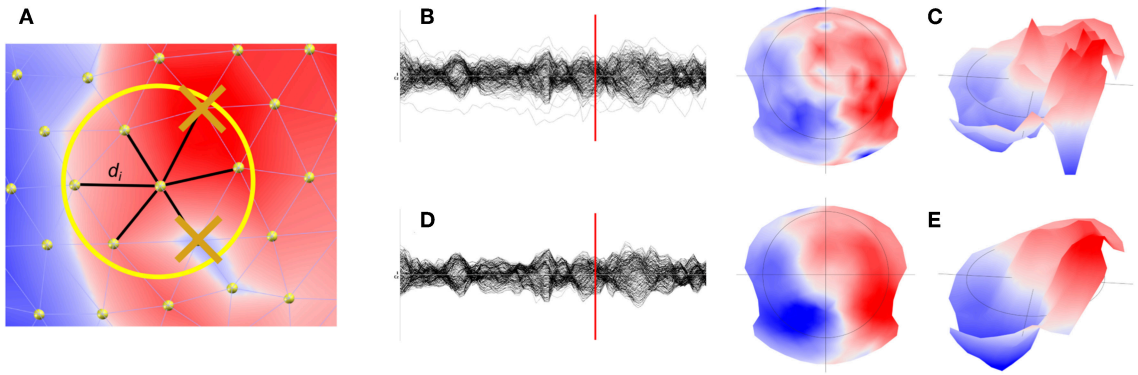

FIGURE 1 | Illustration of the spatial filter implemented in Cartool. **(A)** Determination and removal of the maximal and minimal value of the 6 nearest neighbor of a given electrode. **(B)** Illustration of the waveforms and the map **(C)** at a given time point before filtering. **(D)** Illustration of the effect of the spatial filter on the waveforms and maps **(E)**.

EEG source reconstruction. Once the MRI is pre-processed, the electrodes have to be positioned on the head corresponding to how they were positioned during the recordings. It is obvious that if the position of the electrodes does not correspond to the real position from which the signal was recorded during the experiment, the source localization will not be correct.

MRI Processing

The head model for EEG source imaging is based on the MRI. As mentioned above, whenever possible the individual MRI should be used. It gives information about the shape of the head, the thickness of the skull and the volume of the gray matter within which the solution points for the source localization are defined. Several processing steps are needed in order to properly extract this information. This includes re-sampling and re-orientation, skull stripping, Bias Field correction and separation of gray and white matter. These processing steps are fairly standard and offered in many different software packages, most well-known in the SPM toolbox (48). While Cartool allows to read MRI images and gray masks that have been processed by other software programs, it also has an integrated MRI processing toolbox. It takes particular care of points that are crucial for a proper layout of the solution points, such as assuring that no holes appear in the gray matter mask and that the sagittal plane is properly determined to assure symmetry of the left and right hemisphere. In the following, the way these processing steps are implemented in Cartool are described:

Re-sampling and Re-orientation

Depending on how the MR scanner performed the acquisition and how the participant lied in the scanner, re-sampling and re-orientation of the MRI is needed as a first step. In Cartool, the following geometrical transformations are all built into a 4 × 4 affine transform matrix, which stacks efficiently the successive steps described below, all of them being mathematically linear.

If the acquisition was anisotropic, as is often the case, voxel sizes are not equal in all three dimensions (**Figure 2A**). This is very detrimental for any further 3D processing, like filtering, and needs to be addressed as a very first step. In Cartool this is done by simply up-sampling the lowest resolution axes with some linear rescaling, to end up with the highest resolution in all 3 axes. Once the MRI is made isotropic, the axes have to be re-oriented in a standard way to improve readability and compatibility with other software. As a default, Cartool transforms the MRI to the Right-Anterior-Superior ("RAS") orientation for the three axes X, Y, Z (right-hand system) similar to the MNI template brain. This is done by appropriate 90 degrees rotations (**Figure 2B**).

Once the main axes have been set, adjustments are performed to further improve readability and comparison across subjects, or comparison with the MNI template. First, an optimal sagittal cutting plane is determined by adjusting 2 rotations values, on the Y and Z axes, and 1 translation value on the X axis, until the two halves defined by this plane are most symmetrical. This is of utter importance for the later stage when laying out the solution points in the brain, because it keeps an anatomically realistic balance between the left and right hemispheres. Once the optimal sagittal plane has been found, the best transverse plane is determined. This is highly recommended as the placement of the participant in the MR scanner varies. A tilted head is normalized in Cartool by adjusting 1 rotation value on the X axis, and 2 translation values in Y and Z. The optimal transverse adjustment is the one that gives a mid-sagittal plane that is most similar to the corresponding mid-sagittal plane of the MNI head. This is done by tilting the head and setting the origin above the anterior commissure. Note that these two steps partly solve the co-registration from a given head to the MNI template (**Figure 2C**). Only a final rescaling (3 parameters) is needed to achieve the ultimate 9 parameter co-registration. The last geometrical transform is to resample the MRI to reach the desired target voxel size, which is usually 1 mm^3.

All the steps above are then applied at once on the original MRI, through a 4 × 4 affine transform matrix. Interpolation between the voxels is done with a Lanczos filter, with kernel of size 3, which considers a neighborhood of 216 voxels for each value to be interpolated. The target MRI size is optionally

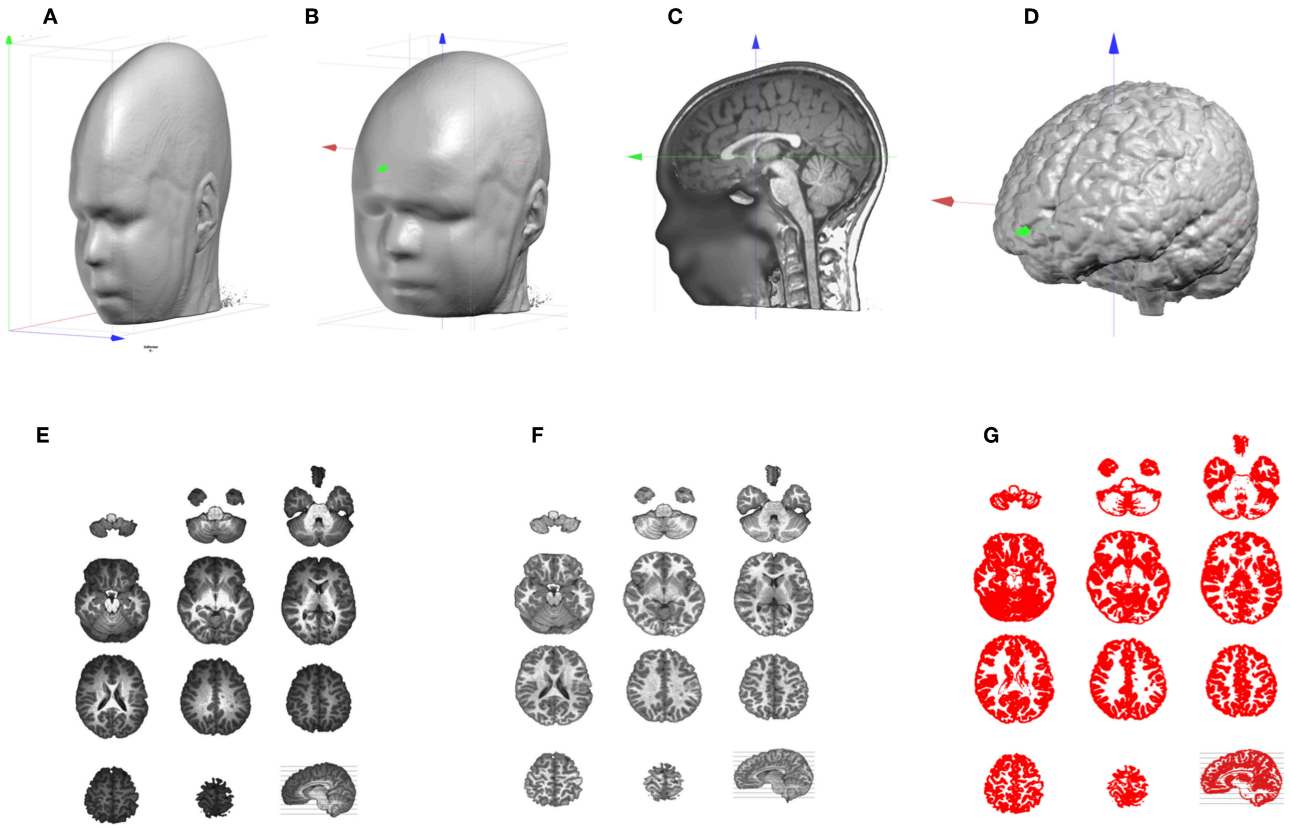

FIGURE 2 | Illustration of the MRI processing pipeline. **(A)** Original anisotropic MRI. **(B)** Result of up-sampling and re-orientation, with red, green, and blue axis pointing, respectively to X, Y, Z. **(C)** Adjustment of the cutting planes and setting of the AC origin. **(D)** Result of the skull-stripping to isolate the brain. **(E)** Brain slices which exhibit the Bias Field of the original MRI. **(F)** Same brain slices post-Bias Field Correction. **(G)** Extraction of the Gray matter.

optimized to include only the transformed head, plus some margin, and drop any useless empty spaces.

Skull-Stripping and Bias Field Correction

At this point, we should have a standardized individual head. The next step in the pipeline is the skull-stripping to separate skull, CSF and brain (**Figure 2D**). Two methods are available in Cartool, one mainly based on morphological operators, the other one on region growing. Both methods were designed for T1 MRIs, but appear to be resilient enough to work on T2 or MP-RAGE images.

MRI scans usually have inhomogeneities in space, called Bias Field. Without correcting for it, a given brain tissue like the gray matter will have different values depending on its physical position in the scanner (**Figure 2E**). This is definitely a non-desired property which will hamper the segmentation of the brain into its constituent tissues. Cartool corrects for the Bias Field of the segmented brain by iteratively equalizing the histogram of the white matter across all 3D directions. Since the white matter has the highest intensity values, it is a good marker for inhomogeneities. Any variations across a given axis are attributed to the Bias Field and are corrected (**Figure 2F**). By repeating this process across all directions, a global approximation of the Bias Field is determined. The validity of this method is reassured by the final histogram of the brain, which shows very clear-cut tissue separation.

Gray Matter Segmentation

The final step of the MRI processing is the separation of white and gray matter. This is needed because EEG source localization usually restricts the source space to the gray matter that contains the synapses where postsynaptic potentials can be generated. Cartool extracts the gray mask by estimating the global intensity distributions of the gray and white matter and the CSF with a Mixture of Gaussians. It classifies each voxel by weighting the Gaussian probabilities, based solely on the voxel intensity, with some neighborhood likelihood (for a given voxel, the greyer the neighbors, the higher the chance to be gray, too). Finally, morphological smoothing operators are applied to fill any possible holes in the gray mask. Note that the produced gray mask is therefore slightly thicker than the actual gray matter, which can be quite thin in some brain areas. The smoothing assures that no gray matter parts are missed (**Figure 2G**).

Determining the Solution Points in the Gray Matter

The volume that has been obtained through the gray matter extraction is called the solution space, and constitutes the volume

in which the electric activity will be allowed to be localized. The solutions space will typically contain 3000–6000 individual solution points and is thus basically a down-sampled version of the gray mask. Because of the Nyquist theorem, down-sampling should be done with some prior smoothing to prevent aliasing effects. Otherwise, this would result in missing solution points or discontinuities in areas where the spatial frequency is higher than the down-sampled spatial frequency.

In Cartool, finding the optimal solution point distribution is done in the following way, given a number of solution points to attain:

1) An initial down-sampling factor is estimated.
2) The gray mask is down-sampled by the current factor, while remaining centered on the optimal center. This keeps the left and right parts as symmetrical as possible.
3) Solution points with <8 neighbors out of a neighborhood of 26 are removed, repeatedly for 3 times.
4) The remaining solution points are counted.
5) If the count is close enough to the requested amount of solution points, the process is stopped. Otherwise, the down-sampling factor is up- or down- regulated according to the current numbers, and the process is repeated.

The solution point extraction is an important step of source localization, very often overlooked, if not totally ignored in the literature. Here are some points that have to be considered:

1) Left-right distribution
   As described above, the MRI has to be realigned to the mid-sagittal plane. That means that the geometrical center of the MRI is going through the YZ plane that cuts the brain in two optimally symmetrical parts. When down-sampling the gray matter into the solution points, the new down-sampled center has to remain in this plane. This will ensure that the resulting solution points will be equally distributed between the left and right hemisphere. Having an asymmetrical distribution of solution points will have an impact on the source localization by giving more weights to one side of the brain and attributing sources to the wrong side. Obviously, a real asymmetrical (pathological) brain will have its mid-sagittal plane set according to its anatomy, and will have an asymmetrical distribution of solution points.
2) Minimum neighborhood
   The inverse process will later need the computation of a discrete Laplacian in the Solution Space. To be able to do that correctly, each solution point has to have enough neighbors. In Cartool, a quite conservative minimum of at least 8 neighbors out of 26 is chosen. Solution points that have less neighbors will be removed.
3) Continuity
   The solution points should cover the whole gray matter without missing points on the thinner parts. It is obvious that source activity cannot be reconstructed on non-existent solution points, leading to a lack of precision for some brain areas. Another risk of missing solution points in some gray matter parts is that neuronal activity coming from this area would be attributed to the solution points closest to the missing part. In order to avoid such effects, Cartool smoothens the gray matter mask as described above to assure continuity of the solution points (**Figure 3**). This is a desired property and not a defect.
4) Number of Solution Points
   The number of solution points is defined by the user, with a recommended range between 3000 and 6000. There are obvious pros and cons for both low and high number of solution points (**Table 2**).

While computer speed is nowadays only a marginal problem, memory limitations can still be an issue. Numerical precision issues come from the fact that inverting large matrices will cumulate more errors than smaller ones. The spatial resolution (grid spacing) and accuracy (to be spot-on) is a sensitive problem. More points mean more spatial resolution because of smaller grid spacing. This increases accuracy but only up to a limit. Accuracy will stop improving after a given number of solution points (i.e., the inverse solution is not "getting better") due to the fact that the quantity of information that is put into the system remains the same, and is set by the number of electrodes. Also, the matrix inversion process can intrinsically provide only a limited level of accuracy.

NUMBER AND POSITIONING OF THE ELECTRODES

Electrode Layout

What is the minimal number of electrodes needed for reliable source localization? This question is often asked, particularly from the clinical community that intends to apply EEG source localization to the EEG that is routinely recorded with the standard 10-20 system, i.e., with only 19 electrodes. Several studies have demonstrated that this low number not only leads to blurring of the solution, but also to incorrect localization (49) compared the effective spatial resolution of different electrode montages (19-129 electrodes) and concluded that "the smallest topographic feature that can be resolved accurately by a 32-channel array is 7 cm in diameter, or about the size of a lobe of the brain". Simulation studies as well as subsampling studies in epileptic patients with known epileptic focus clearly showed that electrode arrays with <32 sensors lead to severe mislocalizations and blurring (3, 28). The significant increase in localization precision has been demonstrated by Brodbeck et al. (47) in a large

TABLE 2 | Pros and Cons of the number of solution points in the inverse space.

Lower number of solution points	Higher number of solution points
(+) Faster to compute the matrices	(–) Longer to compute the matrices
(+) Less memory	(–) More memory
(+) Less numerical precision issues	(–) More numerical precision issues
(+) Smaller matrices and faster display	(–) Larger matrices and slower display
(–) Less spatial resolution	(+) More spatial resolution
(–) Less spatial accuracy	(+) Somewhat more spatial accuracy
(–) Less neighbors around each solution point	(+) More neighbors around each solution point

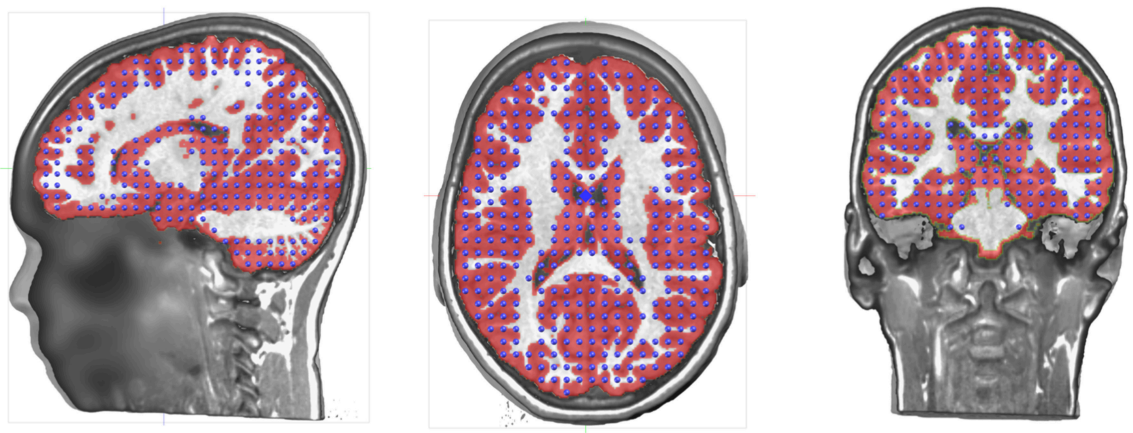

FIGURE 3 | Illustration of the distribution of the solution points in the gray matter.

group of epileptic patients where sensitivity and specificity were compared between high-density (128–256 channels) and routine clinical (19–21 channel) EEG. In a cohort of patients with focal ischemic stroke, (50) demonstrated that more than 64 electrodes were needed to avoid mislocalizations of the affected regions. Recent studies showed that the detection and localization of high frequency oscillations, which are potential markers of epileptic areas, are better detected and localized with high- as compared to low-density EEG (51, 52). Also, localization of seizure onset zone using connectivity analysis in the source space was shown to be more precise with high- compared to low-density EEG (53). The fact that the skull resistance is much lower than previously assumed (see section The LSMAC Head Model), additionally supported the notion that high-density EEG is needed to avoid spatial aliasing, that then leads to mislocalization (54, 55). As the skull is much thinner in babies, even more electrodes are needed in this population (56, 57).

Nevertheless, these results do not necessarily mean that imperfect spatial sampling precludes source localization. Even with <32 electrodes, source localization allows to gain valuable insight about the underlying sources, particularly in applications with well-defined focal activity such as epileptic spikes (15, 58–60).

Besides the number of electrodes, their positioning in terms of coverage of the head plays an important role too. The standard 10–20 system does not include electrodes over the inferior part of the head which disfavors the proper recording of activities in the inferior-basal and anterior part of the temporal lobe where activity originating or propagating from the mesial temporal structures is maximal (61, 62) (**Figure 4B**). Missing these electrodes can lead to mislocalization of activities originating from the mesial temporal lobe (60, 63). It has therefore been recommended that at least 3 inferior electrodes on each side should be added to the standard 10–20 system in clinical routine (64).

3D Electrode Positions

The correct positioning of the electrodes on the surface of the head of the participant's MRI is an important point. Ultimately, the position should correspond to the reality, i.e., to the actual position of the electrodes during the recording, as this has a direct impact on the stability of the source localization.

There are different levels of knowledge of the electrode positions during the recordings. Nowadays, EEG caps or nets are usually used, with the advantage of fixed spacing between electrodes. Many studies rely on these fixed positions determined by the manufacturer and the names of the electrode according to the 10-10 coordinate system. A template 3D-array (often provided by the manufacturer) is then used and it is assumed that the EEG cap is placed and adjusted according to some fixed points (Inion, Nasion, preauricular points, Vertex, etc.). It is crucial that this placement is done correctly and it is recommended that photographs are taken to later assure correspondence of the electrodes to these fixed points when landing the electrode array on the MRI head. A more advanced and recommended method, if available, is to measure the actual position of each electrode for each participant using a 3D digitizer or a photogrammetry system (65). The obviously most accurate method is to put the participant in the scanner with the cap on the head and afterwards mark the artifacts induced by the electrodes on the MR images (**Figure 4A**). This last method bypasses the co-registration procedure described below. However, as it requires an MRI scanner close to the EEG recording room and MRI-compatible EEG caps, this method is rarely possible, except in simultaneous EEG-fMRI studies.

Co-registration of the Electrodes on the MRI Head

In Cartool, the co-registration of the 3D electrode array is done interactively by displaying and manually adjusting the global 3D shape of the electrode array to the shape of the head. This is a way to make use of all the available geometrical information, instead of relying only on a few fiducial positions. The method can adapt to all cases and allows to co-register either an individual or a template electrode array to either an individual or a template MRI head.

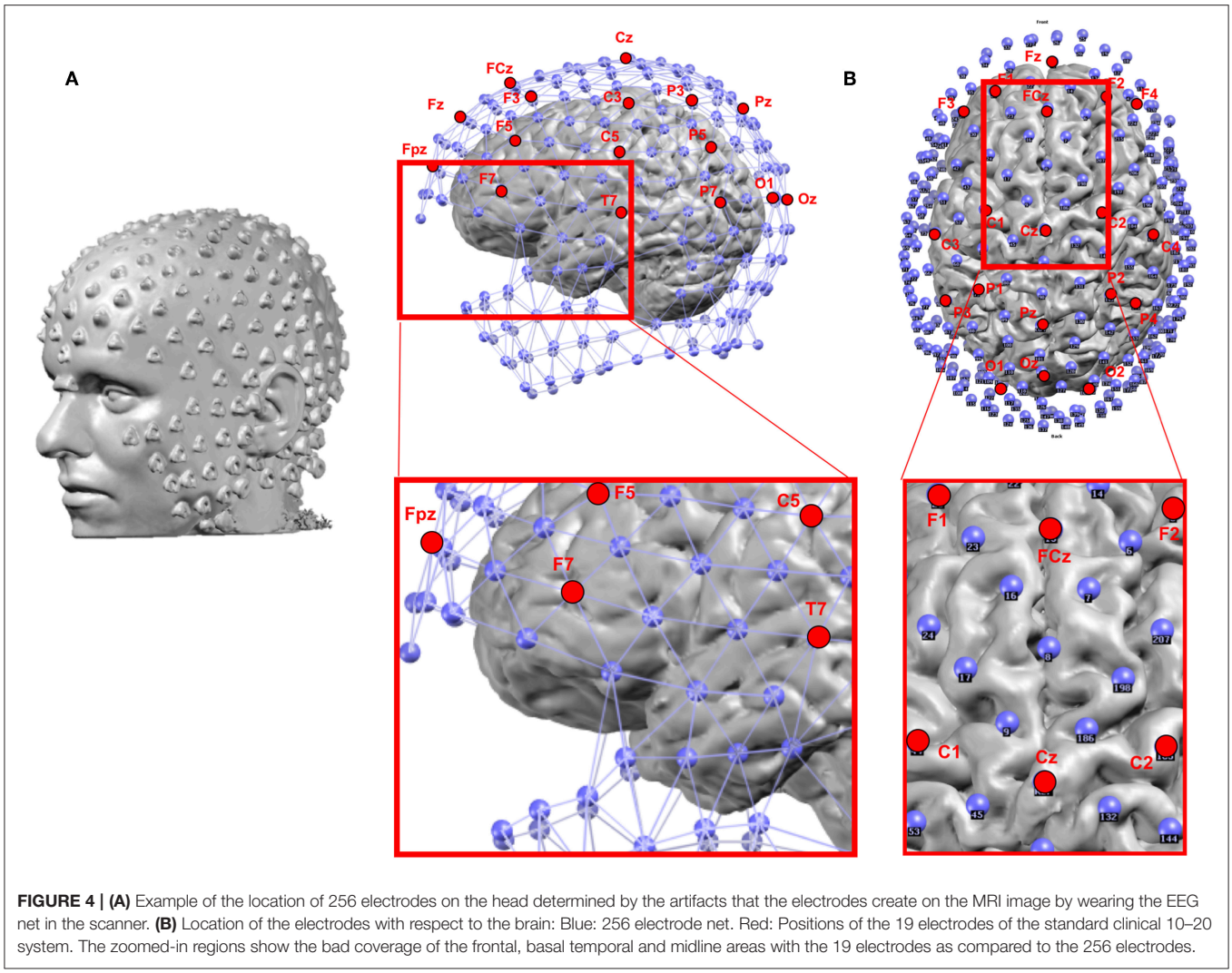

FIGURE 4 | (A) Example of the location of 256 electrodes on the head determined by the artifacts that the electrodes create on the MRI image by wearing the EEG net in the scanner. **(B)** Location of the electrodes with respect to the brain: Blue: 256 electrode net. Red: Positions of the 19 electrodes of the standard clinical 10–20 system. The zoomed-in regions show the bad coverage of the frontal, basal temporal and midline areas with the 19 electrodes as compared to the 256 electrodes.

In detail, the following steps are performed interactively: Both the processed (resampled and reoriented) MRI and the electrode array are displayed on the screen. The operator then virtually adjusts the electrode array on the MRI head, mimicking the way the physical electrodes were set on the subject's head. This is done by shifting the electrode positions in any direction, rotating and stretching them until they convincingly look like the reality. Photographs taken during the recording can help to properly adjust the positions.

Once this adjustment is done, Cartool provides a last useful feature: virtually "gluing" the electrodes on the head. For many reasons, like a template electrode array being used on a real MRI head, and no matter how much care is devoted to the previous steps, many electrodes can end up either being below or above the scalp surface. This in turns will be detrimental to the Lead Field computation by biasing the distances from any given electrode to the brain. By activating this virtual gluing, all electrodes will be perfectly projected perpendicularly on the nearest position on the scalp (**Figure 5**).

CALCULATING THE LEAD FIELD

In order to calculate the lead field, a head model has to be created that incorporates as realistically as possible the shape of the head and the conductivity parameters of the different tissues between the current sources in the brain and the potential on the scalp. There have been substantial advancements in the construction of realistic head models. Still, even the most sophisticated methods are simplified descriptions of the complex organization of head tissues. The often-used realistic models are the Boundary Element Model (BEM) and the Finite Element Model (FEM). Their superiority compared to 3-shell spherical head models has been demonstrated in simulations (66–68) as well as real data (69, 70). The downside of these sophisticated head models is an increased computational load because numerical solutions have to be applied. They are also more sensitive to any mishap happening during the brain and gray matter extraction, as more brain tissues and more parameters are involved. In Cartool, we implemented a method that we called Locally Spherical Model with Anatomical Constraints (LSMAC, see below). It tries to

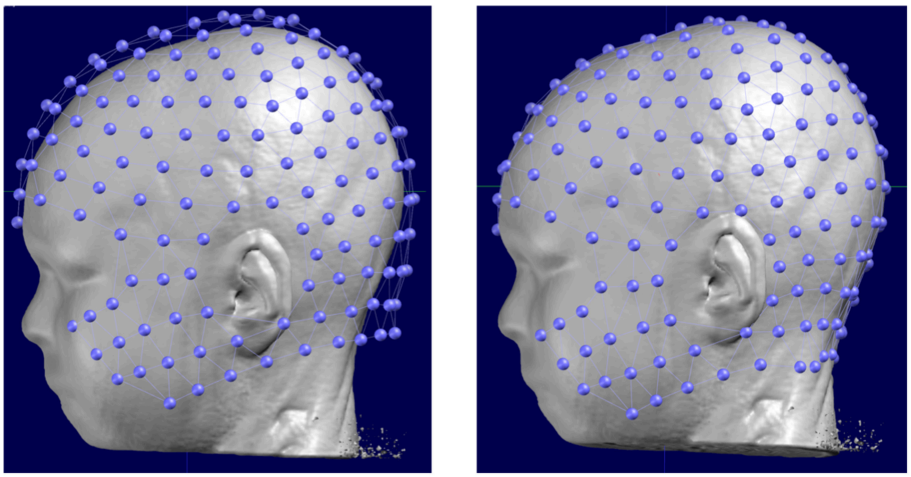

FIGURE 5 | Original position of a template electrode layout with respect to the head of the subject (left) and the corrected positions after manual rotation and translation and the final automatic "gluing" on the scalp.

counteract the computational cost of the BEM and FEM models by using analytical equations while still keeping the realistic aspect of the head geometry and the local variability of the thickness of the skull. Birot et al. (71) compared the LSMAC model with a BEM and a FEM model in a dataset of 38 epileptic patients in whom high-density scalp EEG, intracranial EEG and localization of the resection brain area that rendered the patient seizure-free was available. LSMAC, BEM and FEM were computed from the individual MRI of the patients and source localization was performed on averaged interictal epileptic discharges. Similar source location accuracy with respect to the intracranial recordings and the resected zone was found for all three head models. It was concluded that in such clinical applications, the use of highly sophisticated and difficult to implement head models is not a crucial factor for accurate source localization.

The LSMAC Head Model

The Locally Spherical Model with Anatomical Constraints (LSMAC) (29) is an adaptation of the SMAC head model introduced by Spinelli et al. (24). The LSMAC Lead Field calculation requires the pre-processed full head and the gray mask MRIs, the co-registered electrodes and the location of the solution points. Under each electrode, the inner and outer borders of the skull are then automatically determined and the global resistivity value is locally corrected. This decreases the sources of error in EEG inverse modeling. The borders of the skull are determined by analyzing the gray levels of a radial line, going from the center of the brain to the electrode on the scalp. Since the skull is barely visible in T1 MRI scans, it shows up as dark voxels in contrast to the scalp and the brain. Consequently, the beginning and end of the skull can be identified as borders between light and dark voxels on the line. By measuring these borders repeatedly with slight offsets on the scalp, uncertainty pertaining to noise, low voxel intensities and bone structure variability is adjusted. **Figure 6** shows an example of the skull radii estimation on 3 electrodes.

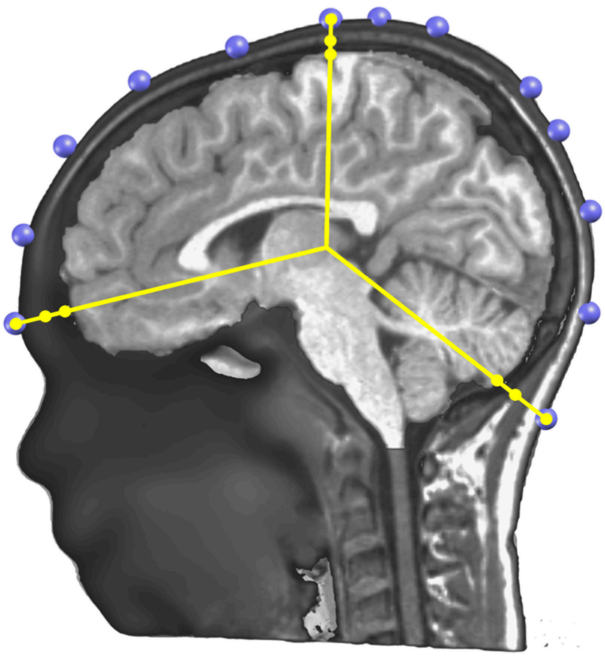

FIGURE 6 | Illustration of the determination of the skull thickness under each electrode. A sagittal cutting plane is shown with the electrodes (in blue) located on the scalp surface, the radius lines (in yellow) extending from the center to each electrode, and on each line three dots showing where the skull and scalp limits are determined.

These skull radii estimate still has some uncertainty due to the nature of the MRI T1 images. To further increase their precision, Cartool requests the user to provide a target age of the subject. Using thickness values described in the literature for different age ranges (72, 73) and linear interpolation of missing

values, a curve of the estimated mean thickness for each age was built (**Figure 7A**). The radii determined from the MRI are then globally rescaled to reach the estimated mean thickness for the given age. This adjustment allows a better estimation of the Lead Field in children, or in the difficult case of newborns. A second advantage of this adjustment is to allow the computation of a Lead Field for any specific age from a fixed template, if the individual MRI was not available.

The skull resistivity has been shown to be much lower than previous literature suggested. The resistivity ratio between the brain and the skull is around 1:10 to 1:30 (74–76), rather than 1:80, as previously assumed (77). Also, the skull resistivity increases with age. Cartool thus has a second built-in curve that gives the relative conductivity of the skull compared to the adjacent tissue (brain, CSF, scalp) as a function of age. The curve is based on a few reported resistivity measures of living tissue (78, 79). According to these reports, the conductivity ratio varied between 1:9.80 (11 years old) to 1:25 (50 years old). An additional estimated value of 1:50 for 100 years old was added to be able to extrapolate the curve past 50 years old, basically following the decreasing trend. When the age of the subject is entered in Cartool, the conductivity value is adapted to this age according to the curve shown in **Figure 7B**.

CALCULATING THE INVERSE SOLUTION

The inverse problem has no unique solution and a priori assumptions have to be incorporated to derive to a unique assumption of the distribution of neuronal activity in the brain that lead to a certain potential field on the scalp. As explained in the Introduction, a number of solutions of the inverse problem have been proposed, incorporating different constraints based on a priori information about the desired source characteristics or on physiological assumptions [for comprehensive reviews see (3, 25–28)]. In Cartool, we implemented three linear distributed source models: the weighted minimum norm solution (21) the low resolution electromagnetic tomography [LORETA; (22)], and the Local AUtoRegressive Average [LAURA; (23)], all being modifications of the minimum norm (NM) solution (18). We validated these implementations in several experimental and clinical studies by comparing them with intracranial recordings, electrocortical stimulation, fMRI, and clinical outcome after surgery [e.g., (47, 80–84)].

Regularization Optimization

Tikhonov regularization is typically used in the case of under-determined system of equations, such as when inverting the Lead Field. Simply put, it factors in the equations a level of EEG noise, and enforces a level of smoothness in the inverted results. The more regularization, the smoother the results and the less the sensitivity to noise. However, too much regularization, by over-smoothing the results, will degrade the accuracy of the localization. We wish to use the most precise amount of regularization despite the fact that the amount of noise is not known in advance, and will vary from case to case. To handle all cases, Cartool computes 13 matrices with increasing regularization factors from 0 (none) to 12 (for very noisy data) times a constant $\propto$, which depends on the selected inverse model. The stack of 13 matrices is then saved into a single file. Later on, when applying an actual EEG to the inverse matrix, its noise level will be evaluated, and the optimal matrix will be chosen.

The general equation for the inverse problem with Tikhonov regularization can be written as:

$$J = W.K^t.(K.W.K^t + \propto_R .I)^+.\Phi \tag{2}$$

With J being the source density, Φ the electric field, K the Lead Field, W some specific inverse weighting factors and I the identity matrix.

The regularization factor $\propto_R$ is set the following way, for R varying from 0 to 12:

$$\begin{aligned} \propto_R &= R. \propto \\ \propto &= \frac{\max\left(\, Eigenvalues\left(K.W.K^t\right)\right)}{20000} \end{aligned} \tag{3}$$

The optimal regularization for a given EEG is defined as the L-corner of the norm of the solution points as a function of the regularization factor R. When Cartool applies the inverse matrix to the data, it automatically defines this L-corner over the whole dataset and uses this optimal regularization factor for all time points. Alternatively, the user can specify a certain regularization factor for each dataset.

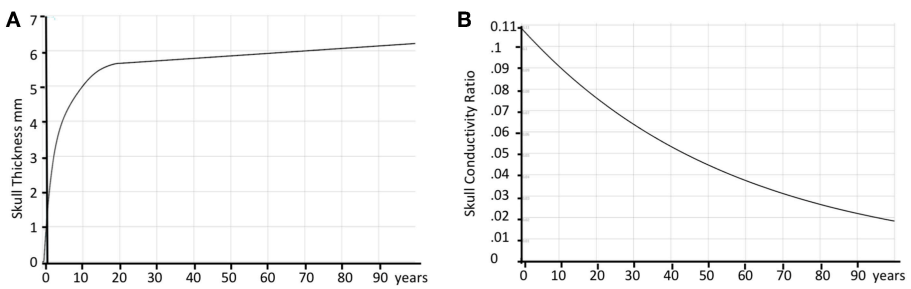

FIGURE 7 | Age correction of skull thickness and skull conductivity. **(A)** Estimated average skull thickness across age. **(B)** Estimated skull conductivity ratios across age.

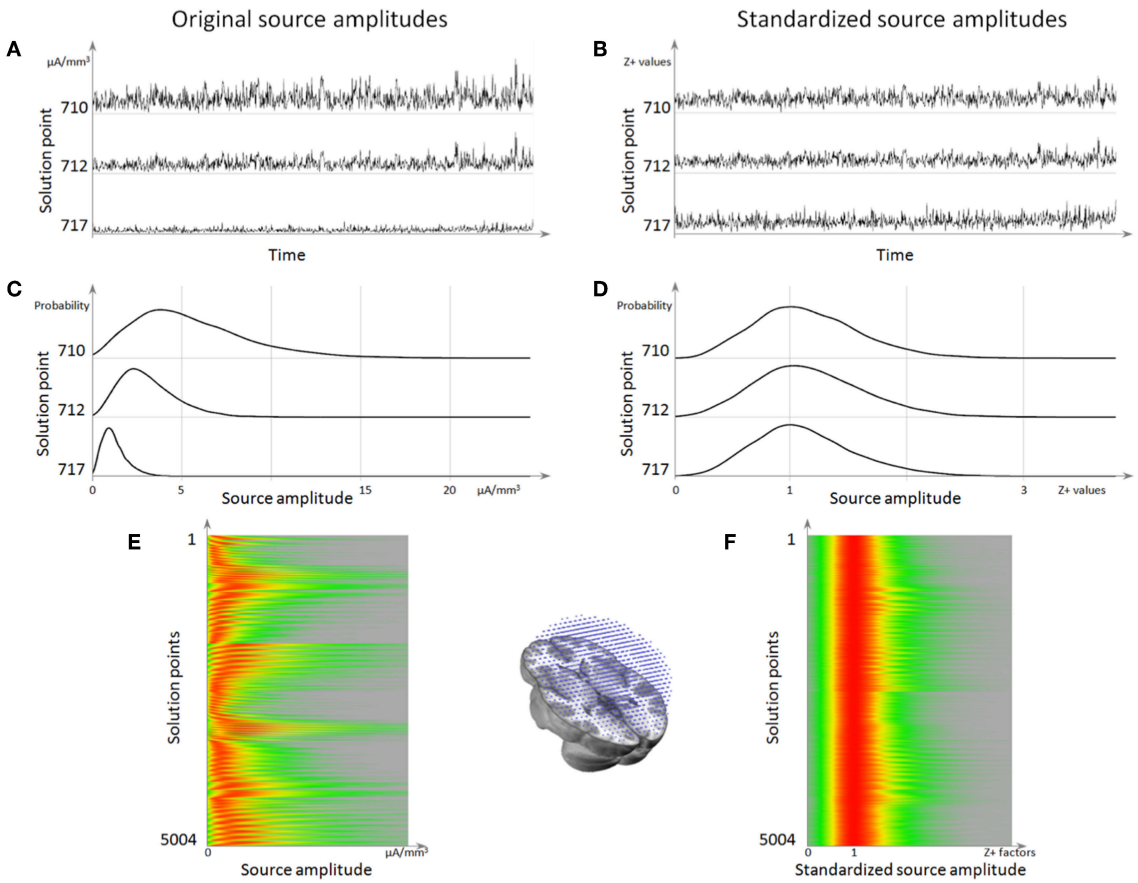

FIGURE 8 | Source localization normalization. **(A)** Time series of 3 solution points showing the difference in mean amplitude (norm) between them. **(B)** The same time series as in **(A)** but after normalization, showing that the 3 solution points now have the same amplitude range. **(C)** Histograms of these 3 solution points, showing that the background activity is the left-most mode of the distribution. **(D)** Histogram after normalization, showing that all the background activity has been centered to 1. **(E)** Histograms for all solution points (vertical axis), with the red color coding for the highest source amplitude probability. **(F)** Histogram of source amplitude probability for each solution point after normalization, showing that all solution points now have a background range from 0 to 1, while retaining their respective highest activities.

Normalization of the Inverse Solution Result

When inspecting the estimated current density at each solution point across time in ongoing (non-averaged) EEG it appears that substantial variability of power is observed across solution points. These variations are supposed to come from geometrical and mathematical approximations that are done during the different steps of the inverse matrix calculation. It is thus necessary to find a way to correct for this power variability, in order to reliably estimate the fluctuations of brain activity over time in individual subjects and to compare them between subjects. In Cartool, we implemented a normalization approach by using the background activity of the norm of the inverse solution over time to estimate a baseline and a scaling factor for each solution point. In order to have a robust estimation, a large enough time sample should be used, preferably the whole pre-processed and artifact-excluded data of a given subject. Still, the correction factors can be satisfactorily computed on as little as a thousand time points, as long as no solution point remains in the same stable state more than half of the sampled time, which might be problematic for example in averaged epileptic spikes or in evoked potentials restricted to the time period of sensory processing or motor responses. The normalization should therefore be applied to non-averaged raw data transformed to the source space. A recent study where this normalization method has been used on resting-state EEG to determine the sources of the EEG microstates in task-induced, self-initiated thoughts, showed that this method reveals brain networks that overlap with those derived by fMRI in the same subjects (85).

Here is a step-by-step description of this specialized normalization:

Given a 3D dipole (sp_x, sp_y, sp_z) at a given solution point sp, we define sp_χ as the squared value of its norm:

$$sp_\chi = {sp_x}^2 + {sp_y}^2 + {sp_z}^2 \quad (4)$$

The noisy part of the data therefore follows a Chi-square distribution of degree 3.

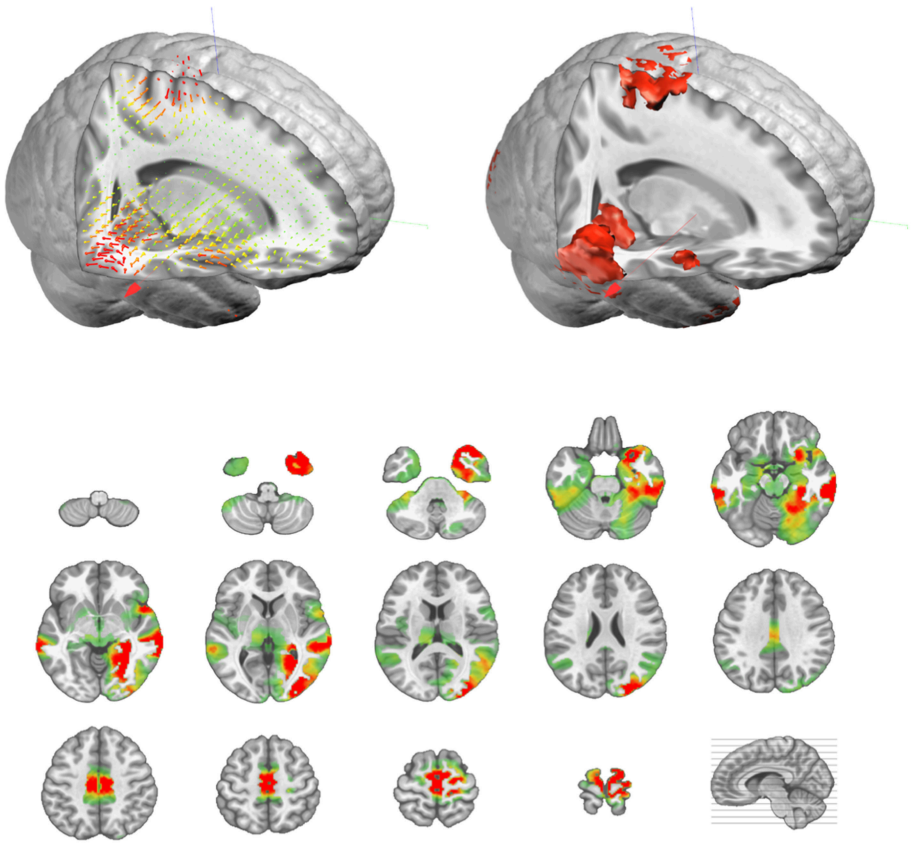

FIGURE 9 | Illustration of the actual vectorial results (top left, in 3D) of the distributed sources, and their corresponding amplitude values (top right, in 3D, and bottom as transverse slices).

The variable sp_χ can be approximated to a normally distributed variable sp_N by (86):

$$sp_N = {sp_\chi}^{0.2887} \tag{5}$$

Having now a normal distribution, sp_N can be standardized into sp_Z by using the regular z-transform:

$$sp_Z = \frac{\left(sp_N - \mu_{sp_N}\right)}{\sigma_{sp_N}} \tag{6}$$

However, the values of μ and σ used for the z-transform have to be calculated only on the noisy part of the data—the background activity from the Chi-square i.e., the lowest values of the probability density function. Hence μ is estimated from the left-most Mode of the sp_N distribution:

$$\mu_{sp_N} = \widehat{Mode_{left}}(sp_N) \tag{7}$$

For the same reason, σ is estimated from the Median of Absolute Deviation (MAD), centered on the previously estimated μ, and computed only with the values below μ:

$$\sigma_{sp_N} = \widehat{MAD_{left}}(sp_N) \tag{8}$$

Both the Mode and the MAD being computed on the left part of the probability density function is key here. In this way it ignores any activity above noise level that might be present in some brain areas while not in others. Rescaling using the actual activities would be incorrect, as it would basically transform them into the baseline. On the other hand, noise can be seen on all solution points and its level is a good estimator of the rescaling that has to be applied. Implementation-wise, these estimators are computed multiple times on random sub-samplings of the data, and the two respective medians of all these estimators are finally taken.

Finally, because we started with positive data (the norm of a dipole), we also wish to end up with positive data in order to avoid any confusion due to having signed results. We define sp_{Z+} as sp_Z shifted by 3 standard deviations to the right, then divided by 3 so that the background mode is finally aligned to 1.

$$sp_{Z+} = \max\left(\left(\mathrm{sp}_Z + 3\right)/3,\ 0\right) \tag{9}$$

After this standardization procedure, the power of the current density is comparable across all solution points, and its noisy component is normally distributed (**Figure 8**).

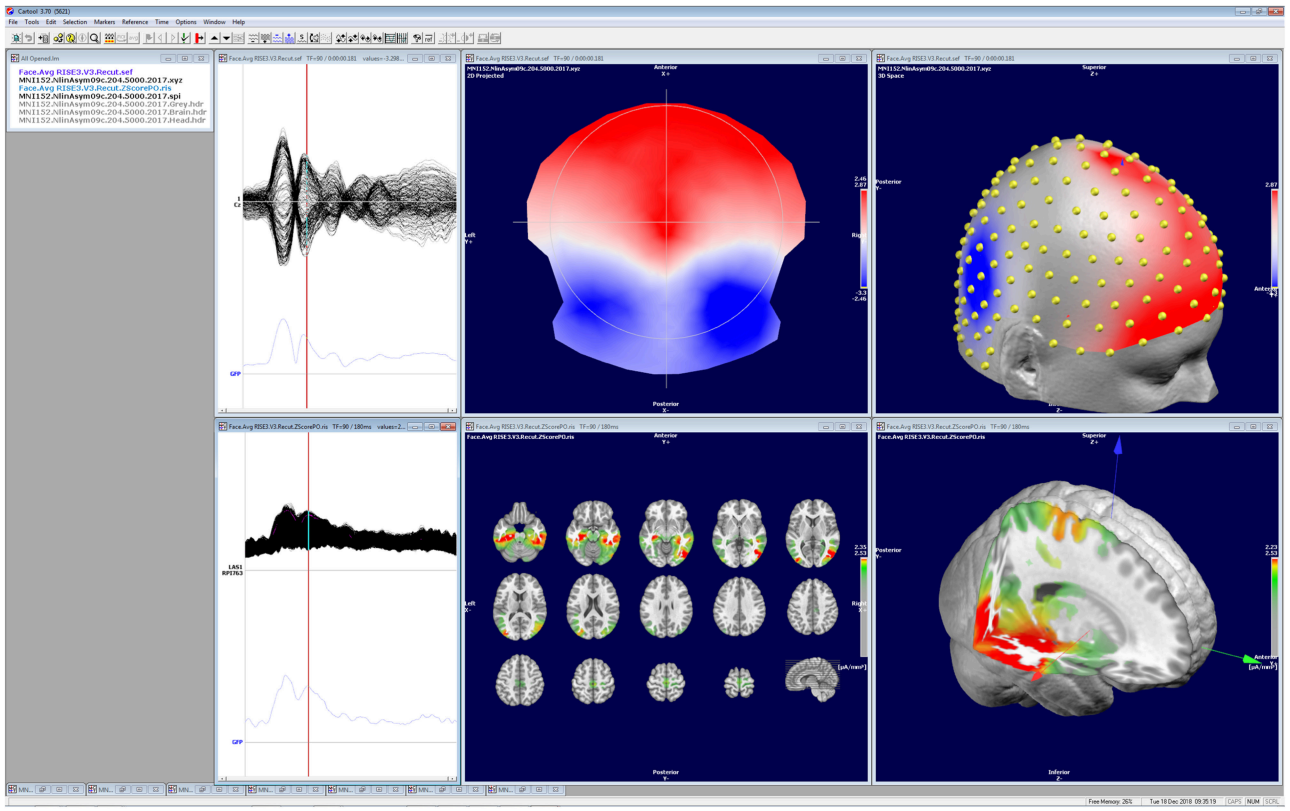

FIGURE 10 | Illustration of the visualization of the data and the results of the different analysis steps as implemented in Cartool. All windows can be independently manipulated in 3D. The screen shot shows a visual evoked potential (face presentation) recorded with 256 electrodes, the corresponding potential map at 188 ms post-stimulus and the estimated sources located in the mesial temporal lobes and the fusiform gyrus.

Results of Inverse Solution: Vectorial vs. Scalar

The output of the inverse matrix multiplication with the EEG results in equivalent dipoles located on each solution point. As each dipole is a 3D vector, it is described as an amplitude in the x-,y-, and z- directions. In most applications, this vectorial information is not relevant and only the norm (amplitude) of the dipoles is saved, i.e. scalar values. This results in positive values at each solution point as displayed in **Figure 9**.

APPLICATIONS OF EEG SOURCE LOCALIZATION

High-density EEG recordings have become standard in many experimental as well as clinical laboratories, given that most manufactures readily provide such systems and that the application of many electrodes has become fairly easy. It therefore does not come as a surprise that EEG source localization is increasingly used to infer to the areas in the brain that generated the activity observed on the scalp (87–89). Concerning clinical applications, the undoubtedly most intense use of EEG source localization is in epilepsy, with the intention to localize the epileptic zone in pharmaco-resistant focal epilepsies (3, 90). The added value of this method in the pre-surgical assessment of these patients has been demonstrated repeatedly, not only for focus localization, but also for localization of eloquent cortex (3, 47, 83, 91–93). Besides the clinical significance, EEG source localization in epilepsy also gives the unique possibility to evaluate the performance and precision of different head- and source-models because intracranial recordings or the outcome after surgery can serve as "gold-standard" (71, 82, 94, 95). The most direct way to evaluate EEG source localization is the simultaneous recording of scalp- and intracranial EEG. A recent study with high-density (256-channel) scalp EEG recorded simultaneously with intracranial local field potentials from deep brain structures in patients undergoing deep brain stimulation demonstrated that EEG source localization is able to sense and properly localize spontaneous Alpha activity generated in the thalamus or the nucleus accumbens (84). This demonstration opens new doors in the use of high-density EEG source imaging, as it shows that source localization is not restricted to the cortex only.

In experimental studies, EEG source imaging has become standard to localize different brain areas involved in sensory, motor, and cognitive functions, most often applied to event-related potentials (89, 96). However, EEG source imaging is also increasingly used to define large-scale network dynamics by applying connectivity measures (97–99). Because of the high

temporal resolution of EEG, functional connectivity measures such as Granger Causality methods are used to study directional connectivity of large-scale networks in the healthy (100–102) and in the pathological (103, 104) brain. It has thereby become clear that such connectivity measures have to be applied in source space and not on the level of the scalp electrodes, since volume conduction and reference-dependency make the interpretability of sensor-based connectivity measures difficult (105–110). Therefore, EEG source imaging is a pre-requisite for functional connectivity analysis [for a recent tutorial paper on EEG connectivity measures see (111)]. It is thus of utmost importance that the source localization is done properly and that the steps described in this review paper are understood and correctly applied.

CONCLUSIONS

This review describes in detail the different steps that are needed to derive from a multichannel scalp EEG recording to the estimation of the distribution of the underlying neuronal sources. It explains the logic underlying each step and the requirements that need to be fulfilled to perform them. It illustrates how these steps are implemented in one particular stand-alone software: Cartool. While this might occasionally give the impression of a software manual rather than a review paper, we do not intend to claim that this software is the only one that allows to perform these steps adequately. Several other stand-alone or open-source software packages exist, commercially or freely available, that have implemented these analysis steps in similar or slightly different ways (30); **Table 1**. We here use the example of Cartool to illustrate the implementation and the usage and to provide a reference for those who use Cartool. In view of the increasing practice of source localization in EEG and MEG applications, it is important that the user well-understands how the software that he/she is using implement the different steps. We also consider it of crucial importance that the data and the results of the analysis are visualized and that the user inspects the data carefully in all different steps and assures that the results make sense (**Figure 10**).

This review also intends to make the user aware of the obstacles and limitations of each step of the analysis and the choices that have to be made. Basic knowledge of the underlying reasons for these choices and how it is implemented in a given software is mandatory to avoid misinterpretation of the results and to properly describe the methods in a publication. Finally, we hope that this review contributes to the global awareness that EEG source imaging is feasible and doable even for non-engineers and provides information about the function of the human brain that cannot be achieved by analysis restricted to the scalp level.

AUTHOR CONTRIBUTIONS

All authors listed have made a substantial, direct and intellectual contribution to the work, and approved it for publication.

FUNDING

This work is supported by the Swiss National Science Foundation (No. 320030_159705) and the Swiss National Center of Competence in Research; Synapsy: the Synaptic Basis of Mental Diseases (NCCR Synapsy Grant # 51NF40-185897).

REFERENCES

1. Helmholtz HLP. Ueber einige gesetze der vertheilung elektrischer ströme in körperlichen leitern mit anwendung aud die thierisch-elektrischen versuche. *Ann Physik und Chemie*. (1853) 9:211–33.
2. Malmivuo J, Plonsey R. *Bioelectromagnetism: Principles and Applications of Bioelectric and Biomagnetic Fields*. New York, NY: Oxford University Press (1995).
3. Michel CM, He B. EEG mapping and source imaging. In: Schomer DL, Silva, FHLd, editors. *Niedermeyer's Electroencephalography*. New York, NY: Oxford University Press (2018). p. 1135–156.
4. Nunez PL, Srinivasan R. *Electric Fields of the Brain: The Neurophysics of EEG*. 2nd ed. New York, NY: Oxford University Press (2006).
5. Fender D. Source localization of brain electrical activity. In: Remond ASGA, editor. *Methods of Analysis of Brain Electrical and Magnetic Signals*. Amsterdam: Elsevier Science Publishers (1987).
6. Nunez PL, Nunez MD, Srinivasan R. Multi-scale neural sources of EEG: genuine, equivalent, and representative. A tutorial review. *Brain Topogr*. (2019) 32:193–214. doi: 10.1101/391318
7. Kavanagh RN, Darcey TM, Lehmann D, Fender DH. Evaluation of methods for three-dimensional localization of electrical sources in the human brain. *IEEE Trans Biomed Eng*. (1978) 25:421–9. doi: 10.1109/TBME.1978.326339
8. He B, Musha T, Okamoto Y, Homma S, Nakajima Y, Sato T. Electric dipole tracing in the brain by means of the boundary element method and its accuracy. *IEEE Trans Biomed Eng*. (1987) 34:406–14. doi: 10.1109/TBME.1987.326056
9. Scherg M, von Cramon D. A new interpretation of the generators of BAEP waves I-V: results of a spatio-temporal dipole model. *Electroencephalogr Clin Neurophysiol*. (1985) 62:290–9. doi: 10.1016/0168-5597(85)90006-1
10. Scherg M, Picton TW. Separation and identification of event-related potential components by brain electric source analysis. In*:* Brunia CHM, Mulder G, Verbaten MN, editors. *Event-Related Brain Research*. Amsterdam: Elsevier (1991). p. 24–37.
11. Mosher JC, Lewis PS, Leahy RM. Multiple dipole modeling and localization from spatio-temporal MEG data. *IEEE Trans Biomed Eng*. (1992) 39:541–57. doi: 10.1109/10.141192
12. Henderson CJ, Butler SR, Glass A. The localization of equivalent dipoles of EEG sources by the application of electrical field theory. *Electroencephalogr Clin Neurophysiol*. (1975) 39:117–30. doi: 10.1016/0013-4694(75)90002-4
13. Ebersole JS. Non-invasive localization of the epileptogenic focus by EEG dipole modeling. *Acta Neurol Scan Suppl*. (1994) 152:20–8. doi: 10.1111/j.1600-0404.1994.tb05179.x
14. Lantz G, Holub M, Ryding E, Rosen I. Simultaneous intracranial and extracranial recording of interictal epileptiform activity in patients with drug resistant partial epilepsy: patterns of conduction and results from dipole reconstructions. *Electroencephalogr Clin Neurophysiol*. (1996) 99:69–78. doi: 10.1016/0921-884X(96)95686-6
15. Sharma P, Scherg M, Pinborg LH, Fabricius M, Rubboli G, Pedersen B, et al. Ictal and interictal electric source imaging in pre-surgical evaluation: a prospective study. *Eur J Neurol*. (2018) 25:1154–60. doi: 10.1111/ene.13676
16. Willemse RB, Hillebrand A, Ronner HE, Vandertop WP, Stam CJ. Magnetoencephalographic study of hand and foot sensorimotor

organization in 325 consecutive patients evaluated for tumor or epilepsy surgery. *Neuroimage Clin*. (2016) 10:46–53. doi: 10.1016/j.nicl.2015.11.002
17. Stefan H, Hummel C, Scheler G, Genow A, Druschky K, Tilz C, et al. Magnetic brain source imaging of focal epileptic activity: a synopsis of 455 cases. *Brain*. (2003) 126:2396–405. doi: 10.1093/brain/awg239
18. Hämäläinen M, Ilmoniemi RJ. Interpreting measured magnetic fields of the brain: minimum norm estimates. *Med Biol Eng Comput*. (1994) 32:25–42.
19. Grave de Peralta Menendez R, Gonzalez Andino SL. A critical analysis of linear inverse solutions. *IEEE Trans Biomed Eng*. (1998) 45, 440–448. doi: 10.1109/10.664200
20. Greenblatt RE. Probabilistic reconstruction of multiple sources in the neuroelectromagnetic inverse problem. *Inverse Problems*. (1993) 9:271–84. doi: 10.1088/0266-5611/9/2/008
21. Wang JZ, Williamson SJ, Kaufman L. Magnetic source images determined by a lead-field analysis: the unique minimum-norm least-squares estimation. *IEEE Trans Biomed Eng*. (1992) 39:665–75. doi: 10.1109/10.142641
22. Pascual-Marqui RD, Michel CM, Lehmann D. Low resolution electromagnetic tomography: a new method for localizing electrical activity in the brain. *Int J Psychophysiol*. (1994) 18:49–65. doi: 10.1016/0167-8760(84)90014-X
23. Grave de Peralta Menendez R, Murray MM, Michel CM, Martuzzi R, Gonzalez Andino SL. Electrical neuroimaging based on biophysical constraints. *NeuroImage*. (2004) 21, 527–539. doi: 10.1016/j.neuroimage.2003.09.051
24. Spinelli L, Andino SG, Lantz G, Seeck M, Michel CM. Electromagnetic inverse solutions in anatomically constrained spherical head models. *Brain Topogr*. (2000) 13:115–25. doi: 10.1023/A:1026607118642
25. Baillet S, Mosher JC, Leahy RM. Electromagnetic brain mapping. *IEEE Signal Process. Magaz*. (2001) 14–30. doi: 10.1109/79.962275
26. He B, Lian J. Electrophysiological Neuroimaging: solving the EEG inverse problem. In: He B, editor. *Neuroal Engineering*. Norwell, MA: Kluwer Academic Publishers (2005). p. 221–61. doi: 10.1007/0-306-48610-5_7
27. He B, Sohrabpour A, Brown E, Liu Z. Electrophysiological source imaging: a noninvasive window to brain dynamics. *Annu Rev Biomed Eng*. (2018) 20:171–96. doi: 10.1146/annurev-bioeng-062117-120853
28. Michel CM, Murray MM, Lantz G, Gonzalez S, Spinelli L, Grave de Peralta R. EEG source imaging. *Clin Neurophysiol*. (2004) 115:2195–222. doi: 10.1016/j.clinph.2004.06.001
29. Brunet D, Murray MM, Michel CM. Spatiotemporal analysis of multichannel EEG: CARTOOL. *Comput Intell Neurosci*. (2011) 2011:813870. doi: 10.1155/2011/813870
30. Baillet S, Friston K, Oostenveld R. Academic software applications for electromagnetic brain mapping using MEG and EEG. *Comput Intell Neurosci*. (2011) 2011:972050. doi: 10.1155/2011/972050
31. Tadel F, Baillet S, Mosher JC, Pantazis D, Leahy RM. Brainstorm: a user-friendly application for MEG/EEG analysis. *Comput Intell Neurosci*. (2011) 2011:879716. doi: 10.1155/2011/879716
32. Delorme A, Mullen T, Kothe C, Akalin Acar Z, Bigdely-Shamlo N, Vankov A, et al. EEGLAB, SIFT, NFT, BCILAB, and ERICA: new tools for advanced EEG processing. *Comput Intell Neurosci*. (2011) 2011:130714. doi: 10.1155/2011/130714
33. Oostenveld R, Fries P, Maris E, Schoffelen JM. FieldTrip: Open source software for advanced analysis of MEG, EEG, and invasive electrophysiological data. *Comput Intell Neurosci*. (2011) 2011:156869. doi: 10.1155/2011/156869
34. Dalal SS, Zumer JM, Guggisberg AG, Trumpis M, Wong DD, Sekihara K, et al. MEG/EEG source reconstruction, statistical evaluation, and visualization with NUTMEG. *Comput Intell Neurosci*. (2011) 2011:758973. doi: 10.1155/2011/758973
35. Litvak V, Mattout J, Kiebel S, Phillips C, Henson R, Kilner J, et al. EEG and MEG data analysis in SPM8. *Comput Intell Neurosci*. (2011) 2011:852961. doi: 10.1155/2011/852961
36. Pernet CR, Garrido M, Gramfort A, Maurits N, Michel C, Pang E. et al. Best practices in data analysis and sharing in neuroimaging using MEEG. (2018). doi: 10.31219/osf.io/a8dhx
37. Grooms JK, Thompson GJ, Pan WJ, Billings J, Schumacher EH, Epstein CM, et al. Infraslow electroencephalographic and dynamic resting state network activity. *Brain Connect*. (2017) 7:265–80. doi: 10.1089/brain.2017.0492
38. Frauscher B, von Ellenrieder N, Zelmann R, Rogers C, Nguyen DK, Kahane P, et al. High-frequency oscillations in the normal human brain. *Ann Neurol*. (2018) 84:374–85. doi: 10.1002/ana.25304
39. Rousselet GA. Does filtering preclude us from studying ERP time-courses? *Front Psychol*. (2012) 3:131. doi: 10.3389/fpsyg.2012.00131
40. Widmann A, Schroger E. Filter effects and filter artifacts in the analysis of electrophysiological data. *Front Psychol*. (2012) 3:233. doi: 10.3389/fpsyg.2012.00233
41. Smith SW. *The Scientist and Engineer's Guide to Digital Signal Processing*. 2nd ed. San Diego, CA: California Technical Publishing (1999).
42. Hogenauer E. A class of digital filters for decimation and interpolation. In: *ICASSP '80. IEEE International Conference on Acoustics, Speech, and Signal Processing*. (1980). p. 271–4. doi: 10.1109/ICASSP.1980.1170846
43. Delorme A, Sejnowski T, Makeig S. Enhanced detection of artifacts in EEG data using higher-order statistics and independent component analysis. *NeuroImage*. (2007) 34:1443–9. doi: 10.1016/j.neuroimage.2006.11.004
44. Delorme A, Makeig S. EEGLAB: an open source toolbox for analysis of single-trial EEG dynamics including independent component analysis. *J Neurosci Methods*. (2004) 134:9–21. doi: 10.1016/j.jneumeth.2003.10.009
45. Perrin F, Pernier J, Bertrand O, Echallier JF. Spherical splines for scalp potential and current density mapping. *Electroencephalogr Clin Neurophysiol*. (1989) 72:184–9. doi: 10.1016/0013-4694(89)90180-6
46. Michel CM, Brandeis D. Data acquisition and pre-processing standards for electrical neuroimaging. In: Michel CM, Koenig T, Brandeis D, Gianotti LRR, Wackermann J, editors. *Electrical Neuroimaging*. Cambridge: Cambridge University Press (2009). p. 79–92.
47. Brodbeck V, Spinelli L, Lascano AM, Wissmeier M, Vargas MI, Vulliemoz S, et al. Electroencephalographic source imaging: a prospective study of 152 operated epileptic patients. *Brain*. (2011) 134:2887–97. doi: 10.1093/brain/awr243
48. Friston K, Ashburner J, Kiebel S, Nichols TE, Penny W. *Statistical Parametric Mapping*. Amsterdam: Elsevier Ltd. (2007). doi: 10.1016/B978-012372560-8/50002-4
49. Srinivasan R, Tucker DM, Murias M. Estimating the spatial Nyquist of the human EEG. *Behav. Res. Methods Ins. Comp*. (1998) 30:8–19. doi: 10.3758/BF03209412
50. Luu P, Tucker DM, Englander R, Lockfeld A, Lutsep H, Oken B. Localizing acute stroke-related EEG changes: assessing the effects of spatial undersampling. *J Clin Neurophysiol*. (2001) 18:302–17. doi: 10.1097/00004691-200107000-00002
51. Kuhnke N, Schwind J, Dumpelmann M, Mader M, Schulze-Bonhage A, Jacobs J. High Frequency oscillations in the ripple band (80-250 Hz) in Scalp EEG: higher density of electrodes allows for better localization of the seizure onset zone. *Brain Topogr*. (2018) 31:1059–72. doi: 10.1007/s10548-018-0658-3
52. Zelmann R, Lina JM, Schulze-Bonhage A, Gotman J, Jacobs J. Scalp EEG is not a blur: it can see high frequency oscillations although their generators are small. *Brain Topogr*. (2014) 27:683–704. doi: 10.1007/s10548-013-0321-y
53. Staljanssens W, Strobbe G, Holen RV, Birot G, Gschwind M, Seeck M, et al. Seizure onset zone localization from ictal high-density EEG in refractory focal epilepsy. *Brain Topogr*. (2017) 30:257–71. doi: 10.1007/s10548-016-0537-8
54. Malmivuo JA, Suihko VE. Effect of skull resistivity on the spatial resolutions of EEG and MEG. *IEEE Trans Biomed Eng*. (2004) 51:1276–80. doi: 10.1109/TBME.2004.827255
55. Ryynanen OR, Hyttinen JA, Malmivuo JA. Effect of measurement noise and electrode density on the spatial resolution of cortical potential distribution with different resistivity values for the skull. *IEEE Trans Biomed Eng*. (2006) 53:1851–8. doi: 10.1109/TBME.2006.873744
56. Fifer WP, Grieve PG, Grose-Fifer J, Isler JR, Byrd D. High-density electroencephalogram monitoring in the neonate (2006). *Clin Perinatol*. 33, 679-691. doi: 10.1016/j.clp.2006.06.011
57. Grieve PG, Emerson RG, Isler JR, Stark RI. Quantitative analysis of spatial sampling error in the infant and adult electroencephalogram. *NeuroImage*. (2004) 21:1260–74. doi: 10.1016/j.neuroimage.2003.11.028

58. Baroumand AG, van Mierlo P, Strobbe G, Pinborg LH, Fabricius M, Rubboli G, et al. Automated EEG source imaging: a retrospective, blinded clinical validation study. *Clin Neurophysiol*. (2018) 129:2403–10. doi: 10.1016/j.clinph.2018.09.015
59. Ding L, Worrell GA, Lagerlund TD, He B. Ictal source analysis: localization and imaging of causal interactions in humans. *NeuroImage*. (2007) 34:575–86. doi: 10.1016/j.neuroimage.2006.09.042
60. Sperli F, Spinelli L, Seeck M, Kurian M, Michel CM, Lantz G. EEG source imaging in pediatric epilepsy surgery: a new perspective in presurgical workup. *Epilepsia*. (2006) 47:981–90. doi: 10.1111/j.1528-1167.2006.00550.x
61. Koessler L, Cecchin T, Colnat-Coulbois S, Vignal JP, Jonas J, Vespignani H, et al. Catching the invisible: mesial temporal source contribution to simultaneous EEG and SEEG recordings. *Brain Topogr*. (2015) 28:5–20. doi: 10.1007/s10548-014-0417-z
62. Rosenzweig I, Fogarasi A, Johnsen B, Alving J, Fabricius ME, Scherg M, et al. Beyond the double banana: improved recognition of temporal lobe seizures in long-term EEG. *J Clin Neurophysiol*. (2014) 31:1–9. doi: 10.1097/WNP.0000000000000019
63. Bach Justesen A, Eskelund Johansen AB, Martinussen NI, Wasserman D, Terney D, Meritam P, et al. Added clinical value of the inferior temporal EEG electrode chain. *Clin Neurophysiol*. (2018) 129:291–5. doi: 10.1016/j.clinph.2017.09.113
64. Seeck M, Koessler L, Bast T, Leijten F, Michel C, Baumgartner C, et al. The standardized EEG electrode array of the IFCN. *Clin Neurophysiol*. (2017) 128:2070–7. doi: 10.1016/j.clinph.2017.06.254
65. Jeon S, Chien J, Song C, Hong J. A preliminary study on precision image guidance for electrode placement in an EEG study. *Brain Topogr*. (2018) 31:174–85. doi: 10.1007/s10548-017-0610-y
66. Akalin Acar Z, Makeig S. Effects of forward model errors on EEG source localization. *Brain Topogr*. (2013) 26:378–96. doi: 10.1007/s10548-012-0274-6
67. Baillet S, Riera JJ, Marin G, Mangin JF, Aubert J, Garnero L. Evaluation of inverse methods and head models for EEG source localization using a human skull phantom. *Phys Med Biol*. (2001) 46:77–96. doi: 10.1088/0031-9155/46/1/306
68. Fuchs M, Wagner M, Kastner J. Development of volume conductor and source models to localize epileptic foci. *J Clin Neurophysiol*. (2007) 24:101–19. doi: 10.1097/WNP.0b013e318038fb3e
69. Guggisberg AG, Dalal SS, Zumer JM, Wong DD, Dubovik S, Michel CM, et al. Localization of cortico-peripheral coherence with electroencephalography. *NeuroImage*. (2011) 57:1348–57. doi: 10.1016/j.neuroimage.2011.05.076
70. Wang G, Worrell G, Yang L, Wilke C, He B. Interictal spike analysis of high-density EEG in patients with partial epilepsy. *Clin Neurophysiol*. (2011) 122:1098–105. doi: 10.1016/j.clinph.2010.10.043
71. Birot G, Spinelli L, Vulliemoz S, Megevand P, Brunet D, Seeck M, et al. Head model and electrical source imaging: A study of 38 epileptic patients. *Neuroimage Clin*. (2014) 5:77–83. doi: 10.1016/j.nicl.2014.06.005
72. Lillie EM, Urban JE, Lynch SK, Weaver AA, Stitzel JD. Evaluation of skull cortical thickness changes with age and sex from computed tomography scans. *J Bone Miner Res*. (2016) 31:299–307. doi: 10.1002/jbmr.2613
73. Roche AF. Increase in cranial thickness during growth. *Hum Biol*. (1953) 25:81–92.
74. Goncalves S, de Munck JC, Verbunt JP, Heethaar RM, da Silva FH. *In vivo* measurement of the brain and skull resistivities using an EIT-based method and the combined analysis of SEF/SEP data. *IEEE Trans Biomed Eng*. (2003) 50:1124–8. doi: 10.1109/TBME.2003.812164
75. Lai Y, van Drongelen W, Ding L, Hecox KE, Towle VL, Frim DM, et al. Estimation of *in vivo* human brain-to-skull conductivity ratio from simultaneous extra- and intra-cranial electrical potential recordings. *Clin Neurophysiol*. (2005) 116:456–65. doi: 10.1016/j.clinph.2004.08.017
76. Oostendorp TF, Delbeke J, Stegeman DF. The conductivity of the human skull: results of *in vivo* and *in vitro* measurements. *IEEE Trans Biomed Eng*. (2000) 47:1487–92. doi: 10.1109/TBME.2000.880100
77. Rush S, Driscoll DA. EEG electrode sensitivity–an application of reciprocity. *IEEE Trans Biomed Eng*. (1969) 16:15–22. doi: 10.1109/TBME.1969.4502645
78. Hoekema R, Wieneke GH, Leijten FS, van Veelen CW, van Rijen PC, Huiskamp GJ, et al. Measurement of the conductivity of skull, temporarily removed during epilepsy surgery. *Brain Topogr*. (2003) 16:29–38. doi: 10.1023/A:1025606415858
79. Latikka J, Kuurne T, Eskola H. Conductivity of living intracranial tissues. *Phys Med Biol*. (2001) 46:1611–6. doi: 10.1088/0031-9155/46/6/302
80. Brodbeck V, Lascano AM, Spinelli L, Seeck M, Michel CM. Accuracy of EEG source imaging of epileptic spikes in patients with large brain lesions. *Clin Neurophysiol*. (2009) 120:679–85. doi: 10.1016/j.clinph.2009.01.011
81. Brodbeck V, Spinelli L, Lascano AM, Pollo C, Schaller K, Vargas MI, et al. Electrical source imaging for presurgical focus localization in epilepsy patients with normal MRI. *Epilepsia*. (2010) 51:583–91. doi: 10.1111/j.1528-1167.2010.02521.x
82. Megevand P, Spinelli L, Genetti M, Brodbeck V, Momjian S, Schaller K, et al. Electric source imaging of interictal activity accurately localises the seizure onset zone. *J Neurol Neurosurg Psychiatry*. (2014) 85:38–43. doi: 10.1136/jnnp-2013-305515
83. Lascano AM, Grouiller F, Genetti M, Spinelli L, Seeck M, Schaller K, et al. Surgically relevant localization of the central sulcus with high-density somatosensory-evoked potentials compared with functional magnetic resonance imaging. *Neurosurgery*. (2014) 74:517–26. doi: 10.1227/NEU.0000000000000298
84. Seeber M, Cantonas LM, Hoevels M, Sesia T, Visser-Vandewalle V, Michel CM. Subcortical electrophysiological activity is detectable with high-density EEG source imaging. *Nat Commun*. (2019) 10:753. doi: 10.1038/s41467-019-08725-w
85. Bréchet L, Brunet D, Birot G, Gruetter R, Michel CM, Jorge J. Capturing the spatiotemporal dynamics of task-initiated thoughts with EEG and fMRI. *Neuroimage*. (2019). doi: 10.1016/j.neuroimage.2019.03.029. [Epub ahead of print].
86. Hernandez F, Johnson RA. The large-sample behavior of transformations to normality. *J Am Stat Assoc*. (1980) 75:855–61.
87. Biasiucci A, Franceschiello B, Murray MM. Electroencephalography. *Curr Biol*. (2019) 29:R80–R85. doi: 10.1016/j.cub.2018.11.052
88. He B, Yang L, Wilke C, Yuan H. Electrophysiological imaging of brain activity and connectivity-challenges and opportunities. *IEEE Trans Biomed Eng*. (2011) 58:1918–31. doi: 10.1109/TBME.2011.2139210
89. Michel CM, Murray MM. Towards the utilization of EEG as a brain imaging tool. *NeuroImage*. (2012) 61:371–85. doi: 10.1016/j.neuroimage.2011.12.039
90. Plummer C, Harvey AS, Cook M. EEG source localization in focal epilepsy: where are we now? *Epilepsia*. (2008) 49:201–18. doi: 10.1111/j.1528-1167.2007.01381.x
91. Feng R, Hu J, Pan L, Wu J, Lang L, Jiang S, et al. Application of 256-channel dense array electroencephalographic source imaging in presurgical workup of temporal lobe epilepsy. *Clin Neurophysiol*. (2015) 127:108–16 doi: 10.1016/j.clinph.2015.03.009
92. Klamer S, Elshahabi A, Lerche H, Braun C, Erb M, Scheffler K, et al. Differences between MEG and high-density EEG source localizations using a distributed source model in comparison to fMRI. *Brain Topogr*. (2015) 28:87–94. doi: 10.1007/s10548-014-0405-3
93. Lascano AM, Perneger T, Vulliemoz S, Spinelli L, Garibotto V, Korff CM, et al. Yield of , high-density electric source imaging (HD-), SPECT and PET in epilepsy surgery candidates. *Clin Neurophysiol*. (2016) 125:150–5. doi: 10.1016/j.clinph.2015.03.025
94. Chowdhury RA, Merlet I, Birot G, Kobayashi E, Nica A, Biraben A, et al. Complex patterns of spatially extended generators of epileptic activity: Comparison of source localization methods cMEM and 4-ExSo-MUSIC on high resolution EEG and MEG data. *NeuroImage*. (2016) 143:175–95. doi: 10.1016/j.neuroimage.2016.08.044
95. Hassan M, Mheich A, Biraben A, Merlet I, Wendling F. Identification of epileptogenic networks from dense EEG: A model-based study. *Conf Proc IEEE Eng Med Biol Soc*. (2015) 2015:5610–3. doi: 10.1109/EMBC.2015.7319664
96. Michel CM, Thut G, Morand S, Khateb A, Pegna AJ, Grave de Peralta R, et al. Electric source imaging of human brain functions. *Brain Res Brain Res Rev*. (2001) 36:108–118. doi: 10.1016/S0165-0173(01)00086-8
97. Astolfi L, de Vico Fallani F, Cincotti F, Mattia D, Marciani MG, Bufalari S, et al. Imaging functional brain connectivity patterns from high-resolution EEG and fMRI via graph theory. *Psychophysiology*. (2007) 44:880–893. doi: 10.1111/j.1469-8986.2007.00556.x

98. Coito A, Michel CM, van Mierlo P, Vulliemoz S, Plomp G. Directed functional brain connectivity based on EEG source imaging: methodology and application to temporal lobe epilepsy. *IEEE Trans Biomed Eng.* (2016) 63:2619–28. doi: 10.1109/TBME.2016.2619665
99. He B, Dai Y, Astolfi L, Babiloni F, Yuan H, Yang L. eConnectome: A MATLAB toolbox for mapping and imaging of brain functional connectivity. *J. Neurosci. Methods.* (2011) 195:261–9. doi: 10.1016/j.jneumeth.2010.11.015
100. Astolfi L, De Vico Fallani F, Cincotti F, Mattia D, Marciani MG, Salinari S, et al. Estimation of effective and functional cortical connectivity from neuroelectric and hemodynamic recordings. *IEEE Trans Neural Syst Rehabil Eng.* (2009) 17:224–33. doi: 10.1109/TNSRE.2008.2010472
101. Coito A, Michel CM, Vulliemoz S, Plomp G. Directed functional connections underlying spontaneous brain activity. *Hum Brain Mapp.* (2019) 40:879–88. doi: 10.1002/hbm.24418
102. Wendling F, Ansari-Asl K, Bartolomei F, Senhadji L. From EEG signals to brain connectivity: a model-based evaluation of interdependence measures. *J Neurosci Methods.* (2009) 183:9–18. doi: 10.1016/j.jneumeth.2009.04.021
103. Coito A, Genetti M, Pittau F, Iannotti G, Thomschewski A, Höller Y, et al. Altered directed connectivity in temporal lobe epilepsy in the absence of interictal spikes: a high density EEG study. *Epilepsia.* (2016) 57:402–11. doi: 10.1111/epi.13308
104. Coito A, Plomp G, Genetti M, Abela E, Wiest R, Seeck M, et al. Dynamic directed interictal connectivity in left and right temporal lobe epilepsy. *Epilepsia.* (2015) 56:207–17. doi: 10.1111/epi.12904
105. Brunner C, Billinger M, Seeber M, Mullen TR, Makeig S. Volume conduction influences scalp-based connectivity estimates. *Front Comput Neurosci.* (2016) 10:121. doi: 10.3389/fncom.2016.00121
106. Chella F, Pizzella V, Zappasodi F, Marzetti L. Impact of the reference choice on scalp EEG connectivity estimation. *J Neural Eng.* (2016) 13:036016. doi: 10.1088/1741-2560/13/3/036016
107. Engel AK, Gerloff C, Hilgetag CC, Nolte G. Intrinsic coupling modes: multiscale interactions in ongoing brain activity. *Neuron.* (2013) 80:867–86. doi: 10.1016/j.neuron.2013.09.038
108. Haufe S, Nikulin VV, Muller KR, Nolte G. A critical assessment of connectivity measures for EEG data: a simulation study. *NeuroImage.* (2013) 64:120–33. doi: 10.1016/j.neuroimage.2012.09.036
109. Schoffelen JM, Gross J. Source connectivity analysis with MEG and EEG. *Hum Brain Mapp.* (2009) 30:1857–65. doi: 10.1002/hbm.20745
110. Van de Steen F, Faes L, Karahan E, Songsiri J, Valdes-Sosa PA, Marinazzo D. Critical comments on EEG sensor space dynamical connectivity analysis. *Brain Topography.* (2016). doi: 10.1007/s10548-016-0538-7
111. He B, Astolfi L, Valdés-Sosa PA, Marinazzo D, Palva SO, Bénar CG, et al. Electrophysiological brain connectivity: theory and applications. *IEEE Trans Biomed Eng.* (2019).

Conflict of Interest Statement: The authors declare that the research was conducted in the absence of any commercial or financial relationships that could be construed as a potential conflict of interest.

frontiers in Neurology

REVIEW
published: 13 June 2019
doi: 10.3389/fneur.2019.00628

Presurgical Functional Cortical Mapping Using Electromagnetic Source Imaging

Rudolf Kreidenhuber[1,2*], *Xavier De Tiège*[3,4] *and Stefan Rampp*[5,6]

[1] Department of Neurology, Christian-Doppler Medical Center, Paracelsus Medical University, Salzburg, Austria, [2] Centre for Cognitive Neuroscience, University of Salzburg, Salzburg, Austria, [3] Laboratoire de Cartographie Fonctionelle du Cerveau, ULB Neuroscience Institute, Université Libre de Bruxelles, Brussels, Belgium, [4] Department of Functional Neuroimaging, Service of Nuclear Medicine, CUB Hôpital Erasme, Université Libre de Bruxelles, Brussels, Belgium, [5] Department of Neurosurgery, University Hospital Erlangen, Erlangen, Germany, [6] Department of Neurosurgery, University Hospital Halle, Halle, Germany

Preoperative localization of functionally eloquent cortex (functional cortical mapping) is common clinical practice in order to avoid or reduce postoperative morbidity. This review aims at providing a general overview of magnetoencephalography (MEG) and high-density electroencephalography (hdEEG) based methods and their clinical role as compared to common alternatives for functional cortical mapping of (1) verbal language function, (2) sensorimotor cortex, (3) memory, (4) visual, and (5) auditory cortex. We highlight strengths, weaknesses and limitations of these functional cortical mapping modalities based on findings in the recent literature. We also compare their performance relative to other non-invasive functional cortical mapping methods, such as functional Magnetic Resonance Imaging (fMRI), Transcranial Magnetic Stimulation (TMS), and to invasive methods like the intracarotid Amobarbital Test (WADA-Test) or intracranial investigations.

Keywords: magnetoencephalography, functional cortical mapping, fMRI, EEG, presurgical

OPEN ACCESS

Edited by:
Sandor Beniczky,
Aarhus University Hospital, Denmark

Reviewed by:
Dragos-Mihai Maliia,
University Emergency Hospital Bucharest, Romania
Jyrki Mäkelä,
Hospital District of Helsinki and Uusimaa, Finland

***Correspondence:**
Rudolf Kreidenhuber
r.kreidenhuber@salk.at

Specialty section:
This article was submitted to Applied Neuroimaging, a section of the journal Frontiers in Neurology

Received: *26 February 2019*
Accepted: *28 May 2019*
Published: *13 June 2019*

Citation:
Kreidenhuber R, De Tiège X and Rampp S (2019) Presurgical Functional Cortical Mapping Using Electromagnetic Source Imaging. Front. Neurol. 10:628. doi: 10.3389/fneur.2019.00628

INTRODUCTION

Functional cortical mapping (FCM) aims at localizing eloquent functional cortex using a range of invasive and non-invasive methods (1). Its main indication is to characterize the anatomical relationship between functionally eloquent cortex and the extent of a planned surgical resection, e.g., of an intracranial tumor or the putative epileptogenic zone in patients with pharmacoresistant focal epilepsy. In the latter patient group, results of FCM are usually interpreted in conjunction with structural magnetic resonance imaging (MRI), neuropsychological findings, positron emission tomography (PET), single photon emission computed tomography (SPECT) and video-electroencephalography (EEG) monitoring (1).

The advent of non-invasive FCM methods has substantially influenced the care of neurosurgical candidates. Indeed, the availability of FCM results based on non-invasive approaches before surgery allows for a better estimation of the risk-benefit ratio of the planned neurosurgical procedure with better patients' counsel, optimized neurosurgical strategies, as well as tailored resection extents. Overlap between functionally eloquent cortex as identified by non-invasive FCM and lesional or epileptogenic zones may even argue against surgery or for alternative therapeutic strategies.

This paper reviews currently available FCM methods with a special emphasis on electromagnetic source imaging. Strengths, weaknesses and limitations of electromagnetic source imaging in relation to other modalities commonly used for mapping of verbal language, sensorimotor, memory, visual, and auditory functions are also presented.

Functional Cortical Mapping Methods

Non-invasive Methods

Anatomical Landmarks

Identification of anatomical landmarks in structural cerebral imaging represents an easy and fast approach to localize functionally eloquent cortex. However, inter-rater reliability is significantly lower than with FCM results, even within the same subject and across successive analyses over several days (2). Furthermore, anatomic variability, lesion-induced plasticity, and displacement considerably limit accuracy and viability of this approach [for references, see, e.g., (3, 4)].

Functional Magnetic Resonance Imaging (fMRI)

Among the various non-invasive FCM techniques that can be used in humans, fMRI is by far the most commonly used (5). Active brain areas are detected indirectly by relying mostly on task-related changes in regional brain perfusion. Blood oxygenation level dependent (BOLD) signal changes can then be detected by fMRI. The resulting spatial resolution of fMRI is excellent (∼1 mm, including deep locations). However, the dependence on the comparably slow hemodynamic response limits its temporal resolution (∼1 s) (6). Furthermore, the neurovascular coupling may be altered by lesional processes in the vicinity, potentially leading to spurious fMRI results (7, 8). Moreover, activation patterns of single patients with brain disorders can be more difficult to interpret than those obtained in individuals or groups of healthy subjects (8, 9).

Electric Source Imaging (ESI) and Magnetic Source Imaging (MSI)

Magnetoencephalography (MEG) and EEG are non-invasive methods that record magnetic and electric fields, respectively. These are generated by excitatory or inhibitory postsynaptic potentials at the apical dendrites of neocortical pyramidal cells. Determination of the anatomical location of the sources generating the measured signal is known as magnetic and electric source imaging (MSI and ESI, respectively). This is achieved by combining MEG or EEG data with structural MRI. For the purpose of clarity, we will henceforth only use MEG and EEG to refer to MSI- or ESI-based FCM.

In contrast to EEG, MEG is sensitive mainly to tangential neocortical source components. Consequently, it detects activity mainly from the sulcal walls, while small areas at the crown or in the sulcal depth barely contribute to detectable signals (10). Sensitivity of both EEG and MEG decreases with increasing cortical depth. The number of sensors, amplitude of background activity and, in EEG, smearing of the field distribution due to variations in skull resistivity, account for differences in recorded signals (11). For a comprehensive review on mechanisms of MEG and EEG signal generation, see (12). Data from EEG and MEG are complementary and combined analysis has been shown to outperform the single modalities alone in the presurgical evaluation of patients with epilepsy in the context of source localization (13). Still, this combined approach is rarely used for FCM and comparable studies for simultaneous FCM in MEG and EEG are, to the best of our knowledge, lacking.

Transcranial Magnetic Stimulation (TMS)

TMS is a non-invasive form of neurostimulation. Magnetic fields applied focally are used to induce or inhibit electric activity of targeted neurons via electromagnetic induction. Neuronavigation using the patient's individual structural MRI (and eventually results from other FCM modalities) allows for better targeted stimulation (nTMS). In the context of FCM, it is used primarily for verbal language and primary motor (M1) cortex localization (14–17) in specialized centers.

Invasive Methods

Intracarotid Amobarbital Test (IAT)

Wada and Rasmussen described in 1960 the intracarotid injection of amobarbital for the lateralization of cerebral speech dominance (18). Sodium amobarbital is injected into a single internal carotid artery via transfemoral arterial catheterization. This procedure transiently suppresses neuronal function of the corresponding brain hemisphere depending on the respective vascular supply, mainly the ipsilateral anterior and middle cerebral arteries. Patients then undergo verbal language and neuropsychological testing during the transient unilateral hemispheric anesthesia, evaluating language and memory functions. The procedure is then repeated for the contralateral hemisphere. The IAT or "Wada-Test" allows for lateralization but not localization of brain areas involved in verbal language and memory functions (19). Limitations and shortcomings include risks of stroke, hemorrhage, infection (morbidity around 3–5%) and the possibility of arterial crossflow to the contralateral hemisphere via the circle of Willis—for reviews or discussions, see, e.g., (20, 21).

Direct Current Stimulation

Direct current stimulation (DCS) is used in awake craniotomy for language-, motor- and memory mapping. For a review, see (22). Intracranial EEG electrodes record local field potentials and can also be used for stimulation purposes. Cortex areas are labeled as eloquent either via gain/loss of the specific function, i.e., motor jerks, speech arrest, memory deficits, or via alterations of simultaneously recorded local field potentials or targeted electromyography (22).

EEG/MEG FUNCTIONAL CORTICAL MAPPING COMPARED TO OTHER METHODS

Verbal Language Function

Presurgical and potentially intraoperative investigation of verbal language function is mandatory to avoid postoperative language deficits if surgery involves resection near (presumed) language eloquent cortex.

Language related cortex is extensive and bilateral, although one hemisphere is usually dominant. Two broad processing streams can be distinguished: a ventral stream for speech comprehension (bilateral, temporal lobes) and a dorsal stream for sensory-motor integration (asymmetric, temporo-parietal junction, and frontal lobe). For comprehensive reviews, see, e.g., (23, 24). In a healthy population, ∼95% of right-handers and ∼76% of left-handers have left—hemisphere language dominance (25, 26). In patients with epilepsy, the rate of left—hemisphere language dominance drops significantly, with rates of 63−96% (right-handers) and 48−75% (left-handers) (26, 27).

Assessment of hemispheric dominance and intra-hemispheric cortical representation of speech processing and production are the main objectives of language FCM (5). IAT has been considered the gold standard for the evaluation of language hemispheric dominance. However, this role has been challenged by non-invasive methods (21). fMRI is the most widely used modality for assessment of language function, but EEG/MEG allow for characterization of temporal, spectral and also spatial dynamics of receptive and expressive language processing (5, 28).

Assessment of Hemispheric Dominance of Receptive Verbal Language Function

A frequently used approach for assessment of hemispheric receptive verbal language dominance was proposed by Papanicolaou et al. (29). It evaluates late (about 200 and 800 ms post stimulus) event related fields by use of an equivalent current dipole model. This approach showed consistent concordance of 86–92% between MEG and IAT results (29–33) and with findings from intracranial cortical stimulation (34).

Other strategies apply beamforming (35) and evaluate the spatial distribution of oscillatory changes related to silent reading. Lateralization of desynchronized/suppressed beta- (13–25 Hz) and gamma-activity (25–50 Hz) in regions of interest is analyzed and used to calculate a laterality index. This method showed concordance with IAT results in 95% of patients. Wilenius et al. (36) found a sensitivity of 67% and a specificity of 100% of stronger MEG responses to vowels than tones in the left hemisphere.

Furthermore, distributed source models, such as e.g., MR-FOCUSS have been successfully used for verbal language lateralization, as demonstrated by Bowyer et al. (37). Their approach of laterality index determination for multiple time intervals showed agreement with IAT results in 89%.

Active participation for the assessment of verbal language dominance using MEG may not be needed, as passive (listening) paradigms have also been described (38, 39).

Intrahemispheric Representation of Speech Processing and Language Production

IAT does not allow for an arterial injection of amobarbital that is selective enough to discriminate the sublobar structures involved in verbal language processing. Therefore, in clinical practice, intrahemispheric verbal language localization is primarily evaluated using fMRI or MEG preoperatively, or using direct current stimulation (DCS) intraoperatively.

Various protocols for the assessment of areas involved in verbal language comprehension (29, 40–42) and production (43, 44) are in routine clinical and research use. Using fMRI or MEG results as starting and end points for tractography further allows estimation of functional white matter pathways for planning of surgery or targeted intraopearative DCS testing (45).

Most studies suggest a high inter-subject variability of language-related activations, as well as high degrees of cortical plasticity in patients with brain disorders (28, 46, 47). Even DCS results have been shown to provide an incomplete representation of verbal language function with consecutive postoperative functional deficits (48).

Furthermore, nTMS, as well as nTMS-based DTI fiber tracking, have been applied successfully (49) but are, to the best of our knowledge, not currently in widespread clinical use.

Validation and Comparison

fMRI possibly provides better prediction of postoperative verbal language and memory deficits compared to IAT (50, 51), and shows concordance with IAT results in about 80–90% of cases (8). fMRI holds the potential to replace IAT for determination of hemispheric language dominance in many cases (5, 52). However, sites of fMRI activation do not necessarily reflect cortex essential for verbal language function and conversely, areas not activated by the fMRI paradigm under use may prove to be relevant (5). The precise intra-hemispheric localization of essential verbal language areas, especially in patients, remains suboptimal (5, 7, 8). Sensitivity of fMRI for DCS sites ranges from 59 to 100%, specificity from 0 to 97% (53).

Multiple approaches have been evaluated and validated for MEG verbal language lateralization. Stimulation paradigms usually test for language comprehension or language production. Agreement with IAT is about 86–92% for word recognition tasks (31, 32), and 78–82% for language production, depending on the specific experimental design (28).

Data on the comparison of localization accuracy of MEG mapping and DCS are sparse (54). Hirata et al. (42) reported distances between MEG activation maxima and DCS positive sites of 6.0 ± 7.1 mm, Simos et al. (34) described concordant results in a case report. Babajani-Feremi et al. (55) showed that the combination of fMRI, high-gamma electrocorticography (ECoG) and MEG predicted postoperative language decline best, while integrating fMRI and MEG provided the best trade-off between model complexity and prediction accuracy. Tarapore et al. (56) compared TMS, DCS, and MEG for language mapping in the same patients and found high sensitivity and specificity (90 and 98%) of TMS for DCS results in a population of 12 patients with lesions around cortical language areas, while MEG results correlated with TMS sites only in 5 subjects and DCS sites in 2 subjects. Other studies support the high sensitivity of TMS for DCS positive sites, but find reduced specificity, e.g., 90.2 and 23.8% by Picht et al. (57). Ille et al. (58) report a sensitivity of 100% and a specificity of 8%. In a separate study (59), the same group could achieve a sensitivity of 98% and a specificity of 83% by combining the results of TMS and fMRI. Comparative EEG, DCS, and/or invasive EEG data for language mapping is not available.

Clinical MEG societies regard MEG as a validated tool for presurgical evaluation of patients in respect to the assessment of verbal language-dominant hemisphere and consider it as a potential replacement for IAT in most patients (60). However, MEG should not be considered as a replacement for DCS or awake surgery to spare eloquent language areas close to resection borders (60). However, the predictive value of DCS itself is debated and limits its value as a gold standard (21). Ilmberger et al. (61) describe DCS positive sites within the resected lesion as significant risk factor for postoperative language disturbances. However, only 53% of patients with such findings developed a new language-related deficit. Furthermore, postoperative language deficits are often only transient although DCS positive sites have been at least partially resected (62). Additionally, Cervenka et al. (63) reported postoperative deficits in 7 of 11 operated patients which were not anticipated by DCS. This may in part be caused by temporal and financial limitations leading to "incomplete mapping," as the authors point out.

Sensorimotor Function

In patients with lesions or epileptogenic zones located at the central region, mapping of sensorimotor cortex is utilized to locate primary somatosensory (S1) and motor (M1) areas (64). While structural landmarks enable the identification of anatomical primary sensorimotor (SM1) cortex, space-occupying lesions may result in considerable displacement and structural alterations. Furthermore, motor areas are especially capable of functional reorganization to neighboring or possibly even remote areas (65). Sensorimotor mapping enables localization of functionally eloquent cortex in the individual patient, and thus the tailoring of resective neurosurgery. Alongside fMRI, DCS and nTMS, MEG has been applied successfully for this indication—for reviews, see (66–68). Studies reporting on EEG–based sensorimotor FCM and its clinical value are however sparse (69, 70) or are evaluated as part of simultaneous EEG/MEG recordings (71, 72).

Somatosensory Functional Cortex Mapping

Clinical MEG/EEG mapping of S1 cortex typically utilizes either electrical or mechanical stimulation. The former follows principles of, e.g., median or tibial nerve electrical stimulation as frequently applied in neurological and neurosurgical practice (3, 6, 73–79). Stimulation sites are chosen according to the location of the lesion and the estimated relation to functional cortex. As the duration of the procedure amounts to only a few minutes, multiple stimulation targets can be evaluated, e.g., for comparison with contralateral cortex. Furthermore, stimulation of several sites can be combined into a single measurement run with only slightly extended duration. One study performed in 325 consecutive patients with various brain disorders demonstrated that the success rate of somatosensory mapping based on electrical median and tibial nerve stimulations was significantly lower for the feet than for the hands (95.3% for the hands vs. 76% for the feet) (77). Electrical stimulation however is rather uncomfortable and associated with high-amplitude stimulation artifacts. Stimulation of the face, as well as investigations of children or pain-sensitive patients are therefore usually performed using pneumatic stimulation (80, 81). This procedure utilizes pneumatic stimulation devices with balloon diaphragms, which are moved using pressurized air. Due to the longer latency and higher variability of pressurization, the onset of the evoked activity occurs later and is less sharp. Somatosensory and motor mapping can be combined into a single recording session to limit the overall measurement duration (82). Presurgical somatosensory FCM in patients with brain lesion located close to the central sulcus is, in most instances, used to properly locate the central sulcus and assess likely functional (i.e., motor function) risks associated with resective surgery [see, e.g., (6)]. Still, this approach provides indirect information about the location of motor function, and might therefore be misleading in certain circumstances (e.g., brain lesion inducing substantial anatomical displacement).

Motor Cortex Mapping

The spectrum of FCM paradigms and analytical techniques to locate M1 cortex mainly rely on motor evoked fields/potentials (MEF/MEP) and on the suppression of rolandic (alpha and) beta rhythm(s). Additional methods can also be used such as cortico-muscular (CMC) or cortico-kinematic (CKC) coherence.

Motor evoked field/potential or readiness paradigms (73, 77, 83–85) utilize either externally cued or self-paced movements or muscle contractions. Most common are finger tapping and hand closing/opening. Simultaneous recording of EMG (electromyography) enables the exact determination of movement onset. Analysis of the averaged signal then evaluates activity approximately 30–40 ms before movement (60).

Motor activity is accompanied by event-related desynchronization (ERD) or suppression of oscillatory activity in the alpha and beta frequency bands (86). This mu-rhythm, alpha- and beta-band suppression can be localized using, e.g., beamforming (3, 77, 87–89). Paradigms include, e.g., hand grasping (88) and finger extension (3), or ankle flexion/extension (77). Importantly, the beta-band movement-related suppression is organized in a somatotopic manner along the precentral gyrus, while this is less clear for the alpha-band suppression, which has been shown to mainly occur close to the hand region of the postcentral gyrus regardless of the body part moved (90). This explains why beta-band suppression is usually preferred over alpha-band suppression for M1 cortex mapping. The success rate of motor mapping based on movement-related beta-band suppression has been shown to be lower for the feet than for the hands (94.6% for the hands vs. 81.8% for the feet (77).

Coherence approaches (3,88) evaluate the functional coupling of neuronal activity with either muscular activity [as measured by electromyography (EMG)] or movement kinematics. Statistical approaches localize cortical areas of significant coupling with these external reference signals. Stimulation paradigms typically utilize isometric contractions for CMC and recording of (active or passive) movement kinematics with, e.g., accelerometers for CKC (4, 91–93). CMC is considered to reflect mainly the efferent flow of motor commands from M1 cortex to the periphery [for a detailed discussion, see, e.g., (94)] while CKC mainly reflects movement-related somatosensory proprioceptive afferent input to the contralateral SM1 cortex (91, 95).

Of note, MEG and fMRI activations may also be used to support identification of the corticospinal tract (83). Aoyama et al. (96) have combined MEG and tractography for planning of stereotactic irradiation of arteriovenous malformations.

Validation and Comparison

MEG-based localization of the SM1 cortex shows high agreement with DCS and fMRI—for a review, see, e.g., (67). Validation based on DCS has been mainly obtained for somatosensory evoked fields (67), to a smaller extent for motor evoked fields (85) or movement-related beta-band suppression (87), and on a few patients for CMC (67). To the best of our knowledge, such validation has not been reported for CKC. Discrepancies between MEG and DCS amount to about 10 mm (81). The comparison of DCS and MEG may however be limited by the spread of the stimulation electrical current, which is largely unknown in the individual case (67), as well as the sensitivity of MEG to sulcal rather than gyral-apical sources. Of note, the intersession reliability of MEG S1 cortex mapping based on electrical median nerve stimulation has been showed to be about 8 mm confidence interval around the estimated location of S1 cortex (79), which is not far from the reported average discrepancy between MEG and DCS.

In comparison to fMRI, MEG shows comparable, and in some patients even superior results (6, 73, 80, 97–102). Mean differences between somatosensory fMRI and MEG results are reported in the range from about 15 mm (73) to 23 mm (70), and for M1 cortex, localizations from 10 mm (73) to 27.9 mm (70). The comparably large variation may be caused by different experimental setups and analysis techniques. Klamer et al. (70), for example, used a distributed source model, whereas, Kober et al. (73) used single equivalent current dipole modeling. In addition, it should be noted that the accuracy of fMRI is also limited by noise, especially in suboptimal recording conditions, which are frequently encountered in clinical practice. High variability may therefore also originate from limited signal-to-noise ratio.

In patients with tumors or vascular lesions in the vicinity of the SM1 cortex, localization of SM1 cortex using fMRI may be difficult due to lesion-induced alterations of regional cerebral blood flow and susceptibility artifacts (103, 104). In these patients, MEG may provide superior results, due to the direct measurement of neuronal activity (105).

MEG also presents an additional key strength over fMRI, which is the ability to investigate in one single MEG session different neurophysiological processes (i.e., evoked magnetic responses, induced magnetic responses, and coupling between peripheral and cortical signals) that can be altered or affected differently by brain lesions or patients' clinical status. Thus, MEG provides the unique opportunity to acquire several MEG "functional localizers" of the SM1 cortex in a reasonable time for the patients (3). "Functional localizer" here refers to a given MEG mapping method to localize the SM1 cortex (see Somatosensory functional cortex mapping and Motor cortex mapping), regardless of the source reconstruction methods used (i.e., equivalent current dipole modeling, minimum norm estimate, spatial filtering approaches). The anatomical convergence of the different MEG functional localizers at the central sulcus has been demonstrated in healthy subjects for hand sensorimotor functional mapping and contributes to the assessment of the confidence level in non-invasive functional mapping results (compared with a uni- or bimodal approach) and to determine the clinical need to undergo further intracranial mapping procedures (3). It also represents a nice way to indirectly validate the localization accuracy of MEG mapping methods not validated by DCS (e.g., CKC) by comparing them with validated methods (e.g., somatosensory evoked fields, motor evoked fields, beta-band suppression). Such approach also increases the yield of MEG in case of failure, inaccurate or atypical localization of one MEG functional localizer or fMRI mapping (3, 67).

Navigated transcranial magnetic stimulation (nTMS) is increasingly applied for presurgical mapping of SM1 cortex (106). A number of studies have shown clinical value for resections of lesions in motor eloquent areas (107–109), as well as a good concordance with DCS (110–113) with, in some cases, smaller distances between nTMS and DCS vs. fMRI and DCS (110). Tarapore et al. (56) evaluated TMS, MEG and DCS for motor mapping in the same population and report distances of 2.13 ± 0.29 mm between TMS and DCS motor sites and 4.71 ± 1.08 mm between MEG and DCS.

Studies evaluating EEG for FCM of SM1 cortex are limited. Klamer et al. (70) compared high-density EEG (hdEEG) and MEG with a similar channel number with fMRI as reference standard. They reported, that, using volume conductor models based on the individual anatomy, source imaging relying on hdEEG may provide localizations that are closer to fMRI than MEG. Mean Euclidean distances were 21.7 mm between EEG and fMRI, and 27.9 mm between MEG and fMRI for motor activity. However, the comparably large deviations of both EEG and MEG suggest that both electromagnetic modalities may be sensitive to different aspects of neural activity than fMRI. This is further supported by deviations of fMRI itself from DCS localizations. Korvenoja et al. (6), for example, reported that fMRI was concordant with intraoperative findings in only 11 of 15 patients. Lascano et al. (69) found good concordance of source imaging relying on hdEEG and fMRI with distances of only 3 to 8 mm. Both, however, deviated from DCS by 13–14 mm. This study further supports the clinical value of EEG especially with a high number of channels. It also highlights the different perspectives of M/EEG, fMRI, and DCS mapping and illustrates the importance of the choice of a gold or, better, reference standard.

Memory Function

Due to the overlap in declarative memory function and lesions associated with mesial temporal lobe epilepsy (MTLE), memory impairment is common in this group of patients. Verbal memory decline can be observed in 30–85% of patients who undergo left temporal resection, whereas non-verbal memory deterioration after right (- or left) temporal resection affects 30–50% (51, 114–116).

IAT is considered the gold standard for the assessment of declarative memory function. Impaired memory performance is usually found in about 20–30 % of cases injected ipsilateral to

the seizure onset zone and in 60–80% after contralateral injection (117–119). Based on these results, several authors consider IAT results as a prognostic tool to predict postsurgical declarative memory, although results on the predictive value of IAT are contradictory and controversial (120–123), and memory results on repeated IAT are much less robust than those of verbal language testing (15).

In addition to the methodological drawbacks of IAT, there is no guarantee that amobarbital can be sufficiently delivered to the targeted hippocampal formation (124, 125).

fMRI, MEG, PET, and TMS, as well as several combined/integrated methods are non-invasive alternatives evaluated for declarative memory functional mapping (126).

In this context, fMRI is by far the most popular and widely used solution. For a comprehensive review, see e.g., (122).

To the best of our knowledge, MEG (or EEG) are not in (routine or validated) clinical use for declarative memory FCM. The most important obstacle might be the detection of hippocampal activation due to the limited sensitivity of MEG to deep sources—a problem that has been addressed, leading to the implementation of research protocols including the evaluation of deep structures via MEG (127–130). Clinical research in this area remains sparse. Maestú et al. (131) investigated verbal episodic memory in 9 patients with left MTLE in comparison to 9 healthy controls. MEG showed a left-hemisphere-dominant activation pattern in healthy controls, whereas patients' activation patterns showed mainly right-hemispheric dominance. Three patients underwent left anterior temporal lobectomy. They showed no significant postoperative memory loss and Engel class 1A/B outcome. These data suggest, that MEG has the potential to be used for memory FCM, but further studies are clearly needed.

Validation and Comparison

Even though it is considered the gold standard, the role of IAT in the prediction of postoperative declarative memory outcome remains controversial. Rathore et al. (123) reported memory outcome data on 116 patients after left anterior temporal lobe resection. Approximately one third of patients had "failed" IAT, meaning that test results indicated ipsilateral memory representation. After resection (operation was performed regardless of IAT-results), no difference was found between the group who failed and those who passed the IAT.

fMRI results show good concordance with IAT, which is also the basis for most validation studies. Throughout the literature, there is a great heterogeneity regarding the experimental paradigms used, but verbal memory tasks show the most consistent and clinically useful results (132).

To the best of our knowledge no validated method of declarative memory functional mapping relying on MEG or EEG exists.

Visual Cortex

Damage to the visual cortex or optic radiations may result in partial or complete anopia, whereas congenital defects or lesions might result in functional reorganization (133, 134). Presurgical FCM provides localization information of potentially displaced primary visual (V1) cortex either using EEG, MEG, or fMRI and thus helps to avoid such damage. Due to the fact that partial anopia is rather accepted by doctors and patients in certain circumstances, visual FCM is of limited clinical value. Therefore, functional mapping of V1 cortex is rarely applied in comparison to, e.g., FCM of verbal language or SM1 areas. Correspondingly, literature on application in clinical settings is sparse, in comparison to studies focusing on basic neuroscientific research of the visual system.

Early components of visual evoked activity in EEG and MEG (visual evoked potentials—VEP and visual evoked fields—VEF) localize to V1 cortex. Paradigms apply pattern reversal stimuli, such as checkerboards, presented to a hemifield or a single quadrant (135–137). Sources of early evoked activity occurring approximately 100 ms after stimulus onset (135, 138), i.e., pattern reversal, can be modeled using single equivalent current dipolar models (135). Presence of a lesion may result in prolonged latencies (139). Robustness of the method is critically dependent on stimulation quality, which is substantially influenced by the projection equipment and the variability of stimulus onset. Similar to approaches in language and motor systems (45, 83), MEG activations have been combined with tractography to support identification of V1 and the optic radiation (140).

Validation and Comparison

EEG-based visual evoked potentials are used for intraoperative neurophysiological monitoring, which evaluates response latencies and amplitudes rather than localization (141). Studies on presurgical EEG-based FCM of V1 cortex are lacking.

DCS, e.g., during invasive Video-EEG monitoring for presurgical evaluation of refractory focal epilepsy, provides high accuracy and selectivity for different aspects of the visual system (142). A comparison of MEG mapping with DCS has not been performed. In principle, TMS can stimulate and thus localize V1 cortex (143), however, clinical evidence is lacking. Consequently, there are no data available relating M/EEG to TMS.

fMRI has shown the ability to accurately localize V1 cortex and differentiate correlates of different stimulus aspects, such as visual field eccentricity and angular position by sophisticated paradigm design (144). Localization accuracy has been evaluated in comparison to DCS in a handful of studies (145, 146), which nevertheless show very high concordance rates. Comparisons between EEG and MEG V1 cortex FCM are not available.

Auditory Cortex

Auditory mapping is clinically applied in patients with lesions or structural alterations within or near Heschl's gyrus (147). Lesional growth may lead to displacement and also reorganization of primary auditory areas. Identification by using anatomical landmarks alone may be challenging in few cases. Cortical deafness as a result of a lesion or surgical procedure is, however, a rare complication due to the redundant bilateral representation (148). This explains why auditory FCM is actually of limited clinical usefulness. Latencies and amplitudes of, e.g., the N100 response or its magnetic counterpart M100 (or N100 m) may be changed in patients with autism (149, 150), dyslexia (151), corticobasal degeneration (152), ischemic lesions (153), and tumors (147).

Auditory stimulation in EEG/MEG recordings typically use monaural presentation of brief sine or click tones with white noise masking of the contralateral ear (60). Averages of 200–500 trials are then analyzed regarding amplitudes and latencies. Localization analysis usually focuses on the N/M100 response and relies on equivalent current dipole modeling. Early brainstem auditory evoked potentials are not well-recorded with MEG (60), but are detectable when using a considerably larger number of averages (154).

Uni- and bilateral auditory stimulation results in bilateral activation of auditory cortices, reflected by bilateral dipolar generators. In EEG, this leads to merging potentials with a maximum negativity over the vertex and positivity over the basal temporal lobes. Due to the different sensitivity and rotated orientation of magnetic fields, the two components are easier to separate in MEG. Furthermore, generators of auditory activity have a predominantly tangential orientation, which improves SNR in MEG (155).

Validation and Comparison

Early studies have shown the accuracy of MEG (156, 157) and EEG (158) to localize auditory evoked activity (159). Scarff et al. (160) conducted EEG-fMRI measurements of auditory evoked activity. They reported good concordance of both methods in the horizontal plane. However, EEG dipoles localized more cranially than fMRI. Increasing the number of electrodes from 64 to 128 improved the concordance. Shahin et al. (161) evaluated auditory activity with simultaneous recordings of MEG and EEG and reported a good concordance regarding localization, although source amplitudes differed depending on the orientation of generators. Between-subject-variability of localizations was lower in MEG compared to EEG. Studies comparing accuracy of MEG, EEG and DCS or nTMS for identification of the auditory cortex in a clinical context are not available.

New Approaches

The evaluation of functional connectivity has gained considerable interest in the last years, partially due to methodological and technical advances. Going beyond the absolute activation and focusing on functional integration patterns between brain areas has opened new opportunities for FCM. These new approaches enable identification of functional networks, rather than task-based individual activated areas. The main hypothesis assumes that this provides a more complete and realistic view of human brain function. While most studies currently focus on physiological activity in healthy subjects, there are promising findings with potential for novel clinical application (162). For example, Doesburg et al. (163) showed functional connectivity and cross-frequency modulation in the gamma and theta frequency bands during a verb generation paradigm in expressive language networks. These findings did not necessarily coincide with the localization of, e.g., task-based gamma power modulations. Although they observed this functional connectivity structure in left- and right-sided regions, cross-frequency modulations were more pronounced in the left frontal cortex and particularly in the inferior frontal gyrus. Such features of neuronal communication may therefore represent candidates for potentially more specific FCM of, e.g., verbal language-related brain areas.

Evaluation of functional connectivity patterns in the resting brain (i.e., in the absence of any explicit task) potentially also provides relevant information for localization of functionally eloquent cortices in fMRI (164) and MEG (165). Martino et al. (164) evaluated such resting state functional connectivity (rsFC) in the vicinity of tumors and compared the results with DCS. Decreased rsFC in the tumor vicinity was associated with absence of eloquent cortex (via DCS) in all cases, while increased rsFC indicated the presence of eloquent cortex (via DCS) in 64% of patients. Tarapore et al. (165) utilized the rsFC method in MEG to predict postoperative functional deficits in patients undergoing glioma surgery. They showed that patients with increased rsFC in the tumor area presented with new neurological deficits in 25% of cases at 6 months after surgery vs. 0% in patients with decreased rsFC. These findings are corroborated by similar results using resting state fMRI data (166). The main limitation of such approaches is currently the limited availability of clinical studies. In addition, analysis methodology is complex and diverse, with little standardization at this point. Furthermore, the specific functional significance of individual resting state and connectivity measures remains largely unclear (166) and requires further investigation.

Machine learning algorithms are transforming multiple medical fields. Clinical applications are already in use in various domains—predominantly in image processing, classification and segmentation (167). Roland et al. (168) used a machine learning approach on resting state fMRI for sensorimotor cortex mapping and compared results with DCS in 16 pediatric patients with epilepsy. The authors report comparable functional localization between the two methods.

In the future, machine learning might find further application in FCM, e.g., based on methods and findings in the field of brain-computer interfaces (169). However, specific analysis protocols, thorough evaluation of the applied algorithms and clinical validation are lacking at this time.

Finally, studies demonstrated that FCM based on the investigation of event related enhancement of high gamma activity as recorded by invasive recordings or electrocorticography during awake craniotomy might be of high interest for the mapping of verbal language and motor eloquent cortex (170–173). Still, this approach is mainly used in some specialized centers and further validation studies are needed.

DISCUSSION

For any validation of FCM methods, the choice of the reference standard used to validate the methods is crucial. DCS either intraoperatively or during invasive monitoring with subdural or depth electrodes is considered as one gold standard. However, data on current flow from the electrodes through the cortex is sparse in addition to how such currents interact with the neuronal architecture beyond single cell responses. In addition, different methods might be sensitive to different aspects of neural

activity. Lascano et al. (69) described a systematic difference between hdEEG and fMRI regarding S1 cortex localization, with fMRI showing more lateral activation. The authors argued that this discrepancy may be caused by EEG detecting early activity in Brodmann area 3b, while fMRI would reflect more integrative processes in the more lateral Brodmann area 1.

In addition, the predictive value of DCS itself may be limited, as illustrated by Ilmberger et al (61). The authors report on the outcome of intraoperative mapping of language functions in 149 tumor patients. One of the main risk factors for early postoperative disturbances was a DCS language-positive site within the tumor. However, only 53% of these patients developed a new postoperative deficit. Furthermore, 7 months after surgery, only pre- or postoperative aphasia, and increased age were associated with persisting deficits. Positive stimulation sites within the resected tumor did no longer show a significant influence. While subtle deficits of language function may not have been considered, the predictive value of DCS was therefore limited to early postoperative language function in a portion of the patients. It ultimately did not affect the outcome after this initial phase. This overestimation of functional involvement, as also found in the non-invasive alternatives, does not necessarily contradict clinical utility. However, it imposes limits on the validity of DCS as a "ground-truth" gold standard, potentially also since it does not and potentially cannot take postoperative reorganization phenomena into account.

In a prospective clinical study by Hermann et al. (46), resection of presumed verbal language eloquent cortex in the superior temporal gyrus was compared with sparing these areas. Postoperative outcomes showed no significant difference in visual confrontation naming. Since intraoperative DCS was not performed, it can only be assumed but is not proven, that language eloquent cortex was resected. As patients underwent classical anterior temporal lobe resections it should be pointed out, that results arguably might have been different, if more extensive resective approaches had been applied. Furthermore, evaluation of subtle verbal language deficits is challenging, especially as postoperative reorganization may mask these.

Tate et al. (174) identified areas in the non-dominant hemisphere, the stimulation of which led to speech arrest. However, only patients with low grade glioma were evaluated, implying that such reorganization may have led to a shift of verbal language-related areas.

Especially in patients with atypical hemispheric dominance, all non-invasive methods show limitations. Bauer et al. (175) published a meta-analysis of fMRI vs. IAT for verbal language lateralization. They reported a concordance rate of 91% in patients with typical language lateralization. However, in patients with atypical lateralization, concordance rate dropped to only 51%. Similarly, while MEG-based verbal language lateralization was concordant with IAT in 32 of 35 patients in a study by Tanaka et al. (176), the remaining were patients with bilateral language representation. In addition, Picht et al. (112) reported overestimation of areas involved in verbal language processing by TMS, underlining that this issue does not seem to be a problem of a single modality, e.g., due to limitation of data quality, etc.

In light of these limitations, non-invasive localization methods that seek to go beyond mere lateralization can provide only a conservative estimate of essential functional cortex. If such areas are spared by the neurosurgical procedure, functional deficit can thus probably be avoided in most cases. However, on the other hand, a portion of these regions could potentially be resected without any functional deterioration, e.g., to achieve gross total resection in tumor surgery or to completely remove the epileptogenic zone. In the context of epilepsy surgery, this "conservative" perspective on functionally eloquent cortex may be warranted, especially as quality of life is the central goal. However, tumor surgery requires more aggressive strategies, which would benefit from increased specificity. Focusing on patients undergoing tumor surgery might therefore help to better determine if this conservative approach is indeed mandatory in all situations.

The current challenge is to identify markers, which provide a more accurate and robust estimation of this essential, necessary cortex.

In general, studies on the direct comparison of different FCM methods in the same patient population are sparse. Most publications focus on the diagnostic accuracy of a single method vs. a mostly invasive reference standard, i.e., DCS or IAT, etc. When postsurgical outcomes are considered, follow-ups are frequently short. Only limited data is available relating presurgical FCM to long-term outcomes and functional reorganization. Results on clinical M/EEG FCM of the auditory or visual system are generally sparse, potentially due to the limited clinical relevance. A main issue for validation of not only M/EEG-based FCM, but also the prognostic value of fMRI, TMS, and even DCS is the very limited availability of prospective, randomized clinical studies.

While EEG and MEG register similar activity with differences in sensitivity, EEG is rarely applied for FCM in a clinical context. This is in stark contrast to the wide utilization of EEG in clinical routine for diagnosis and in neurocognitive studies (177), although these latter ones frequently focus on group sensor-level results rather than specific brain localizations at the individual level. HdEEG is a promising alternative to fMRI and MEG for FCM in a clinical setting though it requires more studies focusing on this application.

Both MEG and EEG are sparsely used for FCM in tumor patients in comparison to, e.g., fMRI, while most clinical MEG centers perform functional mapping in the context of epilepsy surgery (178, 179). Reasons for the sparse application may be limited availability of reimbursement in many countries and the subsequent constrained access to MEG, but also HdEEG. Furthermore, a wide spectrum of methodological approaches without a clear gold-standard procedure complicates implementation and application in clinical routine, while technical challenges, e.g., to integrate results into neuronavigation, have been solved (81, 180, 181). Further development of existing clinical practice guidelines (60, 182) as well as

comparative and prospective studies would certainly impact practical application.

In conclusion, electromagnetic source imaging provides additional information for functional mapping with reasonable spatial resolution, exquisite temporal resolution and direct information about neural activity. Due to their non-invasive nature, these methods can be applied early in the presurgical workup and can be utilized to optimize the application of invasive means, such as DCS. Further evaluation is needed to investigate their respective clinical added-value.

AUTHOR CONTRIBUTIONS

All authors listed have made a substantial, direct and intellectual contribution to the work, and approved it for publication.

ACKNOWLEDGMENTS

XD is Postdoctorate Clinical Master Specialist at the Fonds de la Recherche Scientifique (FRS-FNRS, Brussels, Belgium). The MEG project at the CUB Hôpital Erasme is financially supported by the Fonds Erasme (Brussels, Belgium).

REFERENCES

1. Rosenow F, Lüders H. Presurgical evaluation of epilepsy. *Brain.* (2001) 124:1683–700. doi: 10.1093/brain/124.9.1683
2. Towle VL, Khorasani L, Uftring S, Pelizzari C, Erickson RK, Spire J-P, et al. Noninvasive identification of human central sulcus: a comparison of gyral morphology, functional MRI, dipole localization, and direct cortical mapping. *Neuroimage.* (2003) 19:684–97. doi: 10.1016/S1053-8119(03)00147-2
3. Bourguignon M, Jousmäki V, Marty B, Wens V, Beeck MO de, Bogaert PV, et al. Comprehensive functional mapping scheme for non-invasive primary sensorimotor cortex mapping. *Brain Topogr.* (2013) 26:511–23. doi: 10.1007/s10548-012-0271-9
4. Bourguignon M, De Tiège X, Op de Beeck M, Pirotte B, Van Bogaert P, Goldman S, et al. Functional motor-cortex mapping using corticokinematic coherence. *Neuroimage.* (2011) 55:1475–9. doi: 10.1016/j.neuroimage.2011.01.031
5. Duncan JS, Winston GP, Koepp MJ, Ourselin S. Brain imaging in the assessment for epilepsy surgery. *Lancet Neurol.* (2016) 15:420–33. doi: 10.1016/S1474-4422(15)00383-X
6. Korvenoja A, Kirveskari E, Aronen HJ, Avikainen S, Brander A, Huttunen J, et al. Sensorimotor cortex localization: comparison of magnetoencephalography, functional MR imaging, and intraoperative cortical mapping. *Radiology.* (2006) 241:213–22. doi: 10.1148/radiol.2411050796
7. Bartsch AJ, Homola G, Biller A, Solymosi L, Bendszus M. Diagnostic functional MRI: illustrated clinical applications and decision-making. *J Magn Reson Imaging.* (2006) 23:921–32. doi: 10.1002/jmri.20579
8. D'Esposito M, Deouell LY, Gazzaley A. Alterations in the BOLD fMRI signal with ageing and disease: a challenge for neuroimaging. *Nat Rev Neurosci.* (2003) 4:863–72. doi: 10.1038/nrn1246
9. Kuchcinski G, Mellerio C, Pallud J, Dezamis E, Turc G, Rigaux-Viodé O, et al. Three-tesla functional MR language mapping: comparison with direct cortical stimulation in gliomas. *Neurology.* (2015) 84:560–8. doi: 10.1212/WNL.0000000000001226
10. Hillebrand A, Barnes GR. A quantitative assessment of the sensitivity of whole-head MEG to activity in the adult human cortex. *Neuroimage.* (2002) 16:638–50. doi: 10.1006/nimg.2002.1102
11. de Jongh A, de Munck JC, Gonçalves SI, Ossenblok P. Differences in MEG/EEG epileptic spike yields explained by regional differences in signal-to-noise ratios. *J Clin Neurophysiol.* (2005) 22:153–8. doi: 10.1097/01.WNP.0000158947.68733.51
12. Riitta Hari MD, Aina Puce P. *MEG-EEG Primer*. Oxford University Press Available at: http://oxfordmedicine.com/view/10.1093/med/9780190497774.001.0001/med-9780190497774 (accessed September 15, 2018)
13. Aydin Ü, Vorwerk J, Dümpelmann M, Küpper P, Kugel H, Heers M, et al. Combined EEG/MEG can outperform single modality EEG or MEG source reconstruction in presurgical epilepsy diagnosis. *PLoS ONE.* (2015) 10:e0118753. doi: 10.1371/journal.pone.0118753
14. Picht T. Current and potential utility of transcranial magnetic stimulation in the diagnostics before brain tumor surgery. *CNS Oncol.* (2014) 3:299–310. doi: 10.2217/cns.14.25
15. Lehtinen H, Mäkelä JP, Mäkelä T, Lioumis P, Metsähonkala L, Hokkanen L, et al. Language mapping with navigated transcranial magnetic stimulation in pediatric and adult patients undergoing epilepsy surgery: comparison with extraoperative direct cortical stimulation. (2018) 3:224–35. doi: 10.1002/epi4.12110
16. Krieg SM, Sabih J, Bulubasova L, Obermueller T, Negwer C, Janssen I, et al. Preoperative motor mapping by navigated transcranial magnetic brain stimulation improves outcome for motor eloquent lesions. *Neuro Oncol.* (2014) 16:1274–82. doi: 10.1093/neuonc/nou007
17. Ille S, Sollmann N, Butenschoen VM, Meyer B, Ringel F, Krieg SM. Resection of highly language-eloquent brain lesions based purely on rTMS language mapping without awake surgery. *Acta Neurochir.* (2016) 158:2265–75. doi: 10.1007/s00701-016-2968-0
18. Wada J, Rasmussen T. Intracarotid injection of sodium amytal for the lateralization of cerebral speech dominance 1960. *J Neurosurg.* (2007) 106:1117–33. doi: 10.3171/jns.2007.106.6.1117
19. Rouleau I, Robidoux J, Labrecque R, Denault C. Effect of focus lateralization on memory assessment during the intracarotid amobarbital procedure. *Brain Cogn.* (1997) 33:224–41. doi: 10.1006/brcg.1997.0894
20. Loddenkemper T, Morris HH, Lineweaver TT, Kellinghaus C. Repeated intracarotid amobarbital tests. *Epilepsia.* (2007) 48:553–8. doi: 10.1111/j.1528-1167.2007.00982.x
21. Papanicolaou AC, Rezaie R, Narayana S, Choudhri AF, Abbas-Babajani-Feremi null, Boop FA, et al. On the relative merits of invasive and non-invasive pre-surgical brain mapping: new tools in ablative epilepsy surgery. *Epilepsy Res.* (2018) 142:153–5. doi: 10.1016/j.eplepsyres.2017.07.002
22. Szelényi A, Bello L, Duffau H, Fava E, Feigl GC, Galanda M, et al. Intraoperative electrical stimulation in awake craniotomy: methodological aspects of current practice. *Neurosurgical Focus.* (2010) 28:E7. doi: 10.3171/2009.12.FOCUS09237
23. Hickok G. The functional neuroanatomy of language. *Phys Life Rev.* (2009) 6:121–43. doi: 10.1016/j.plrev.2009.06.001
24. Middlebrooks EH, Yagmurlu K, Szaflarski JP, Rahman M, Bozkurt B. A contemporary framework of language processing in the human brain in the context of preoperative and intraoperative language mapping. *Neuroradiology.* (2017) 59:69–87. doi: 10.1007/s00234-016-1772-0
25. Pujol J, Deus J, Losilla JM, Capdevila A. Cerebral lateralization of language in normal left-handed people studied by functional MRI. *Neurology.* (1999) 52:1038–43. doi: 10.1212/WNL.52.5.1038
26. Springer JA, Binder JR, Hammeke TA, Swanson SJ, Frost JA, Bellgowan PSF et al. Language dominance in neurologically normal and epilepsy subjectsA functional MRI study. *Brain.* (1999) 122:2033–46. doi: 10.1093/brain/122.11.2033
27. Helmstaedter C, Kurthen M, Linke DB, Elger CE. Patterns of language dominance in focal left and right hemisphere epilepsies: relation to MRI findings, EEG, sex, and age at onset of epilepsy. *Brain Cogn.* (1997) 33:135–50. doi: 10.1006/brcg.1997.0888
28. Pirmoradi M, Béland R, Nguyen DK, Bacon BA, Lassonde M. Language tasks used for the presurgical assessment of epileptic patients with MEG. *Epileptic Disorders.* (2010) 12:97–108. doi: 10.1684/epd.2010.0314
29. Papanicolaou AC, Simos PG, Castillo EM, Breier JI, Sarkari S, Pataraia E, et al. Magnetocephalography: a noninvasive alternative

to the Wada procedure. *J Neurosurgery.* (2004) 100:867–76. doi: 10.3171/jns.2004.100.5.0867
30. Breier JI, Simos PG, Wheless JW, Constantinou JE, Baumgartner JE, Venkataraman V, et al. Language dominance in children as determined by magnetic source imaging and the intracarotid amobarbital procedure: a comparison. *J Child Neurol.* (2001) 16:124–30. doi: 10.1177/088307380101600211
31. Breier JI, Simos PG, Zouridakis G, Wheless JW, Willmore LJ, Constantinou JE, et al. Language dominance determined by magnetic source imaging: a comparison with the Wada procedure. *Neurology.* (1999) 53:938–45. doi: 10.1212/WNL.53.5.938
32. Doss RC, Zhang W, Risse GL, Dickens DL. Lateralizing language with magnetic source imaging: validation based on the Wada test. *Epilepsia.* (2009) 50:2242–8. doi: 10.1111/j.1528-1167.2009.02242.x
33. Papanicolaou AC, Simos PG, Breier JI, Zouridakis G, Willmore LJ, Wheless JW, et al. Magnetoencephalographic mapping of the language-specific cortex. *J Neurosurg.* (1999) 90:85–93. doi: 10.3171/jns.1999.90.1.0085
34. Simos PG, Papanicolaou AC, Breier JI, Wheless JW, Constantinou JE, Gormley WB, et al. Localization of language-specific cortex by using magnetic source imaging and electrical stimulation mapping. *J Neurosurg.* (1999) 91:787–96. doi: 10.3171/jns.1999.91.5.0787
35. Hirata M, Kato A, Taniguchi M, Saitoh Y, Ninomiya H, Ihara A, et al. Determination of language dominance with synthetic aperture magnetometry: comparison with the wada test. *Neuroimage.* (2004) 23:46–53. doi: 10.1016/j.neuroimage.2004.05.009
36. Wilenius J, Lehtinen H, Paetau R, Salmelin R, Kirveskari E. A simple magnetoencephalographic auditory paradigm may aid in confirming left-hemispheric language dominance in epilepsy patients. *PLoS ONE.* (2018) 13:e0200073. doi: 10.1371/journal.pone.0200073
37. Bowyer SM, Moran JE, Weiland BJ, Mason KM, Greenwald ML, Smith BJ, et al. Language laterality determined by MEG mapping with MR-FOCUSS. *Epilepsy Behav.* (2005) 6:235–41. doi: 10.1016/j.yebeh.2004.12.002
38. Rezaie R, Narayana S, Schiller K, Birg L, Wheless JW, Boop FA, et al. Assessment of hemispheric dominance for receptive language in pediatric patients under sedation using magnetoencephalography. *Front Hum Neurosci.* (2014) 8:657. doi: 10.3389/fnhum.2014.00657
39. Van Poppel M, Wheless JW, Clarke DF, McGregor A, McManis MH, Perkins FF, et al. Passive language mapping with magnetoencephalography in pediatric patients with epilepsy. *J Neurosurg Pediatr.* (2012) 10:96–102. doi: 10.3171/2012.4.PEDS11301
40. Kamada K, Sawamura Y, Takeuchi F, Kuriki S, Kawai K, Morita A, et al. Expressive and receptive language areas determined by a non-invasive reliable method using functional magnetic resonance imaging and magnetoencephalography. *Neurosurgery.* (2007) 60:296–305; discussion 305–306. doi: 10.1227/01.NEU.0000249262.03451.0E
41. Breier JI, Castillo EM, Simos PG, Billingsley-Marshall RL, Pataraia E, Sarkari S, et al. Atypical language representation in patients with chronic seizure disorder and achievement deficits with magnetoencephalography. *Epilepsia.* (2005) 46:540–8. doi: 10.1111/j.0013-9580.2005.48904.x
42. Hirata M, Goto T, Barnes G, Umekawa Y, Yanagisawa T, Kato A, et al. Language dominance and mapping based on neuromagnetic oscillatory changes: comparison with invasive procedures. *J f Neurosurg.* (2009) 112:528–38. doi: 10.3171/2009.7.JNS09239
43. Bowyer SM, Fleming T, Greenwald ML, Moran JE, Mason KM, Weiland BJ, et al. Magnetoencephalographic localization of the basal temporal language area. *Epilepsy Behav.* (2005) 6:229–34. doi: 10.1016/j.yebeh.2004.12.003
44. Kamada K, Takeuchi F, Kuriki S, Todo T, Morita A, Sawamura Y. Dissociated expressive and receptive language functions on magnetoencephalography, functional magnetic resonance imaging, and amobarbital studies. case report and review of the literature. *J Neurosurg.* (2006) 104:598–607. doi: 10.3171/jns.2006.104.4.598
45. Kamada K, Todo T, Masutani Y, Aoki S, Ino K, Morita A, et al. Visualization of the frontotemporal language fibers by tractography combined with functional magnetic resonance imaging and magnetoencephalography. *J Neurosurg.* (2007) 106:90–8. doi: 10.3171/jns.2007.106.1.90
46. Hermann B, Davies K, Foley K, Bell B. Visual confrontation naming outcome after standard left anterior temporal lobectomy with sparing versus resection of the superior temporal gyrus: a randomized prospective clinical trial. *Epilepsia.* (1999) 40:1070–6. doi: 10.1111/j.1528-1157.1999.tb00821.x
47. Mnatsakanyan L, Vadera S, Ingalls CW, Zheng J, Sazgar M, Hsu FP, et al. Language recovery after epilepsy surgery of the Broca's area. *Epilepsy Behav Case Rep.* (2018) 9:42–5. doi: 10.1016/j.ebcr.2017.06.002
48. Hamberger MJ, Williams AC, Schevon CA. Extraoperative neurostimulation mapping: results from an international survey of epilepsy surgery programs. *Epilepsia.* (2014) 55:933–9. doi: 10.1111/epi.12644
49. Raffa G, Quattropani MC, Scibilia A, Conti A, Angileri FF, Esposito F, et al. Surgery of language-eloquent tumors in patients not eligible for awake surgery: the impact of a protocol based on navigated transcranial magnetic stimulation on presurgical planning and language outcome, with evidence of tumor-induced intra-hemispheric plasticity. *Clin Neurol Neurosurg.* (2018) 168:127–39. doi: 10.1016/j.clineuro.2018.03.009
50. Sabsevitz DS, Swanson SJ, Hammeke TA, Spanaki MV, Possing ET, Morris GL, et al. Use of preoperative functional neuroimaging to predict language deficits from epilepsy surgery. *Neurology.* (2003) 60:1788–1792. doi: 10.1212/01.WNL.0000068022.05644.01
51. Bonelli SB, Powell RHW, Yogarajah M, Samson RS, Symms MR, Thompson PJ, et al. Imaging memory in temporal lobe epilepsy: predicting the effects of temporal lobe resection. *Brain.* (2010) 133:1186–99. doi: 10.1093/brain/awq006
52. Coolen T, Dumitrescu AM, Bourguignon M, Wens V, Urbain C, De Tiège X. Presurgical electromagnetic functional brain mapping in refractory focal epilepsy. *Z Epileptol.* (2018) 31:203–12. doi: 10.1007/s10309-018-0189-7
53. Giussani C, Roux F-E, Ojemann J, Sganzerla EP, Pirillo D, Papagno C. Is preoperative functional magnetic resonance imaging reliable for language areas mapping in brain tumor surgery? review of language functional magnetic resonance imaging and direct cortical stimulation correlation studies. *Neurosurgery.* (2010) 66:113–20. doi: 10.1227/01.NEU.0000360392.15450.C9
54. Schmid E, Thomschewski A, Taylor A, Zimmermann G, Kirschner M, Kobulashvili T, et al. Diagnostic accuracy of functional magnetic resonance imaging, wada test, magnetoencephalography, and functional transcranial doppler sonography for memory and language outcome after epilepsy surgery: a systematic review. *Epilepsia.* (2018) 59:2305–17. doi: 10.1111/epi.14588
55. Babajani-Feremi A, Holder CM, Narayana S, Fulton SP, Choudhri AF, Boop FA, et al. Predicting postoperative language outcome using presurgical fMRI, MEG, TMS, and high gamma ECoG. *Clin Neurophys.* (2018) 129:560–71. doi: 10.1016/j.clinph.2017.12.031
56. Tarapore PE, Findlay AM, Honma SM, Mizuiri D, Houde JF, Berger MS, et al. Language mapping with navigated repetitive TMS: proof of technique and validation. *NeuroImage.* (2013) 82:260–72. doi: 10.1016/j.neuroimage.2013.05.018
57. Picht T, Krieg SM, Sollmann N, Rösler J, Niraula B, Neuvonen T, et al. A comparison of language mapping by preoperative navigated transcranial magnetic stimulation and direct cortical stimulation during awake surgery. *Neurosurgery.* (2013) 72:808–19. doi: 10.1227/NEU.0b013e3182889e01
58. Ille S, Sollmann N, Hauck T, Maurer S, Tanigawa N, Obermueller T, et al. Impairment of preoperative language mapping by lesion location: a functional magnetic resonance imaging, navigated transcranial magnetic stimulation, and direct cortical stimulation study. *J Neurosurg.* (2015) 123:314–24. doi: 10.3171/2014.10.JNS141582
59. Ille S, Sollmann N, Hauck T, Maurer S, Tanigawa N, Obermueller T, et al. Combined noninvasive language mapping by navigated transcranial magnetic stimulation and functional MRI and its comparison with direct cortical stimulation. *J Neurosurg.* (2015) 123:212–25. doi: 10.3171/2014.9.JNS14929
60. Burgess RC, Funke ME, Bowyer SM, Lewine JD, Kirsch HE, Bagić AI. American clinical magnetoencephalography society clinical practice guideline 2: presurgical functional brain mapping using magnetic evoked fields. *J Clin Neurophysiol.* (2011) 28:355–61. doi: 10.1097/WNP.0b013e3182272ffe
61. Ilmberger J, Ruge M, Kreth F-W, Briegel J, Reulen H-J, Tonn J-C. Intraoperative mapping of language functions: a longitudinal neurolinguistic analysis. *J Neurosurgery.* (2008) 109:583–92. doi: 10.3171/JNS/2008/109/10/0583

62. Sanai N, Mirzadeh Z, Berger MS. Functional outcome after language mapping for glioma resection. *N Engl J Med.* (2008) 358:18–27. doi: 10.1056/NEJMoa067819
63. Cervenka MC, Corines J, Boatman-Reich DF, Eloyan A, Sheng X, Franaszczuk PJ, et al. Electrocorticographic functional mapping identifies human cortex critical for auditory and visual naming. *NeuroImage.* (2013) 69:267. doi: 10.1016/j.neuroimage.2012.12.037
64. De Tiège X, Connelly A, Liégeois F, Harkness W, Clark CA, Chong WK, et al. Influence of motor functional magnetic resonance imaging on the surgical management of children and adolescents with symptomatic focal epilepsy. *Neurosurgery.* (2009) 64:856–64; discussion 864. doi: 10.1227/01.NEU.0000343741.54200.58
65. Ward N. Assessment of cortical reorganisation for hand function after stroke. *The Journal of Physiology.* (2011) 589:5625–32. doi: 10.1113/jphysiol.2011.220939
66. Mäkelä JP. 5.03 - Bioelectric measurements: magnetoencephalography. In: Brahme A, editor. *Comprehensive Biomedical Physics*. Oxford: Elsevier (2014). p. 47–72.
67. Mäkelä JP, Forss N, Jääskeläinen J, Kirveskari E, Korvenoja A, Paetau R. Magnetoencephalography in neurosurgery. *Neurosurgery.* (2006) 59:493–510; discussion 510–511. doi: 10.1227/01.NEU.0000232762.63508.11
68. Stufflebeam SM, Tanaka N, Ahlfors SP. Clinical applications of magnetoencephalography. *Hum Brain Mapp.* (2009) 30:1813–23. doi: 10.1002/hbm.20792
69. Lascano AM, Grouiller F, Genetti M, Spinelli L, Seeck M, Schaller K, et al. Surgically relevant localization of the central sulcus with high-density somatosensory-evoked potentials compared with functional magnetic resonance imaging. *Neurosurgery.* (2014) 74:517–26. doi: 10.1227/NEU.0000000000000298
70. Klamer S, Elshahabi A, Lerche H, Braun C, Erb M, Scheffler K, et al. Differences between MEG and high-density EEG source localizations using a distributed source model in comparison to fMRI. *Brain Topogr.* (2015) 28:87–94. doi: 10.1007/s10548-014-0405-3
71. Bast T, Wright T, Boor R, Harting I, Feneberg R, Rupp A, et al. Combined EEG and MEG analysis of early somatosensory evoked activity in children and adolescents with focal epilepsies. *Clin Neurophysiol.* (2007) 118:1721–35. doi: 10.1016/j.clinph.2007.03.037
72. Sutherling WW, Crandall PH, Darcey TM, Becker DP, Levesque MF, Barth DS. The magnetic and electric fields agree with intracranial localizations of somatosensory cortex. *Neurology.* (1988) 38:1705–14. doi: 10.1212/WNL.38.11.1705
73. Kober H, Nimsky C, Möller M, Hastreiter P, Fahlbusch R, Ganslandt O. Correlation of sensorimotor activation with functional magnetic resonance imaging and magnetoencephalography in presurgical functional imaging: a spatial analysis. *Neuroimage.* (2001) 14:1214–28. doi: 10.1006/nimg.2001.0909
74. Mäkelä JP, Kirveskari E, Seppä M, Hämäläinen M, Forss N, Avikainen S, et al. Three-dimensional integration of brain anatomy and function to facilitate intraoperative navigation around the sensorimotor strip. *Hum Brain Mapp.* (2001) 12:180–92. doi: 10.1002/1097-0193(200103)12:3<180::AID-HBM1014>3.0.CO;2-N
75. Cheyne D, Bostan AC, Gaetz W, Pang EW. Event-related beamforming: a robust method for presurgical functional mapping using MEG. *Clin Neurophysiol.* (2007) 118:1691–704. doi: 10.1016/j.clinph.2007.05.064
76. Willemse RB, de Munck JC, van't Ent D, Ris P, Baayen JC, Stam CJ, et al. Magnetoencephalographic study of posterior tibial nerve stimulation in patients with intracranial lesions around the central sulcus. *Neurosurgery.* (2007) 61:1209–17; discussion 1217–8. doi: 10.1227/01.neu.0000306099.45764.5c
77. Willemse RB, Hillebrand A, Ronner HE, Vandertop WP, Stam CJ. Magnetoencephalographic study of hand and foot sensorimotor organization in 325 consecutive patients evaluated for tumor or epilepsy surgery. *Neuroimage Clin.* (2016) 10:46–53. doi: 10.1016/j.nicl.2015.11.002
78. Vitikainen A-M, Lioumis P, Paetau R, Salli E, Komssi S, Metsähonkala L, et al. Combined use of non-invasive techniques for improved functional localization for a selected group of epilepsy surgery candidates. *Neuroimage.* (2009) 45:342–8. doi: 10.1016/j.neuroimage.2008.12.026
79. Solomon J, Boe S, Bardouille T. Reliability for non-invasive somatosensory cortex localization: Implications for pre-surgical mapping. *Clin Neurol Neurosurg.* (2015) 139:224–229. doi: 10.1016/j.clineuro.2015.10.001
80. Roberts TP, Rowley HA. Mapping of the sensorimotor cortex: functional MR and magnetic source imaging. *AJNR Am J Neuroradiol.* (1997) 18:871–880.
81. Schiffbauer H, Berger MS, Ferrari P, Freudenstein D, Rowley HA, Roberts TPL. Preoperative magnetic source imaging for brain tumor surgery: a quantitative comparison with intraoperative sensory and motor mapping. *J Neurosurg.* (2002) 97:1333–42. doi: 10.3171/jns.2002.97.6.1333
82. Castillo EM, Simos PG, Wheless JW, Baumgartner JE, Breier JI, Billingsley RL, et al. Integrating sensory and motor mapping in a comprehensive MEG protocol: clinical validity and replicability. *Neuroimage.* (2004) 21:973–83. doi: 10.1016/j.neuroimage.2003.10.020
83. Kamada K, Houkin K, Takeuchi F, Ishii N, Ikeda J, Sawamura Y, et al. Visualization of the eloquent motor system by integration of MEG, functional, and anisotropic diffusion-weighted MRI in functional neuronavigation. *Surg Neurol.* (2003) 59:352–361; discussion 361-362. doi: 10.1016/S0090-3019(03)00018-1
84. Lin PT, Berger MS, Nagarajan SS. Motor field sensitivity for preoperative localization of motor cortex. *J Neurosurg.* (2006) 105:588–594. doi: 10.3171/jns.2006.105.4.588
85. Gaetz W, Cheyne D, Rutka JT, Drake J, Benifla M, Strantzas S, et al. Presurgical localization of primary motor cortex in pediatric patients with brain lesions by the use of spatially filtered magnetoencephalography. *Oper Neurosurg.* (2009) 64:ONS177–86. doi: 10.1227/01.NEU.0000316433.10913.32
86. Jasper H, Penfield W. Electrocorticograms in man: effect of voluntary movement upon the electrical activity of the precentral gyrus. *Arch F Psychiatr U Z Neur.* (1949) 183:163–74. doi: 10.1007/BF01062488
87. Nagarajan S, Kirsch H, Lin P, Findlay A, Honma S, Berger MS. Preoperative localization of hand motor cortex by adaptive spatial filtering of magnetoencephalography data. *J Neurosurg.* (2008) 109:228–37. doi: 10.3171/JNS/2008/109/8/0228
88. Taniguchi M, Kato A, Fujita N, Hirata M, Tanaka H, Kihara T, et al. Movement-related desynchronization of the cerebral cortex studied with spatially filtered magnetoencephalography. *Neuroimage.* (2000) 12:298–306. doi: 10.1006/nimg.2000.0611
89. Willemse RB, de Munck JC, Verbunt JPA, van 't Ent D, Ris P, Baayen JC, et al. Topographical organization of mu and Beta band activity associated with hand and foot movements in patients with perirolandic lesions. *Open Neuroimag J.* (2010) 4:93–9. doi: 10.2174/1874440001004010093
90. Salmelin R, Hämäläinen M, Kajola M, Hari R. Functional segregation of movement-related rhythmic activity in the human brain. *Neuroimage.* (1995) 2:237–43. doi: 10.1006/nimg.1995.1031
91. Piitulainen H, Bourguignon M, De Tiège X, Hari R, Jousmäki V. Corticokinematic coherence during active and passive finger movements. *Neuroscience.* (2013) 238:361–70. doi: 10.1016/j.neuroscience.2013.02.002
92. Piitulainen H, Bourguignon M, De Tiège X, Hari R, Jousmäki V. Coherence between magnetoencephalography and hand-action-related acceleration, force, pressure, and electromyogram. *Neuroimage.* (2013) 72:83–90. doi: 10.1016/j.neuroimage.2013.01.029
93. Piitulainen H, Bourguignon M, Hari R, Jousmäki V. MEG-compatible pneumatic stimulator to elicit passive finger and toe movements. *Neuroimage.* (2015) 112:310–7. doi: 10.1016/j.neuroimage.2015.03.006
94. Hari R, Bourguignon M, Piitulainen H, Smeds E, De Tiège X, Jousmäki V. Human primary motor cortex is both activated and stabilized during observation of other person's phasic motor actions. *Philos Trans R Soc Lond B Biol Sci.* (2014) 369:20130171. doi: 10.1098/rstb.2013.0171
95. Bourguignon M, Piitulainen H, De Tiège X, Jousmäki V, Hari R. Corticokinematic coherence mainly reflects movement-induced proprioceptive feedback. *NeuroImage.* (2015) 106:382–90. doi: 10.1016/j.neuroimage.2014.11.026
96. Aoyama H, Kamada K, Shirato H, Takeuchi F, Kuriki S, Iwasaki Y, et al. Visualization of the corticospinal tract pathway using magnetic resonance axonography and magnetoencephalography for stereotactic irradiation planning of arteriovenous malformations. *Radiother Oncol.* (2003) 68:27–32. doi: 10.1016/S0167-8140(03)00032-X

97. Beisteiner R, Erdler M, Teichtmeister C, Diemling M, Moser E, Edward V, et al. Magnetoencephalography may help to improve functional MRI brain mapping. *Eur J Neurosci.* (1997) 9:1072–7. doi: 10.1111/j.1460-9568.1997.tb01457.x
98. Beisteiner R, Gomiscek G, Erdler M, Teichtmeister C, Moser E, Deecke L. Comparing localization of conventional functional magnetic resonance imaging and magnetoencephalography. *Eur J Neurosci.* (1995) 7:1121–4. doi: 10.1111/j.1460-9568.1995.tb01101.x
99. Morioka T, Yamamoto T, Mizushima A, Tombimatsu S, Shigeto H, Hasuo K, et al. Comparison of magnetoencephalography, functional MRI, and motor evoked potentials in the localization of the sensory-motor cortex. *Neurol Res.* (1995) 17:361–7. doi: 10.1080/01616412.1995.11740343
100. Morioka T, Mizushima A, Yamamoto T, Tobimatsu S, Matsumoto S, Hasuo K, et al. Functional mapping of the sensorimotor cortex: combined use of magnetoencephalography, functional MRI, and motor evoked potentials. *Neuroradiology.* (1995) 37:526–30. doi: 10.1007/s002340050149
101. Shimizu H, Nakasato N, Mizoi K, Yoshimoto T. Localizing the central sulcus by functional magnetic resonance imaging and magnetoencephalography. *Clin Neurol Neurosurg.* (1997) 99:235–8. doi: 10.1016/S0303-8467(97)00096-6
102. Inoue T, Shimizu H, Nakasato N, Kumabe T, Yoshimoto T. Accuracy and limitation of functional magnetic resonance imaging for identification of the central sulcus: comparison with magnetoencephalography in patients with brain tumors. *Neuroimage.* (1999) 10:738–48. doi: 10.1006/nimg.1999.0501
103. Lehéricy S, Biondi A, Sourour N, Vlaicu M, du Montcel ST, Cohen L, et al. Arteriovenous brain malformations: is functional MR imaging reliable for studying language reorganization in patients? Initial observations. *Radiology.* (2002) 223:672–82. doi: 10.1148/radiol.2233010792
104. Silva MA, See AP, Essayed WI, Golby AJ, Tie Y. Challenges and techniques for presurgical brain mapping with functional MRI. *Neuroimage Clin.* (2018) 17:794–803. doi: 10.1016/j.nicl.2017.12.008
105. Juenger H, Ressel V, Braun C, Ernemann U, Schuhmann M, Krägeloh-Mann I, et al. Misleading functional magnetic resonance imaging mapping of the cortical hand representation in a 4-year-old boy with an arteriovenous malformation of the central region. *J Neurosurg Pediatr.* (2009) 4:333–8. doi: 10.3171/2009.5.PEDS08466
106. Raffa G, Scibilia A, Conti A, Ricciardo G, Rizzo V, Morelli A, et al. The role of navigated transcranial magnetic stimulation for surgery of motor-eloquent brain tumors: a systematic review and meta-analysis. *Clin Neurol Neurosurg.* (2019) 180:7–17. doi: 10.1016/j.clineuro.2019.03.003
107. Krieg SM, Shiban E, Droese D, Gempt J, Buchmann N, Pape H, et al. Predictive value and safety of intraoperative neurophysiological monitoring with motor evoked potentials in glioma surgery. *Neurosurgery.* (2012) 70:1060–70; discussion 1070–1. doi: 10.1227/NEU.0b013e31823f5ade
108. Krieg SM, Picht T, Sollmann N, Bährend I, Ringel F, Nagarajan SS, et al. Resection of motor eloquent metastases aided by preoperative nTMS-based motor maps-comparison of two observational cohorts. *Front Oncol.* (2016) 6:261. doi: 10.3389/fonc.2016.00261
109. Vitikainen A-M, Salli E, Lioumis P, Mäkelä JP, Metsähonkala L. Applicability of nTMS in locating the motor cortical representation areas in patients with epilepsy. *Acta Neurochir.* (2013) 155:507–18. doi: 10.1007/s00701-012-1609-5
110. Forster M-T, Hattingen E, Senft C, Gasser T, Seifert V, Szelényi A. Navigated transcranial magnetic stimulation and functional magnetic resonance imaging: advanced adjuncts in preoperative planning for central region tumors. *Neurosurgery.* (2011) 68:1317–24; discussion 1324–5. doi: 10.1227/NEU.0b013e31820b528c
111. Picht T, Schmidt S, Woitzik J, Suess O. Navigated brain stimulation for preoperative cortical mapping in paretic patients: case report of a hemiplegic patient. *Neurosurgery.* (2011) 68:E1475–80; discussion E1480. doi: 10.1227/NEU.0b013e318210c7df
112. Picht T, Schmidt S, Brandt S, Frey D, Hannula H, Neuvonen T, et al. Preoperative functional mapping for rolandic brain tumor surgery: comparison of navigated transcranial magnetic stimulation to direct cortical stimulation. *Neurosurgery.* (2011) 69:581–588; discussion 588. doi: 10.1227/NEU.0b013e3182181b89
113. Paiva WS, Fonoff ET, Marcolin MA, Cabrera HN, Teixeira MJ. Cortical mapping with navigated transcranial magnetic stimulation in low-grade glioma surgery. *Neuropsychiatr Dis Treat.* (2012) 8:197–201. doi: 10.2147/NDT.S30151
114. Gleissner U, Helmstaedter C, Schramm J, Elger CE. Memory outcome after selective amygdalohippocampectomy: a study in 140 patients with temporal lobe epilepsy. *Epilepsia.* (2002) 43:87–95. doi: 10.1046/j.1528-1157.2002.24101.x
115. Gleissner U, Helmstaedter C, Schramm J, Elger CE. Memory outcome after selective amygdalohippocampectomy in patients with temporal lobe epilepsy: one-year follow-up. *Epilepsia.* (2004) 45:960–2. doi: 10.1111/j.0013-9580.2004.42203.x
116. Helmstaedter C, Kurthen M, Lux S, Reuber M, Elger CE. Chronic epilepsy and cognition: a longitudinal study in temporal lobe epilepsy. *Ann Neurol.* (2003) 54:425–32. doi: 10.1002/ana.10692
117. Powell GE, Polkey CE, Canavan AG. Lateralisation of memory functions in epileptic patients by use of the sodium amytal (Wada) technique. *J Neurol Neurosurg Psychiatry.* (1987) 50:665–72. doi: 10.1136/jnnp.50.6.665
118. Rausch R, Babb TL, Engel J, Crandall PH. Memory following intracarotid amobarbital injection contralateral to hippocampal damage. *Arch Neurol.* (1989) 46:783–8. doi: 10.1001/archneur.1989.00520430077022
119. Wyllie E, Naugle R, Chelune G, Lüders H, Morris H, Skibinski C. Intracarotid amobarbital procedure: II. lateralizing value in evaluation for temporal lobectomy. *Epilepsia.* (1991) 32:865–9. doi: 10.1111/j.1528-1157.1991.tb05543.x
120. Loring DW, Meador KJ, Lee GP, Nichols ME, King DW, Gallagher BB, et al. Wada memory performance predicts seizure outcome following anterior temporal lobectomy. *Neurology.* (1994) 44:2322. doi: 10.1212/WNL.44.12.2322
121. Chan S, Andrew A, Roberts D, Bujarski K, Thadani V, Kobylarz E, et al. Wada memory performance does not predict memory and seizure outcome after epileptic surgery (P6.229). *Neurology.* (2017) 88:P6.229.
122. Limotai C, Mirsattari SM. Role of functional MRI in presurgical evaluation of memory function in temporal lobe epilepsy. *Epilepsy Res Treat.* (2012) 2012:687219. doi: 10.1155/2012/687219
123. Rathore C, Alexander A, Sarma PS, Radhakrishnan K. Memory outcome following left anterior temporal lobectomy in patients with a failed Wada test. *Epilepsy Behav.* (2015) 44:207–12. doi: 10.1016/j.yebeh.2015.02.011
124. McMackin D, Dubeau F, Jones-Gotman M, Gotman J, Lukban A, Dean G, et al. Assessment of the functional effect of the intracarotid sodium amobarbital procedure using co-registered MRI/HMPAO-SPECT and SEEG. *Brain Cogn.* (1997) 33:50–70. doi: 10.1006/brcg.1997.0884
125. de Silva R, Duncan R, Patterson J, Gillham R, Hadley D. Regional cerebral perfusion and amytal distribution during the Wada test. *J Nucl Med.* (1999) 40:747–52.
126. Dale AM, Halgren E. Spatiotemporal mapping of brain activity by integration of multiple imaging modalities. *Currt Opin Neurobiol.* (2001) 11:202–8. doi: 10.1016/S0959-4388(00)00197-5
127. Mikuni N, Nagamine T, Ikeda A, Terada K, Taki W, Kimura J, et al. Simultaneous recording of epileptiform discharges by MEG and subdural electrodes in temporal lobe epilepsy. *Neuroimage.* (1997) 5:298–306. doi: 10.1006/nimg.1997.0272
128. Hopf L, Quraan MA, Cheung MJ, Taylor MJ, Ryan JD, Moses SN. Hippocampal lateralization and memory in children and adults. *J Int Neuropsychol Soc.* (2013) 19:1042–52. doi: 10.1017/S1355617713000751
129. Riggs L, Moses SN, Bardouille T, Herdman AT, Ross B, Ryan JD. A complementary analytic approach to examining medial temporal lobe sources using magnetoencephalography. *Neuroimage.* (2009) 45:627–42. doi: 10.1016/j.neuroimage.2008.11.018
130. Moses SN, Hanlon FM, Ryan JD. Dynamic imaging of deep brain structures with MEG: contributions to understanding human memory. *Magnetoencephalography.* (2011). doi: 10.5772/29133
131. Maestú F, Campo P, García-Morales I, del Barrio A, Paul N, del Pozo F, et al. Biomagnetic profiles of verbal memory success in patients with mesial temporal lobe epilepsy. *Epilepsy Behav.* (2009) 16:527–33. doi: 10.1016/j.yebeh.2009.09.007
132. Towgood K, Barker GJ, Caceres A, Crum WR, Elwes RDC, Costafreda SG, et al. Bringing memory fMRI to the clinic: comparison of seven memory

fMRI protocols in temporal lobe epilepsy. *Hum Brain Mapp.* (2015) 36:1595–608. doi: 10.1002/hbm.22726
133. Slotnick SD, Moo LR, Krauss G, Hart JJ. Large-scale cortical displacement of a human retinotopic map. *NeuroReport.* (2002) 13:41. doi: 10.1097/00001756-200201210-00013
134. Pang EW, Chu BHW, Otsubo H. Occipital lobe lesions result in a displacement of magnetoencephalography visual evoked field dipoles. *J Clin Neurophysiol.* (2014) 31:456. doi: 10.1097/WNP.0000000000000077
135. Nakasato N, Seki K, Fujita S, Hatanaka K, Kawamura T, Ohtomo S, et al. Clinical application of visual evoked fields using an MRI-linked whole head MEG system. *Front Med Biol Eng.* (1996) 7:275–83.
136. Alberstone CD, Skirboll SL, Benzel EC, Sanders JA, Hart BL, Baldwin NG, et al. Magnetic source imaging and brain surgery: presurgical and intraoperative planning in 26 patients. *J Neurosurg.* (2000) 92:79–90. doi: 10.3171/jns.2000.92.1.0079
137. Ganslandt O, Buchfelder M, Hastreiter P, Grummich P, Fahlbusch R, Nimsky C. Magnetic source imaging supports clinical decision making in glioma patients. *Clin Neurol Neurosurg.* (2004) 107:20–6. doi: 10.1016/j.clineuro.2004.02.027
138. Armstrong RA, Slaven A, Harding GF. Visual evoked magnetic fields to flash and pattern in 100 normal subjects. *Vision Res.* (1991) 31:1859–64. doi: 10.1016/0042-6989(91)90180-D
139. Grover KM, Bowyer SM, Rock J, Rosenblum ML, Mason KM, Moran JE, et al. Retrospective review of MEG visual evoked hemifield responses prior to resection of temporo-parieto-occipital lesions. *J Neurooncol.* (2006) 77:161–6. doi: 10.1007/s11060-005-9014-z
140. Inoue T, Fujimura M, Kumabe T, Nakasato N, Higano S, Tominaga T. Combined three-dimensional anisotropy contrast imaging and magnetoencephalography guidance to preserve visual function in a patient with an occipital lobe tumor. *Min Minimally Invasive Neurosurg.* (2004) 47:249–52. doi: 10.1055/s-2004-818519
141. Wiedemayer H, Fauser B, Armbruster W, Gasser T, Stolke D. Visual evoked potentials for intraoperative neurophysiologic monitoring using total intravenous anesthesia. *J Neurosurg Anesthesiol.* (2003) 15:19–24. doi: 10.1097/00008506-200301000-00004
142. Lee HW, Hong SB, Seo DW, Tae WS, Hong SC. Mapping of functional organization in human visual cortex: electrical cortical stimulation. *Neurology.* (2000) 54:849–54. doi: 10.1212/WNL.54.4.849
143. Romero JR, Ramirez DM, Aglio LS, Gugino LD. Brain mapping using transcranial magnetic stimulation. *Neurosurg Clin N Am.* (2011) 22:141–52 vii. doi: 10.1016/j.nec.2010.11.002
144. DeYoe EA, Raut RV. Visual mapping using blood oxygen level dependent functional magnetic resonance imaging. *Neuroimaging Clin N Am.* (2014) 24:573–84. doi: 10.1016/j.nic.2014.08.001
145. Hirsch J, Ruge MI, Kim KH, Correa DD, Victor JD, Relkin NR, et al. An integrated functional magnetic resonance imaging procedure for preoperative mapping of cortical areas associated with tactile, motor, language, and visual functions. *Neurosurgery.* (2000) 47:711–21; discussion 721–2. doi: 10.1227/00006123-200009000-00037
146. Kapsalakis IZ, Kapsalaki EZ, Gotsis ED, Verganelakis D, Toulas P, Hadjigeorgiou G, et al. Preoperative evaluation with FMRI of patients with intracranial gliomas. *Radiol Res Pract.* (2012) 2012:727810. doi: 10.1155/2012/727810
147. Nakasato N, Yoshimoto T. Somatosensory, auditory, and visual evoked magnetic fields in patients with brain diseases. *J Clin Neurophysiol.* (2000) 17:201–11. doi: 10.1097/00004691-200003000-00009
148. Häusler R, Levine RA. Auditory dysfunction in stroke. *Acta Otolaryngol.* (2000) 120:689–703. doi: 10.1080/000164800750000207
149. Gage NM, Siegel B, Callen M, Roberts TPL. Cortical sound processing in children with autism disorder: an MEG investigation. *Neuroreport.* (2003) 14:2047–51. doi: 10.1097/00001756-200311140-00008
150. Oram Cardy JE, Flagg EJ, Roberts W, Brian J, Roberts TPL. Magnetoencephalography identifies rapid temporal processing deficit in autism and language impairment. *Neuroreport.* (2005) 16:329–32. doi: 10.1097/00001756-200503150-00005
151. Stefanics G, Fosker T, Huss M, Mead N, Szucs D, Goswami U. Auditory sensory deficits in developmental dyslexia: a longitudinal ERP study. *Neuroimage.* (2011) 57:723–32. doi: 10.1016/j.neuroimage.2011.04.005
152. Mizuno T, Takanashi Y, Nakase T, Makino M, Iwamoto K, Nakajima K, et al. Clinical application of magnetoencephalography in a patient with corticobasal degeneration. *J Neuroimaging.* (1999) 9:45–47. doi: 10.1111/jon19999145
153. Mäkelä JP, Hari R, Valanne L, Ahonen A. Auditory evoked magnetic fields after ischemic brain lesions. *Ann Neurol.* (1991) 30:76–82. doi: 10.1002/ana.410300114
154. Parkkonen L, Fujiki N, Mäkelä JP. Sources of auditory brainstem responses revisited: contribution by magnetoencephalography. *Hum Brain Mapp.* (2009) 30:1772–82. doi: 10.1002/hbm.20788
155. Destoky F, Philippe M, Bertels J, Verhasselt M, Coquelet N, Vander Ghinst M, et al. Comparing the potential of MEG and EEG to uncover brain tracking of speech temporal envelope. *Neuroimage.* (2019) 184:201–13. doi: 10.1016/j.neuroimage.2018.09.006
156. Pantev C, Hoke M, Lehnertz K, Lütkenhöner B, Fahrendorf G, Stöber U. Identification of sources of brain neuronal activity with high spatiotemporal resolution through combination of neuromagnetic source localization (NMSL) and magnetic resonance imaging (MRI). *Electroencephalogr Clin Neurophysiol.* (1990) 75:173–84. doi: 10.1016/0013-4694(90)90171-F
157. Papanicolaou AC, Baumann S, Rogers RL, Saydjari C, Amparo EG, Eisenberg HM. Localization of auditory response sources using magnetoencephalography and magnetic resonance imaging. *Arch Neurol.* (1990) 47:33–7. doi: 10.1001/archneur.1990.00530010041016
158. Picton TW, Alain C, Woods DL, John MS, Scherg M, Valdes-Sosa P, et al. Intracerebral sources of human auditory-evoked potentials. *Audiol Neurootol.* (1999) 4:64–79. doi: 10.1159/000013823
159. Verkindt C, Bertrand O, Perrin F, Echallier JF, Pernier J. Tonotopic organization of the human auditory cortex: N100 topography and multiple dipole model analysis. *Electroencephalogr Clin Neurophysiol.* (1995) 96:143–56. doi: 10.1016/0168-5597(94)00242-7
160. Scarff CJ, Reynolds A, Goodyear BG, Ponton CW, Dort JC, Eggermont JJ. Simultaneous 3-T fMRI and high-density recording of human auditory evoked potentials. *Neuroimage.* (2004) 23:1129–42. doi: 10.1016/j.neuroimage.2004.07.035
161. Shahin AJ, Roberts LE, Miller LM, McDonald KL, Alain C. Sensitivity of EEG and MEG to the N1 and P2 auditory evoked responses modulated by spectral complexity of sounds. *Brain Topogr.* (2007) 20:55–61. doi: 10.1007/s10548-007-0031-4
162. Pang EW, Snead III OC. From structure to circuits: the contribution of MEG connectivity studies to functional neurosurgery. *Front Neuroanat.* (2016) 10:67. doi: 10.3389/fnana.2016.00067
163. Doesburg SM, Vinette SA, Cheung MJ, Pang EW. Theta-modulated gamma-band synchronization among activated regions during a verb generation task. *Front Psychol.* (2012) 3:195. doi: 10.3389/fpsyg.2012.00195
164. Martino J, Honma SM, Findlay AM, Guggisberg AG, Kirsch HE, Berger MS, et al. Resting functional connectivity in patients with brain tumors in eloquent areas. *Ann Neurol.* (2011) 69:521–32. doi: 10.1002/ana.22167
165. Tarapore PE, Martino J, Guggisberg AG, Owen J, Honma SM, Findlay A, et al. Magnetoencephalographic imaging of resting-state functional connectivity predicts postsurgical neurological outcome in brain gliomas. *Neurosurgery.* (2012) 71:1012–22. doi: 10.1227/NEU.0b013e31826d2b78
166. Lang S, Duncan N, Northoff G. Resting-state functional magnetic resonance imaging: review of neurosurgical applications. *Neurosurgery.* (2014) 74:453–64; discussion 464–5. doi: 10.1227/NEU.0000000000000307
167. Zaharchuk G, Gong E, Wintermark M, Rubin D, Langlotz CP. Deep learning in neuroradiology. *Am J Neuroradiol.* (2018) 39:1776–84. doi: 10.3174/ajnr.A5543
168. Roland JL, Hacker CD, Snyder AZ, Shimony JS, Zempel JM, Limbrick DD, et al. A comparison of resting state functional magnetic resonance imaging to invasive electrocortical stimulation for sensorimotor mapping in pediatric patients. *NeuroImage Clin.* (2019) 23:101850. doi: 10.1016/j.nicl.2019.101850
169. Lotte F, Bougrain L, Cichocki A, Clerc M, Congedo M, Rakotomamonjy A, et al. A review of classification algorithms for EEG-based brain-computer interfaces: a 10 year update. *J Neural Eng.* (2018) 15:031005. doi: 10.1088/1741-2552/aab2f2
170. Kambara T, Sood S, Alqatan Z, Klingert C, Ratnam D, Hayakawa A, et al. Presurgical language mapping using event-related high-gamma

activity: the detroit procedure. *Clin Neurophysiol.* (2018) 129:145–54. doi: 10.1016/j.clinph.2017.10.018
171. Kamada K, Ogawa H, Kapeller C, Prueckl R, Guger C. Rapid and low-invasive functional brain mapping by realtime visualization of high gamma activity for awake craniotomy. *Conf Proc IEEE Eng Med Biol Soc.* (2014) 2014:6802–5. doi: 10.1109/EMBC.2014.6945190
172. Brunner P, Ritaccio AL, Lynch TM, Emrich JF, Wilson JA, Williams JC, et al. A practical procedure for real-time functional mapping of eloquent cortex using electrocorticographic signals in humans. *Epilepsy Behav.* (2009) 15:278–86. doi: 10.1016/j.yebeh.2009.04.001
173. Pastori C, Francione S, Pelle F, de Curtis M, Gnatkovsky V. Fluency tasks generate beta-gamma activity in language-related cortical areas of patients during stereo-EEG monitoring. *Brain Language.* (2016) 163:50–6. doi: 10.1016/j.bandl.2016.09.006
174. Tate MC, Herbet G, Moritz-Gasser S, Tate JE, Duffau H. Probabilistic map of critical functional regions of the human cerebral cortex: broca's area revisited. *Brain.* (2014) 137:2773–82. doi: 10.1093/brain/awu168
175. Bauer PR, Reitsma JB, Houweling BM, Ferrier CH, Ramsey NF. Can fMRI safely replace the Wada test for preoperative assessment of language lateralisation? a meta-analysis and systematic review. *J Neurol Neurosurg Psychiatry.* (2014) 85:581–8. doi: 10.1136/jnnp-2013-305659
176. Tanaka N, Liu H, Reinsberger C, Madsen JR, Bourgeois BF, Dworetzky BA, et al. Language lateralization represented by spatiotemporal mapping of magnetoencephalography. *Am J Neuroradiol.* (2013) 34:558–63. doi: 10.3174/ajnr.A3233
177. Lopes da Silva F. EEG and MEG: relevance to neuroscience. *Neuron.* (2013) 80:1112–28. doi: 10.1016/j.neuron.2013.10.017
178. Bagić AI. Disparities in clinical magnetoencephalography practice in the United States: a survey-based appraisal. *J Clin Neurophysiol.* (2011) 28:341–7. doi: 10.1097/WNO.0b013e3181ce162a
179. De Tiège X, Lundqvist D, Beniczky S, Seri S, Paetau R. Current clinical magnetoencephalography practice across Europe: are we closer to use MEG as an established clinical tool? *Seizure.* (2017) 50:53–9. doi: 10.1016/j.seizure.2017.06.002
180. Rezai AR, Hund M, Kronberg E, Zonenshayn M, Cappell J, Ribary U, et al. The interactive use of magnetoencephalography in stereotactic image-guided neurosurgery. *Neurosurgery.* (1996) 39:92–102. doi: 10.1097/00006123-199607000-00018
181. Ganslandt O, Steinmeier R, Kober H, Vieth J, Kassubek J, Romstöck J, et al. Magnetic source imaging combined with image-guided frameless stereotaxy: a new method in surgery around the motor strip. *Neurosurgery.* (1997) 41:621–7; discussion 627–8. doi: 10.1227/00006123-199709000-00023
182. Hari R, Baillet S, Barnes G, Burgess R, Forss N, Gross J, et al. IFCN-endorsed practical guidelines for clinical magnetoencephalography (MEG). *Clin Neurophysiol.* (2018) 129:1720–47. doi: 10.1016/j.clinph.2018.03.042

Conflict of Interest Statement: The authors declare that the research was conducted in the absence of any commercial or financial relationships that could be construed as a potential conflict of interest.

frontiers in Neurology

REVIEW
published: 17 July 2019
doi: 10.3389/fneur.2019.00721

Network Perspectives on Epilepsy Using EEG/MEG Source Connectivity

Pieter van Mierlo[1]*, *Yvonne Höller*[2], *Niels K. Focke*[3] and *Serge Vulliemoz*[4]

[1] Medical Image and Signal Processing Group, Ghent University, Ghent, Belgium, [2] Faculty of Psychology, University of Akureyri, Akureyri, Iceland, [3] Clinical Neurophysiology, University Medicine Göttingen, Göttingen, Germany, [4] EEG and Epilepsy Unit, University Hospital of Geneva, Geneva, Switzerland

The evolution of EEG/MEG source connectivity is both, a promising, and controversial advance in the characterization of epileptic brain activity. In this narrative review we elucidate the potential of this technology to provide an intuitive view of the epileptic network at its origin, the different brain regions involved in the epilepsy, without the limitation of electrodes at the scalp level. Several studies have confirmed the added value of using source connectivity to localize the seizure onset zone and irritative zone or to quantify the propagation of epileptic activity over time. It has been shown in pilot studies that source connectivity has the potential to obtain prognostic correlates, to assist in the diagnosis of the epilepsy type even in the absence of visually noticeable epileptic activity in the EEG/MEG, and to predict treatment outcome. Nevertheless, prospective validation studies in large and heterogeneous patient cohorts are still lacking and are needed to bring these techniques into clinical use. Moreover, the methodological approach is challenging, with several poorly examined parameters that most likely impact the resulting network patterns. These fundamental challenges affect all potential applications of EEG/MEG source connectivity analysis, be it in a resting, spiking, or ictal state, and also its application to cognitive activation of the eloquent area in presurgical evaluation. However, such method can allow unique insights into physiological and pathological brain functions and have great potential in (clinical) neuroscience.

Keywords: EEG/MEG source connectivity, epilepsy, interictal epileptiform discharges, seizures, resting state

OPEN ACCESS

Edited by:
Sandor Beniczky,
Aarhus University Hospital, Denmark

Reviewed by:
Jordi A. Matias-Guiu,
Hospital Clínico San Carlos, Spain
Ioana Mindruta,
University of Bucharest, Romania

***Correspondence:**
Pieter van Mierlo
pieter.vanmierlo@UGent.be

Specialty section:
This article was submitted to Applied Neuroimaging, a section of the journal Frontiers in Neurology

Received: *29 January 2019*
Accepted: *18 June 2019*
Published: *17 July 2019*

Citation:
van Mierlo P, Höller Y, Focke NK and Vulliemoz S (2019) Network Perspectives on Epilepsy Using EEG/MEG Source Connectivity. Front. Neurol. 10:721. doi: 10.3389/fneur.2019.00721

INTRODUCTION

Epilepsy is commonly considered an archetypical network disease (1), with seizures and interictal activity generated and spreading in networks involving one or both hemispheres. There is a growing body of imaging evidence suggesting that epilepsy affects both structural (2, 3) and functional brain network properties (4–7). Interestingly, even in idiopathic/genetic generalized epilepsy, there is a certain level of focality both in resting-state imaging (7) as well as for generators of epileptiform activity (8) and seizures (9, 10). These structural and functional network properties are investigated using brain connectivity analysis.

Brain connectivity can be categorized into structural, functional and effective connectivity (11). Structural connectivity refers to the white matter connections in the brain and can be examined *in vivo* with MRI measuring the motion of water along the axons. Functional and effective connectivity entangle the neuronal communication between brain regions. These types of connectivity can be calculated when signals are sampled over multiple time points, such as brain activity recorded via EEG, MEG, but also fMRI, or PET. According to Friston (12),

"functional connectivity is defined as statistical dependencies among remote neurophysiological events, while effective connectivity refers explicitly to the influence that one neural system exerts over another, either at a synaptic or population level." Functional or effective connectivity is measured in terms of similarities between signals and shows complementary information with regard to structural connectivity (13). With the growing enthusiasm for connectivity it is often overlooked that in reality, all we have are statistical interdependencies of signals, which should be interpreted cautiously.

The main difference between functional and effective connectivity is that functional connectivity characterizes whether the activity of two units are linked, while effective connectivity also examines the direction of communication, i.e., which is the driver or receiver of information. This does not tell us whether there exists a physical/structural connection (14), but the size of the predictability lets us estimate how likely it is that one unit influences the other. Therefore, the common understanding is that effective connectivity entails directed information flow from one system/region to another while functional connectivity assesses undirected information flow. Functional or effective connectivity can be time-resolved or averaged over a certain period and optionally within a specific frequency band.

The most classical measures for functional connectivity are correlation and coherence, which reflects the similarity between signals in the time and frequency domain, respectively. Intuitively speaking, coherence is a correlation of two signals in the frequency domain (15). Other connectivity measures consider the phase of the oscillations in the electrophysiological signals, the so-called measures of synchronization. The phase indicates whether the oscillation is at a specific time point t at a peak, trough, or transitions between these two states (such as for instance, zero crossings). If two signals exhibit the same phases at the same point in time, they are said to oscillate synchronously. Determining the phase of two signals allows calculating the difference in phase, the phase lag, which in turn may inform us about propagation effects, if the one signal exhibits a later phase than the other signal. The phase lag is suggested to reflect signal propagation and can be studied to examine effective connectivity. In addition to bivariate measures that consider pairs of signals, multivariate measures are designed in order to remove shared properties between multiple signals, such as, for example, partial coherence (16). Most measures of effective connectivity are described under the umbrella term Granger causality (17). This concept considers two signals X and Y and examines whether the activity at time point t of signal X can be predicted (statistically) by the activity at the earlier time points t-k of signal Y. Among them, partial directed coherence (18) and directed transfer function (19) are commonly used to study epilepsy. Next to these data driven analysis approaches, effective connectivity can also be estimated based on underlying biophysical models with a priori assumptions about the organization of the network as in Dynamic Causal Modeling (DCM) and other neural mass models. DCM in EEG or MEG takes biologically plausibility of causal models into account, and thus yields an informed estimate of connectivity (20).

The connectome estimated using functional or effective connectivity algorithms contains a large amount of data, which can complicate the biophysical interpretation. The connectome is composed of values indicating the relatedness of each region-by-region combination. In addition, each of these values can be estimated optionally for defined time-windows and/or frequency ranges. That is, the final result may characterize the data in up to four dimensions: region × region × time × frequency. In order to reduce the dimensionality of these complex data and to extract meaningful patterns, topological graph analysis can be performed. The importance of specific nodes and the general architecture can be characterized by local and global network characteristics (21). Local indices identify important information hubs, which distribute or merge information to a large number of other nodes, or select so-called rich-clubs of highly interconnected nodes. Global indices measure the organization of the network into small worlds where only neighboring regions exchange information, or whether the network is organized in a centralized way. Regions with high outflow are considered drivers of information transfer in the network. Efficient information transfer across the network is measured by efficiency or path length. Segregation characterized by groups of highly connected regions for specialization can be measured by the clustering coefficient (22). The clear advantage of deriving network characteristics is that it reduces the statistical challenge posed by the multidimensional problem in terms of multiple comparisons. High dimensional data can lead to false discoveries when the statistical approach does not deal adequately with the high dimensionality. However, a large degree of integration can obscure localized phenomena. Therefore, the degree of integration needs to be chosen carefully in line with the current clinical problem or research question.

Functional and effective connectivity are commonly used to gain insight into the network nature of epilepsy (23). On the one hand, connectivity analysis is used to identify how epilepsy and years of seizures and/or interictal activity affect the brain network (24). Furthermore, cognitive improvement or decline can be linked to changes in specific brain networks in epilepsy patients (25). On the other hand, because seizures and spikes spread rapidly in the brain, connectivity analysis is used as a tool to localize the seizure onset zone (SOZ) and the irritative zone (IZ) (26). Here, a big advantage is that non-invasive connectivity analysis can be validated based on resections that rendered the patients seizure free or intracranial EEG recordings that are often available in these patients.

MEG/EEG SOURCE CONNECTIVITY

The electrical activity of active neurons can be recorded at the scalp surface as voltage differences across EEG electrodes. In addition, the neuronal currents in the brain generate magnetic fields that can be measured outside the scalp surface by the MEG sensors. Compared to other neuroimaging techniques such as PET and fMRI, EEG, and MEG have a superior temporal resolution but an inferior spatial resolution. Despite this inferior spatial resolution, the temporal resolution and the fact that

EEG and MEG directly measures neuronal activity makes them highly valuable techniques to study functional and especially effective connectivity. Combining neuroimaging techniques with high spatial resolution with a technique with high temporal resolution, such as EEG-fMRI, is a valid approach to examine slow changes in blood supply based on spiking activity (27–29) or at rest (30) and, therefore, provides an excellent validation for localization accuracy of source connectivity (31). Nevertheless, because MRI induces artifacts such as ballistocardiographic artifact, the EEG signals recorded within the MRI scanner are more noisy and therefore less suitable to be used for connectivity analysis compared to EEG measured outside the MRI scanner.

There are a number of studies applying connectivity algorithms to the electrophysiological signals recorded from the MEG/EEG sensors, so called functional and effective connectivity in sensor space. While this is the most straightforward way to estimate connectivity, this approach suffers from important methodological limitations and these studies should be interpreted with caution. First, due to the volume conduction effect, every source in the brain, i.e., activity in a brain region large enough to generate measurable EEG/MEG signals, is picked up by all recording EEG/MEG sensors simultaneously (32). The main orientation of the activated neurons, the distance to the sensors and the conductive properties of the tissue define how much each source is picked up by each sensor. Because of this volume conduction effect, connectivity analysis performed in sensor space can potentially lead to false connections, given the fact that distant electrode can share common information from several sources (33, 34). Second, the choice of the EEG reference can influence the estimated functional integration and segregation (35). Therefore, the connectivity pattern derived in sensor space does not necessarily reflect the connections of underlying cortical regions. One (partial) solution is to apply connectivity measures to the sensor signals that are specifically designed to deal with the volume conduction effect such as the imaginary part of the coherence (36). Another option to circumvent the volume conduction effect is to study the EEG/MEG signals in source space (37). First, EEG source imaging is performed on the signals to project them into brain/source space. It is of utmost importance to choose a proper forward model and inverse technique to estimate the neuronal activity in the volumes of interest. Even in source space it is important to choose the measure for connectivity carefully, otherwise the artifacts of volume conduction may still be present even in reconstructed source time series as zero-lag correlations (33, 37). Nevertheless, it is an advantage that source space connectivity is a more direct representation of the connectivity pattern between brain regions instead of electrodes as this clearly augments the information gain for clinical and research questions concerning epilepsy. This makes the information from source space connectivity analysis much more intuitive to understand.

In the following, we provide a brief explanation on how EEG/MEG source space connectivity can be calculated from EEG and MEG measurements. In **Figure 1** an example pipeline how to extract source space connectivity patterns from EEG/MEG is depicted. In a first step, EEG/MEG sensor signals are recorded. In this step, it is important to assure optimal quality of the measurements. These recordings are then usually preprocessed to remove environmental and physiological noise. For example, this is done by excluding segments of data contaminated by eye or muscle artifacts. Decomposition techniques such as independent component analysis (ICA) are frequently used to remove eye blinks or cardiac artifacts. However, one should be cautious since ICA might introduce spurious connectivity as it removes shared activity from all sensors. In other words, ICA employs a calculation on all channels that might introduce similarity between the signals. The effects of ICA artifact removal on subsequent connectivity analyses is not clearly quantified yet and should be clarified in future studies. Also filtering of the EEG and MEG signals should be done carefully in order to prevent the introduction of phase differences. Therefore, it is recommended to use zero-phase shift filters, for instance, to remove 50/60 Hz power line noise and to refrain from filtering as much as possible (38).

In a second step, the EEG/MEG signals are projected from sensor to source space using EEG/MEG source imaging (ESI/MSI). ESI/MSI is applied to all time points of the chosen preprocessed epoch. For each time point a source image is generated. From the source images, the activity in the ROIs that are defined based on a cortical parcellation (based on an atlas or specifically defined for the study) can be estimated over time. It is also possible to reconstruct EEG/MEG time courses on a voxel- or vertex-level in higher spatial resolution, although this increases the computational resources needed and is limited by the spatial resolution of modalities. M/ESI requires a forward model that characterizes the electrical and magnetic field propagation in the subject's head. From the individual's MRI, this electromagnetic head model is constructed that links brain activity to the recorded scalp potentials. For EEG the use of a complex head model that specifies each tissue class is recommended, while for MEG simpler models usually suffice. This is because the spread of magnetic fields are not affected by electric conductance, in contrary to electric fields; i.e., the complex architecture of the head, including cerebrospinal fluid, dura, skull, fatty tissue, and skin, all of which having different conductance, does not influence magnetic fields (39). This enables the use of much simpler head models in MEG, even the very simple "single shell" model are still frequently used (40, 41). Nevertheless, it has been shown that not including CSF and not distinguishing gray and white matter in the head models can introduce source space connectivity errors both in EEG and MEG (42). The inverse solution techniques depend on the forward model to estimate the neuronal activity from the M/EEG. These head models can be divided into dipole modeling techniques, where the number of estimated sources in the brain is much smaller than the number of sensors, and distributed inverse solution techniques that estimate the activity in many sources in the brain using different methods of regularization (43). Most commonly used inverse techniques for M/EEG source space connectivity are distributed techniques such as weighted minimum norm, beamforming and low resolution brain electromagnetic tomography (LORETA). It has been shown that the optimal choice of the inverse solution depends both on the spatial and synchronization profile of the interacting cortical sources (44). Also, the intrinsic difference

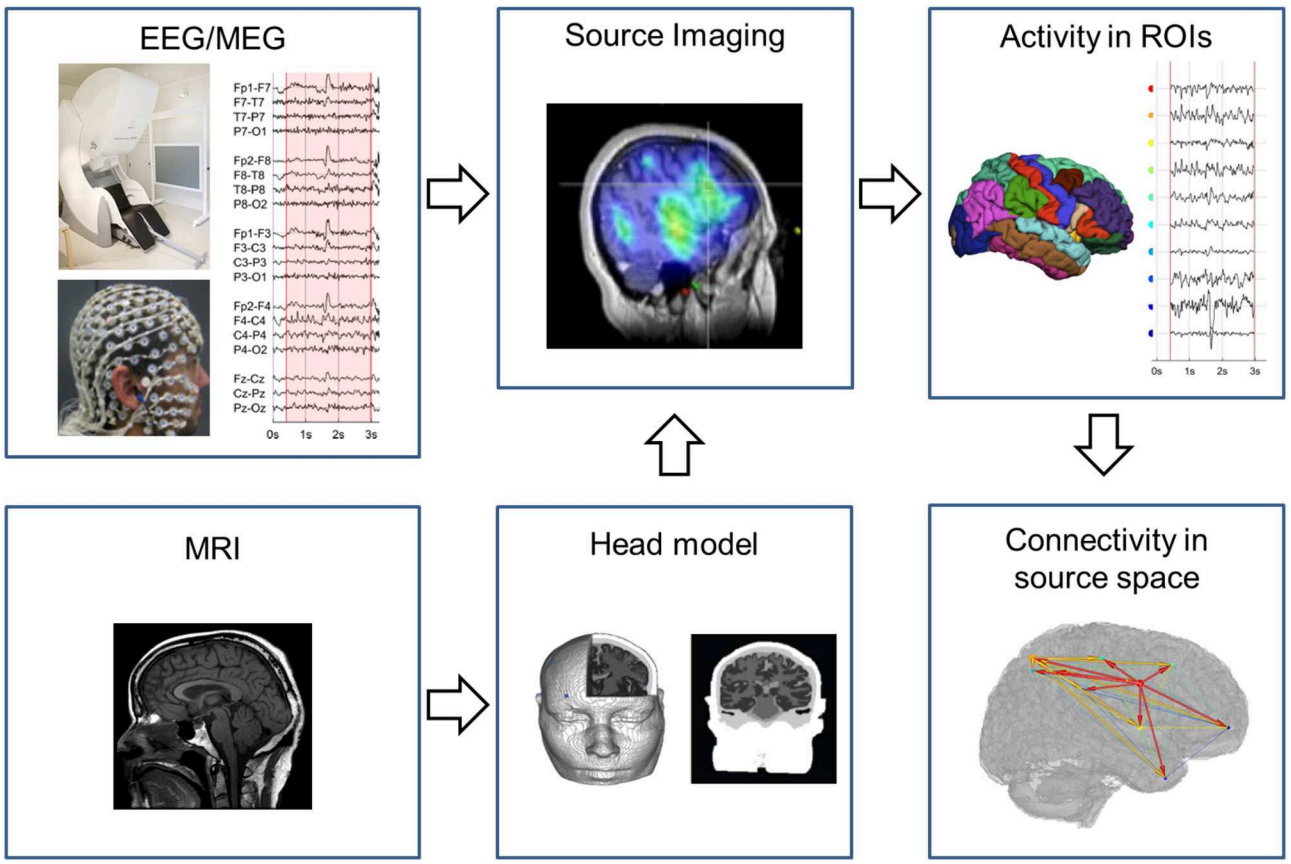

FIGURE 1 | Pipeline to obtain EEG/MEG source connectivity. The EEG/MEG signals in sensor space are source imaged using a head model constructed based on a template or patient specific MRI. In the brain regions of interest the neuronal activity is estimated over time and fed in the connectivity analysis to obtain the connectivity pattern in source space.

between EEG and MEG influences the result. MEG is particularly sensitive to tangential dipoles, whereas it is "blind" to pure radial sources, while the EEG is more sensitive to radial sources (45, 46). Hence, one could expect that some source connections are particularly well detectable with MEG (if they are largely tangential to the skull convexity), whereas others should be better detectable with EEG or a combination of both techniques.

In a last step, connectivity measures, as introduced above, can be applied to the estimated neuronal activity in the ROIs to obtain the connectivity pattern in source space. Graph analysis can be applied on this connectome to extract local and global characteristics of the network.

For source-level analysis of EEG/MEG signals several non-commercial software packages offer tools and functions. For example, EEGLAB (47), CARTOOL (48), Fieldtrip (49), Brainstorm (50), eConnectome (51), and the MNE software (52) offer both, source-transformation and connectivity analysis.

SOURCE CONNECTOMES IN EPILEPSY

In this section, we provide an overview how EEG/MEG source space connectivity has been used in epilepsy patients to study ictal, interictal, and resting state activity.

Ictal

Ding et al. studied EEG source space connectivity in 20 seizures of 5 patients (53). The brain source with highest outgoing information flow was estimated within 15 mm of the EZ that was defined by lesions visible on MRI or hyper perfusion seen in ictal SPECT. Given that the resection location in the patients was not mentioned, it remains unclear if the presumed EZ corresponded with the true EZ. In a follow-up study, Lu et al. (54) showed the value of using more electrodes to localize the SOZ based on EEG source space connectivity by comparing different electrode setups (76, 64, 48, 32, and 21 electrodes). In the 10 investigated patients with ILAE class 1 or 2 post-operative outcome, the SOZ was estimated within 10 mm of the resection in 16/23 seizures and within 20 mm in 22/23 seizures. The gain in sensitivity to localize the SOZ when increasing the number of scalp electrodes has been confirmed by Staljanssens et al. (26). However, the study compared the same data with the full number of sponge-electrodes (265) from a high-impedance amplifier to a reduced subset (reduced sequentially up to 32 channels). The drawback of this approach is that low-density systems typically used in a clinical setting have different amplifiers and electrodes, such that the data quality is not directly comparable between both situation and therefore the

result of reducing the number of electrodes should be interpreted with caution.

Currently, the recording length using high density EEG is limited to overnight recordings, at most. The resulting difficulty to record seizures with high density EEG pushed for ictal connectivity analysis based on clinical video-EEG. The largest cohort study so far was performed by Staljanssens et al. (55). One hundred and eleven seizures in 27 patients all with Engel class 1 outcome were localized using EEG source connectivity and ESI power. They showed that source space connectivity, compared to ESI power, significantly increases the performance from 42 to 94% to localize the SOZ within 10 mm from the resection. Despite the fact that several studies (26, 53–57) show the potential of ictal source localization using EEG source connectivity, there is only limited data available about their sensitivity and specificity in extra-temporal lobe epilepsy or in patients that did not become seizure free, which hampers the use of these methods in a clinical setting.

EEG source connectivity has also been used to investigate the network topology during a seizure as a marker of transient functional reorganization. Elshoff et al. showed that the topology changes from a star-like topography with the SOZ as the main hub in the beginning of the seizure to a circular pattern with no hub in the middle of the seizure (**Figure 2**). These results suggest an important information transfer from the SOZ at seizure onset, that was reduced during the seizure and resulted in a reduction of the efficiency of information transfer (58). Japaridze et al. used the same approach in 15 children with continuous spike waves during sleep and reported network abnormalities involving notably the thalamus although the possibility of EEG to estimate activity in the thalamus remains very questionable (59). Klamer et al. studied seizures and auras of a patient with musicogenic epilepsy using DCM based on prior selection of regions of interest from fMRI (60). In this application, the technique was used to infer hidden neuronal states from measurements of brain activity, to localize the SOZ from simultaneous high density EEG/MEG. Two sources were apparent from previous functional MRI investigation: one frontal and one mesiotemporal. Using DCM they found that the best model explaining the recording consisted in the mesiotemporal brain region driving the frontal regions. In later invasive EEG recordings the right hippocampus was confirmed as SOZ. It is important to note that the regions of interest were selected based on results of the fMRI analysis and on previous literature; without these priors, the results of the source connectivity analysis might have been considerably different.

Interictal Epileptic Discharges

EEG and MEG are sensitive to different type of spikes. EEG is more sensitive to spikes arising from cortex in which the pyramidal neurons are aligned perpendicular to the skull, while MEG is more sensitive to tangential sources. One recent study reported that about 8% of spike types (from ∼300 patients) were only visible in MEG (61), whereas another study reported an added sensitivity of 18% for MEG vs. EEG in 22 epilepsy patients (62). The problem with all studies is that EEG and MEG channel count and coverage are often not directly comparable. MEG usually has >250 sensors, while EEG is often recorded with ∼1/10 of these. A head-to-head comparison of MEG and high density EEG is still lacking.

M/ESI applied to interictal spikes has been increasingly validated by large independent studies showing its accuracy as a surrogate marker of epileptic activity. M/ESI has high sensitivity and specificity to predict epilepsy surgery outcome by localizing the irritative zone that generates the spikes (63–66). The feasibility to use MEG source connectivity to localize spikes has been shown by Dai et al. (67). Dai et al. selected time points of interest visually and, from these selected epochs, regions of interest that—according to visual inspection—exhibited significant activity. We stress that, in order to improve objectivity of source connectivity, it is absolutely necessary to follow standardized rules or statistical approaches to select regions of interest.

Storti et al. (68) performed source analysis and Granger-based connectivity on high density EEG in 12 patients with focal epilepsy. They found that connectivity could distinguish between spike onset and propagation zones. In this study, only half of the patients were operated and post-operatively seizure free so that validation was only partially available.

Given the fact that M/ESI is increasingly validated to localize the irritative zone, using source connectivity will probably not add much information to localize the origin of the spike but could be used for mapping large-scale network aspects of interictal activity and their clinical diagnostic and prognostic correlates. Coito et al. studied the time-varying frequency specific directed connectivity between brain regions during spikes in temporal epilepsy using high density EEG (25). They found that the spike network in 16 temporal lobe epilepsy patients was more bilateral in right temporal epilepsy including some frontal connections as shown in **Figure 3**. Interestingly, this pattern was concordant with the neurocognitive profile of these patients showing more verbal and visuospatial alterations as well as impaired executive function (frontal) in right temporal lobe epilepsy at group level. These results are promising but limited to patients with a sufficient number of recorded spikes. So far, the clinical relevance of spike-related connectivity analysis regarding the risk of recurrence, drug treatment response, and prediction of post-operative outcome has not been assessed.

A DCM study on children with centrotemporal spikes found the strongest outflow in the central cortex, temporo-parietal junction and temporal pole with projections toward frontal regions and the contralateral hemisphere (69). The population chosen in this study unfortunately prevents invasive validation of this interesting approach based on a neural mass model.

Non Spiking "Resting State" and Cognition

Apart from studying the brain during seizures or interictal "spiking" periods, there is an increasing interest to examine the "resting state" of the brain. Studies of resting-state connectivity could be interesting to understand more about the default state of the brain that might influence spike and seizure generation. In fact, there are several studies showing that network connectivity is altered in resting epileptic brains.

High density EEG source connectivity identified the posterior cingulate cortex as the strongest driver in healthy subjects (70),

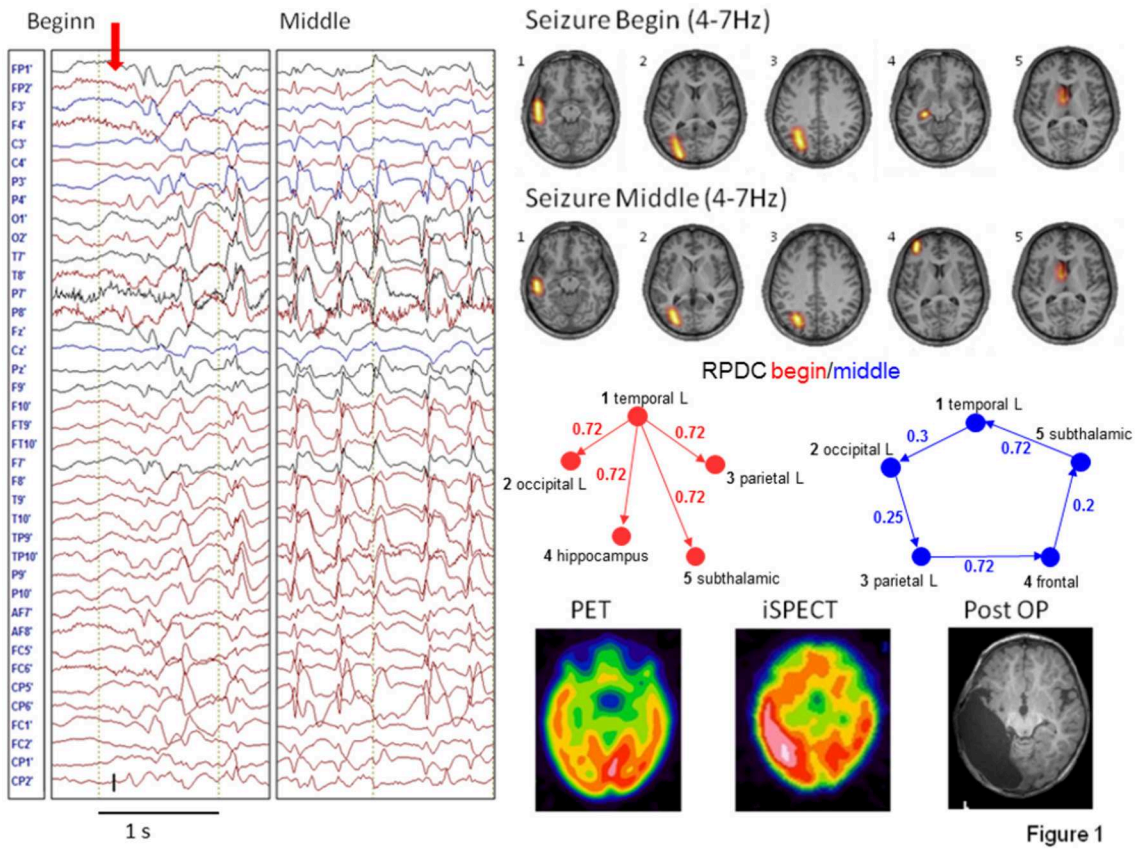

FIGURE 2 | Figure reproduced from Elshoff et al. (58). In the beginning of the seizure a star-shaped network topology with the SOZ as main hub is found, while during the middle of the seizure a circular network was found. Permission granted to reproduce under the terms of the Creative Commons Attribution License.

while in 20 patients with temporal lobe epilepsy, the maximum outflow was in the ipsilateral medial temporal lobe (24). It needs to be considered that measures for connectivity that are frequency specific such as the partial directed coherence in Coito et al. (24) require selection of a frequency range of interest. In their study, Coito et al. (24) selected the alpha range, because the main drivers were found in this frequency band. The choice of the frequency band may contribute to variation of results across studies. However, a follow-up study used a classifier to distinguish between patients and controls with a high accuracy of 91% and to lateralize the focus in 90% of patients in the absence of visible EEG abnormality. This could offer a potential powerful diagnostic biomarker (71) (**Figure 4**). It needs to be mentioned, however, that classification analysis by use of machine learning has undergone significant change over the last years. Initial enthusiasm was often based on biased selection of characteristics (features) by which the groups of interest would be separated. The main problem consisted in inappropriate subset selection approaches, leading to overfitting the results to the analyzed sample, thus, great results of sensitivity and specificity, but poor generalizability. Verhoeven et al. (71) illustrate that iterative algorithms with a random selection procedure reveal instability in the selected features—illustrating the effect of fitting the model to the sample. To conclude, studies using machine learning techniques should always be interpreted by taking into account the feature subset selection algorithm and how cross-validation is done.

In generalized epilepsy (19 patients with drug naive juvenile myoclonic epilepsy), Clemens et al. performed source-based connectivity analysis from EEG recordings (19 electrodes) using correlation measures. They found increased alpha band connectivity and decreased beta band connectivity as well as larger integration compared to controls (72). These alterations occurred mostly in the somatosensory integration areas. Although not obtained with the same approach as the directed connectivity study in temporal lobe epilepsy described above, this study points out to a very different pattern of connectivity alterations that strengthen the potential diagnostic role of M/EEG source connectivity analysis for epilepsy classification in the absence of visible interictal activity.

However, some studies report increased connectivity (5, 7), and other studies report decreased connectivity (6, 73) or complex patterns of increased and decreased connectivity (24). It is likely that these differences are influenced by the type of epilepsy studied (genetic/idiopathic vs. focal/lesional epilepsy), clinical differences (e.g., seizure rate/freedom), the

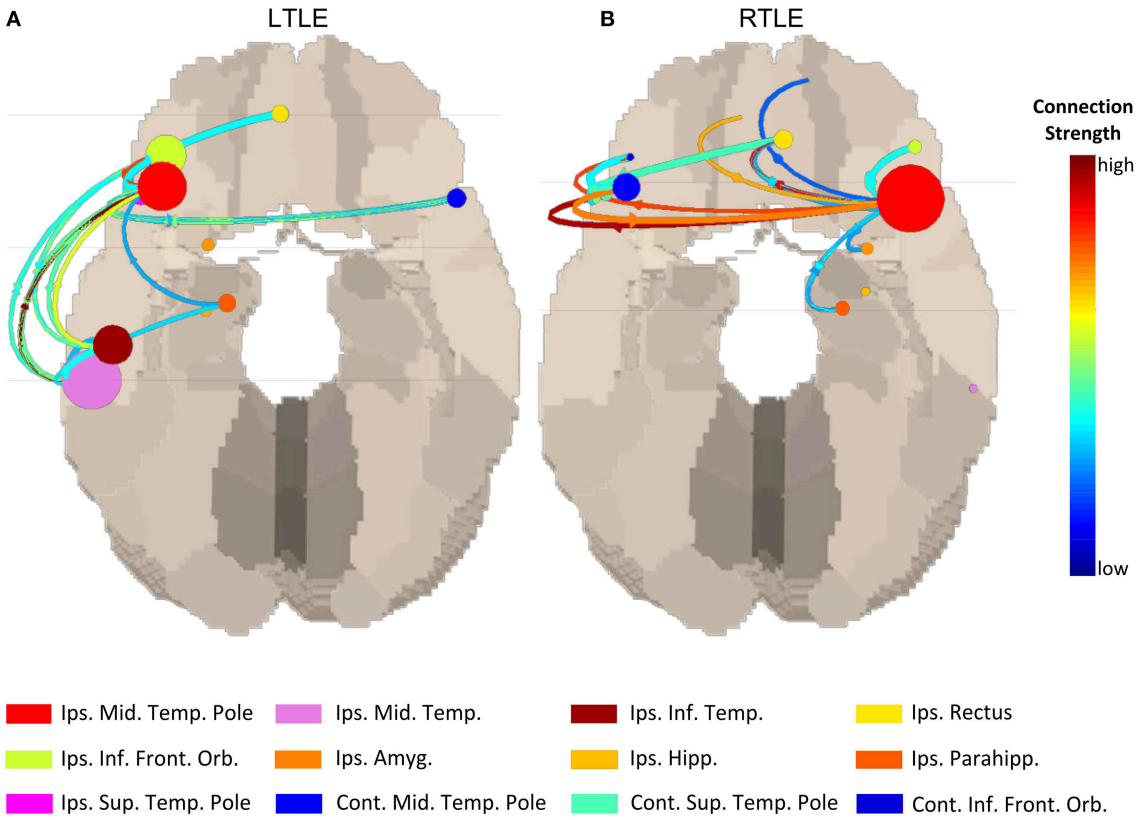

FIGURE 3 | Source connectivity pattern during interictal spikes at group level left temporal lobe epilepsy vs. right temporal lobe epilepsy. In the right temporal lobe epilepsy group more contralateral connectivity can be seen compared to the left temporal lobe epilepsy group which corresponded with more contralateral neuropsychological deficits in this group. Figure adapted from Coito et al. (25). Permission for reuse granted by John Wiley and Sons (License Number 4518770594674). Spike-related network patterns in **(A)** LTLE and **(B)** RTLE.

methods such as the choice of the frequency band, processing variants used and, possibly, medication (74). All these factors will need to be better addressed in future studies to allow better comparability. Currently, there is no established standard for this type of "resting-state" network analysis and there is only a limited understanding of the confounding technical and biological factors. Nevertheless, at least in some syndromes like idiopathic generalized epilepsy there is a spatial overlap between regions that show network alterations (3, 7) and spike sources (9) suggesting a biological link between them.

Under physiological conditions, the brain is constantly active, as is evident from EEG/MEG discharges even in the deepest stages of sleep. Moreover, the "resting state," i.e., the status of the brain without an active external task, is not a homogenous, single state but rather a combination/interplay of different states. Indeed scalp EEG data can be decomposed into alternating stable scalp voltage topographies called "microstates," (75). Future connectivity studies of the resting-state might gain from considering the different microstates separately. In these future studies, oversimplification of microstates to a few basic configurations is not recommendable. Larger scale evaluation of generalizability of microstates is first needed before choosing a set of pre-defined resting-state patterns. Moreover, comparison of microstates to the time-restricted view of source space connectivity is of interest, as time scale plays an important role in determining directed networks.

DISCUSSION

What Have We Learned (so Far) From the Connectomes

Localization

For interictal epileptic activity and non-spiking periods, existing studies have not focused at localizing pathological activity but rather at describing the large-scale brain networks and the patterns of connections across individual patients and groups of patients vs. healthy subjects. It remains to be determined if the analysis of interictal connectivity provides an added value over "plain" source localization for estimating the epileptogenic zone and post-operative outcome. For seizure analysis, very promising localizing results have been found for ictal recordings, using high density as well as low density recordings in patients with good post-operative outcome. So far only retrospective ictal connectivity studies were done in limited and homogeneous cohorts. Prospective studies need to confirm these findings in larger groups of patients with temporal and extra-temporal lobe

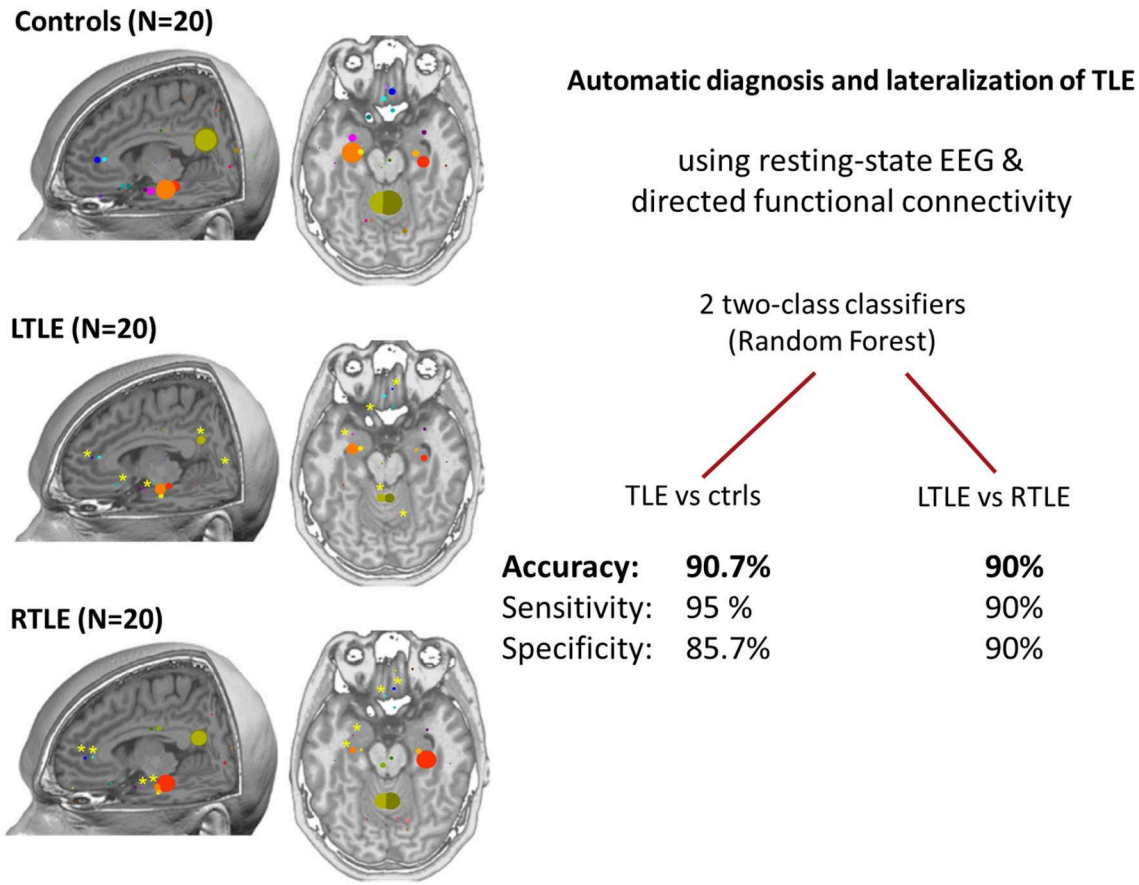

FIGURE 4 | Patterns of connectivity in non-spiking high density EEG (24). **Left**: comparison between healthy controls, left temporal lobe epilepsy and right temporal lobe epilepsy (20 subjects in each group). In controls, posterior cingulate and medial temporal structures are strong drivers of the network, the maximum being in the posterior cingulate cortex. In patients, there is a global reduction of the drivers with the maximum located in the ipsilateral medial temporal structures at group level. **Right**: the use of machine learning (two random forest classifiers) allowed achieving very high accuracy for the prediction of individual subjects suggesting a role of this analysis as a biomarker (71). Permission for reuse granted by John Wiley and Sons (License Number 4518770257321).

epilepsy and a variety of post-operative outcome to bring these techniques closer to clinical utility.

Diagnosis

The source connectivity during interictal spikes was shown to be concordant with cognitive deficits at group level (25). More contralateral spreading of the spikes was seen in right temporal lobe epilepsy compared to left temporal lobe epilepsy, which was in agreement with more contralateral neuropsychological deficits in right temporal lobe epilepsy. This is an indication that source connectivity has an additional potential diagnostic value. Nevertheless, the diagnostic added value should surpass the group level and be applicable to the individual patients before it can be used in patient treatment and follow-up.

There are promising results supporting connectivity analysis for improving the diagnosis of epilepsy and classification in the absence of visible EEG abnormalities (71). Further studies should include drug naive (first seizure) subjects, other types of epilepsies (generalized and focal) as well as patients with other neurological disorders (with and without structural abnormalities) including non-epileptic seizures. This would allow better estimating the sensitivity and specificity of such non-spiking EEG connectivity analysis that could assist the clinician in frequently difficult differential diagnoses. Indeed, abnormal connectivity patterns have been reported in 18 patients with non-epileptic seizures vs. controls (76). Abnormal findings based on high density EEG and phase-lag/synchronization measures affected mostly basal ganglia outflow although the ability of EEG connectivity to map connections from subcortical structures remains controversial. In patients with a first seizure, a connectivity study based on synchronization likelihood between scalp signals found that increased connectivity in the theta band was associated with an epilepsy diagnosis. In the absence of visible epileptic activity, connectivity could predict the diagnosis of epilepsy with sensitivity of 51% and specificity of 73% (77). In another study, increased theta band connectivity extracted from MEG in sensor space was shown to correlate with a higher number of epileptic seizures in brain tumor patients, indicating the potential to be used as biomarker for tumor-related epilepsy (78). Despite the methodological limitations

related to scalp signal analysis, these studies pave the way for similar investigations on the diagnostic and prognostic added value of M/EEG connectivity analysis in source space. Also, connectivity results in source space might be more intuitive for the physician than in sensor space because connections between brain regions are easier to understand than connections between sensors that do not necessarily represent the connectivity of proximal brain regions.

Predicting Outcome

The benefits of interictal, ictal, or resting state connectivity as a predictor of disease evolution (recurrence after first seizure, response to drug treatment, or epilepsy surgery) have not been formally studied and the same needs for validation and comparison of methods discussed in the previous section also apply here.

Regarding vagal nerve stimulation, Wostyn et al. (79) studied source activity and connectivity of the P300 response with the vagal nerve stimulation system on/off and found that good response to therapy was correlated with specific patterns of source activity and connectivity, mostly involving the limbic system, insula, and the orbitofrontal region. However, the study only investigated EEG after implantation of the vagal nerve stimulator. It remains unclear if effective connectivity patterns can predict whether patients will respond or not to vagal nerve stimulation.

Future Perspectives and Clinical Application

M/EEG source space connectivity techniques allow studying temporal patterns measured with M/EEG. For instance, it could be used to investigate network aspects of specific phenomena such as focal slowing [especially temporal, frontal, or occipital intermittent rhythmic delta activity (80)] and link specific patterns to specific forms of epilepsy (81). Furthermore, source space connectivity patterns could shed more light on how these M/EEG patterns are generated in the brain, and distinguish which patterns of focal slowing are potential surface correlates of epileptogenic activity from deeper regions.

Methodological Considerations

There exist a multitude of source localization methods and connectivity methods. It remains unclear which techniques should be used. Additional validation and comparison between source space connectivity methods is crucially needed in large patient cohorts with invasive validation. A pilot study showed that weighted minimum norm approach and phase-lag value were the best combination of inverse model and connectivity analysis on simulated data with application in only one patient (82). Such rigorous comparative approaches must be encouraged in broader clinical populations.

Several studies used informed selection of regions of interest in order to perform connectivity analysis, while others followed a rather data-driven approach. The drawback of the data-driven approach is that the selection of the interesting edges of the network is typically based on the magnitude of activity and/or interaction. However, the most meaningful regions do not necessarily exhibit the largest activity/connectivity with respect to the clinical question. For example, physiological process may exhibit a more prominent network than the pathological epileptic connection patterns. On this background, it is worth considering hypothesis driven analysis of source connectivity. However, in order to maintain objectivity, the grounds for selecting the regions of interest must be well motivated. One approach is to base the selection process on additional data. For example, resting-state fMRI or EEG-fMRI can be used to identify regions of interests that will be further investigated by MEG/EEG source connectivity (30). DCM, originally developed for fMRI, can also be understood as an informed approach and was earlier proposed to be used for estimating source space connectivity (83) and was used to determine the role of a-priori selected brain regions for seizure generation (84).

Currently, there is a lack of validation studies to bring source space connectivity into clinical practice. Even M/EEG source localization is still only performed in a modest number of centers worldwide, e.g., in the E-PILEPSY consortium electromagnetic source localization is only used at 12 out of 25 centers in the presurgical evaluation (85). Calculating source space connectivity is more complex than source localization alone. Given that the integration of source localization has already proven to be difficult in clinical practice, it can be anticipated that this will be an even larger challenge for source space connectivity. First, well designed prospective studies should show that source space connectivity has clear added value compared to the visual analysis of the electrophysiologist today on a patient specific level. Later, the methods should be available in standardized software with appropriate clearance for clinical use. Software for clinical use must come along with high usability, so that clinical-technical staff can do the necessary steps of processing (a) without risk of running into pitfalls that are common in source imaging and (b) within a workable time range, which is notoriously limited in clinical contexts. Next to this, standardized paradigms must be defined and tested, similarly to neuropsychological tests, in order to determine whether eloquent areas can be mapped by source connectivity analysis in pre-surgical evaluation. These paradigms must take into account the fact that network analyses require temporal information. Indeed, source-level connectivity needs different data properties than simple source-transformation of single events such as peaks of event related components. Only when all these limitations are overcome, can source connectivity be considered in clinical practice to assist in patient treatment and follow-up.

On the upper end of the EEG frequency range there are also promising fields of action for source connectivity: high frequency oscillations (HFOs), occurring above 80 Hz, have gathered great interest over the last two decades (86–88). However, evidence that HFOs might serve as an indicator for the region that needs to be resected in order to achieve seizure freedom is limited to invasive EEG recordings (89). MEG beamformer-based virtual sensors allowed to distinguish infrequent HFOs in MEG, from noise (90). It is of further interest whether measures of directed connectivity

can inform us better about the very local propagation patterns of HFOs. Multiple potential clinical as well as basic science implications warrant the technical effort to approach this new perspective. For instance, the differential propagation patterns of HFOs might distinguish pathological from physiological HFOs on surface recordings—a problem that is hard to tackle so far (91).

A further crucial approach is the validation of the methods applied to EEG and MEG by concurrently recorded intracranial signals from regions deep within the brain. These studies offer unique validation opportunities, by providing direct evidence that the sources derived from surface recorded signals indeed correlate with the neuronal activities linked to specific cognitive functions recorded directly from the responsible brain areas. For instance, Crespo-García et al. (92) used simultaneous intracranial EEG and MEG and showed that hippocampal slow-theta activity was negatively correlated with spatial accuracy for memorized locations. Other studies mostly investigated the circumstances in which intracranial epileptic discharges can be detected with non-invasive recordings (93).Time-derived connectivity analysis and single-event analysis would critically depend on such simultaneous recordings for validation.

Brain Networks in Cognition

Epilepsy offers unique opportunities to examine the physiological foundations of human cognition when basic science is conducted in patients undergoing invasive recordings. Results obtained from surface EEG in healthy participants can be source-transformed, and the localization can serve to select patients undergoing epilepsy surgery according to their medically indicated placement of invasive electrodes. For example, Ponz et al. (94) identified disgust-effects in event-related potentials with generators in the left anterior insula, as localized by source transformation of 64-channel surface EEG in 21 healthy participants. Two patients suffering from left frontotemporal epilepsy underwent presurgical investigation with depth cortical electrodes. These case studies confirmed early emotion effects in insular and orbitofrontal electrodes when undergoing the same cognitive testing procedure. In another study, Dalal et al. (95) demonstrated the localizability of sources derived from both, MEG and EEG, obtained during self-paced finger movements to the sensorimotor cortex, where the localization was confirmed again by electrocorticography from two epilepsy patients. Selecting patients with specific combination of intracranial electrodes could also be used for investigating network characteristics and validating connectivity analysis in these cognitive processes.

Taking this approach into the other direction, knowledge obtained in basic cognitive neurosciences can inform the localization of eloquent areas for the surgical management of patients who are candidates for epilepsy surgery (96). Adequate design of cognitive paradigms to be used in order to activate the eloquent area is often based on prior research in healthy samples, as well as the validation of the respective analysis pipeline. For example, MEG sources for language localization and lateralization can guide preoperative decision making (97, 98). This technique, be it based on EEG or MEG, can easily be extended to other questions regarding the boundaries of eloquent and to-be resected tissue (99–101). However, there is no report regarding the additional information that could be gained by source-level connectivity. Coito et al. (25) reported that the difference in source-level network patterns during interictal spikes in right and left temporal lobe epilepsy overlapped with neuropsychological deficits. However, whether such cognitive correlates may be detectable also in the absence of spikes by EEG/MEG source-level connectivity needs to be determined in future studies. Research projects addressing source-level connectivity and cognition in epilepsy are highly warranted, as connections between eloquent areas and pathological regions may significantly contribute to the outcome if the pathological region or a crucial connection is targeted surgically.

Box 1 | Summary Box

EEG/MEG source imaging is performed on signals to project them into brain/source space.
Connectivity analysis can reveal epileptic networks, which show specific patterns:

- **ictal hyperconnectivity**: higher connectivity and, specifically, higher outgoing information flow from the epileptogenic zone (53, 54, 58) reflects (initial) spreading activation patterns of seizures.
- **interictal epileptic discharge propagation**: directed connectivity reveals propagation patterns of spikes and, thus, their origin (25, 68).
- **diagnosis in the absence of epileptiform activity**: source connectivity patterns distinguish patients from healthy controls (3, 24, 70–72, 76–78).

Future directions should address outcome prediction (79), model validation (82), concurrent recording with intracranial signals (92), standardized cognitive stimulation protocols for assessing the eloquent area, for bringing source connectivity analysis into clinical practice.

CONCLUSION

Source connectivity derived from EEG or MEG opens up new perspectives on the network disease epilepsy (see **Box 1**). We can more intuitively "see" the origin and spread of pathological or physiological activity and this information can be integrated into clinical decision making. Studies in limited cohorts have shown that source connectivity can be used to localize the epileptogenic zone from ictal epochs and interictal spikes, and that diagnosis of epilepsy from resting state M/EEG is feasible. Nevertheless, several obstacles need to be overcome to bring these techniques into clinical use: (i) source connectivity methods should be standardized and validated with respect to invasive recordings in large patient cohorts, (ii) software with appropriate clearance for clinical use that has high usability and requires limited time of the staff should be developed, (iii) prospective validation studies that show the added value of source connectivity over visual analysis need to be conducted in large heterogeneous patient cohorts, and (iv) standard paradigms and the respective analysis

pipelines that allow to test functioning of eloquent areas need to be designed.

AUTHOR CONTRIBUTIONS

PvM provided the technical description of MEG/EEG source connectivity, ictal connectomes in epilepsy, combined contributions, and feedback by all authors and helped with the revision. YH described the background on connectivity, cognitive applications, future applications, and took care of the revision. NF provided insights into research and applications of MEG source connectivity, and clinical applications. SV summarized studies about interictal epileptiform discharges, detailed future perspectives, and clinical applications. All authors have edited, commented, and revised all sections of the manuscript and confirmed its final version.

FUNDING

PvM was funded by the Swiss National Science Foundation grant Nos. 179873 and 180365. YH was supported by the Austrian Science Fund (FWF): T 798-B27 and by the PMU-FFF: A-16/02/021-HÖL. NF was funded by Deutsche 1203 Forschungsgemeinschaft grant Nos. FO750/5-1 and FO750/7-1. SV was funded by Swiss National Science Foundation grant Nos. 169198 and 170873 and the Foundation Gertrude von Meissner. Part of this work was performed within the FLAG-ERA/JTC 2017 SCALES project.

REFERENCES

1. Kramer MA, Cash SS. Epilepsy as a disorder of cortical network organization. *Neuroscientist.* (2012) 18:360–72. doi: 10.1177/1073858411422754
2. Focke NK, Yogarajah M, Bonelli SB, Bartlett PA, Symms MR, Duncan JS. Voxel-based diffusion tensor imaging in patients with mesial temporal lobe epilepsy and hippocampal sclerosis. *Neuroimage.* (2008) 40:728–37. doi: 10.1016/j.neuroimage.2007.12.031
3. Focke NK, Diederich C, Helms G, Nitsche MA, Lerche H, Paulus W. Idiopathic-generalized epilepsy shows profound white matter diffusion-tensor imaging alterations. *Hum Brain Mapp.* (2013) 35:3332–42. doi: 10.1002/hbm.22405
4. van Diessen E, Diederen SJH, Braun KPJ, Jansen FE, Stam CJ. Functional and structural brain networks in epilepsy: what have we learned? *Epilepsia.* (2013) 54:1855–65. doi: 10.1111/epi.12350
5. Elshahabi A, Klamer S, Sahib AK, Lerche H, Braun C, Focke NK. Magnetoencephalography Reveals a Widespread Increase in Network Connectivity in Idiopathic/Genetic Generalized Epilepsy. *PLoS ONE.* (2015) 10:e0138119. doi: 10.1371/journal.pone.0138119
6. Englot DJ, Hinkley LB, Kort NS, Imber BS, Mizuiri D, Honma SM, et al. Global and regional functional connectivity maps of neural oscillations in focal epilepsy. *Brain.* (2015) 138:2249–62. doi: 10.1093/brain/awv130
7. Li Hegner Y, Marquetand J, Elshahabi A, Klamer S, Lerche H, Braun C, et al. Increased functional MEG connectivity as a hallmark of mri-negative focal and generalized epilepsy. *Brain Topogr.* (2018) 31:863–74. doi: 10.1007/s10548-018-0649-4
8. Klamer S, Ethofer T, Torner F, Sahib AK, Elshahabi A, Marquetand J, et al. Unravelling the brain networks driving spike-wave discharges in genetic generalized epilepsy-common patterns and individual differences. *Epilepsia Open.* (2018) 3:485–94. doi: 10.1002/epi4.12252
9. Bai X, Vestal M, Berman R, Negishi M, Spann M, Vega C, et al. Dynamic time course of typical childhood absence seizures: EEG, behavior, and functional magnetic resonance imaging. *J Neurosci.* (2010) 30:5884–93. doi: 10.1523/JNEUROSCI.5101-09.2010
10. Seneviratne U, Cook M, D'Souza W. Focal abnormalities in idiopathic generalized epilepsy: a critical review of the literature. *Epilepsia.* (2014) 55:1157–69. doi: 10.1111/epi.12688
11. Friston KJ. Functional and effective connectivity in neuroimaging: a synthesis. *Hum Brain Mapp.* (1994) 2:56–78. doi: 10.1002/hbm.460020107
12. Friston KJ. Functional and effective connectivity: a review. *Brain Connect.* (2011) 1:13–36. doi: 10.1089/brain.2011.0008
13. Horwitz B. The elusive concept of brain connectivity. *Neuroimage.* (2003) 19:466–70. doi: 10.1016/S1053-8119(03)00112-5
14. Lehnertz K. Assessing directed interactions from neurophysiological signals—an overview. *Physiol Meas.* (2011) 32:1715–24. doi: 10.1088/0967-3334/32/11/R01
15. Walter DO. Coherence as a measure of relationship between EEG records. *Electroenceph Clin Neurophysiol.* (1968) 24:282.
16. Gersch W, Goddard GV. Epileptic focus location: spectral analysis method. *Science.* (1970) 169:701–2. doi: 10.1126/science.169.3946.701
17. Granger CWJ. Investigating causal relations by econometric models and cross-spectral methods. *Econometrica.* (1969) 37:424. doi: 10.2307/1912791
18. Baccalá LA, Sameshima K. Partial directed coherence: a new concept in neural structure determination. *Biol Cybern.* (2001) 84:463–74. doi: 10.1007/PL00007990
19. Kaminski MJ, Blinowska KJ. A new method of the description of the information flow in the brain structures. *Biol Cybern.* (1991) 65:203–10. doi: 10.1007/BF00198091
20. David O, Kiebel SJ, Harrison LM, Mattout J, Kilner JM, Friston KJ. Dynamic causal modeling of evoked responses in EEG and MEG. *Neuroimage.* (2006) 30:1255–72. doi: 10.1016/j.neuroimage.2005.10.045
21. Lehnertz K, Ansmann G, Bialonski S, Dickten H, Geier C, Porz S. Evolving networks in the human epileptic brain. *Physica D.* (2014) 267:7–15. doi: 10.1016/j.physd.2013.06.009
22. Bassett DS, Sporns O. Network neuroscience. *Nat Neurosci.* (2017) 20:353–64. doi: 10.1038/nn.4502
23. van Mierlo P, Papadopoulou M, Carrette E, Boon P, Vandenberghe S, Vonck K, et al. Functional brain connectivity from EEG in epilepsy: Seizure prediction and epileptogenic focus localization. *Progr Neurobiol.* (2014) 121:19–35. doi: 10.1016/j.pneurobio.2014.06.004
24. Coito A, Genetti M, Pittau F, Iannotti GR, Thomschewski A, Höller Y, et al. Altered directed functional connectivity in temporal lobe epilepsy in the absence of interictal spikes: a high density EEG study. *Epilepsia.* (2016) 57:402–11. doi: 10.1111/epi.13308
25. Coito A, Plomp G, Genetti M, Abela E, Wiest R, Seeck M, et al. Dynamic directed interictal connectivity in left and right temporal lobe epilepsy. *Epilepsia.* (2015) 56:207–17. doi: 10.1111/epi.12904
26. Staljanssens W, Strobbe G, Holen RV, Birot G, Gschwind M, Seeck M, et al. Seizure onset zone localization from ictal high-density EEG in refractory focal epilepsy. *Brain Topogr.* (2017) 30:257–71. doi: 10.1007/s10548-016-0537-8
27. Watanabe S, Dubeau F, Zazubovits N, Gotman J. Temporal lobe spikes: EEG-fMRI contributions to the "mesial vs. lateral" debate. *Clin Neurophysiol.* (2017) 128:986–91. doi: 10.1016/j.clinph.2017.03.041
28. Pittau F, Ferri L, Fahoum F, Dubeau F, Gotman J. Contributions of EEG-fMRI to assessing the epileptogenicity of focal cortical dysplasia. *Front Comput Neurosci.* (2017) 11:8. doi: 10.3389/fncom.2017.00008
29. Moeller F, Stephani U, Siniatchkin M. Simultaneous EEG and fMRI recordings (EEG-fMRI) in children with epilepsy. *Epilepsia.* (2013) 54:971–82. doi: 10.1111/epi.12197
30. Centeno M, Carmichael DW. Network connectivity in epilepsy: resting state fMRI and EEG-fMRI contributions. *Front Neurol.* (2014) 5:93. doi: 10.3389/fneur.2014.00093
31. Lei X, Wu T, Valdes-Sosa PA. Incorporating priors for EEG source imaging and connectivity analysis. *Front Neurosci.* (2015) 9:284. doi: 10.3389/fnins.2015.00284

32. Winter WR, Nunez PL, Ding J, Srinivasan R. Comparison of the effect of volume conduction on EEG coherence with the effect of field spread on MEG coherence. *Stat Med.* (2007) 26:3946–57. doi: 10.1002/sim.2978
33. Haufe S, Nikulin VV, Müller K-R, Nolte G. A critical assessment of connectivity measures for EEG data: a simulation study. *Neuroimage*. (2013) 64:120–33. doi: 10.1016/j.neuroimage.2012.09.036
34. Van de Steen F, Faes L, Karahan E, Songsiri J, Valdes-Sosa PA, Marinazzo D. Critical comments on EEG sensor space dynamical connectivity analysis. *Brain Topogr.* (2019) 32:643–54. doi: 10.1007/s10548-016-0538-7
35. Trujillo LT, Stanfield CT, Vela RD. The Effect of Electroencephalogram (EEG) reference choice on information-theoretic measures of the complexity and integration of EEG signals. *Front Neurosci.* (2017) 11:425. doi: 10.3389/fnins.2017.00425
36. Nolte G, Bai O, Wheaton L, Mari Z, Vorbach S, Hallett M. Identifying true brain interaction from EEG data using the imaginary part of coherency. *Clin Neurophysiol.* (2004) 115:2292–307. doi: 10.1016/j.clinph.2004.04.029
37. Anzolin A, Presti P, Van de Steen F, Astolfi L, Haufe S, Marinazzo D. Effect of head volume conduction on directed connectivity estimated between reconstructed EEG sources. *bioRxiv [Preprint].* (2018). doi: 10.1101/251223
38. Florin E, Gross J, Pfeifer J, Fink GR, Timmermann L. The effect of filtering on Granger causality based multivariate causality measures. *Neuroimage*. (2010) 50:577–88. doi: 10.1016/j.neuroimage.2009.12.050
39. Hämäläinen M, Hari R, Ilmoniemi RJ, Knuutila J, Lounasmaa OV. Magnetoencephalography—theory, instrumentation, and applications to noninvasive studies of the working human brain. *Rev Mod Phys.* (1993) 65:413–97. doi: 10.1103/RevModPhys.65.413
40. Nolte G. The magnetic lead field theorem in the quasi-static approximation and its use for magnetoencephalography forward calculation in realistic volume conductors. *Phys Med Biol.* (2003) 48:3637–52. doi: 10.1088/0031-9155/48/22/002
41. Lalancette M, Quraan M, Cheyne D. Evaluation of multiple-sphere head models for MEG source localization. *Phys Med Biol*. (2011) 56:5621–35. doi: 10.1088/0031-9155/56/17/010
42. Cho J-H, Vorwerk J, Wolters CH, Knösche TR. Influence of the head model on EEG and MEG source connectivity analyses. *Neuroimage*. (2015) 110:60–77. doi: 10.1016/j.neuroimage.2015.01.043
43. Hallez H, Vanrumste B, Grech R, Muscat J, De Clercq W, Vergult A, et al. Review on solving the forward problem in EEG source analysis. *J Neuroeng Rehabil.* (2007) 4:46. doi: 10.1186/1743-0003-4-46
44. Hincapié A-S, Kujala J, Mattout J, Pascarella A, Daligault S, Delpuech C, et al. The impact of MEG source reconstruction method on source-space connectivity estimation: a comparison between minimum-norm solution and beamforming. *Neuroimage.* (2017) 156:29–42. doi: 10.1016/j.neuroimage.2017.04.038
45. Ahlfors SP, Han J, Belliveau JW, Hämäläinen MS. Sensitivity of MEG and EEG to source orientation. *Brain Topogr.* (2010) 23:227–32. doi: 10.1007/s10548-010-0154-x
46. Hunold A, Funke ME, Eichardt R, Stenroos M, Haueisen J. EEG and MEG: sensitivity to epileptic spike activity as function of source orientation and depth. *Physiol Meas*. (2016) 37:1146–62. doi: 10.1088/0967-3334/37/7/1146
47. Delorme A, Makeig S. EEGLAB: an open source toolbox for analysis of single-trial EEG dynamics including independent component analysis. *J Neurosci Methods*. (2004) 134:9–21. doi: 10.1016/j.jneumeth.2003.10.009
48. Brunet D, Murray MM, Michel CM. Spatiotemporal analysis of multichannel EEG: CARTOOL. *Comput Intell Neurosci.* (2011) 2011:813870. doi: 10.1155/2011/813870
49. Oostenveld R, Fries P, Maris E, Schoffelen J-M. FieldTrip: open source software for advanced analysis of MEG, EEG, and invasive electrophysiological data. *Comput Intell Neurosci.* (2011) 2011:156869. doi: 10.1155/2011/156869
50. Tadel F, Baillet S, Mosher JC. Brainstorm: a user-friendly application for MEG/EEG analysis. *Comput Intell Neurosci*. (2011) 2011:879716. doi: 10.1155/2011/879716
51. He B, Dai Y, Astolfi L, Babiloni F, Yuan H, Yang L. eConnectome: A MATLAB toolbox for mapping and imaging of brain functional connectivity. *J Neurosci Methods*. (2011) 195:261–9. doi: 10.1016/j.jneumeth.2010.11.015
52. Gramfort A, Luessi M, Larson E, Engemann D, Strohmeier D, Brodbeck C, et al. MNE software for processing MEG and EEG data. *Neuroimage*. (2014) 86:446–60. doi: 10.1016/j.neuroimage.2013.10.027
53. Ding L, Worrell GA, Lagerlund TD, He B. Ictal source analysis: localization and imaging of causal interactions in humans. *Neuroimage*. (2007) 34:575–86. doi: 10.1016/j.neuroimage.2006.09.042
54. Lu Y, Yang L, Worrell GA, He B. Seizure source imaging by means of FINE spatio-temporal dipole localization and directed transfer function in partial epilepsy patients. *Clin Neurophysiol*. (2012) 123:1275–83. doi: 10.1016/j.clinph.2011.11.007
55. Staljanssens W, Strobbe G, Van Holen R, Keereman V, Gadeyne S, Carrette E, et al. EEG source connectivity to localize the seizure onset zone in patients with drug resistant epilepsy. *NeuroImage*. (2017) 16:689–98. doi: 10.1016/j.nicl.2017.09.011
56. Sohrabpour A, Ye S, Worrell GA, Zhang W, He B. Noninvasive electromagnetic source imaging and granger causality analysis: an electrophysiological connectome (eConnectome) approach. *IEEE Trans Biomed Eng.* (2016) 63:2474–87. doi: 10.1109/TBME.2016.2616474
57. Martinez-Vargas JD, Strobbe G, Vonck K, Mierlo PV, Castellanos-Dominguez1 G. Improved localization of seizure onset zones using spatiotemporal constraints and time-varying source connectivity. *Front Neurosci.* (2017) 11:156. doi: 10.3389/fnins.2017.00156
58. Elshoff L, Muthuraman M, Anwar AR, Deuschl G, Stephani U, Raethjen J, et al. Dynamic imaging of coherent sources reveals different network connectivity underlying the generation and perpetuation of epileptic seizures. *PLoS ONE*. (2013) 8:e78422. doi: 10.1371/journal.pone.0078422
59. Japaridze N, Muthuraman M, Dierck C, von Spiczak S, Boor R, Mideksa KG, et al. Neuronal networks in epileptic encephalopathies with CSWS. *Epilepsia*. (2016) 57:1245–55. doi: 10.1111/epi.13428
60. Klamer S, Rona S, Elshahabi A, Lerche H, Braun C, Honegger J, et al. Multimodal effective connectivity analysis reveals seizure focus and propagation in musicogenic epilepsy. *Neuroimage*. (2015) 113:70–7. doi: 10.1016/j.neuroimage.2015.03.027
61. Ebersole JS, Wagner M. Relative yield of MEG and EEG spikes in simultaneous recordings. *J Clin Neurophysiol*. (2018) 5:443–53. doi: 10.1097/WNP.0000000000000512
62. Duez L, Beniczky S, Tankisi H, Hansen PO, Sidenius P, Sabers A, et al. Added diagnostic value of magnetoencephalography (MEG) in patients suspected for epilepsy, where previous, extensive EEG workup was unrevealing. *Clin Neurophysiol*. (2016) 127:3301–5. doi: 10.1016/j.clinph.2016.08.006
63. Brodbeck V, Spinelli L, Lascano AM, Wissmeier M, Vargas MI, Vulliemoz S, et al. Electroencephalographic source imaging: a prospective study of 152 operated epileptic patients. *Brain.* (2011) 134(Pt 10):2887–97. doi: 10.1093/brain/awr243
64. Rikir E, Koessler L, Gavaret M, Bartolomei F, Colnat-Coulbois S, Vignal JP, et al. Electrical source imaging in cortical malformation-related epilepsy: a prospective EEG-SEEG concordance study. *Epilepsia*. (2014) 55:918–32. doi: 10.1111/epi.12591
65. Lascano AM, Perneger T, Vulliemoz S, Spinelli L, Garibotto V, Korff CM, et al. Yield of MRI, high-density electric source imaging (HD-ESI), SPECT and PET in epilepsy surgery candidates. *Clin Neurophysiol.* (2016) 127:150–5. doi: 10.1016/j.clinph.2015.03.025
66. Sharma P, Scherg M, Pinborg LH, Fabricius M, Rubboli G, Pedersen B, et al. Ictal and interictal electric source imaging in pre-surgical evaluation: a prospective study. *Eur J Neurol.* (2018) 25:1154–60. doi: 10.1111/ene.13676
67. Dai Y, Zhang W, Dickens DL, He B. Source connectivity analysis from MEG and its application to epilepsy source localization. *Brain Topogr.* (2011) 25:157–66. doi: 10.1007/s10548-011-0211-0
68. Storti SF, Galazzo IB, Khan S, Manganotti P, Menegaz G. Exploring the epileptic brain network using time-variant effective connectivity and graph theory. *IEEE J Biomed Health Informat*. (2017) 21:1411–21. doi: 10.1109/JBHI.2016.2607802

69. Adebimpe A, Bourel-Ponchel E, Wallois F. Identifying neural drivers of benign childhood epilepsy with centrotemporal spikes. *NeuroImage*. (2018) 17:739–50. doi: 10.1016/j.nicl.2017.11.024
70. Coito A, Michel CM, Vulliemoz S, Plomp G. Directed functional connections underlying spontaneous brain activity. *Hum Brain Mapp*. (2018) 40:879–88. doi: 10.1002/hbm.24418
71. Verhoeven T, Coito A, Plomp G, Thomschewski A, Pittau F, Trinka E, et al. Automated diagnosis of temporal lobe epilepsy in the absence of interictal spikes. *NeuroImage*. (2018) 17:10–5. doi: 10.1016/j.nicl.2017.09.021
72. Clemens B, Puskas S, Bessenyei M, Emri M, Spisak T, Koselak M, et al. EEG functional connectivity of the intrahemispheric cortico-cortical network of idiopathic generalized epilepsy. *Epilepsy Res*. (2011) 96:11–23. doi: 10.1016/j.eplepsyres.2011.04.011
73. Bernhardt BC, Bernasconi A, Liu M, Hong S-J, Caldairou B, Goubran M, et al. The spectrum of structural and functional imaging abnormalities in temporal lobe epilepsy. *Ann Neurol*. (2016) 80:142–53. doi: 10.1002/ana.24691
74. Höller Y, Helmstaedter C, Lehnertz K. Quantitative pharmaco-electroencephalography in antiepileptic drug research. *CNS Drugs*. (2018) 32:839–48. doi: 10.1007/s40263-018-0557-x
75. Michel CM, Koenig T. EEG microstates as a tool for studying the temporal dynamics of whole-brain neuronal networks: a review. *Neuroimage*. (2018) 180:577–93. doi: 10.1016/j.neuroimage.2017.11.062
76. Barzegaran E, Carmeli C, Rossetti AO, Frackowiak RS, Knyazeva MG. Weakened functional connectivity in patients with psychogenic non-epileptic seizures (PNES) converges on basal ganglia. *J Neurol Neurosurg Psychiatr*. (2015) 87:332–7. doi: 10.1136/jnnp-2014-309483
77. Douw L, de Groot M, van Dellen E, Heimans JJ, Ronner HE, Stam CJ, et al. "Functional connectivity" is a sensitive predictor of epilepsy diagnosis after the first seizure. *PLoS ONE*. (2010) 5:e10839. doi: 10.1371/journal.pone.0010839
78. Douw L, van Dellen E, de Groot M, Heimans JJ, Klein M, Stam CJ, et al. Epilepsy is related to theta band brain connectivity and network topology in brain tumor patients. *BMC Neurosci.*. (2010) 11:103. doi: 10.1186/1471-2202-11-103
79. Wostyn S, Staljanssens W, De Taeye L, Strobbe G, Gadeyne S, Van Roost D, et al. EEG derived brain activity reflects treatment response from vagus nerve stimulation in patients with epilepsy. *Int J Neural Syst*. (2017) 27:1650048. doi: 10.1142/S0129065716500489
80. Cobb WA. Rhythmic slow discharges in the electro-encephalogram. *J Neurol Neurosurg Psychiatr*. (1945) 8:65–78. doi: 10.1136/jnnp.8.3-4.65
81. Brigo F. Intermittent rhythmic delta activity patterns. *Epilepsy Behav*. (2011) 20:254–6. doi: 10.1016/j.yebeh.2010.11.009
82. Hassan M, Merlet I, Mheich A, Kabbara A, Biraben A, Nica A, et al. Identification of interictal epileptic networks from dense-EEG. *Brain Topogr*. (2016) 30:60–76. doi: 10.1007/s10548-016-0517-z
83. Lemieux L, Daunizeau J, Walker MC. Concepts of connectivity and human epileptic activity. *Front Syst Neurosci*. (2011) 5:12. doi: 10.3389/fnsys.2011.00012
84. Vaudano AE, Laufs H, Kiebel SJ, Carmichael DW, Hamandi K, Guye M, et al. Causal hierarchy within the thalamo-cortical network in spike and wave discharges. *PLoS ONE*. (2009) 4:e6475. doi: 10.1371/journal.pone.0006475
85. Mouthaan BE, Rados M, Barsi P, Boon P, Carmichael DW, Carrette E, et al. Current use of imaging and electromagnetic source localization procedures in epilepsy surgery centers across Europe. *Epilepsia*. (2016) 57:770–6. doi: 10.1111/epi.13347
86. Allen PJ, Fish DR, Smith SJM. Very high-frequency rhythmic activity during SEEG suppression in frontal lobe epilepsy. *Electroencephalogr Clin Neurophysiol*. (1992) 82:155–9. doi: 10.1016/0013-4694(92)90160-J
87. Fried I, Wilson CL, Maidment NT, Engel J, Behnke E, Fields TA, et al. Cerebral microdialysis combined with single-neuron and electroencephalographic recording in neurosurgical patients. *J Neurosurg*. (1999) 91:697–705. doi: 10.3171/jns.1999.91.4.0697
88. Jacobs J, Zijlmans M, Zelmann R, Chatillon C-É, Hall J, Olivier A, et al. High-frequency electroencephalographic oscillations correlate with outcome of epilepsy surgery. *Ann Neurol*. (2010) 67:209–20. doi: 10.1002/ana.21847
89. Höller Y, Kutil R, Klaffenböck L, Thomschewski A, Höller PM, Bathke AC, et al. High-frequency oscillations in epilepsy and surgical outcome. A meta-analysis. *Front Hum Neurosci*. (2015) 9:574. doi: 10.3389/fnhum.2015.00574
90. van Klink N, Hillebrand A, Zijlmans M. Identification of epileptic high frequency oscillations in the time domain by using MEG beamformer-based virtual sensors. *Clin Neurophysiol*. (2016) 127:197–208. doi: 10.1016/j.clinph.2015.06.008
91. Höller P, Trinka E, Höller Y. High-frequency oscillations in the scalp electroencephalogram: mission impossible without computational intelligence. *Comput Intell Neurosci*. (2018) 2018:1–9. doi: 10.1155/2018/1638097
92. Crespo-García M, Zeiller M, Leupold C, Kreiselmeyer G, Rampp S, Hamer HM, et al. Slow-theta power decreases during item-place encoding predict spatial accuracy of subsequent context recall. *Neuroimage*. (2016) 142:533–43. doi: 10.1016/j.neuroimage.2016.08.021
93. Dubarry AS, Badier JM, Trébuchon-Da Fonseca A, Gavaret M, Carron R, Bartolomei F, et al. Simultaneous recording of MEG, EEG and intracerebral EEG during visual stimulation: from feasibility to single-trial analysis. *Neuroimage*. (2014) 99:548–58. doi: 10.1016/j.neuroimage.2014.05.055
94. Ponz A, Montant M, Liegeois-Chauvel C, Silva C, Braun M, Jacobs AM, et al. Emotion processing in words: a test of the neural re-use hypothesis using surface and intracranial EEG. *Soc Cogn Affect Neurosci*. (2013) 9:619–27. doi: 10.1093/scan/nst034
95. Dalal SS, Guggisberg AG, Edwards E, Sekihara K, Findlay AM, Canolty RT, et al. Five-dimensional neuroimaging: localization of the time–frequency dynamics of cortical activity. *Neuroimage*. (2008) 40:1686–700. doi: 10.1016/j.neuroimage.2008.01.023
96. Shibasaki H, Ikeda A, Nagamine T. Use of magnetoencephalography in the presurgical evaluation of epilepsy patients. *Clin Neurophysiol*. (2007) 118:1438–48. doi: 10.1016/j.clinph.2007.03.002
97. Doss RC, Zhang W, Risse GL, Dickens DL. Lateralizing language with magnetic source imaging: validation based on the Wada test. *Epilepsia*. (2009) 50:2242–8. doi: 10.1111/j.1528-1167.2009.02242.x
98. Pirmoradi M, Jemel B, Gallagher A, Tremblay J, D'Hondt F, Nguyen DK, et al. Verbal memory and verbal fluency tasks used for language localization and lateralization during magnetoencephalography. *Epilepsy Res*. (2016) 119:1–9. doi: 10.1016/j.eplepsyres.2015.11.015
99. Pataraia E, Baumgartner C, Lindinger G, Deecke L. Magnetoencephalography in presurgical epilepsy evaluation. *Neurosurg Rev*. (2002) 25:141–59. doi: 10.1007/s10143-001-0197-2
100. Nagarajan S, Kirsch H, Lin P, Findlay A, Honma S, Berger MS. Preoperative localization of hand motor cortex by adaptive spatial filtering of magnetoencephalography data. *J Neurosurg*. (2008) 228–37. doi: 10.3171/JNS/2008/109/8/0228
101. Burgess RC, Funke ME, Bowyer SM, Lewine JD, Kirsch HE, Bagić AI. American clinical magnetoencephalography society clinical practice guideline 2. *J Clin Neurophysiol*. (2011) 28:355–61. doi: 10.1097/WNP.0b013e3182272ffe

Conflict of Interest Statement: PvM is a co-founder and shareholder of Epilog NV (Ghent, Belgium). SV is an advisor and shareholder of Epilog NV (Ghent, Belgium).

The remaining authors declare that the research was conducted in the absence of any commercial or financial relationships that could be construed as a potential conflict of interest.

frontiers in Neurology

ORIGINAL RESEARCH
published: 20 August 2019
doi: 10.3389/fneur.2019.00855

Taking the EEG Back Into the Brain: The Power of Multiple Discrete Sources

Michael Scherg[1]*, *Patrick Berg*[1], *Nobukazu Nakasato*[2] and *Sándor Beniczky*[3]

[1] Research Department, BESA GmbH, Gräfelfing, Germany, [2] Department of Epileptology, Tohoku University, Sendai, Japan, [3] Department of Clinical Neurophysiology, Danish Epilepsy Centre, Aarhus University Hospital, Aarhus, Denmark

Background: In contrast to many neuroimaging modalities, clinical interpretation of EEG does not take advantage of post-processing and digital signal analysis. In most centers, EEG is still interpreted at sensor level, exactly as half a century ago. A major task in clinical EEG interpretation is the identification of interictal epileptiform discharges (IEDs). However, due to the overlap of background activity, IEDs can be hard to detect in the scalp EEG. Since traditional montages, like bipolar and average reference, are linear transformations of the recorded channels, the question is whether we can provide linear transformations of the digital EEG to take it back into the brain, at least on a macroscopic level. The goal is to improve visibility of epileptiform activities and to separate out most of the overlap.

Methods: Multiple discrete sources provide a stable linear inverse to transform the EEG into source space with little cross-talk between source regions. The model can be based on a few dipoles or regional sources, adapted to the individual EEG and MRI data, or on selected standard sources evenly distributed throughout the brain, e.g. below the 25 EEG standard electrodes.

Results: Auditory and somatosensory evoked potentials serve as teaching examples to show how various source spaces can reveal the underlying source components including their loss or alteration due to lesions. Source spaces were able to reveal the propagation of source activities in frontal IEDs and the sequential activation of the major nodes of the underlying epileptic network in myoclonic epilepsy. The power of multiple discrete sources in separating the activities of different brain regions was also evident in the ongoing EEG of cases with frontal cortical dysplasia and bitemporal lobe epilepsy. The new source space 25 made IEDs more clearly visible over the EEG background signals. The more focal nature of source vs. scalp space was quantitatively confirmed using a new measurement of focality.

Conclusion: Multiple discrete sources have the power to transform the EEG back into the brain by defining new EEG traces in source space. Using standard source space 25, these can provide for improved clinical interpretation of EEG.

Keywords: EEG, epilepsy, evoked potentials, source space, source montages, dipole source localization, multiple discrete sources, linear transformation

OPEN ACCESS

Edited by:
Christian Gaser,
Friedrich Schiller University Jena, Germany

Reviewed by:
Roman Rodionov,
University College London, United Kingdom
Radek Janca,
Czech Technical University in Prague, Czechia
Charles Akos Szabo,
Long School of Medicine at UT Health San Antonio, United States

***Correspondence:**
Michael Scherg
mscherg@besa.de

Specialty section:
This article was submitted to Applied Neuroimaging, a section of the journal Frontiers in Neurology

Received: *19 February 2019*
Accepted: *23 July 2019*
Published: *20 August 2019*

Citation:
Scherg M, Berg P, Nakasato N and Beniczky S (2019) Taking the EEG Back Into the Brain: The Power of Multiple Discrete Sources. Front. Neurol. 10:855. doi: 10.3389/fneur.2019.00855

INTRODUCTION

The dipolar activities of the different brain regions appear widespread over the scalp and generate a complex overlap in the EEG. Although the radially oriented activities of the cortical convexity are more prominent in the EEG, two thirds of the cortex lie in fissures and lead to widely distributed topographies on the scalp as illustrated in **Figure 1**. When trying to localize a focal interictal epileptiform discharge (IED), we are looking for a negative peak in the scalp EEG based on the fact that the pyramidal cells at the crown of a gyrus are depolarized at their apical dendrites. Thus, the primary, intracellular currents flow radially into the depth parallel to the cortical columns. The associated return currents form closed loops (**Figure 1**). Only a small portion of the current passes the skull and returns along the scalp. This creates the positive peaks on the scalp at the maximum exit zone (illustrated by the light red arrows in **Figure 1**) and the negative peaks at the maximum reentry zone (light blue arrows).

With an ideal radial current, the scalp negativity is exactly over the superficial cortical generator (**Figure 1**, left). If the depolarization occurs on one side of a sulcus that goes straight into the depth, the associated tangential current creates a scalp topography with symmetric negative and positive poles perpendicular to the sulcus, with the positivity on the active side (**Figure 1**, right). Normally, focal IEDs involve both sulcal and superficial cortex or deeper parts of sulci. The resulting net orientation of the primary current is oblique. The associated negative and positive peaks are unequal and somewhat shifted away from the active cortex (**Figure 1**, middle). In fact, the negative peaks can be far away from the active cortex especially if the focus is deeper in the brain, leading, for example, to the so-called "paradoxical" or "false" lateralization over the wrong hemisphere. Thus, a key problem of interpreting the EEG is its crucial dependence on the orientation of the active cortex.

The other problem is the traditional concept of the EEG. When observing a spike in the EEG, our primary thought is: Where is the source of this spike? Intuitively, we assume a single source for a prominent spike or a peak in an evoked potential (**Figure 2**). However, considering the complex overlap on the scalp, we might pose a different question: What do the different brain regions contribute to cause this spike or peak? This new approach implies that we can confirm the existence of a focal origin only, if we can show that no region in the brain except one is contributing substantially. This is the basic concept of reverse source imaging (RSI) using multiple discrete sources (MDS), as detailed below.

Obviously, we cannot uniquely reconstruct the activity of all pyramidal cells from the few recorded EEG channels, not even of all gyri and sulci in the brain. This is the so-called inverse problem of EEG, i.e. to estimate the regions in the 3D-brain that contribute to the 2D-voltage distribution on the scalp surface. **Figure 2** illustrates different approaches how to solve the inverse problem. Take, for example, the prominent N100 peak of late auditory evoked potentials (LAEP) at mid-frontal electrodes. Using a single dipole, you localize into the middle of the brain with high goodness of fit (GoF: 97%), but not bilaterally into the auditory cortices (AC) as expected (1, 2). The assumption of a single source is not valid. Similarly, beamformers mis-localize to one equivalent center (**Figure 2A**) unless you assume two symmetric beams pointing into each hemisphere. Distributed source models, on the other hand, use thousands of equivalent dipoles in the brain volume, or hundreds in the cortical gray matter. This requires additional mathematical, non-physiological assumptions. For example, smoothness in source space is used in LORETA (3). CLARA, i.e. LORETA applied recursively (4, 5), separates two foci around the right and left auditory cortices in this LAEP elicited by auditory stimuli of varying intensity (6). However, foci in distributed source images are smeared and shift over time and the small activity of cingulate gyrus (CG), imaged by the MDS model in **Figure 2C**, was not detected.

MDS models are an alternative to project the scalp data into the brain, here onto three fixed regional sources bilaterally in AC and in CG. Prior to discussing this approach in detail, we need to lay out viable concepts of source space and linear transformations to take the EEG back into the brain on a macroscopic level. At the same time, we must ascertain that our assumptions are appropriate for the data to be analyzed.

In contrast to MRI or CT, EEG is still interpreted at sensor level. Most clinicians reading EEG inspect only raw data. Although accessing undistorted raw signals is important, reluctance to include signal processing into clinical practice precludes any progress in this field. In fact, clinical EEG has proven to be one of the most conservative fields in medicine, where trainees are still taught exactly the same routines as their tutors were several decades ago.

Therefore, this paper documents how to create a new perspective onto the EEG by taking it back into brain source space. This is achieved by simple linear transformations of the scalp EEG in addition to digital filtering in the time domain. First, we need to outline the concepts of equivalent sources, of local and global source spaces and of linear transformations. Then, we can illustrate how brain source space provides additional insight into IEDs and evoked potentials.

BASIC CONCEPTS OF EQUIVALENT SOURCES AND BRAIN SOURCE SPACE

The Local Source Space

In evoked potentials, the situation appears relatively simple. In the ascending pathways, the local source space is defined by a specific fiber tract leaving a nucleus (7) or crossing a boundary of the volume conductor (8). In sensory cortex, perception occurs in small, circumscribed cytoarchitectonic areas. Thus, the dipole currents of the cortical columns sum up to an equivalent dipole with high precision (**Figure 3A**). Accordingly, the scalp potential is relatively small ($<5\ \mu V$). In the case of an IED, the activated area is often much larger, especially in mesial temporal lobe epilepsy with up to 10–20 cm^2 (9). If we assume a circular shape of the activated cortical patch, this would correspond to a diameter of ∼3.6–5 cm and amplitudes $>100\ \mu V$ on the scalp. In extra-temporal-lobe epilepsy, IED amplitudes are often smaller ($\sim 30\ \mu V$), but this still requires a patch diameter of

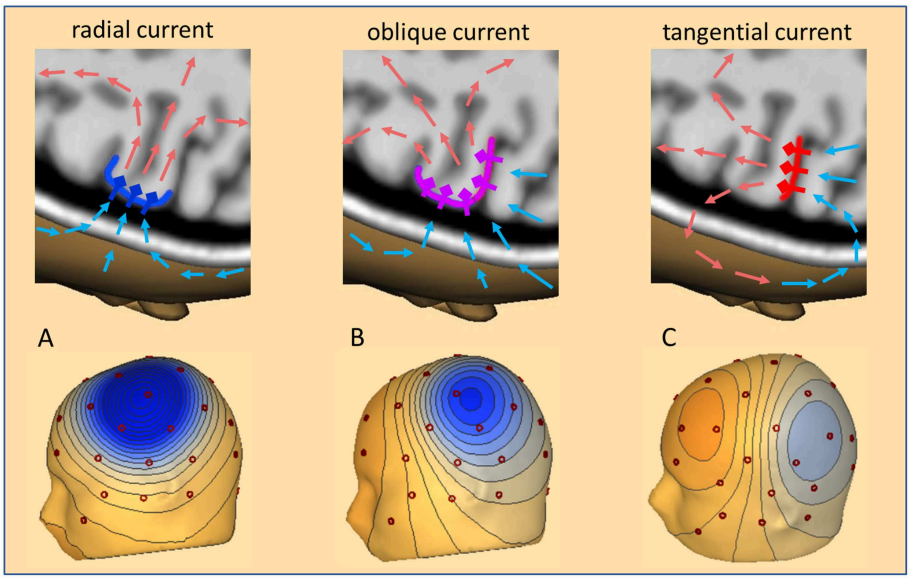

FIGURE 1 | Cortical currents, volume currents, and scalp topography. Three cases of IED current inflow into a focal cortical patch are illustrated: **(A)** radial (dark blue), **(B)** oblique (pink), **(C)** tangential (red). Pyramidal cells and their apical dendrites are symbolized by diamonds and thick outward bars. A subset of return current loops is depicted by arrows in light red to illustrate where they create positive and light blue where they create negative voltages. Depending on the net orientation of the cortical patch, the zone of maximal inflow from scalp into depth shifts from above the patch **(A)**, to more posterior **(B)** and fully posterior **(C)**. These currents create the typical 3D-voltage topographies on the scalp related to a focal IED at the cortical convexity **(A)**, in the depth of a sulcus **(C)**, and, the more common case of an oblique net current involving both superficial and sulcal cortex **(B)**.

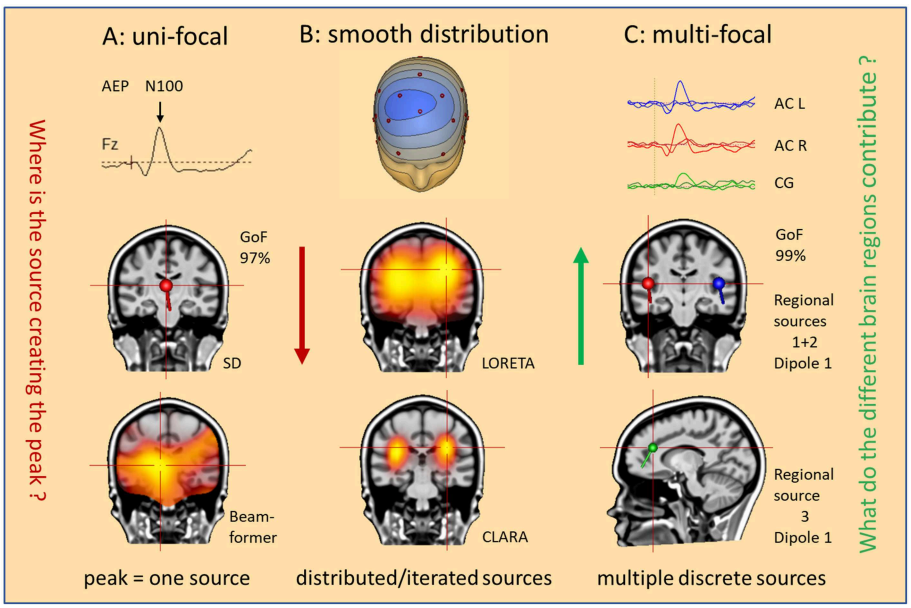

FIGURE 2 | What is our hypothesis? Three hypotheses are illustrated as mental starting points to understand the origin of the N100 peak of the LAEP. **(A)** Uni-focal: a single dipole (SD) or beamformer will localize to an equivalent center in the middle of the brain. **(B)** Smooth distribution: activity appears widely distributed in the Brain (LORETA); separate foci can be better isolated by iteration of the smeared images (CLARA). **(C)** Multifocal: what do the different brain regions contribute? Multiple discrete sources (RS1–RS3) model the three regions (AC L, AC R, CG) involved in the generation of this LAEP. The answer is the source waveforms shown on top.

∼2.5–3.0 cm. Thus, an IED may involve most of the crown of a gyrus (**Figure 3B**), the whole gyrus (**Figure 3C**) or even several gyri as well as large parts of sulci.

How do we define an adequate model for this seemingly extended local source space? An equivalent dipole summarizes the dipolar potentials of a small cortical patch (Ø < 1 cm) with

extreme accuracy. It is located near the center of the patch and oriented parallel to the net current flow of the patch (**Figure 3A**). If the patch is curved and more extended, the equivalent dipole moves deeper into the white matter (**Figure 3B**). If an IED extends uniformly around a gyrus (**Figure 3C**) the equivalent dipole locates at the bottom of the gyrus, deep in the white matter. In all cases, the equivalent dipole lies at the center of an imaginary near-to-planar cross-section of the activated patch. As shown on the right, we can close the activated patch by a cross-section having a dipole density equal to the patch and obtain zero-potential outside, because the net dipolar currents of a closed surface cancel. By mentally adding the same cross-section with the opposite dipole current density, we add nothing and create zero potential from the upper closed surface. What remains is the opposite dipole field of the added near-to-planar cross-section. Thus, the shape of the gyrus above the cross-section has no influence whatsoever on the EEG scalp potential. We only observe the dipolar potentials coming from the equivalent, uniformly active cross-section at the bottom.

What is the magnitude of the negative scalp peak in these three cases having the same radial orientation of the net current flow? The superficial patch A produces a small and focal negative peak; the wider patch B involves a much larger surface leading to higher magnitude. Interestingly, the widespread activation around the gyrus in case C leads to the smallest peak for two reasons: (1) the effective cross-section is small, (2) the equivalent dipole is considerably deeper in the brain. However, the shape of the voltage map in these 3 cases changes only slightly with the increasing depth of the equivalent radial dipole.

What about the accuracy of the forward estimation of the scalp potentials, if we use an equivalent dipole at the center of the patch as our source model instead of the whole dipole sheet at the cross-section? Repeating previous simulations (10) we used 40 standard electrodes and 6 hexagonally arranged equivalent dipoles plus a center dipole below Cz to mimic the scalp potentials of a superficial circular cortical sheet placed at the outer cortical convexity (eccentricity: 80%). The difference in residual variance (RV) between the potentials created by the sheets and a single center dipole was <0.01% for the small hexagons around each dipole, 0.02% for a patch of 5.2 cm^2 spanned by the 7 dipoles (Ø $\sim$ 2.6 cm) and only 0.17% for a patch of 20 cm^2 (Ø $\sim$ 5 cm). As expected from the curved surface (**Figure 3**) the fitted equivalent dipole stayed below Cz and moved into the depth to the level of the cross-section, i.e. to 76% eccentricity with the patch of 5.2 cm^2 and to 67% with 20 cm^2. Even in this last, worst case, the observed inaccuracy was more than one dimension smaller than the typical errors of 2–5% when fitting a dipole to an averaged IED.

Thus, in view of the substantial background noise still remaining after averaging, there is no way to estimate the extent of an IED source from the scalp EEG, because source extent is counteracted by the shielding of the brain activity due to the insulating skull and the highly conducting layers of CSF and skin. Conductivities and thicknesses of theses tissues vary greatly between individuals and cannot be precisely rendered from MRI. Less conducting skulls, e.g. in older subjects, and thicker tissues lead to increased shielding, more widespread topographies and deeper equivalent dipoles. If we force distributed dipoles into the cortical folds based on the individual MRI, the extent of activation along the cortical surface is mostly determined by the assumed tissue parameters. Even the amplitude of the scalp peaks is only a crude indicator of the extent, as can be seen from **Figure 3** and by comparing large IED amplitudes in children having focal cortical dysplasia with small IEDs in the elderly having large polar areas involved in temporal lobe epilepsy.

So far, we have only considered radial sources at one point in time. If we look at the evolution of an IED over time, we can take snapshots at different time-points from onset to peak to compare the dipolar scalp maps with the location of the activated cortex and the related equivalent dipole (**Figure 4**). Given the idealized situation that an IED starts at the anterior wall of a sulcus perpendicular to the convexity, our snapshots show an equivalent tangential dipole at onset (−16 ms, red), followed by an oblique dipole when superficial cortex becomes involved (−8 ms, pink) and a radial dipole (0 ms, blue) when the activity of the superficial cortex peaks while the tangential, sulcal onset activity is crossing zero after its first peak (cf. related arrows along source waveforms in **Figure 4**, right). The equivalent dipole is always located at the center of the smallest cross-section that is equivalent to the complex patch of activated cortex. Location changes minimally while dipole orientation is changing continuously.

This type of model is called a moving dipole model. However, the brain structures are fixed and not moving. This is taken into account by the so-called regional source model (2, 10, 11). The regional source is fixed to the local brain structure by assuming one equivalent location in the depth of the gyrus. This model is more robust, because it assumes only one location over time and not a new location at each point in time. Allowing for a small error in location, e.g. in source depth, is not critical, because the resulting change in scalp topography is minimal as shown before. Dynamics is modeled by 3 time-varying dipole vectors describing the local current flow over time in any direction (**Figure 4**, right). Thus, by having 3 dipole vectors at a common location oriented, e.g. along the orthogonal x,y,z-axes of the AC-PC or Talairach coordinate system, dipole current in any direction is fully projected into this local source space, i.e. one calculates the dipole orientation and magnitude at each point in time and projects this onto the 3 axes.

The main advantage of the regional source is that the axes can be rotated to obtain fixed orientations to match the local anatomy (**Figure 4**, right bottom) without any change in the resulting model of the observed scalp waveforms. Thus, we can choose the first dipole to be tangential in order to estimate the sulcal IED onset activity oriented into and perpendicular to the posterior wall of the active gyrus while the 2nd dipole is oriented radially into the depth to model the superficial cortex-negative IED. The third dipole serves to image the local current along the gyrus—often quite small in evoked potentials and IEDs. Thus, we obtain 3 source waveforms (12) for each regional source in the brain. When oriented appropriately, we can identify the local area of earliest onset and the local propagation, e.g. from sulcus to surface, by inspecting the source waveforms (**Figure 4**).

Could we try to localize the sulcal, superficial and 3rd dipoles independently (**Figure 4**, right top)? We would have to find time-points when the signal from one region is large with zero overlap

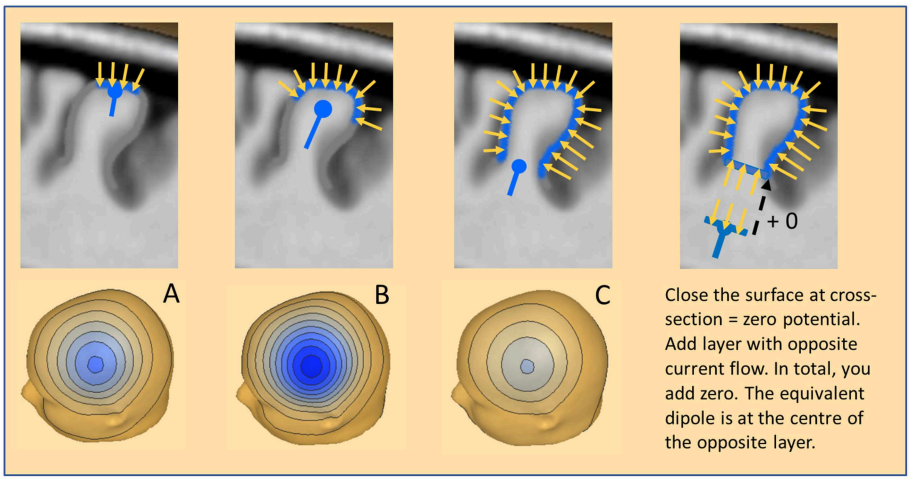

FIGURE 3 | The equivalent dipole. Three cases of cortical patches are illustrated with a resulting net inward current of radial orientation: **(A)** Small patch on the crown of a gyrus. **(B)** More extended patch spreading into the sulci. **(C)** Large patch involving both crown and deep sulci. The equivalent radial dipole sums the local currents along the cortical columns and is moving progressively deeper. For more details see text.

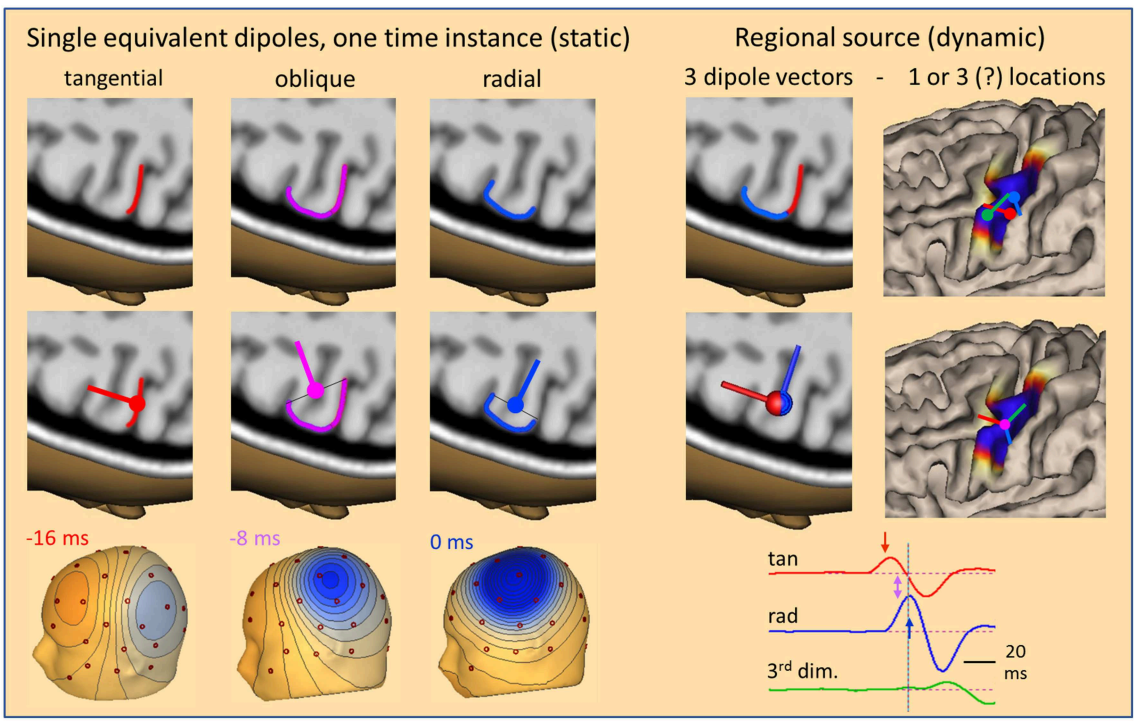

FIGURE 4 | The local source space. Using snapshots at one time instance as in **Figure 1**, we can define the local source space by a single equivalent dipole (**left**) moving from the sulcus (−16 ms, tangential) into the white matter (−8 ms, oblique) and closer to the surface (0 ms, radial). The changes in location are very small, but orientation changes completely, rotating from tangential through oblique to radial within 16 ms. The cross-sections of the active patch at each time are illustrated by lines. The equivalent dipole is located at their midpoint. An alternative local source space is defined by a regional source (**right**) having 3 orthogonal dipoles at a common center location to describe the 3-dimensional volume currents with high precision and rotational invariance. When rotated appropriately, the radial dipole depicts the superficial and the 1st tangential dipole the sulcal currents. Their source waveforms (right bottom) show the contribution of the local source space to the measured data. For more details see text.

from the others, but this rarely happens. For example, when trying to fit the tangential onset, activity is weak and noisy and localization is unstable. If we try to fit a later activity, overlap from the previously activated surfaces will bias localization. In contrast, if we fit one common location to the time course of the IED, this is much more stable, because the regional source

model needs less parameters. Assume an averaged IED with 25 channels and 20 time samples involving just one gyrus. The 3 locations and 3 orientations of a moving dipole can be estimated at every time point to reduce the number of parameters from the measured 500 values to 120. Using a regional source, the estimate is more robust and needs only 63 parameters, i.e. 3 for location and 20 for each source waveform. However, the greatest benefit of the oriented dipole vectors of a fixed regional source is that they provide a straight-forward linear transformation of the scalp signals into the local source space matching functional anatomy as shown below.

The Global Source Space

A simulation is presented in **Figure 5** to show how to extend the local source space concepts into the global source space of the brain. Assume a focal IED starting out in the right mesial frontal lobe. After averaging, some EEG background noise is still present. The activity is modeled by a single dipole (red) pointing into the right CG almost horizontally and slightly downward. As activation pattern, a biphasic spike has been assumed with the first peak modeling the surface negativity, i.e. the depolarization of the pyramidal cells by the current flowing into a small cortical patch in right CG. Using a regional source with 3 orthogonal dipoles, the first dipole takes up all the early activity peaking at −16 ms after orienting the local source space along the dipole field at this onset peak.

Next, we assume that the local IED is propagating to the right and then to the left lateral frontal cortex (FC). Propagation via the connecting fiber tracts is faster to ipsilateral (right, 16 ms) than contralateral (left, 22 ms) due to the shorter ipsilateral pathway. Again, the local IEDs in these propagated regions show biphasic patterns. These might be spread out a bit more in time due to temporal dispersion and larger in amplitude due to recruiting larger cortical patches in the propagated regions. Again, we place 2 regional sources into the propagated right and left lateral frontal regions and orient each source at its maximum. Now, the first dipole of each source is depicting the biphasic source waveform of the IED in each region. The temporal sequence of deep onset and subsequent propagation to ipsi- and contralateral is fully reconstructed by the source waveforms of this MDS model.

The scalp signals, simulated at 40 standard electrodes (**Figure 6**), show severe overlap with a broad mid-frontal negative peak shifting from right to the left between 0 and 6 ms. The deeper tangential onset activity (−16 ms) is quite weak. It is barely seen in the scalp waveforms (**Figure 6**, red arrow) but clearly visible in the 3D onset map. As illustrated above for oblique dipoles in fissures, we observe a "false" lateralization of the negativity over the left hemisphere at a location to where the negative pole of the red dipole is pointing (**Figure 5**). The overlap at the scalp has been separated by projecting the 40 scalp signals into this individual source space defined by the 3 regional sources, fixed to the anatomy and not moving over time. The first dipole of each regional source has been oriented to the maximum activity of each source while the other two dipoles show no significant activity along their spatial orientation. They only reflect EEG background noise and some small cross-talk due to slight smoothing of the inverse linear operator used to limit the influence of noise (cf. Methods).

What do we see when using 25 fixed regional sources distributed evenly throughout the brain placed, e.g. below the 25 standard electrodes (13) of the International Federation of Clinical Neurophysiology (IFCN) at an eccentricity of 70%? Five of these sources lie in a para-coronal frontal plane: frontocentral (FC) mesial, right, left, temporal anterior (TA) right and left, approximately below Fz, F4, F3, F10, F9 (**Figure 5B**). Their projected activities show the propagated IEDs in the frontal-central source channels FC R and FC L with correct peak timing. Since the real sources were more superior, FC M sums up a part of both activities to compensate for the inaccurate localization. The onset activity in the depth (eccentricity 38%) is barely seen, but picked up correctly by the tangential, 2nd dipole of FC M. It is reduced in amplitude, because it is shared with other nearby sources, mainly with the 2nd, tangential dipole of FC R. Thus, we could state correctly that the weak onset activity is coming from between and below FC M and FC R. Less cross-talk is observed when looking selectively at the 25 radial source activities below the 25 standard electrodes. This subset of the transformation of the 40 scalp signals into the standard 25 brain regions, i.e. into 75 signals, 3 for each regional source, shows deblurred and more focal signals in the regions near the real sources as compared to the 25 average-referenced signals at the scalp (**Figure 6**, middle).

When combining the 25 regional sources with the simulated source dipoles into a mixed MDS model, one can construct a specially weighted inverse transformation that renders the 3 source activities correctly and has only a very small cross-talk to the nearby standard sources (**Figure 6**, right). Again, the deeper onset activity is more attenuated than in the individual MDS model with 3 regional sources (**Figure 5**, left), since the 25 standard sources act like a partially shielding dipole layer at 70% eccentricity. Yet, this example illustrates one powerful aspect of MDS: The 25 regional sources act as additional probe sources and their small source waveforms document that no significant activity is contributed to the averaged IED by all the other brain regions. How shall we find the active, contributing regions in the brain? This is the critical point of MDS models to be discussed further below.

A different global source space is defined, if we distribute many equivalent sources evenly either throughout the brain or along the cortical surface (**Figure 5**). In a distributed source model, each brain voxel or cortical patch is modeled by an equivalent dipole. Typically, the current distribution is estimated independently at each point in time and displayed in the brain volume or on the cortical surface. The few scalp potential values−40 in this example—are converted into ∼500–5,000 color values of a 3D- or 2D-image (**Figures 5C,D**). This under-determination requires a mathematical constraint like minimum norm or smoothness is space to obtain an image (14). To reduce the smearing of foci (**Figure 2**, LORETA), images can be iterated to become more focused. For example, after a few steps using CLARA (4, 5), foci became either separated (**Figures 5C,D**, 0 and 6 ms) or lumped together into an intermediate focus in the brain volume (**Figure 5D**, −16 ms). When source space was restricted to the cortical surface, however, foci were incorrectly projected to

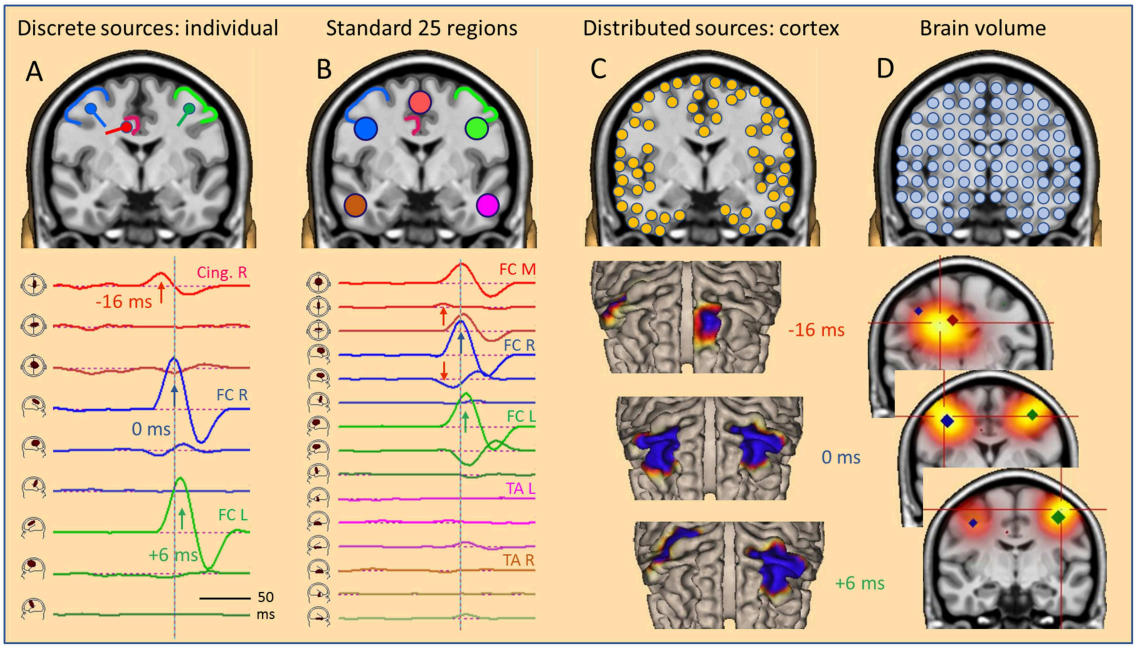

FIGURE 5 | The global source space. EEG/MEG can be modeled by: **(A)** multiple discrete sources (MDS) adapted to the individual data, **(B)** standard source regions, grossly distributed within the brain, **(C)** distributed sources confined to the gray-white matter boundary of the cortex, **(D)** sources distributed throughout the brain volume. Results in a simulated case of an IED propagating from right CG (**A**, red) to right (**A**, blue) and left frontal (**A**, green) superficial cortex depend severely on the choice of global source space. With a small number of sources **(A,B)**, temporal dynamics is revealed by the source waveforms (bottom). However, the large number of sources in distributed models requires the display of a time series of images, either on the cortical surface (**C**, cortical CLARA) or in the brain volume (**D**, CLARA). Typically, distributed source images are calculated independently from one time point to the next. Thus, foci appear smeared and moving over time. Their extent depends more on scaling and other factors used to create the images than the underlying extent of active cortex. For more details see text.

different gyri along the poles of the underlying deep dipole field (**Figure 5C**, −16 ms).

Using three different types of global source spaces in this simulated example, the following effects were observed:

- Individual regional sources fixed to the anatomy accurately reconstructed the source activities of the few generating cortical areas.
- Standard source space 25 with regional sources covering the whole brain provided a gross overview over magnitudes and patterns of activity in the brain.
- Distributed sources provided smoothed images on the cortical surface or in the brain volume. Some locations and the moving of foci were incongruent with the simulation.

TRANSFORMATION INTO SOURCE SPACE: AEP AND SEP AS TEACHING EXAMPLES

The recipe of how to take the EEG back into the brain, i.e. how to calculate the linear inverse, will be detailed in section Materials and Methods. The inverse differs between distributed sources and individual or standard source spaces based on MDS. Whereas distributed models use just one regularization parameter to invert the lead-fields in data space (14), inversion in source space allows for specific regularization of each source to make the inverse stable and exempt specific sources from smoothing (**Figure 6**) or to remove, e.g. ECG artifacts completely (15, 16).

Auditory Evoked Potentials (AEP)

Figure 7 shows data and source waveform matrices to illustrate how and why we can take the EEG back into the brain on a macroscopic level. The middle latency auditory evoked potential (MAEP) of a patient with a deafferented left auditory cortex (AC) appears widespread over the scalp (2, 17). The signals along a coronal chain of 12 electrodes—perpendicular to the supra-temporal plane and lateral surface of the temporal lobe—are linearly transformed to estimate the 4 currents flowing out of AC in vertical and lateral directions (2, 18), i.e. opposite to the inward orientation of IED dipoles. Despite the widespread distribution over the scalp, the source waveforms show that the vertical N19-P30 activity only arises from right AC (Rv). The deafferented left AC (dipole Lv) does not exhibit any primary activity. The lateral, radial activities were small in this case and showed only a weak cross-talk to the left (Ll). Evidently, fixed dipoles associated with specific functional areas in the brain are needed to create such a linear source reconstruction—silent cortex cannot be localized.

The 4 equivalent dipoles were seeded at the mean fitted locations of 42 subjects (19). They were used to calculate the forward solution, i.e. the topography, or leadfield matrix L having 4 columns and 12 rows. Each column contains the voltages calculated at the 12 electrodes in a 4-shell head model using

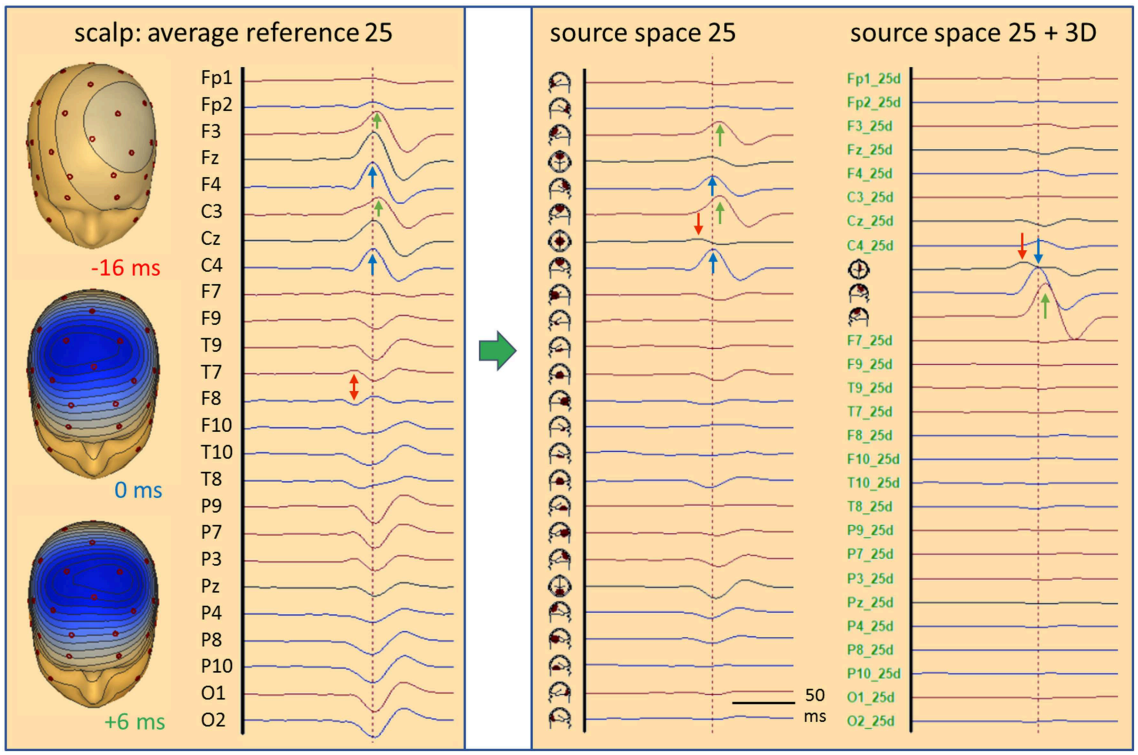

FIGURE 6 | Standard source space 25. In the simulated case of a propagating frontal IED (cf. **Figure 5**), transformation from scalp (**left**) into source space (**right**) is illustrated. The same sequence of channels from Fp1 to O2 is used to compare the scalp potential with the radial current below each electrode (source space 25). Source channels F9–10 and T9–10 have specific orientations (see text). Time scale is expanded to visualize the different latencies; amplitude scales are relative to enable comparison. The weak onset activity of CG (red arrows, −16 ms) is barely seen on the scalp, but has an oblique dipolar map. Peak latencies appear earlier in the right frontal-central channels F4 and C4 (blue, 0 ms) than left F3 and C3 (green, 6 ms). In source space 25, the activity appears more focused to the frontal-central region with much less cross-talk to other regions. The superficial right and left frontal activities appear better separated (blue, green). On the right, source space 25+3D shows the combination of the 3 simulated source dipoles with the 25 standard regional sources. This isolates the IED and the flat signals of the 25 standard regions document that they are not involved in the averaged IED. The near-to-tangential onset (red arrow) is seen more clearly now as compared to source space 25. For more details see text.

unit currents oriented along one of the 4 dipoles. Using simple linear algebra, the pseudo-inverse of the L-matrix is used as linear operator to transform the scalp data matrix D into the brain source wave matrix S. This macroscopic transformation is stable and unique because the number of signals is condensed from 12 into 4. The 4 inverse vectors have an important property: They render 100% of the source signal they represent, but 0% of the other sources (20). Thus, the first source waveform shows the N19-P30 component of the intact AC, while the second source waveform reveals the loss of activity in the deafferented AC, because there is no cross-talk from dipole source 1 to the location of any of the other 3 sources and vice versa.

The MDS model of the LAEP shown in **Figure 2C** was created assuming multiple discrete foci by seeding a symmetric pair of regional sources bilaterally into AC (2). After orientation, their first dipoles depicted the vertical P50-N100 complex of the LAEP while their second dipoles showed only a small radial N150. No source components along the Sylvian fissure were seen to rise above the EEG background remaining after averaging. This residual noise was shared by all source waveforms. At high stimulus intensities, a prominent additional component arose around 115 ms and was localized to CG using the grand average LAEP (6). Therefore, a third regional source was seeded at this anterior mid-line location to check the activity of this region at low intensities. There was a peak of activity around 115 ms, smaller than N100, but clearly dissociated in latency and shape from the AC source waveforms after orienting the source to this peak (**Figure 2C**).

The dipole topographies of this MDS model defined a unique linear transformation of the 32 scalp signals to reconstruct the dynamics of the 9 source activities in the 3 regions. Interestingly, this model explained only 2% more of data variance at the peak of N100 (GoF 99%) as compared to a single dipole in the middle of the brain (**Figure 2A**), because of the similar scalp topographies of the almost parallel vertical currents in the depth of the left and right Sylvian fissures. However, when taking the temporal evolution into account, the source waveforms revealed the different dynamics of AC and CG during the whole interval from 30 to 150 ms (GoF 98.8%). This separation—possible despite the severe overlap of right and left N100 with N115 at the mid-frontal scalp (**Figure 2A**)—underlines the power of MDS. The

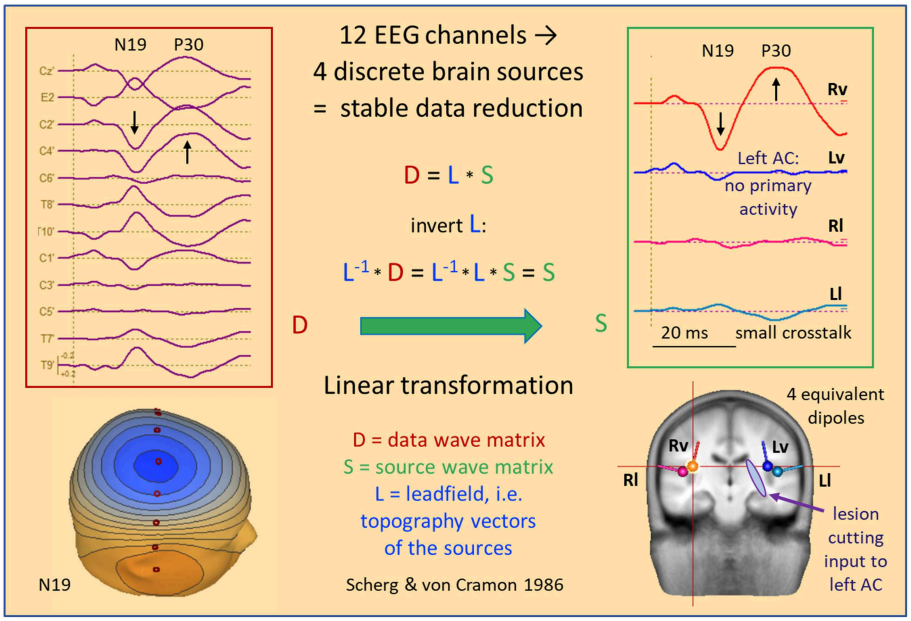

FIGURE 7 | MAEP of a patient with a white matter lesion cutting the input to left AC (2). The distance between scalp traces corresponds to 0.6 μV and transforms into 10 nAm between source waveforms. Filter settings: 10 Hz forward to 200 Hz. The 12 EEG channels in the coronal plane show a right sided dipolar map with the negativity of N19 near the vertex. MAEP scalp potentials are displayed positive up and dipoles with the orientation outward of the cortex—opposite to IEDs—to display P30 upward in the scalp and source waveforms. The linear transformation into standard AEP cortical source space reduces the data to the vertical (Rv, Lv) and lateral (Rl, Ll) activities of the Heschl's gyrus on both sides. Thus, it is immediately apparent that the primary activity of left AC is completely abolished by the lesion whereas the healthy right AC exhibits the typical N19-P30 pattern of the MAEP.

same fixed model with 3 regional sources successfully revealed the different gating effects of P50 in AC and CG despite very poor signal-to-noise ratios (SNR) in the individual data (21).

Somatosensory Evoked Potentials (SEP)

The median-nerve SEP seems a better candidate for hypothesis A of **Figure 2**. The N20 peak with its clear tangential dipolar map (**Figure 8**) invites to localize this peak by a single dipole (24). However, the primary activity of the somatosensory area 3b at the posterior wall of the central sulcus is not where the onset occurs. N20 is preceded by the neural activities of the stimulated afferent pathway. These activities are not over at the latency of N20 and their overlap at the scalp can lead to mis-localization when using only one equivalent dipole. The error depends on the magnitude and orientation of the deep afferent activity that is creating a frontal scalp negativity at the time of N20, thus modifying the dipolar map of N20, and on the distribution of scalp electrodes over the upper and lower head (22, 23).

Figure 8 shows the 31 scalp signals of an SEP average to 10,000 stimuli of the right median-nerve. The 3D scalp maps show the N14 peak of the ascending neural volley and two distinct maps over the contralateral sensorimotor cortex, a tangential map around 20 ms (posterior N20) and a radial positivity around 24 ms (P24). Related deflections are marked in the widespread distribution of the SEP over the upper scalp. As reported (11, 22, 23), the underlying biphasic components associated with N14, N16, N20, and P24 can be separated by seeding a vertical dipole into the brain stem, an oblique dipole in the contralateral thalamus oriented along the ascending thalamocortical tract and fitting a regional source into the contralateral hand area. After rotating the 1st dipole of the RS to the peak of N20 and keeping the 2nd dipole radial outward, we observe the separation of the biphasic N20 and P24 components while no activity is seen along the postcentral-gyrus (3rd dipole). The 32 scalp signals have been projected into SEP source space, i.e. reduced to 5 equivalent source waveforms, by using the inverse linear operator L^{-1} of the 5 dipole topographies.

What can we read from the source waveforms? (A) The 4 peaks reveal the timing of the ascending activity from entering the brain volume (N14) at the foramen magnum (8) over the thalamic output (N16) to the initial cortical activations of area 3b (N20) and superficial areas 1 and 2 (P24). (B) The near-tangential N20 dipole summates the activities of the central sulcus while the radial P24 dipole summates all superficial activities of the contralateral sensorimotor cortex. Further distinctions and separate localizations of P24 and N20 from the 32 scalp channels are impossible. (C) Most importantly, each source waveform shows a flat baseline before the activity starts rising. There is no cross-talk from earlier onto later activities confirming the focal nature of the earlier activities, and the later activities are not influenced by the on-going overlap from the earlier sources. Thus, the SEP can be localized more accurately by having a multi-focal hypothesis (**Figure 2C**) und using an MDS model in which the deep sources are represented and allowed to be simultaneously active when fitting a regional source into the

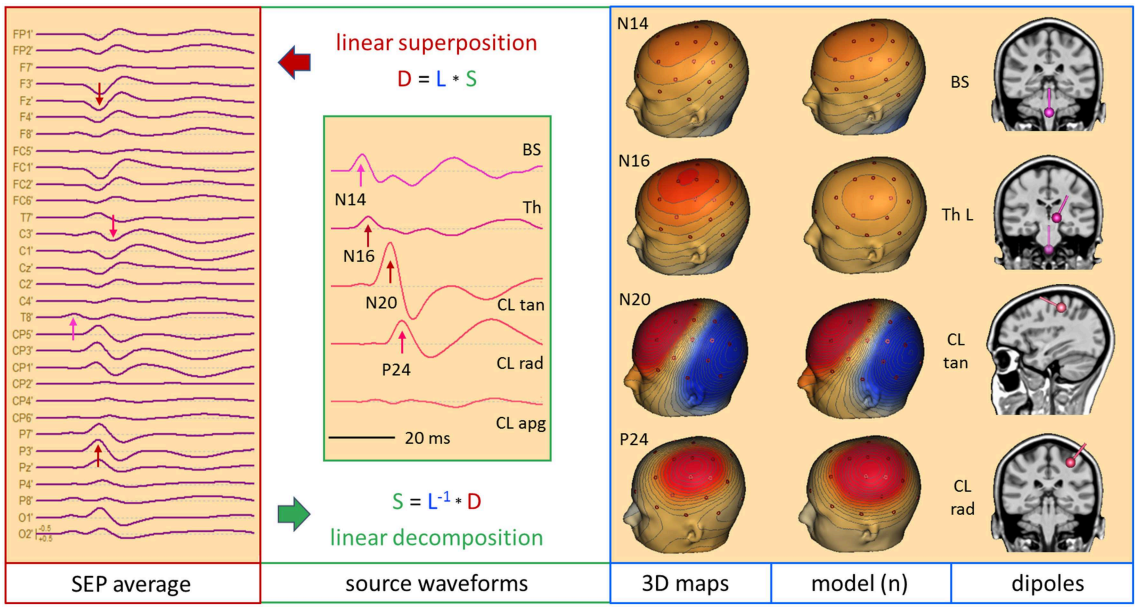

FIGURE 8 | Right median-nerve SEP recorded with 31 channels and high SNR. The distance between scalp traces corresponds to 2 μV and transforms into 30 nAm between source waveforms. Filter settings: 20 Hz forward to 200 Hz. Scalp waveforms show negative up and source waveforms the current flow into the direction of the dipole vector (right). The dipole model consists of a vertical source in the brainstem (BS), an oblique source in left thalamus (Th L) and a regional source (CL) in the contralateral left central hand area (22, 23). The regional source has been rotated to separate the near-to-tangential N20 component (CL tan) from the radial P24 (CL rad). The linear inverse L^{-1} is based on the model topographies of the 5 dipoles shown in column model (n). They are quite similar to the 3D maps at the peaks of N14, N20, and P24. At N16, there is still considerable overlap from N14. L^{-1} reduces the 31 scalp signals to 5 source waveforms showing the separation of the underlying components N14, N16, N20, and P24, labeled by their first peaks. The 3rd dipole of the regional source CL is oriented along the postcentral gyrus (CL apg). Its flat source waveform confirms that (a) no evoked current is flowing along the gyrus, (b) N20 and P24 components fully model the activity of CL, and (c) the model consisting of the preceding 4 dipoles is sufficient to explain and decompose the data.

primary somatosensory cortex, e.g. for presurgical functional mapping (22).

Figure 9 depicts the left median-nerve SEP of the same subject to illustrate the effects of projecting the scalp data into three different source spaces. First, we use the same discrete model with 5 individual sources. The N14 dipole is seeded into the brainstem and oriented to the scalp data while the N16 dipole is mirrored into the opposite thalamus. The added regional source fits into the hand area of the opposite hemisphere and separates the tangential N20 and radial P24 components without showing activity along the gyrus (**Figure 9**, individual sources). The five source waveforms show a sequence and patterns similar to the right median-nerve SEP.

What happens if we project the scalp SEP into a standard source space constructed to reveal the different source components of the SEP? The source montage in **Figure 9** (right) consists of 3 deep dipoles (brainstem and thalamus L & R) with fixed locations and orientations and two regional sources seeded bilaterally into the hand areas in a standard brain with the 1st dipole oriented perpendicular to the central sulcus, the 2nd radially and the 3rd along the postcentral gyrus. Additional sources are placed into secondary somatosensory cortex at the central operculum L & R, bilaterally into frontal and parietal cortex, and into three midsagittal areas to account for overlap from these regions. The N14, N20, and P24 components are very similar to the individual MDS while the deep N16 is quite small in trace ThR due to shielding by the more superficial sources as explained above. The cross-talk to other regions is small and they do not exhibit own activities due to the high number of averages. Again, the other sources act as probes. They confirm the origin of the SEP in brainstem and right sensorimotor cortex and show that the secondary somatosensory areas in both central opercular areas (cOL, cOR) are not activated during fast repetitive stimulation.

This separation is possible, because the different equivalent dipolar sources of the SEP project to the scalp according to the laws of physics. Even when using a simple multi-shell head model, we can predict their model maps on the scalp and reconstruct their source activities quite accurately (**Figure 8**) provided the maps are not linearly dependent (i.e. one map is highly similar to any combination of the others). In contrast, a purely mathematical decomposition of the data, e.g. independent (ICA) or principal components analysis (PCA), is unable to provide this separation of the underlying physiological components (**Figure 9**, left).

EEG: STANDARD SOURCE SPACE 25

As shown in **Figure 6**, we can construct a source space using a limited number of sources, for example one source below each of the standard 25 EEG electrodes of the IFCN (13) to get a gross overview of the EEG activities arising from different

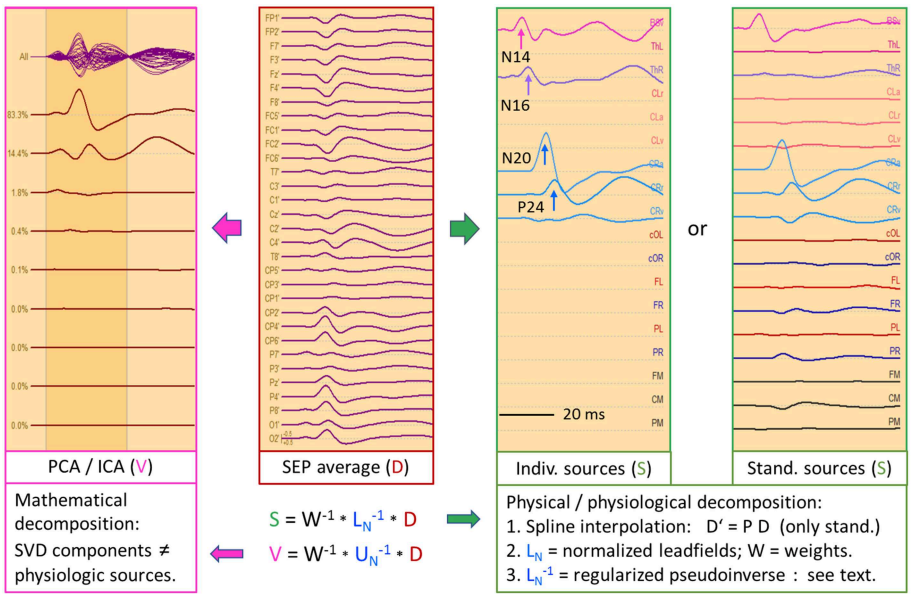

FIGURE 9 | Left median-nerve SEP—same subject, scaling and filtering as in **Figure 8**. Here, different types of linear decompositions are illustrated. First, one can use the 5 individual sources as in **Figure 8**, mirror locations and orientation from right to left, and adjust orientations to the peaks of N14, N24, and P24. The separation of components is highly similar to **Figure 8**, but the generators are now in the right hemisphere, contralateral to stimulation. When using the standard SEP source montage (**right**), one can immediately observe the separation of N14, N20, and P24, although N20 and P24 have not been oriented optimally, so that some activity is shared with the 3rd dipole of CR. The other regions do not contribute to the SEP in this time range and partially shield the deep radial generator of N16 in the right thalamus. This separation in matrix S is enabled by using an appropriate physical and physiological model defined by the leadfields of the sources. If we use a blind, purely mathematical decomposition of the data matrix D, e.g. singular value decomposition (SVD) or ICA, the resulting waveforms V do not show an interpretable decomposition (**left**).

brain regions. Each of the 25 brain regions below the electrodes is represented by a regional source oriented such that the first dipole points into the adjacent cortex (**Figure 10**, middle). For most sources, the primary orientation is radial to model the activity of the superficial cortex. Two inferior sources are oriented differently to depict the activities of the temporal pole (F9/F10) and temporal base (T9/T10) in their first dipole source waveforms. Only the first dipoles of each regional source are displayed in source-space montage 25 to obtain a legible overview (**Figure 10**, right).

For better comparison of scalp and brain signals, electrode and source traces are arranged in the same sequence. Considering the typical sequence of longitudinal and transverse montages (13), the fronto-polar (Fp) and superior frontal channels (F) are displayed at the top, followed by the central channels (C), each group going transversally from left to right. In the middle, the temporal left (TL) and right (TR) groups are displayed going from anterior over inferior to posterior. The temporal groups start with channels F7 and F8, respectively, for convenient perception of temporal polar IEDs. At the bottom, the parietal (P) channels are displayed followed by occipital (O).

Typical EEG rhythms and IEDs are more focused in source space 25, and the source channels where IEDs appear maximally are considerably less contaminated by overlap from other brain regions as compared to the scalp maximum. **Figure 10** shows a spike in a case having left frontal cortical dysplasia (25). Source activity is maximal below Fp1 and weaker below F3 and F7. On the scalp, the spike peak appears more widespread from Fp1 to F9. In the preceding 500 ms, the fronto-polar and frontal sources show much less cross-talk of rhythmic activity from the other brain regions. Also, the central μ- and parietal-occipital α-rhythms appear clearer and more focused in source space.

Figure 11 shows 6 s of EEG in a 67-year old female having mesial temporal lobe (mTL) sclerosis with frequent bilateral independent spiking. In source space, four different spike types can be seen almost perfectly focused to the temporal basal and polar traces. One can distinguish immediately whether a spike has propagated from its mesial origin (not visible on the scalp) to the temporal basal or polar cortex. The polar spikes predominate at the inferior-temporal scalp while the basal spikes produce more widespread and smaller scalp peaks. However, scalp voltage maps show the typical polar and basal topographies. EEG background appears much more separated in source space, cf. frontal rhythms in seconds 1 and 2 and parietal rhythms in seconds 4 and 5 (black arrows). The preceding baselines are much clearer in the source traces, because cross-talk from other brain regions is less. Thus, IEDs are more easily detected in source space.

This was confirmed by the new focality measure illustrated in **Supplementary Figure 1** and defined in section Materials and Methods. Mean focality of the 65 left-temporal IEDs

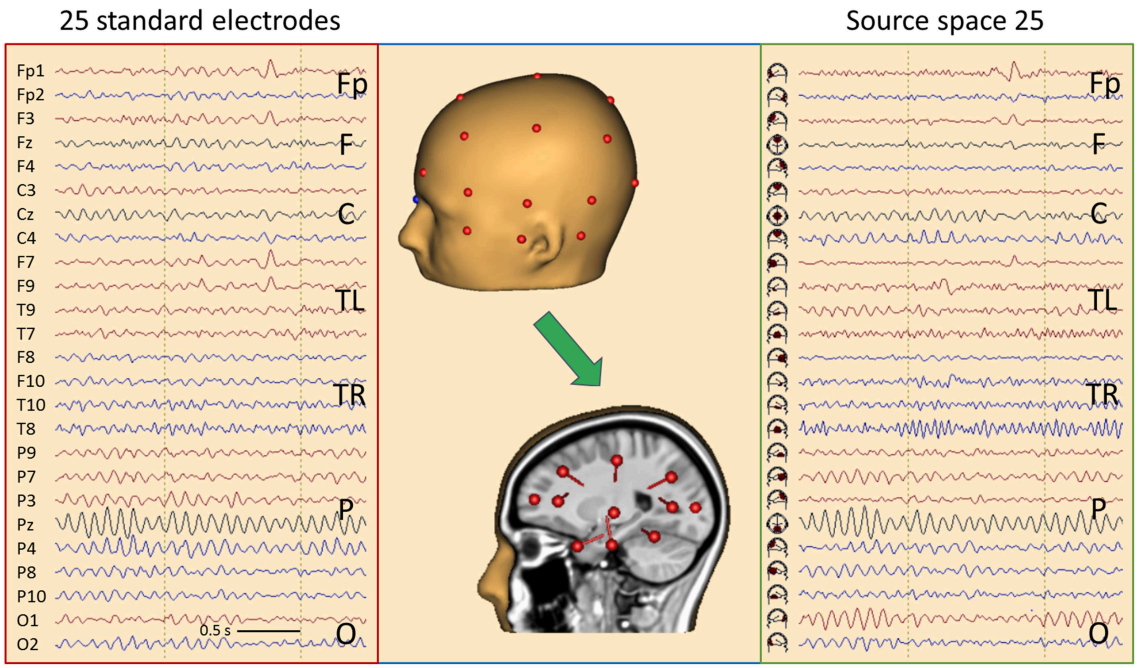

FIGURE 10 | Comparison of the scalp EEG at 25 standard electrodes in average reference (**left**) with standard source space 25 (**right**) using the same sequence of channels in a case with left frontal cortical dysplasia (25). Filter settings optimized for IED review: 2–35 Hz, zero-phase characteristic (26). A spike is seen in second 2, appearing more focal in source space. In addition, the spread of central μ-rhythm onto frontal channels is greatly reduced in source space, making the frontal spike stand out more clearly. In the center the underlying principle of "taking the EEG back into the brain" is illustrated showing the electrodes on the one hand and the underlying source dipoles on the other. For more details see text.

in this mTL case was 79.5% in source and 65.8% in scalp space ($p < 0.001$, V = 2,104, Wilcoxon two-sided signed rank test). Taking the two most prominent averaged IED types detected by BESA Epilepsy in 25 adults (27), i.e. comparing 50 averaged IEDs of different temporal and extratemporal orgins, mean focality was 71.8% in source and 64.6% in scalp space ($p < 0.001$, V = 981).

The transformation from scalp to brain occurs purely in the spatial domain and does not depend on the temporal dynamics of the EEG. The same linear inverse operator is applied to each EEG sampling point. Hence, a source-space montage is simply a spatial filter combining the recorded scalp signals into a new EEG montage. Instead of subtracting the signals of neighboring electrodes, as in bipolar montages, specific weights are given to each scalp signal to enhance activity coming from the region below the selected electrode while suppressing activities from other regions as much as possible (26). As detailed in Materials and Methods, the linear inverse is stabilized by spline interpolation of the 25 scalp signals onto 81 standard electrodes and slight smoothing of the spatial filter in source space to create 75 source waveforms, i.e. 3 for each regional source. Because the full set of 75 EEG traces is hard to review on a single page, separate source montages with subsets of the 75 signals can be selected to observe, for example, tangentially oriented IEDs in sulci, if these are not apparent in the standard subset of 25 traces showing predominantly the radial activity of each region.

PROPAGATING IEDs IN STANDARD AND INDIVIDUAL SOURCE SPACES

Frontal IED: EEG and MEG

Figure 12 depicts an average of 84 frontal spikes simultaneously recorded with EEG and MEG in a 23 year-old male (16). The EEG shows maximum negativity at F8 reaching out to T8, C4, and F4 with slightly different latencies. An almost synchronous smaller positivity is seen at F3 and F7 while 20 ms later a negativity is barely noticeable at C3 and T7. The maps show a near-to-tangential pattern at onset (0 ms), an oblique pattern at 15 ms with the strongest negativity and a contralateral dipolar pattern at 25 ms.

Source space 25 separated the radial inward activity below F8 (pink arrow) more clearly from the preceding peaks below F4 and T8 (red). Their opposite polarity indicated a tangential activity in between, similar to the contralateral activity occuring later with opposite source peaks below F3 and T7 (green). The fronto-central subset of all 75 source channels (montage 25-FC) showed the strongest regional activity below F4 throughout the onset-to-peak interval (0–15 ms, red and pink arrows). This was followed by the activities of the more central superior (7 ms, below C4), anterior-inferior frontal (15 ms, F8) and contralateral sources (28 ms, F3), as confirmed by MEG (**Figure 13**).

The individual EEG source space (**Figure 12**, right) was determined by fitting two regional sources and converting them into separate dipoles oriented to separate onset and peak

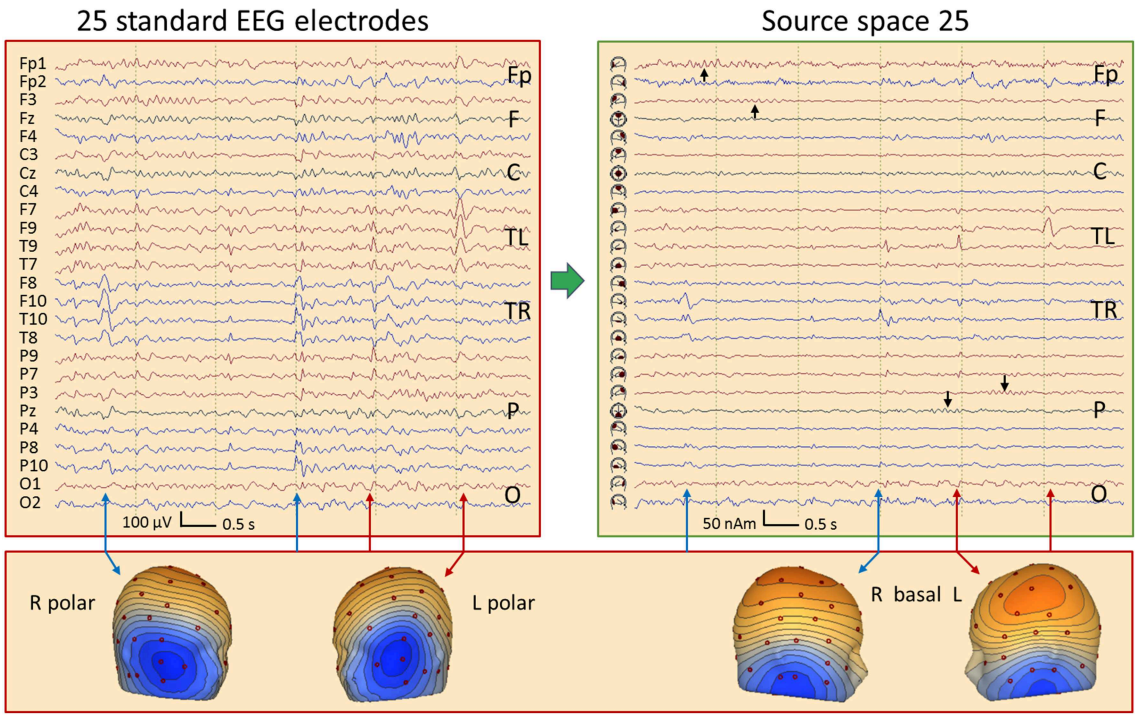

FIGURE 11 | Comparison of the scalp EEG at 25 standard electrodes in average reference (left) with standard source space 25 (right) in a case with bitemporal spiking. Filter settings optimized for IED review: 2–35 Hz, zero-phase characteristic (26). Right (blue arrows) and left (red) polar spikes are seen at the beginning and end of the displayed 6-s EEG segment, most prominent in the inferior channels F10 and F9. In the middle of the segment, IEDs with more complex distributions are seen on the scalp. Transformation into source space 25 provides a much clearer picture: The polar temporal lobe spikes can be identified immediately in the source waveforms below F10 and F9. Basal temporal spikes are seen on the right below T10 (blue) and on the left (red) below T9 (2 spikes emerging clearly, the 1st immediately after the right basal spike below T10). In source space, the temporal spikes appear considerably more focal and emerge much more clearly from the EEG background. In addition, overlap from frontal and parietal EEG rhythms (black arrows) is strongly reduced.

activities. In the right hemisphere, only the contributing sulcal onset (red) and superficial peak (pink) dipoles were retained in the model together with the contralateral sulcal dipole (green). Their source waveforms provide a dynamic image of the propagation from sulcal to superficial cortex within right frontal cortex and to left frontal with a delay of ∼26 ms.

What does the simultaneously recorded MEG tell us about the propagation in this case (**Figure 13**)? MEG is blind to superficial radial currents, but looks at sulcal activities with higher resolution than EEG. First, we transformed the 102 magnetometers signals into source space M29 while removing ECG artifacts (16). The 29 regional sources were rotated to display the maximum of the two tangential dipole activities in each source trace. Thus, the onset activity of the right frontal cortex appeared very clearly (red arrow), followed by more central (pink) and more anterior (blue) ipsilateral activities. The contralateral left frontal activity (green) peaked ∼20 ms later. MEG flux maps showed a dipolar onset pattern (0 ms) followed by a complex, seemingly 2-dipolar pattern at 12 ms and a contralateral dipolar pattern at 32 ms. The individual source space was constructed by fitting 4 dipoles sequentially (11) using the onset phase for dipole 1 and the zero-crossings of the preceding activities for dipoles 2–4 to localize at times with low interference. This revealed an intriguing local propagation pattern in the 4 source waveforms consistent with the individual MRI: From the sulcal onset zone at a rear wall in the inferior frontal gyrus (red dipole, peak at −4 ms: tan), propagation occurred both toward more superior cortex (pink, 10 ms: up) and to the anterior, opposite side of the spiking gyral section (blue, 16 ms: opp). About 20 ms later, propagated activity peaked in contralateral frontal cortex (green, 30 ms: c.lat).

How could such a separation be achieved? The 3 ipsilateral dipoles had different orientations with distinct topographies in the 102-sensor array, and, in this MDS model, their locations were sufficiently different to avoid linear dependence. This would occur when assuming 3 dipoles at exactly the same location, because MEG is sensitive only to 2 tangential dimensions. The source waveforms document that the linear inverse was able to transform the 102 magnetometer signals into 4 source signals with excellent separation of onset and propagated activities for two reasons: (1) There was no cross-talk from one activity to the next. Initially, only the onset region showed activity rising above background; next, the upper source activity started rising while the anterior, opposite wall was still inactive; finally, the 3 ipsilateral dipole activities combined to create the complex superficial flux pattern seen at 12 ms while contralateral source

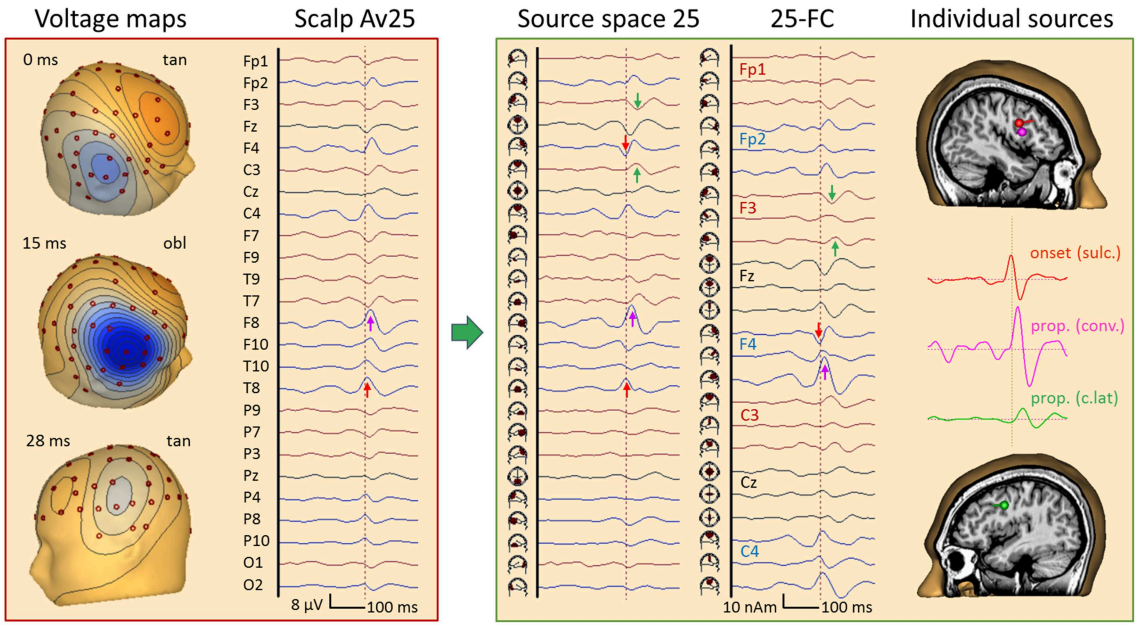

FIGURE 12 | Right frontal propagating IED, 84 averages, EEG results. Filtering: 5 Hz forward to 40 Hz to reveal IED onset (26). In the virtual average-reference montage Av25 (26), the earliest IED peak is seen at T8 (red arrow) followed by F8 (pink). In source space 25, the peak below T8 appears earlier (0 ms) and synchronous with a peak of opposite polarity under F4, indicating an origin between the 2 regions. The corresponding onset map appears tangential, followed by an oblique map with a strong surface negative peak at 15 ms near F8 (pink arrow) and another near-to-tangential map over the left frontal cortex at 26 ms. The left frontal IED appears below F3 and C3 (green) in source space 25. When inspecting all frontal-central channels of source space 25 (25-FC), the strongest peak (15 ms) is seen in the 2nd tangential trace of the regional source below F4 while the earlier onset is seen in the 1st trace. The individual source model needed 3 dipoles to separate the sulcal onset (red, peak at 0 ms) from the larger peak activity (pink, 15 ms) in the same frontal-central region on the right. The 3rd source waveform (green, 26 ms) isolated the IED propagated to the left.

activity just started. The latter was much easier to separate, of course, because its flux map has only little overlap with the maps of the 3 right frontal dipoles. (2) There was no enhancement of background noise in the baselines of the source waveforms prior to the IED. This would appear when coming closer to linear dependence.

The orientations and locations of the tangential onset dipoles in EEG and MEG matched. They point to the same origin at a time when EEG activity was still weak. This underlines that averaging is needed to distinguish IED onset from EEG background in order to localize the triggering onset zone.

A Case of Myoclonic Epilepsy: Findings in EEG and MEG Source Space

Figure 14 displays the jerk-locked average of 474 myoclonic spikes from a simultaneous EEG-MEG recording of a 36-year-old female with cortical reflex myoclonus. The EMG, recorded from the first dorsal interosseus muscle on the left (FDIL), shows the time of the jerk involving the left-hand digits 1–2. In the unfiltered EEG, widespread rhythmic activities precede the jerk, relatively steady in the occipital channels O1-O2, but progressively building up in central channels Cz and C4 toward the jerk. At C4 and F4, a small spike-like discharge is riding on the rhythmic activity, best recognized in source space 25. It precedes the EMG peak by about 20 ms. Averaging would have completely reduced the rhythmic activity, if it were not time-locked to the jerk. Here, we observed only partial reduction suggesting that the steady posterior 10-Hz rhythm is driving the central rhythmic buildup until the depolarization in the central area is sufficient to gate the initiation of the myoclonic jerk.

Using principal components analysis over the first 3 EEG cycles prior to the jerk, we could define 2 spatial components (11, 15) to model the rhythmic activities with centers of gravity in the midst of parietal (PC1, purple) and central cortex (PC2, dark blue). After using two forward low filters at 10 Hz and 50 Hz to reduce the overlap of the slow activity and expanding the time scale, the averaged IED was localized using 4 dipole sources in MEG (**Figure 14** right, bottom): Source 1, peaking 22 ms prior to the jerk of the left hand, was located at and pointed into right somatosensory cortex (SC, red). Source 2 localized at the precentral motor knob (MC, green, −17 ms), source 3 near right SMA (blue, −11 ms) and source 4 near the left, contralateral motor knob (MC L, brown, −10 ms). Finally, dipole orientations were fitted to the data, independently for EEG and MEG, since MEG dipoles only render the tangential and not the full, oblique current vectors as EEG does.

The onset dipole of the IED in SC was tangential with similar source magnitudes of the upward peaks in EEG and MEG source waveforms (red arrows). Similarly, the MC dipole, peaking 5 ms later, was tangential in EEG and MEG with comparable magnitudes. The SMA dipole (blue) showed a predominant radial current 6 ms later. Hence, the SMA peak was considerably larger

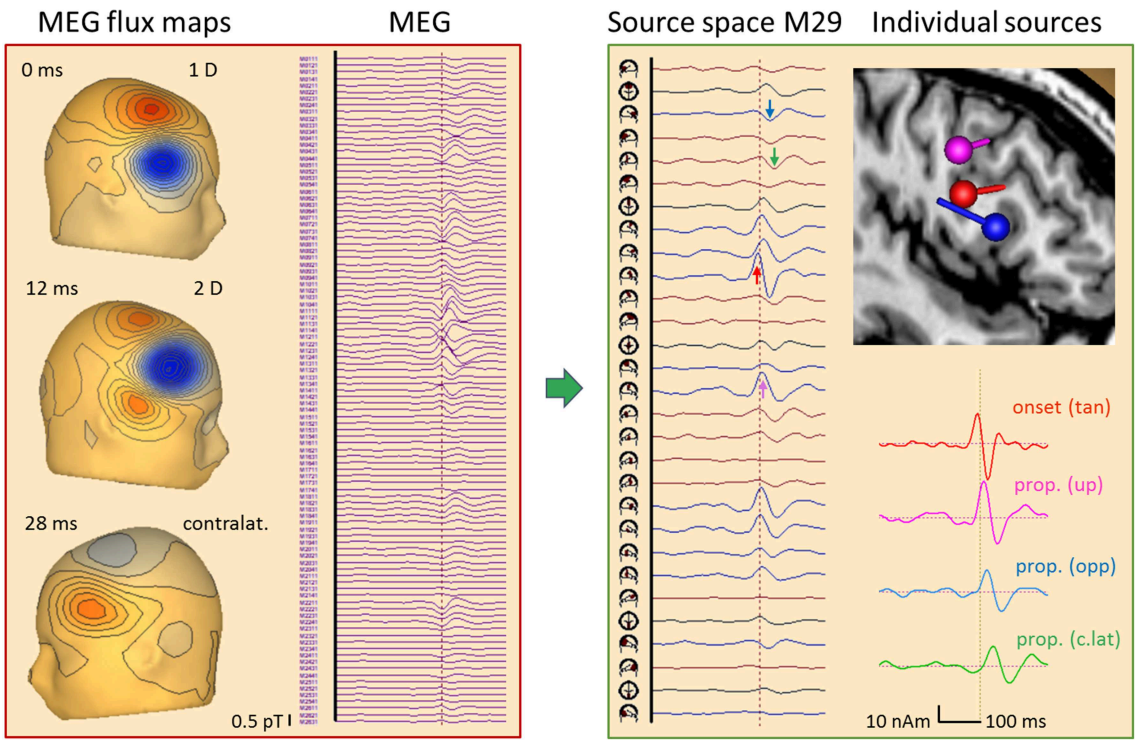

FIGURE 13 | Right frontal propagating IED, 84 averages, MEG results. Time epoch and filtering same as in **Figure 12**. The 102 magnetometer signals (left) are transformed into source space M29 (16). Each source has 2 tangential dipoles and is rotated to show the maximum tangential activity in each of the 29 regions. The onset shows the largest peak at the right frontal source (red arrow) followed by a delayed peak below C4 (pink) and later peaks below F8 (blue) and F3 (green). A multiple discrete source model with 4 dipoles was sufficient (see text) to separate the onset (red) from activities propagated upwards (pink), forward to the other side of the gyrus (blue) and to contralateral (green), as seen clearly by the increasing delay of the typical biphasic spike pattern in the 4 source waveforms. The flux map at 12 ms illustrates that localization by a single dipole is no longer possible when the propagated activities start overlapping in a complex way.

in the EEG source waveform. The tangential dipole activity of the left motor knob (brown) was relatively weak both in MEG and EEG, but could be localized precisely using MEG. The larger downward peak in the EEG source waveform (black arrow) following the positive onset peak of SC reflects the second phase of the IED with a large inward current into sensorimotor cortex. How much of this predominantly radial activity originated in SC or in MC, could not be fully resolved using EEG due to the closeness of both source regions. MEG, however, rendered only the tangential part of the inflow into the motor knob and showed minimal interference between the SC and MC dipoles because their orientations differed sufficiently in the tangential plane (**Figure 14**, right).

Figure 15 depicts the SEP average of 375 left-median nerve stimuli in this patient. Here, the EEG rhythms were averaged out due to the asynchrony with the stimulation randomized around 3 per second. In addition to the giant SEP component P25 (28) peaking at C4 and P4 with a latency of 22 ms, the median-nerve stimulus elicited jerks occurring at 40 ms as seen in the EMG (black arrow). The stimulus artifact, seen as the first peak in EMG, was removed from the EEG by 2 spatial components using the SEP source space (**Figure 9**) as surrogate model to correct the EEG in analogy to ECG-artifact correction (15). This correction defines a linear operator that was applied to the leadfields during source modeling to prevent bias in localization. When inspecting the waveforms in standard SEP source space (**Figure 15**, left), N20 was seen at a latency of 18 ms in the first tangential trace of the right central sensorimotor cortex (CR). The giant P25 was maximal in the radial trace, but also quite large in the first tangential trace of CR with inverted polarity relative to N20 (green arrows). Thus, P25 showed an oblique dipole pattern with a large positive scalp peak in the 3D-map between C4 and P4. A similar pattern was seen in left sensorimotor cortex (CL) about 9 ms later (brown arrows).

In this patient having myoclonic epilepsy, an enhanced neuronal network was activated following right median-nerve stimulation as suggested by the jerks occuring ∼40 ms later in the left hand (black arrow in EMG channel FDIL) and weaker jerks seen in the EMG of the right FDI ∼50 ms post-stimulus. MDS analysis of the somatosensory evoked potentials (SEP) and magnetic fields (SEF) revealed six nodes of this network. These involved not only somatosensory, but also right and left motor cortex as suggested by multiple discrete source analysis (**Figure 15**, right). The first deflection, i.e. N20, localized to the known postcentral area 3b (peaking 18 ms after the stimulus and −22 ms prior to the jerk, red). Adding a more superficial and

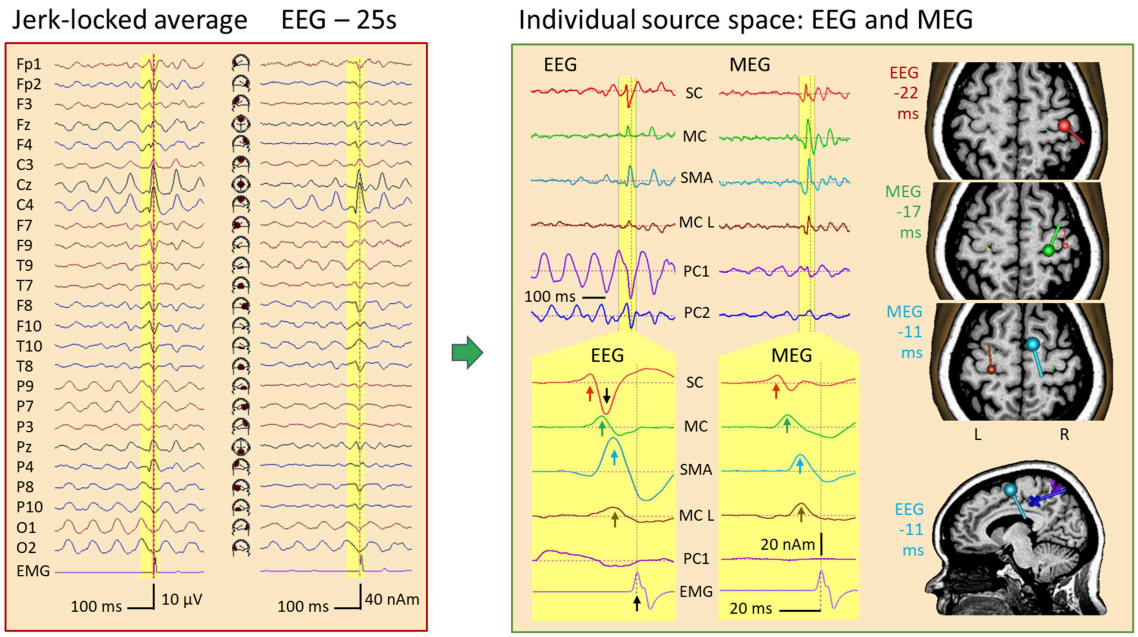

FIGURE 14 | IED in a case of myoclonic epilepsy. Left: jerk-locked average displayed in scalp EEG montage Av25 and source space 25. The motor potential (MP) preceding the left-hand jerk (EMG/FDIL at bottom) is riding on a central 10-Hz EEG rhythm and is most prominent below C4 in source space 25. Right: An MDS model with 4 dipoles and 2 PCA-components modeling the parietal (PC1) and central (PC2) 10-Hz oscillations separates the sharp jerk-locked transient in the wideband EEG and MEG averages from the rhythmic activities (right top). After expanding time scale for better visualization of the yellow pre-jerk epoch, and forward filtering (see text), 4 components could be isolated both in EEG and MEG (for details, see text): IED onset in right somatosensory cortex (SC, red, 22 ms prior to jerk), discharges of right motor knob (MC, green, −17 ms), SMA (blue, −11 ms) and contralateral, left motor knob (MC L, brown, −10 ms). The orientation and strength of source current at these times is illustrated by the dipoles in the slices of the individual MRI, colored accordingly. The posterior mid-line centers of the oscillatory EEG components PC1 and PC2 are shown by crosses in the sagittal slice at −11 ms.

lateral dipole to model the somatosensory areas 1–2, the P22 activity could be isolated both in EEG and MEG (pink, −20 ms). Two sources were needed to separate P25 from the continuing overlap of the somatosensory activities that had started earlier: a near-to-tangential dipole in the lower parts of the motor knob, likely area 4 (MC 4, green, −18 ms) and a more superficial oblique dipole at the crown of the motor knob (MC 6, yellow, −17 ms). The next two nodes were modeled by dipoles in the SMA (blue, −13 ms) and in the left, contralateral motor knob (−10 ms, brown). This model could be constructed either by seeding the dipoles using the individual MRI and the known anatomical locations of the sensorimotor areas representing the first 2 digits, or by using localizations from MEG and EEG. In both approaches, the key was to optimize orientations such that each dipole source waveform had a flat baseline prior to its onset (black arrows).

DISCUSSION

Since the 10–20 electrode system was introduced in 1958 (29), reviewing EEG in longitudinal or transverse bipolar montages became clinical standard. To better observe signals from the temporal lobe, e.g. IEDs, the IFCN recommended to include more inferior electrodes and record from a minimum of 25 electrodes in 2017 (13). In addition to bipolar montages that depict the scalp potential gradients over the upper head, the common average reference montage (CA) of these 25 electrodes was proposed for additional EEG overview (30). All these montages, however, look only at the voltage distribution over the surface of the head.

Hjorth's source derivation (31) was the first attempt to take the EEG from scalp into depth by using a linear transformation corresponding to a simplified Laplacian operator that subtracts the signals of all surrounding electrodes from that at the center electrode. Nowadays, using spherical-splines interpolation (32), the Laplacian or current-source-density (CSD) distribution over the scalp can be estimated more accurately including the boundaries of the electrode array (26). CSD measures the currents flowing from the brain into the scalp through the skull. Thus, CSD maps represent a smoothed reconstruction of the voltage distribution on the brain surface as proposed previously by Freeman (33). Although CSD deblurs the EEG to some extent (34, 35), it faces the same problem as cortical grid recordings of correctly localizing the origin of the underlying oblique dipolar maps. Furthermore, CSD maps are noisier than average-referenced EEG and more difficult to read.

Attempts to take the EEG review beyond the scalp and cortical surface into the brain have been rare but successful by using so-called source montages (20, 26, 30, 36–39). As documented in these papers and illustrated in **Figures 6**, **9–12**, **15**, standard source spaces based on MDS models can (a) render the signals of

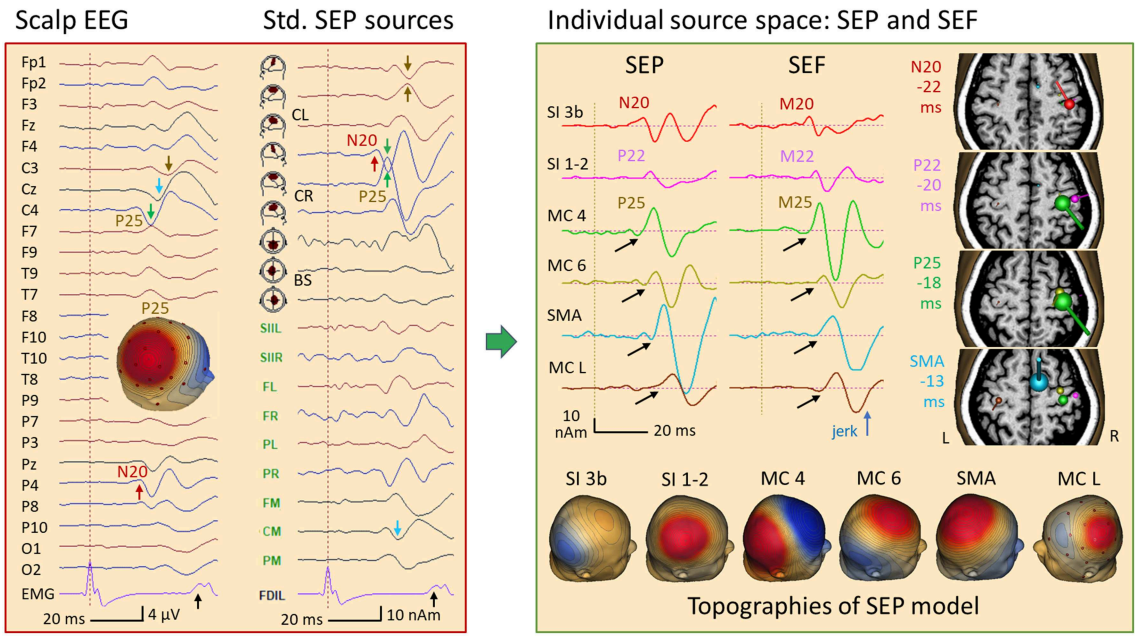

FIGURE 15 | Left median-nerve SEP in a case of myoclonic epilepsy. Left: SEP average in AV25 montage and in SEP source space. Following a weak N20 (P4, red arrow), the giant P25 (28) is seen at C4 (green arrow) and P4. The EMG showed a jerk ∼40 ms after stimulation of the left hand and, a weaker jerk of the right hand ∼10 ms later. In SEP standard source space, the regional source CR (below C4) displays the N20 in the 1st trace, perpendicular to the central sulcus. Then, it shares the huge P25 component with the radial 2nd source trace of CR (green arrows), resulting in the strong positive peak of P25 between C4 and P4 in the scalp map. A similar giant P25 pattern is seen ∼10 ms later in the left central region (CL, brown). Right: an MDS model with 6 dipoles resolved the complex overlap both in EEG and MEG (for details see text): N20 (red) is followed by the more radial post-central P22 (pink), by the pre-central P25 (shared by 2 sources in MC 4, green and MC 6, yellow) and activities in SMA (blue) and the contralateral, left motor cortex (MC L, brown). The peak times relative to the left-hand jerk are given next to the MRI slices used to display MEG dipole orientations and strengths at the peak times of N20, P22, P25, and SMA. Below, the 6 forward EEG topographies of the MDS are depicted. Using their inverse matrix, the 32 scalp EEG channels and, independently, the 122 MEG channels could be taken back into the brain to separate the activities of the nodes of the network underlying this case of myoclonic epilepsy. Black arrows indicate the onset of the later activities that had no obvious cross-talk with the earlier activities.

focal brain activities more precisely, i.e. with less contamination from other brain areas, (b) indicate where their origin is located, and (c) demonstrate that the separation is adequate by showing that no or only little cross-talk from other brain regions is seen in the source waveforms (2, 37).

The separation of different brain activities can be optimally tuned by using individual dipole source configurations with equivalent dipoles fixed to known brain structures or fitted to data with high signal-to-noise ratio (SNR). However, dipole orientations in individual MDS models are the key to separate earlier from later source components. The orientation of each dipole has to be fitted to match the recorded scalp maps at time points when the other sources are relatively inactive. Tuning is done using the source waveforms as control to check that cross-talk from earlier onto later sources is minimal, as seen for example in **Figures 5–9**, **14**, **15**. Finding the orientation of an IED onset dipole is relatively easy, but finding the orientation of subsequent dipoles to model the regions involved in propagation becomes more complicated, the more dipoles are comprised in the model (11, 12, 25).

The distance between the different active regions in the presented case of cortical reflex myoclonus was just sufficient to prevent linear dependence between the dipole topographies of the forward model (**Figure 15**, right), because 4 dipoles could be used to separate the postcentral somatosensory (N20, P22) and precentral motor components (MC 4, MC 6) instead of just one regional source with 3 dipoles that would have been quite an accurate model for this region. This separation was only possible by sequentially adapting orientations to minimize cross-talk between source waveforms as seen by the flat onset phases prior to the rising of each activity and the lack of large activities following N20 and P22 (**Figure 15**, black arrows). If the linear inverse operators were inadequate, activities would spread onto the other sources, as seen in standard source space when generators are between the model sources (**Figure 6**) or not individually oriented (**Figures 9**, **15**). In contrast, the separation of the source activities from the more distant central SMA and left motor cortex was not critical. Thus, the linear inverse using 6 dipoles could clearly depict the biphasic discharge patterns of the sources of SEP and SEF related to the propagation from primary sensory to primary motor areas, and further on to SMA and contralateral MC (**Figure 15**).

For the spontaneous jerks in this case of cortical reflex myoclonus, propagation of a typical spike pattern from SC to MC could be documented with inward orientation of the source dipoles into the cortex as expected for IEDs. In addition, the

afferent nerve conduction time of 18 ms as defined by the latency of N20 and the efferent conduction times as defined from the source peaks in MC relative to the EMG peaks (MC R to FDIL: 17–18 ms; MC L to FDIR: 19 ms) were highly similar. In contrast, the first activity seen in the averaged spontaneous jerks occurred 6 ms earlier in SC, 22 ms prior to the jerk, i.e. at the same relative latency at which the postcentral N20 occurred prior to the jerks elicited by stimulation. Thus, the spontaneous myoclonic IEDs appeared triggered by the activity in SC and not by MC. A similar time lag of 6 ms between SC and MC has been reported previously for tibial nerve SEPs recorded epi-cortically (40). In fact, when looking at the wideband EEG source waveforms, a rhythmic buildup over 1–2 cycles prior to the IED could be seen in SC, but not in MC (**Figure 14**, right top).

This imaging of propagation was possible, because the models of the 4–6 discrete dipoles were overdetermined and stable, not only in EEG, but also in MEG. The better spatial resolution of MEG due to the larger number of recording channels having precise relative locations, seemed to compensate for the lack of the "radial" current dimension in MEG, since the SEF model could separate 6 source waveforms highly similar to the SEP model. Thus, we could decompose the complex signals in the surface SEP and SEF into six similar, yet successive biphasic patterns with an overlap becoming progressively more severe with increasing latency. Separation was consistent between EEG and MEG and comparable to the separation of the source waveforms underlying the jerk-locked averaged activity. Due to the lack of inferior electrodes, the activities of the afferent and efferent nerve volleys were not resolved, although the standard SEP montage in **Figure 15** suggested such activity in the brainstem trace (BS) prior to the left-hand jerks.

The presented cases illustrate the power of discrete sources in taking the EEG back into the brain when using individually adapted equivalent dipoles to separate the different brain activities underlying evoked potentials and focal IEDs in line with several previous studies (2, 25, 41–43). During EEG and MEG review, however, sources are not known a priori. Hence, standard source spaces covering the whole brain are required to separate the activities of the different regions (16, 26, 37). As shown in **Figures 10**, **11** and previously (20, 26, 37–39), source montages provide a more focal view, approximate localization and reduction of overlap from other sources. Thus, abnormal signals like IEDs can be recognized more easily. This was confirmed quantitatively by the focality measure introduced here.

After a few similar IEDs have been found, they can be averaged and their spatial vectors, derived from source localization of a regional probe source or from PCA (**Figure 6**), can be combined with the standard sources. This creates a linear inverse proving focality, if only little activity is contributed by other regions (cf. hypotheses in **Figure 2**). This principle of reverse source imaging (RSI), applied e.g. by minimizing the cross-talk while moving the probe source, has not yet been exploited and promises to become a very helpful adjunct to source localization of IEDs in the future.

Source montages are based on fixed MDS models (26, 37). Thus, they define a time-invariant linear inverse transformation to take the EEG back into the brain on an approximate, macroscopic level. Because sources are fixed, it is the resulting compound activities of the source waveforms (12, 26, 37) that fully contain the dynamic evolution of the source activity in each brain region. There is no restriction on their temporal dynamics whatsoever; source waveforms are simply linear combinations of the recorded EEG or MEG signals like traditional montages. Being unconstrained, the source waveforms are the result of our testing whether the hypothesized source configuration can explain the data adequately. Thus, the source waveforms reveal immediately when in time an MDS is decomposing the data appropriately and when cross-talk or interference might be occurring.

For example, the decomposition of the SEP in **Figure 15** was critical when trying to separate the activities of the posterior (area 3b: N20) and anterior walls (area 4: P25) of the central fissure, because the model had to include two closely located dipoles with almost anti-parallel orientations. Despite this near-to-linear dependence, the onset-to-peak phases of N20 and P25 could be well separated as documented by little crosstalk between all sources prior to the peak of P25 and by the fact that the smaller N20 dipole could be localized accurately to the postcentral gyrus in the onset phase. It remained fixed and displayed the same N20 peak when more sources were added to the EEG model. The second upward peak in the N20 source waveform, however, increased in comparison to the MEG source waveform of M20 since it interacted with the downward peak following P25—an indication that the activation of sensorimotor cortex had become more complex at this later time when more sources were involved. Here, the macroscopic linear decomposition of this SEP data recorded with 29 electrodes had come to its limits.

In contrast, spatio-temporal dipole modeling (STDM) and dynamic causal modeling (DCM) parametrize the waveforms of the compound source activities in addition to source locations and orientations in order to reduce the overall number of unknown parameters and to impose temporal constraints. Whereas, the first STDM studies used empirical biphasic or bi-peaked waveshapes (1, 7), the compound source activities of the more recent DCM methods (44) are based on a physiologically informed network model of the underlying sources. In any case, the goal is to find a model with relatively few temporal and spatial parameters. As shown previously (1, 7), STDM parameters can be estimated in a robust way even when using only few recording channels, because the abundance of the spatio-temporal information is reduced to a small number of parameters far below the degrees of freedom in the data (10). Estimation of these parameters, however, is complicated, because spatial and temporal parameters are severely dependent in a non-linear way.

STDM is based on the assumption that "the neural substrate generating the surface evoked potentials can be defined as consisting of a limited number of neural subsets (generators)…" (1). The activity of each generator—"stationary, as is the spatial organization of the underlying neural structure"—is described by "an equivalent dipole located in, or in close proximity to the neural substrate" and the "temporal course of dipole magnitude is thought to depict the compound discharge processes of the underlying structure." The generators add "linearly to the scalp potential according to the laws of electrostatics (spatio-temporal

superposition)" and their contribution on the scalp can be approximated by choosing "a particular head model" (1). These spatial assumptions also apply to DCM and MDS. STDM and DCM, however, do not estimate the source activities by a simple linear transformation. In addition to the 5 spatial parameters required for each dipole source having unit magnitude (i.e. 3 locations and 2 orientations), the time-varying dipole magnitude is modeled in STDM by e.g. 4∼10 parameters describing peak amplitudes, onset, peak and offset times. When applying STDM to AEPs, the strong data reduction allowed for the separation of 6 components of the afferent activity in the brainstem—redefining the origin of the brainstem AEP (7)—and of two components bilaterally in the auditory cortex (1), despite the availability of only 12 scalp EEG channels.

The assumptions underlying STDM are also valid for IEDs. IEDs are generated by a small number of connected regions, i.e. a network with a limited number of nodes. Each underlying cortical patch can be modeled by a fixed equivalent source with a relatively simple bi- or triphasic waveshape as seen in the source waveforms of **Figures 12–14**. Thus, the propagation around a gyrus and to neighboring areas as shown by the MEG decomposition of a frontal spike in **Figure 13**, could be resolved with more stability, if the typical spike waveshapes were modeled by a few temporal parameters in addition to the 5 spatial parameters of each equivalent dipole. This would lead to an enormous reduction in degrees of freedom and, thus, STDM appears quite promising in providing a robust separation of the components underlying averaged IEDs. However, software to adapt such an STDM model to IEDs is currently not available. Neither has DCM been applied to focal, lesion-related IEDs, to our knowledge, possibly due to the computationally very demanding Bayesian methods required by DCM (44). However, DCM models have been applied to understand the networks underlying electrographic seizures using EEG/ECoG (45).

MDS models are also the key to measure connectivity between brain regions (46). The strong overlap due to volume conduction makes most scalp signals highly correlated, as evidenced by the focality measure introduced here. As illustrated above, a linear inverse can be constructed to isolate the activities of two brain regions without any contamination by mutual volume conduction, if the regularization coefficients of the two regions are set to zero. Thus, their mutual cross-talk is zero. Their connectivity can be assessed, if the other brain regions are modeled by a standard source space. Cross-talk of the other regions is projected onto the two sources of interest with the same phase. This interference can be removed using out of phase coherence (47). For connectivity analysis, one ideally constructs specific source spaces using prior information from multi-modal functional imaging and individual structural MRI (48).

To conclude, taking the EEG back into the brain using a standard or specific source space is a prerequisite to analyze the networks underlying IEDs and evoked- or event-related potentials. If the results of reviewing the EEG in standard source space are inconclusive, functional and structural information from other modalities should be used to create more specific individual source spaces.

MATERIALS AND METHODS

Subjects and Data

The presented EEG and MEG examples were available as digitized, anonymized data from past studies in various evoked potential laboratories and epilepsy units at the Max-Planck-Institute for Psychiatry in Munich (1, 7, 10, 17), at the Kohnan Hospital and Tohoku University of Sendai (49), and at the University Hospitals of Aarhus (16), Heidelberg (25, 26, 50), Iowa (51), and Munich (6). For all studies, informed consent of the subjects and approval of the local ethics committees had been obtained.

Software and Digital Signal Processing

Digital signal processing was performed using BESA Research 7.0 (BR7), BESA MRI 2.0 (BM), and BESA Simulator 1.4 (BESA GmbH, Gräfelfing, Germany). Standard MDS models were created by seeding sources into the standard MRI of BR7 in Talairach space within the source analysis module of BR7. Individual MDS models were created using sequential fitting strategies (11, 25) while visually minimizing cross-talk between source waveforms. Individual source locations as well as LORETA and CLARA images were visualized in Talairach space using the source analysis module of BR7 and structural T1-weighted MRI images were rendered using BM.

Using specific batch functions, individual and standard source montages were saved to be applied effectively while inspecting continuous EEG data using a digital zero-phase-shift filter of 2–35 Hz to reduce artifacts and enhance perception of IEDs (26). IEDs were averaged using wideband filter settings in the ERP module of BR7 and the averages were filtered with a forward low filter of 5 Hz to obtain a clear baseline prior to onset and a zero-phase-shift high filter at 40 Hz to reduce artifacts of higher frequencies. Averaged evoked potential filter settings depended on the time range of the observed components and are specified in the figures.

Source Space Transformations

Scalp and Source Montages Are Linear Transformations

EEG data can be described as a matrix D_r with as many rows as recorded channels. Each column contains the recorded voltages at one sampling point in time. EEG data is typically recorded against a common reference that is often defined by a hardware average of the signals from two or more recorded electrodes, e.g. F3 and F4. Thus, signals are biased, because the voltage difference is small to nearby and large to remote electrodes. To remove this bias, bipolar montages are created by subtracting neighboring channels. In the average reference montage, bias is removed by subtracting the signal averaged over all channels from each channel. Thus, bipolar montages measure the voltage gradients along the scalp in longitudinal or transverse directions while the average reference comes close to showing the "true" voltage at each electrode, if the electrodes cover the upper and lower head with sufficient equidistant spacing (26).

These montages are special forms of linear combinations, defined by multiplying the recorded matrix D_r with a linear

operator B to create a bipolar montage D_B or with A to create the average reference matrix D:

$$D_B = B\ D_r \quad (1)$$

$$D = A\ D_r \quad (2)$$

Similarly, the signals in source space are described by a matrix S using a special inverse linear transformation matrix T^{-1}:

$$S = T^{-1}\ D = T^{-1}A\ D_r \quad (3)$$

Each row of A, B or T^{-1} contains the weight factors used to multiply the recorded channels in order to obtain one channel in the bipolar, average referenced or source montage. The weight factors of A and B have been published (26). For example, a bipolar channel simply uses a weight factor of +1 for the positive, −1 for the negative, and 0 for the other channels. The inverse matrix T^{-1} has more specific, non-zero factors for each recorded channel. For example, T^{-1} of **Figure 7** has 4 rows, one for each source, and 12 columns with the source-specific factors for each recorded channel.

How can we calculate T^{-1}, i.e. the different weight factors needed to reconstruct each channel in the individual and standard source spaces from the recorded channels?

Linear Overlap: The Forward Model With Fixed Sources

According to the laws of physics, the signals of all sources in the brain (rows in S) overlap linearly at the scalp to form the EEG together with some remaining noise, i.e. the signals not explained by the chosen set of discrete sources (noise matrix N):

$$D = T\ S + N = A\ L\ S + N \quad (4)$$

The contribution of each source to the EEG is defined by its voltage map on the scalp. Thus, the columns of the topography matrix T contain the average-referenced maps due to unit currents at each source. Using a volume conductor model of the head (forward model), one can predict the reference-free scalp maps of each source by calculating matrix L, the so-called leadfield vectors (26). To equate the average-reference matrix D with the predicted voltages, we must apply A also onto L to obtain T. The amount of signal contributed to the EEG signals d_i (t) (rows *i* in D, $i = 1 \ldots$.nchans) at each point in time by source k is given by the magnitude of the (still unknown) source waveform signals s_k (t) (rows k in S, $k = 1 \ldots$.ns) multiplied with the fixed, time-independent topography vector k, i.e. the column k of T.

The Inverse Linear Operator: Individual and Standard Source Spaces

After having defined matrix T by a specific forward model, one can calculate S by applying the linear inverse T^{-1} onto Equation (4) from the left:

$$S = T^{-1}\ D - T^{-1}\ N \quad (5)$$

since the product of the forward and inverse matrices is the identity matrix I:

$$T\ T^{-1} = I \quad (6)$$

Since T is not a square matrix, T^{-1} is given by the Moore-Penrose pseudoinverse (41). Prior to inversion, the forward column vectors of T are normalized to avoid bias against deep sources in the brain and to enable noise reduction and smoothing by regularization (**Figure 9**):

$$T_N = T\ W^{-1} \quad (7)$$

The diagonal in W contains the root-mean-square magnitudes of each topography vector and the norm of each column in T_N is 1. The pseudoinverse of T_N is given by

$$T_N^{-1} = (T_N^T T_N + R)^{-1}\ T_N^T \quad (8)$$

The correlation matrix of the topographies (T_N^T is the transpose of T_N) is the kernel of the inverse with values of 1 in the main diagonal. In individual source spaces with few sources (ns < nchans) the regularization matrix R can be set to zero. Thus, source activities are not smoothed and there is no cross-talk between sources, because applying T_N^{-1} from the left onto T_N produces the identity matrix, i.e. each signal is rendered maximally while spread from the other sources is suppressed (20).

In standard source spaces with more source dipoles (ns ∼ nchans), the coefficients in the diagonal regularization matrix R can be set specifically for each source to a small percentage of 1 as, for example, to 1.2% in source space 25. This results in little cross-talk and moderate smoothing as can be seen in **Figures 6**, **8–12**. Furthermore, the recorded data matrix D_r is first projected onto 81 standard electrodes by the linear operator P using spherical splines interpolation as for mapping (26). This projection is also very convenient, if a noisy recording channel has to be excluded, because the leadfields L can be pre-calculated for the 81 standard-electrodes using the standard sources.

In summary, the EEG is taken back into the brain by a single linear inverse operator, if we combine the series of linear operations into a single linear transformation matrix M acting on the recorded data:

$$S = M\ D_r = (W^{-1}T_N^{-1}P\ A)D_r \quad (9)$$

P is the unity matrix I in discrete individual source models and the spline-interpolation matrix (dimension: 81*nchans) in standard MDS models. In distributed source models (ns >> nchans), the inverse is calculated in sensor and not in source space (14), because the number of sources is too large for inversion in source space. This leads to more smoothing. Furthermore, regularization with different coefficients for specific sources is impossible. When inverting in source space, however, ECG components are removed completely, if their regularization coefficients are set to zero (15), and source activities of a particular brain region can be rendered without cross-talk to other regions.

As shown above, equivalent dipoles and regional sources have a high accuracy in modeling the activity of a relatively large brain area. In addition, the linear inverse T^{-1} is minimizing the noise

term N in Equation (5) as it represents an implicit least-squares-fit of the source waveforms S to the data D. Therefore, a small number of dipoles in the individual source spaces and 25 regional sources in standard source space 25 were sufficient to model D with little noise in all cases presented here. Typically, residual variance (RV) in standard source spaces was below 1%, i.e. the noise projected by matrix N onto the different source regions was small.

Focality in Source and Scalp Space

Focality was defined to measure the spread of activity over the channels in scalp vs. source space as follows: In each space, the channel having maximum signal was determined within a selected epoch (IEDs: −50: +150 ms relative to peak). Next, the maximum signal was correlated with itself and all other channels to obtain a vector of squared covariance coefficients sorted by magnitude and normalized to 100%. Cumulative focality was calculated by summing the magnitudes from the largest to the n-largest values to obtain F(n) as illustrated in **Supplementary Figure 1**.

DATA AVAILABILITY

The raw data supporting the conclusions of this manuscript will be made available by the authors, without undue reservation, to any qualified researcher.

ETHICS STATEMENT

The presented EEG and MEG examples were available as digitized, anonymized data from past studies in various evoked potential laboratories and epilepsy units at the Max-Planck-Institute for Psychiatry in Munich (1, 7, 10, 17), at the Kohnan Hospital and Tohoku University of Sendai (48), and at the University Hospitals of Aarhus (16), Heidelberg (25, 27, 49), Iowa (50), and Munich (6). For all studies, informed consent of the subjects and approval of the local ethics committees had been obtained.

AUTHOR CONTRIBUTIONS

MS analyzed the EEG and MEG data and designed all figures. PB performed simulations and specific software developments for this study and critically reviewed the manuscript. NN and SB provided the data from their epilepsy units, contributed to data interpretation, and critical revision of manuscript and figures.

ACKNOWLEDGMENTS

We are grateful to all colleagues who have taken care to record EEG, MEG, and MRI data of high quality at their institutions and provided this data for this and previous studies.

SUPPLEMENTARY MATERIAL

The Supplementary Material for this article can be found online at: https://www.frontiersin.org/articles/10.3389/fneur.2019.00855/full#supplementary-material

Supplementary Figure 1 | Assessment of focality: Nine IEDs (1-s segments) are shown in scalp space (middle) and standard source space 25 (top). The visual impression of higher focality in source as compared to scalp space, i.e. the IED signal spreads less and with smaller magnitude over the channels in source than scalp space, is quantified by the new measure of focality F(n) summing the cumulative variance of the correlation with the largest signal from the largest to the n-th largest channel (see Materials and Methods). The focality diagrams at the bottom show focality in % for segments 2 (left) and 5 (middle). In segment 2, focality is considerably larger in source space at lower n-values while the more widespread IED in segment 5 exhibits similar focality in source and scalp space. The diagram at the lower right depicts source focality together with the difference of focality in source vs. scalp space over the 65 left temporal IEDs of the mTL patient shown in **Figure 11**. The difference is >0 in all but 2 IEDs. This proves the much higher focality in source space ($p < 0.001$).

REFERENCES

1. Scherg M, Von Cramon D. Two bilateral sources of the late AEP as identified by a spatio-temporal dipole model. *Electroencephalogr Clin Neurophysiol.* (1985) 62:32–44. doi: 10.1016/0168-5597(85)90033-4
2. Scherg M, Von Cramon D. Evoked dipole source potentials of the human auditory cortex. *Electroencephalogr Clin Neurophysiol.* (1986) 65:344–60. doi: 10.1016/0168-5597(86)90014-6
3. Pascual-Marqui RD, Michel CM, Lehmann D. Low resolution electromagnetic tomography: a new method for localizing electrical activity in the brain. *Int J Psychophysiol.* (1994) 18:49–65. doi: 10.1016/0167-8760(84)90014-X
4. Jordanov T, Hoechstetter K, Berg P, Paul-Jordanov I, Scherg M. CLARA: classical LORETA analysis recursively applied. *F1000Posters.* (2014) 5:895. Available online at: https://f1000research.com/posters/1096116
5. Beniczky S, Rosenzweig I, Scherg M, Jordanov T, Lanfer B, Lantz G, et al. Ictal EEG source imaging in presurgical evaluation: high agreement between analysis methods. *Seizure.* (2016) 43:1–5. doi: 10.1016/j.seizure.2016.09.017
6. Hegerl U, Gallinat J, Mrowinski D. Intensity dependence of auditory evoked dipole source activity. *Int J Psychophysiol.* (1994) 17:1–13. doi: 10.1016/0167-8760(94)90050-7
7. Scherg M, von Cramon D. A new interpretation of the generators of BAEP waves I-V: results of a spatio-temporal dipole model. *Electroencephalogr Clin Neurophysiol.* (1985) 62:290–9. doi: 10.1016/0168-5597(85)90006-1
8. Kimura J, Mitsudome A, Yamada T, Dickins QS. Stationary peaks from a moving source in far-field recording. *Electroencephalogr Clin Neurophysiol.* (1984) 58:351–61. doi: 10.1016/0013-4694(84)90061-0
9. Tao JX, Ray A, Hawes-Ebersole S, Ebersole JS. Intracranial EEG substrates of scalp EEG interictal spikes. *Epilepsia.* (2005) 46:669–76. doi: 10.1111/j.1528-1167.2005.11404.x
10. Scherg M. Fundamentals of dipole source potential analysis. In: Grandori F, Hoke M, Romani GL, editors. *Auditory Evoked Magnetic Fields and Electric Potentials. Vol. 6. Advances in Audiology.* Basel: Karger (1990). p. 40–69.
11. Scherg M, Berg P. New concepts of brain source imaging and localization. In: Barber C, Celesia G, Comi GC, Mauguière F, editors. *Functional Neuroscience.* Amsterdam: Elsevier Science (1996). p. 127–37.
12. Scherg M. Functional imaging and localization of electromagnetic brain activity. *Brain Topogr.* (1992) 5:103–11. doi: 10.1007/BF01129037
13. Seeck M, Koessler L, Bast T, Leijten F, Michel C, Baumgartner C, et al. The standardized EEG electrode array of the IFCN. *Clin Neurophysiol.* (2017) 128:2070–7. doi: 10.1016/j.clinph.2017.06.254

14. Pascual-Marqui RD, Sekihara K, Brandeis D, Michel CM. Imaging the electric neuronal generators of EEG/MEG. In: Michel CM, Koenig T, Brandeis D, Gianotti LRR, Wackermann J, editors. *Electrical Neuroimaging*. Cambridge: University Press (2009). p. 49–78. doi: 10.1017/CBO9780511596889.004
15. Berg P, Scherg M. A multiple source approach to the correction of eye artifacts. *Electroencephalogr Clin Neurophysiol.* (1994) 90:229–41. doi: 10.1016/0013-4694(94)90094-9
16. Beniczky S, Duez L, Scherg M, Hansen PO, Tankisi H, Sidenius P, et al. Visualizing spikes in source-space: rapid and efficient evaluation of magnetoencephalography. *Clin Neurophysiol.* (2016) 127:1067–72. doi: 10.1016/j.clinph.2015.07.017
17. Scherg M, von Cramon D. Psychoacoustic and electrophysiologic correlates of central hearing disorders in man. *Eur Arch Psychiatry Neurol Sci.* (1986) 236:56–60. doi: 10.1007/BF00641060
18. Scherg M, Picton TW. Separation and identification of event-related potential components by brain electric source analysis. In: Brunia CHM, Mulder G, Verbaten MN, editors. *Event-related Potentials of the Brain*. Amsterdam: Elsevier (1991). p. 24–37.
19. Scherg M, von Cramon D. Dipole source potentials of the auditory cortex in normal subjects and in patients with temporal lobe lesions. In: Grandori F, Hoke M, Romani GL, editors. *Auditory Evoked Magnetic Fields and Electric Potentials. Vol. 6. Advances in Audiology*. Basel: Karger (1990). p. 40–69.
20. Scherg M, Bast T, Hoechstetter K, Ille N, Weckesser D, Bornfleth H, et al. Brain source montages improve the non-invasive diagnosis in epilepsy. *Int Congress Ser.* (2014) 1270C:15–9. doi: 10.1016/j.ics.2004.04.035
21. Weisser R, Weisbrod M, Roehrig M, Rupp A, Schroeder J, Scherg M. Is frontal lobe involved in the generation of auditory evoked P50? *Neuroreport.* (2001) 12:3303–7. doi: 10.1097/00001756-200110290-00031
22. Buchner H, Adams L, Knepper A, Rüger R, Laborde G, Gilsbach JM, et al. Preoperative localization of the central sulcus by dipole source analysis of early somatosensory evoked potentials and three-dimensional magnetic resonance imaging. *J Neurosurg.* (1994) 80:849–56. doi: 10.3171/jns.1994.80.5.0849
23. Buchner H, Adams L, Müller A, Ludwig I, Knepper A, Thron A, et al. Somatotopy of human hand somatosensory cortex revealed by dipole source analysis of early somatosensory evoked potentials and 3D-NMR tomography. *Electroencephalogr Clin Neurophysiol.* (1995) 96:121–34. doi: 10.1016/0168-5597(94)00228-7
24. Aydin Ü, Vorwerk J, Küpper P, Heers M, Kugel H, Galka A, et al. Combining EEG and MEG for the reconstruction of epileptic activity using a calibrated realistic volume conductor model. *PLoS ONE.* (2014) 9:e93154. doi: 10.1371/journal.pone.0093154
25. Scherg M, Bast T, Berg P. Multiple source analysis of interictal spikes: goals, requirements, and clinical value. *J Clin Neurophysiol.* (1999) 16:214–24. doi: 10.1097/00004691-199905000-00003
26. Scherg M, Ille N, Bornfleth H, Berg P. Advanced tools for digital EEG review: virtual source montages, whole-head mapping, correlation, and phase analysis. *J Clin Neurophysiol.* (2002) 19:91–112. doi: 10.1097/00004691-200203000-00001
27. Scherg M, Ille N, Weckesser D, Ebert A, Ostendorf A, Boppel T, et al. Fast evaluation of interictal spikes in long-term EEG by hyper-clustering. *Epilepsia.* (2012) 53: 1196–204. doi: 10.1111/j.1528-1167.2012.03503.x
28. Kakigi R, Shibasaki H. Generator mechanisms of giant somatosensory evoked potentials in cortical reflex myoclonus. *Brain.* (1987) 110(Pt 5):1359–73. doi: 10.1093/brain/110.5.1359
29. Jasper HH. The ten-twenty electrode system. *Electroencephalogr Clin Neurophysiol.* (1958) 10: 371–5.
30. Rosenzweig I, Fogarasi A, Johnsen B, Alving J, Fabricius ME, Scherg M, et al. Beyond the double banana: improved recognition of temporal lobe seizures in long-term EEG. *J Clin Neurophysiol.* (2014) 31:1–9. doi: 10.1097/WNP.0000000000000019
31. Hjorth B. An on-line transformation of EEG scalp potentials into orthogonal source derivations. *Electroencephalogr Clin Neurophysiol.* (1975) 39:526–30. doi: 10.1016/0013-4694(75)90056-5
32. Perrin F, Pernier J, Bertrand O, Echallier JF. Spherical splines for scalp potential and current density mapping. *Electroencephalogr Clin Neurophysiol.* (1989) 72:184–7. doi: 10.1016/0013-4694(89)90180-6
33. Freeman WJ. Use of spatial deconvolution to compensate for distortion of EEG by volume conduction. *IEEE Trans Biomed Eng.* (1980) 27:421–9. doi: 10.1109/TBME.1980.326750
34. Junghofer M, Elbert T, Leiderer P, Berg P, Rockstroh B. Mapping EEG-potentials on the surface of the brain: a strategy for uncovering cortical sources. *Brain Topogr.* (1997) 9:203–17. doi: 10.1007/BF01190389
35. Gevins A, Le J, Leong H, McEvoy LK, Smith ME. Deblurring. *J Clin Neurophysiol.* (1999) 16:204–13. doi: 10.1097/00004691-199905000-00002
36. Scherg M. From EEG source localization to source imaging. *Acta Neurol Scand.* (1994) 152(Suppl. 1):29–30. doi: 10.1111/j.1600-0404.1994.tb05180.x
37. Scherg M, Ebersole JS. Brain source imaging of focal and multifocal epileptiform EEG activity. *Neurophysiol Clin.* (1994) 24:51–60. doi: 10.1016/S0987-7053(05)80405-8
38. Assaf BA, Ebersole JS. Continuous source imaging of scalp ictal rhythms in temporal lobe epilepsy. *Epilepsia.* (1997) 38:1114–23. doi: 10.1111/j.1528-1157.1997.tb01201.x
39. Assaf BA, Ebersole JS. Visual and quantitative ictal EEG predictors of outcome after temporal lobectomy. *Epilepsia.* (1999) 40:52–61. doi: 10.1111/j.1528-1157.1999.tb01988.x
40. Hitomi T, Ikeda A, Matsumoto R, Kinoshita M, Taki J, Usui K, et al. Generators and temporal succession of giant somatosensory evoked potentials in cortical reflex myoclonus: epicortical recording from sensorimotor cortex. *Clin Neurophysiol.* (2006) 117:1481–6. doi: 10.1016/j.clinph.2006.03.029
41. Scherg M, Vajsar J, Picton TW. A source analysis of the late human auditory evoked potentials. *J Cogn Neurosci.* (1989) 1:336–55. doi: 10.1162/jocn.1989.1.4.336
42. Vanni S, Warnking J, Dojat M, Delon-Martin C, Bullier J, Segebarth C. Sequence of pattern onset responses in the human visual areas: an fMRI constrained VEP source analysis. *Neuroimage.* (2004) 21:801–17. doi: 10.1016/j.neuroimage.2003.10.047
43. Bledowski C, Cohen Kadosh K, Wibral M, Rahm B, Bittner RA, Hoechstetter K, et al. Mental chronometry of working memory retrieval: a combined functional magnetic resonance imaging and event-related potentials approach. *J Neurosci.* (2006) 26:821–9. doi: 10.1523/JNEUROSCI.3542-05.2006
44. David O, Kiebel SJ, Harrison LM, Mattout J, Kilner JM, Friston KJ. Dynamic causal modeling of evoked responses in EEG and MEG. *Neuroimage.* (2006) 30:1255–72. doi: 10.1016/j.neuroimage.2005.10.045
45. Cooray GK, Sengupta B, Douglas PK, Friston K. Dynamic causal modelling of electrographic seizure activity using Bayesian belief updating. *Neuroimage.* (2016) 125:1142–54. doi: 10.1016/j.neuroimage.2015.07.063
46. Hoechstetter K, Bornfleth H, Weckesser D, Ille N, Berg P, Scherg M. BESA source coherence: a new method to study cortical oscillatory coupling. *Brain Topogr.* (2004) 16:233–8. doi: 10.1023/B:BRAT.0000032857.55223.5d
47. Nolte G, Bai O, Wheaton L, Mari Z, Vorbach S, Hallett M. Identifying true brain interaction from EEG data using the imaginary part of coherency. *Clin Neurophysiol.* (2004) 115:2292–307. doi: 10.1016/j.clinph.2004.04.029

48. Lei X, Wu T, Valdes-Sosa PA. Incorporating priors for EEG source imaging and connectivity analysis. *Front Neurosci.* (2015) 9:284. doi: 10.3389/fnins.2015.00284
49. Iwasaki M, Nakasato N, Shamoto H, Nagamatsu K, Kanno A, Hatanaka K, et al. Surgical implications of neuromagnetic spike localization in temporal lobe epilepsy. *Epilepsia.* (2002) 43:415–24. doi: 10.1046/j.1528-1157.2002.30801.x
50. Hoechstetter K, Rupp A, Stancák A, Meinck HM, Stippich C, Berg P, et al. Interaction of tactile input in the human primary and secondary somatosensory cortex–a magnetoencephalographic study. *Neuroimage.* (2001) 14:759–67. doi: 10.1006/nimg.2001.0855
51. Yamada T, Azuma Y, Yanagisawa T. Interaction of somatosensory evoked potentials within the same nerve and between the two different nerves: including high-frequency oscillation (HFO). *Suppl Clin Neurophysiol.* (2006) 59:205–12. doi: 10.1016/S1567-424X(09)70032-7

Conflict of Interest Statement: MS is shareholder and employee of BESA GmbH, a company developing software for advanced EEG and MEG analysis. PB is a free-lance employee of BESA GmbH.

The remaining authors declare that the research was conducted in the absence of any commercial or financial relationships that could be construed as a potential conflict of interest.

frontiers in Neurology

REVIEW
published: 10 September 2019
doi: 10.3389/fneur.2019.00933

Evidence for the Role of Magnetic Source Imaging in the Presurgical Evaluation of Refractory Epilepsy Patients

Evelien Carrette[1]* *and Hermann Stefan*[2]

[1] Reference Centre for Refractory Epilepsy, Ghent University Hospital, Ghent, Belgium, [2] Department of Neurology-Biomagnetism, University Hospital Erlangen, Erlangen, Germany

Magnetoencephalography (MEG) in the field of epilepsy has multiple advantages; just like electroencephalography (EEG), MEG is able to measure the epilepsy specific information (i.e., the brain activity reflecting seizures and/or interictal epileptiform discharges) directly, non-invasively and with a very high temporal resolution (millisecond-range). In addition MEG has a unique sensitivity for tangential sources, resulting in a full picture of the brain activity when combined with EEG. It accurately allows to perform source imaging of focal epileptic activity and functional cortex and shows a specific high sensitivity for a source in the neocortex. In this paper the current evidence and practice for using magnetic source imaging of focal interictal and ictal epileptic activity during the presurgical evaluation of drug resistant patients is being reviewed.

Keywords: magnetic source imaging, refractory epilepsy, presurgical evaluation, equivalent current dipole modeling, magnetoencephalagraphy (MEG)

OPEN ACCESS

Edited by:
Sandor Beniczky,
Aarhus University Hospital, Denmark

Reviewed by:
Gabriel Gonzalez-Escamilla,
University Medical Centre, Johannes Gutenberg University Mainz, Germany
Lene Duez,
Aarhus University Hospital, Denmark

***Correspondence:**
Evelien Carrette
evelien.carrette@ugent.be

Specialty section:
This article was submitted to Applied Neuroimaging, a section of the journal Frontiers in Neurology

Received: *12 February 2019*
Accepted: *12 August 2019*
Published: *10 September 2019*

Citation:
Carrette E and Stefan H (2019) Evidence for the Role of Magnetic Source Imaging in the Presurgical Evaluation of Refractory Epilepsy Patients. Front. Neurol. 10:933. doi: 10.3389/fneur.2019.00933

Since the first MEG recordings in 1968 performed by Dr. Cohen using a single channel, the MEG technique has been optimized. The increase in the number of channels toward the whole head dewars with more than 300 sensors we use today, resulted in a breakthrough of MEG in the presurgical evaluation of patients with drug resistant epilepsy.

Using MEG in the work-up of epilepsy patients holds many advantages which are clear and multiple; just like EEG, MEG is able to measure the brain activity, and therefore the epilepsy specific information, directly (independent of blood flow), non-invasively and with a very high temporal resolution in the order of milliseconds. Thanks to its unique sensitivity to tangential sources it gives the full picture when combined with EEG, it allows accurate source imaging and shows a specific sensitivity for neocortical sources.

Typically patients with epilepsy who undergo MEG are in supine position during the recording session lasting in European centers about 90 min (range 60–420 min) and are encouraged to fall asleep or are even sleep deprivated (1).

In the MEG data recorded different features are being used to study the disease and more specifically to localize the epileptogenic zone (EZ) as precise as possible to plan surgical procedures in drug resistant epilepsy patients. Like stated in the position statement paper by the American Clinical MEG Society (AMEGS) MEG should be used as a non-redundant method to localize the EZ in people with drug resistant

localization related epilepsy, especially if those cases were the standard and established presurgical evaluation modalities fail in providing sufficient information (2).

EQUIVALENT CURRENT DIPOLE MODELING—PRACTICAL GUIDELINES

In this review mainly source localization obtained by equivalent current dipoles (ECD) is being discussed. This inverse solution localizes a point source assuming that all recorded magnetic signal is explained by a single dipole source. To check the reliability of this dipole several indicators are calculated for example the goodness of fit or the correlation coefficient.

ECD modeling is widely used for clinical source localization of interictal epileptiform discharges and today the only solution approved by clinical guidelines (2).

In contrast, when distributed methods are being used to perform magnetic source imaging, maps of the location and the extent of the generators are being displayed, however the yield of this inverse method has not been clinically validated yet and is therefore beyond the scope of this paper.

Today the proposed and accepted MSI pipeline to perform ECD modeling is illustrated in **Figure 1**. Based on the guideline provided by the American MEG Society (2) some elaboration on the following important steps in the pipeline should be mentioned:

- Visual identification of well-defined IED's is of major importance and this can include spikes and sharp waves. Research on the value of modeling slow-wave and/or fast activity is ongoing.
- The importance and difficulty of selecting a specific or several time-points in the IED waveform for source analysis. Typically, the peak of a spike-wave is being chosen as this time-point can guarantee a good signal-to-noise ratio (SNR) however might not represent the origin of the spike. Alternatively, a point on the rising phase of the IED should be checked and if SNR allows also the onset of the discharge. As described in the guideline, it is possible to trust the modeled spike-peak if the dipolar field pattern is stable (no rotation) over the whole spike-course. In case rotation of the field is evident, it is being suggested to look for an earlier source throughout the whole time-course of the spike to check for propagation. As SNR will be lower in this case, results need to be interpreted with more caution. Averaging might of course increase SNR (see lower).
- Evaluation of reliability of the ECD using solution parameters like goodness of fit, total error, coefficient of correlation or confidence interval are used however cannot guarantee appropriateness of the model. In case of ECD it is important to understand (1) the pro's and con's of the dipole model, (2) the character of the cortical spike sources, and (3) the current recommendations on MSI.
- Averaging of IED is not common or standard practice for MSI. It holds the advantage that SNR increases and therefore allows to model earlier phases of the IED time-course which might hold benefits (3), however it might blur differences in location or time course if similar IED are taken together nevertheless they arise from different and separated sources.

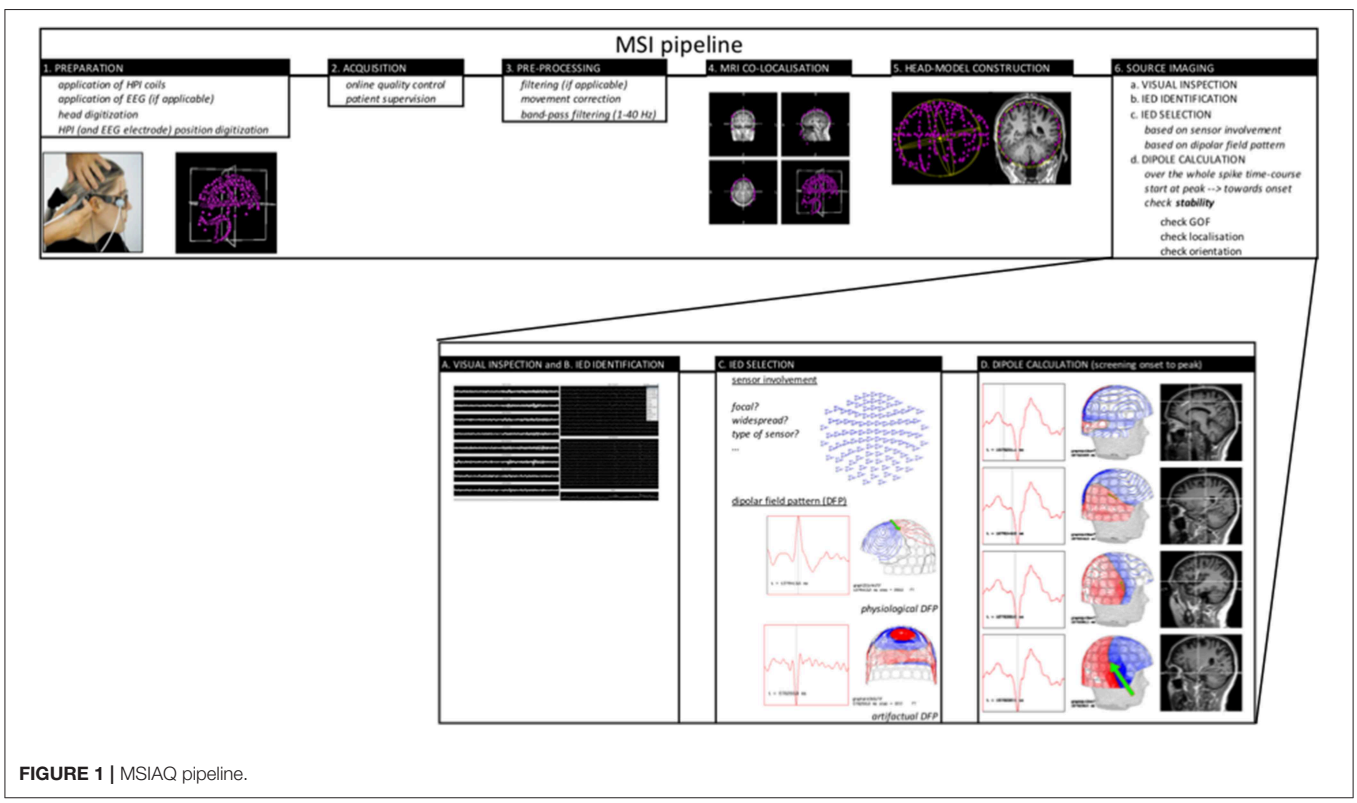

FIGURE 1 | MSIAQ pipeline.

THE VALUE OF INTERICTAL MSI

Spike Yield and Sensitivity

Given the acquisition circumstances, the most common feature measured with MEG is the interictal epileptiform discharge (IED) rather than a seizure. Depending on the localization of the so-called "irritative zone" sensitivity to detect IEDs with MEG differ. The average reported sensitivity to detect clinically significant IEDs is about 75% (3–5).

Studies on simultaneously recorded scalp EEG and MEG comparing IED's, show a complementarity between both techniques. This complementarity is a result of the difference in sensitivity of EEG and MEG for radial and tangential sources in the brain. This difference is caused by the different orientation of the apical dendrites of the pyramidal cells in the gyri or sulci. MEG is selectively sensitive for sources that are tangentially orientated corresponding to the neurons on the banks of the sulci, whereas EEG on the otherhand is mainly sensitive for radially orientated sources corresponding to the neurons on the top of the gyri (and in a lesser extend also for tangential sources). This explains why both techniques, EEG and MEG should be considered complementary (6). Illustratively Ebersole and Ebersole state in their paper "that the brain without sulci, but with major fissures, is a simplified but reasonable, model of the cortical generator for scalp EEG and the brain "seen" by MEG appears to have no gyral crowns over the convexity but rather erode sulci and fissures" (7). Therefore, it is clear that the full image can only be "seen" by combining both techniques.

In literature investigating the sensitivity of EEG and MEG, it is being described that in more than half of patients IEDs can be identified both on scalp EEG and MEG, in 7% of patients only EEG show IED and in 18% only MEG show IED. In 21% of patients no IEDs can be recorded with any of the two modalities. Interestingly they additionally showed that 47% of patients who did not show IEDs on scalp EEG did had spikes during 1 h of MEG recording, supporting the performance of MEG in EEG negative patients (8–11). Duez et al. compered the number of epileptiform discharge (ED) clusters between MEG and (high-density) EEG (64–80 electrodes) and found that 72% of ED clusters were visible both in MEG and EEG, in 15% only on EEG and in 13% only in MEG. More than 1/4 of ED clusters was visible in only 1 modality showing the importance of simultaneous EEG and MEG recording (12). In the recent study by Plummer et al. comparing simultaneous recorded MEG and HD-EEG report IED only in HD-EEG in 42%, only in MEG in 16% and seen in both modalities in 42%. This somewhat different result compared to earlier studies (high number of IED reported only for HD-EEG) might be a result of the additional 12 electrodes that were placed inferior temporal which is not standard practice (13).

In addition, Ebersole and Wagner recently reported on the importance of taking into account "the number of spike "types" recorded by EEG and MEG in addition to the spike frequency." They explain that this can only be done by combing EEG and MEG both for the recording and for the source modeling. They conclude that the absolute number of spikes can have some clinical significance, but that in the context of epilepsy surgery it is more important to identify the number of foci the spikes arise from. They showed that using only MEG would have let to missing at least 1 spike "type," clear and evident in EEG, in almost 50% of the patients (14).

Studies have compared subdural recordings with simultaneous MEG recordings and showed that all MEG spikes had subdural counterparts, whereas 56% of the subdural recorded spikes were shown on MEG. However for lateral neocortical, insular, intra-sylvian, and (frontal) interhemispheric foci this percentage rose to 75–90% of spikes (5, 9, 15, 16).

With similar studies it was shown that in neocortical epilepsy MEG picks up IED that extend no more than 3–4 cm^2 of activated lateral frontal neocortex on the subdural electrodes, up to 6 cm^2 for more basal frontal and temporal neocortex whereas other studies showed that scalp EEG only detects IED when >10 cm^2 of the neocortex is activated (17, 18). However, these studies did not use the HD-EEG set-ups available today.

Ideal is the combination of EEG and MEG to increase spike-yield (19). Indeed Heers et al. compared the spike yield in EEG, MEG and EEG/MEG following sleep deprivation and reported, respectively, 51, 60, and 71% IED detection (10).

Due to this high sensitivity for the cortical convexity, MEG has recently been claimed complementary with SEEG and subdural invasive EEG recording. Vadera and colleagues performed simultaneous MEG and SEEG. They showed that MEG was able to fill the gaps in-between the recorded brain activity from the depth electrodes and allowed a more tailored resection of only a small amount of brain tissue (20).

Diagnostic Accuracy and Added Value

Patient Type

In epilepsy surgery the best outcomes are described for patients with mesial temporal lobe epilepsy (Engel I in up to 90%). This is not the case for patients with neocortical epilepsy. In these patients the current presurgical evaluation is not sufficient. The inclusion of MEG might be an important step as literature agrees on the fact that MEG is more sensitive for *neocortical sources* compared to deep sources.

Different studies have focused on the difficulties known in frontal lobe epilepsy (FLE) where scalp EEG is often not able to detect interictal or ictal activity due to fast propagation, muscle activity and source orientation whereas MEG could (21). They found that the resection of monofocal clusters in FLE and the tailoring of the resection by including clusters adjacent to the lesion correlated both significantly with good postsurgical outcome (22). Wu et al. retrospectively evaluated the correlation between semiology and MEG in seven patients with FLE and found in FLE that MEG non-invasively complemented the localization hypotheses obtained by ictal semiology (23). Ossenblok et al. optimized the procedures for localizing IED in FLE. Their conclusion was that MEG can be used as a "fast screening method for identifying the distinct categories of spikes and brain areas responsible for these spikes." Moreover, the simultaneous recording of EEG and MEG allowed them to compare both modalities directly for FLE and showed superiority of the MEG spike yield and localization over EEG (16).

The *insular cortex* is a second region that often causes difficulties in the current conventional presurgical work-up.

Mohamed et al. retrospectively looked into their 14 insular cases and compared the MEG, FDG-PET and ictal SPECT result to the resection margin. They described three different patterns of MEG spike sources, (1) posterior operculo-insular cluster, (2) anterior operculo-insular cluster or (3) no cluster but rather diffuse perisylvian distribution. In the patient group that underwent surgery and had an anterior operculo-insular cluster, MEG provided superior information to ictal SPECT in 4/6 patients and to interictal PET in 5/6 patients (24). Park and colleagues described an interesting case with insular epilepsy in whom the IEDs simultaneously recorded on EEG and MEG were best explained by ECD in the anterior temporal lobe as seen in patients with TLE. However, the IEDs that were only measured by MEG and not seen simultaneously on EEG were best explained by ECDs adjacent to the insular lesion. This case report shows the potential of MEG to detect insular activity that is undetectable by scalp EEG (25). Different studies confirmed the role of MEG in the identification of the epileptogenic zone (EZ) in insular cases by confirming results with intracranial monitoring or following resective surgery (26, 27). In addition Yin et al. report on the importance of non-invasively recorded HFO (rippels associated with spikes) with MEG which show to be valuable for the localization of the EZ in insular epilepsy. They showed that resection of insular tissue generating ripples during IED's was more successful then when tissue was resected that only generated IED, however this difference was not statistical significant (28).

Comparable reports are available for sources in the *fronto-parietal operculum* (29) and *medial occipital region* (30).

Nevertheless, MEG seems more sensitive for neocortical sources, studies did confirm that *mesial temporal* spikes can be detected by MEG and in these patients too MEG can add crucial information to the presurgical work-up. Kaiboriboon evaluated the ability of MEG to detect mesial temporal spikes and found a sensitivity of 86%. In 60% of patients with non-localizing ictal video-EEG monitoring (VEM) and 67% of patients with non-localizing MRI, MEG showed well-localized IEDs ipsi-lateral to the side of surgery (31).

Non-lesional neocortical patients form the most difficult group of patients for the planning of resective surgery. Only 35% of the non-lesional extra-temporal lobe cases are rendered seizure free following epilepsy-surgery (32). MEG has shown to be useful as a guide to identify very subtle lesions with and without post-processing techniques (see infra) or high-resolution (surface coil) imaging (33–35) or to implant patients with intracranial electrodes (36). Definitely when focal MEG clusters are observed, this is very valuable in the presurgical decision-making and shown to be a positive predictive factors for successful resective surgery (27, 36, 37). In this complex patient group, Jeong et al. compared MEG with other presurgical investigations and compared all to the intracranial golden standard. It was shown that in 86% of patients MEG lateralizes correctly. For ictal VEM this is the case for 78%, for PET 70%, and 57% for ictal SPECT. On a lobar level, MEG and ictal VEM correctly identified the involved lobe in 65% of cases, PET in 57% of cases and ictal SPECT in 52% of cases (38). In the study by Itabashi including patients with very subtle (initially missed) focal cortical dysplasia (FCD), it was suggested that "MEG-guided a posteriori review of MRI" should become a routine part of a clinical practice and definitely in the preparation for a multidisciplinary presurgical meeting. In this role MEG could contribute to avoiding invasive evaluations and lead to improved surgical outcome (33, 39). Aydin et al. suggest in their paper to combine EEG/MEG source analysis with high resolution zoomed MR imaging, limited to small areas centered at the EMEGS source location as a new diagnosis strategy (35).

Besides the important role of MEG in non-lesional cases, it also has an important value in *lesional cases*. Kim et al. showed that the number of MEG dipole clusters and the proportion of dipoles in the resection cavity was not associated with seizure free outcome for the whole group of children however for cases with localized neocortical MRI lesions MEG source localization successfully localized the peri-lesional epileptogenic zone (40). A few important epileptogenic lesions are Focal Cortical Dysplasias (FCD), cavernoma's and tubers in Tuberous Sclerosis. These will be discussed in more detail below.

A FCD is a highly and intrinsically epileptogenic lesion. Over 76% of patients with these lesions become intractable to AED however studies have shown that 50–70% of patients can be rendered seizure free following epilepsy surgery. Presurgical evaluation of these patients is therefore mandatory and MRI is as always important as it identifies these lesions by showing blurring of the gray-white matter, cortical thickening, and abnormal signs in the white matter (41). However, these abnormalities might also be microscopic and not visible or only subtle on optimal imaging. Many studies focus on the role of MEG in the identification of these subtle but highly epileptogenic lesions (27, 39, 42). Due to the intrinsic epileptogenicity of the lesion neurophysiology, and also MEG, plays an important role in the delineation of the extent of a FCD in the cortex (often beyond what is visible on MRI) and to predict the outcome following the removal of FCD lesions (41, 43, 44). Therefore the estimation of the spiking volume might be important like shown by Bouet et al. and classical equivalent current dipole models might fail to provide this estimation (45). FCD often generate (spike-independent) discharges in the beta-frequency-band. Heers et al. localized these discharges using Dynamic Imaging of Coherent Sources and found coherence between simultaneous MEG and intracranial EEG. The sources of the beta band activity localized within <2 cm of the epileptogenic FCD (46). In patients with FCD and MEG dipole clusters, the complete removal of the clusters is associated with good postsurgical outcome (38). Wilenius et al. described that in patients with MEG dipole clusters and Engel class I or II 49% of the clusters on average was removed, whereas the corresponding value in patients with Engel class III or IV was only 5.5% (42). Especially for FCD type II related epilepsy MEG showed to be a very strong tool. In the study by Kasper et al. MEG was combined with MRI post-processing techniques like for example MRI acquisition and morphometric analysis (MAP) and showed excellent surgical outcomes with 81% reaching Engel I compared to published series. The MEG sensitivity in this cohort was 95% in FCDII, compared to 70% reported from unselected epilepsy series (47).

Besides the associated refractory epilepsy, the high risk for bleeding makes cavernoma a clear indication for epilepsy surgery. Epilepsy is caused by the associated mass effect, gliosis and hemosiderine and therefore, in contrast to FCD, the tissue adjacent to the cavernoma, rather than the lesion, exhibits hyperexcitability. Studies in patients with cavernoma have shown that it might be important to perform more than a pure lesionectomy and for the delineation of the extent of resection needed, MEG might play an important role as you are able to map the epileptic activity on the structural image (48, 49). In case of multiple cavernoma MEG will mainly reveal the complexity but will contribute to the decision-making whether or not further invasive work-up is useful (48). Unfortunately in 20–40% of patients with cavernoma, multiple of these lesions can be identified.

Besides for cavernoma and FCD, MEG might play an important role in the presurgical evaluation of patients with tuberous sclerosis and brain tumors or in patients who need a second or third surgery when earlier procedures failed to control epilepsy. In post-operative situations MEG is superior over EEG because the magnetic field is not distorted by the skull defects. El Tahry and colleagues focused on the value of MEG in this patient population and compared MEG with ictal SPECT. They showed that MEG alone was successful in these patients after failed resective surgery. Only ictal SPECT with an early injection ($<$20 s) also had a good localization value (50).

Localizing Accuracy

In 2008 Lau et al. performed a systematic review of the available literature based on the *DARE scientific quality criteria* and concluded that "there was insufficient evidence in the current literature to support the relationship between the use of MEG in surgical planning and seizure-free outcome after epilepsy surgery" (51). However, this review received a lot of methodological critics.

Today the number of these specific studies comparing MSI result with the resection and postoperative outcome has only increased and therefore the evidence for its value in the presurgical evaluation became only more established. Very recently Mouthaan et al. performed an extensive meta-analysis on "the diagnostic accuracy and quality of evidence of interictal high resolution electric and magnetic source imaging (ESI and MSI) to localize the epileptogenic regions in the presurgical epilepsy evaluation." The quality appraisal was based in a modified QUADAS-2 framework. Based on database searches they found almost 2000 abstracts that they screened and kept about 100 abstracts to do a full text assessment of which they excluded 47 articles for various quality reasons (no full text available, no study, different aim/objective, different index test, not the outcome of interest, …). For the other 51 articles they performed a full data extraction and quality appraisal. Only from 11 studies enough data could be captured to draw the anticipated conclusions [eight on MSI (236 patients) and three on ESI (127 patients)] as only studies without zero values in the 2×2 contingency tables were included. The study quality was however generally assessed as "poor" and no study was free of bias (selection of operated patients only, interference of source localization with surgical plan/decision, …) however they could conclude that the diagnostic accuracy analysis reveals for MSI and ESI a good surgical outcome in, respectively, 130/236 patients (54%) and 86/127 patients (67%). They additionally showed that the number of patients with a good surgical outcome is higher in the concordant group (76%) than in the non-concordant group (28%). There overall conclusion was that "both source localization techniques have a relatively high sensitivity (82%) and low specificity (53%) for the identification of the EZ. The diagnostic accuracy of MSI and HR-ESI to localize the EZ is strongly affected by poor study quality and likely biased toward overestimation therefore the results need to be interpreted with caution and independent support from other diagnostic tools is required to proceed to surgery. Higher quality studies, allowing unbiased MSI and ESI evaluation, are needed to judge results in light of source estimate size and resection size" (52).

Over the last 20 years, many studies investigated the role of MEG within the presurgical evaluation and confronted the MEG results with the golden standard available i.e., seizure outcome following resection and/or invasive recording and a few are described below.

Stefan et al. performed a retrospective study including 455 cases and concluded that MEG identified the correct lobe in 89% of cases and added information in 33% and crucial information in 10% (3). Papanicolaou et al. evaluated 41 patients that underwent MEG, IVEM, and resection. The seizure outcome was correlated to the overlap with the resection cavity and it was shown that IVEM was correct in 54% of cases and MEG in 56%. When groups were analyzed separately it was shown that MEG might be less beneficial relative to IVEM in ETLE compared to TLE (53). Knowlton et al. showed "a positive predictive value of MSI for seizure localization of 82–90% depending on whether computed against ICEEG alone or in combination with surgical outcome" (54). Knowlton et al. showed that a highly localized MSI result was significantly associated with seizure–free outcome for the entire surgical population (55). Kim and colleagues showed that the number of MEG dipole clusters and the proportion of dipoles in the resection cavity was not associated with seizure free outcome for the whole group however for cases with localized MRI lesions MEG source localization successfully localized the perilesional epileptogenic zone (40). Based on the retrospective analysis of the value of MEG performed at Cleveland between 2009 and 2012, Vadera et al. found that when preoperative MEG studies were fused with postoperative MRI, for 30/65 patients the MEG cluster was located within the resection cavity, for 28/65 completely outside the cavity and for 7/65 partially within. When postoperative outcome was analyzed they found that 74% of patients was seizure free at 1 year follow-up and 60% at 2 year follow-up. Correlation with the MEG result showed significantly improved likelihood of seizure freedom with complete clusterectomy in patients with localization outside the temporal lobe (56). Englot et al. reported on 132 surgical cases with at least 1 year post-operative follow-up of whom 70% had Engel I outcome. In 78% of cases MEG revealed IED and this result was compared with the (sub)lobe of resection, ECoG result and/or MRI lesion. They concluded that a concordant and specific MEG result predicted seizure freedom with an OR

of 5.11 (57). The recent study by Duez et al. concluded that analyzing their combined dataset of MEG and EEG yielded significantly higher OR than separate analysis of both datasets, emphasizing the clinical importance of recording MEG and EEG simultaneously (12).

Nevertheless the recent paper by Plummer et al. focusses on the comparison between MSI, HD-EEG source imaging (EEG recording with coverage of the inferior temporal region with 12 additional electrodes) and simultaneous MEG and HD-EEG SI. In this paper they did not use the ECD model but used averaged data and distributed source modeling (sLORETA) and concluded, in contrast with their hypothesis, that independent source MEG and HD-EEG source imaging is superior to combined modeling (13).

In conclusion; based on different studies the clinical utility of MEG is ranging from 20 to 100% sensitivity and (3, 4, 51, 58, 59) from <10 to 100% specificity (51, 58–60). The positive predictive value is reported to be as high as 90% when compared to intracranial findings and association with surgical outcome (54, 60–63).

Therapeutic Impact and Added Value

The cornerstone investigation in the presurgical evaluation is scalp video-EEG monitoring (VEM). Despite the cheap cost of EEG, VEM is a rather expensive investigation, as it requires long-term admission at the hospital. In addition, MEG is a fast and more patient-friendly screening tool. Paulini and colleagues compared MEG with VEM and found that when long-term VEM gives insufficient localizing information, a (short) MEG session does in about half of patients (5). In 2004 Pataraia et al. investigated the added value of MEG compared to interictal and ictal VEM and used the surgery to confirm the results. In over 30% of cases MEG and VEM provided equivalent results however in 40% of patients additional information was available. When EEG was non-localizing MEG contributed to the localization of the region that was subsequently resected in 59% and when EEG was only partially localizing, MEG contributed significantly in 73% (4).

Different studies evaluated how the inclusion of MEG in the decision-making process changed or would have changed the patient management (**Table 1**). Overall studies reach a consensus that adding MEG to the presurgical evaluation protocol will change the management of about 1/5 up to 2/3 patients (depending on the inclusion level) (55, 62, 64–66). Very recently Duez et al. evaluated the effect of simultaneous EEG and MEG source imaging and revealed changed management in 34% of patients and these changes were useful in 80% (12). The type of patients included in the different studies can explain this broad difference in added value. Like mentioned in the study by Mohamed et al. mixing lesional and non-lesional cases for example just like combining the straight forward and "difficult" cases in one study like in the study by De Tiege et al. results in an underestimation of the added benefit of MSI. In contrary the study by Duez et al. only included the more complex cases which might lead to an overestimation (12). Overall the value of MEG (and EEG) source imaging is clearly large in especially the non-lesional cases.

The study by Mohamed et al. could, due to their inability to provide reliable MEG results in a timely matter, assess the presumed impact of MEG retrospectively and in this way provide more clear evidence of the impact of MEG. They saw via this unique set-up that in 68% the management would have been different if the MEG results would have been available in time. In the subgroup of patients who in the meanwhile underwent surgery the inclusion of MEG in the work-up would have modified the resection in ∼20% of patients possibly preventing negative outcomes and in another subgroup the unavailability of MEG led to a set of unnecessary/complicated intracranial recordings, surgical failures, and reoperations (66).

Guidance of Invasive Video-EEG Monitoring

The most important role of MEG today is the optimal guidance of invasive video-EEG monitoring (IVEM). IVEM is an invasive and expensive procedure associated with medical risks. However, for many patients it is their ultimate chance to be considered an eligible epilepsy surgery candidate. The planning of the implantation scheme is crucial and MEG has shown to be an ideal non-invasive investigation to guide this implantation especially in non-lesional cases (12, 36, 55, 66). Knowlton showed this elegantly in his study mentioned above (**Table 1**), including all patients planned for intracranial implantation. In this group in 23% MEG resulted in extra electrode coverage and in 39% of these cases these extra electrode-contacts involved the seizure onset (55). Also in the study by Mohamed it became clear that MEG is very important to optimally plan an intracranial implantation. Not only to make sure to end up with clinically relevant coverage of the seizure onset zone but also to minimize procedural risks to patients by allowing direct surgery without intracranial implantation, by reducing the number of contacts or excluding patients with a diffuse or inoperable epileptic area. This important role of source imaging within the presurgical evaluation, namely the optimal planning of the location of the intracranial electrodes, was confirmed in the recent study by Duez et al. showing changes in the location of the electrodes in 16.5% and offering the ability to implant electrodes in an additional 7% of patients that would not have been investigated without. In this study the source imaging allowed to skip intracranial recordings in 9.4% of patients and direct them to surgery immediately and withheld 1% of patients from undergoing surgical procedures (12).

The potential of MEG to identify the "primary irritative zone" via time-course analysis of the whole spike when interictal activity is complex (for example due to deep source) might be crucial in the planning of the IVEM, namely by predicting the patterns of spikes on ECoG or SEEG (67–70). Agirre-Arrizubieta compared 12 consecutive patients who underwent MEG before their implantation with electrodes with a control group that underwent an IVEM without MEG and were matched for implantation type. The groups were however not comparable when considering the complexity of the cases, as the MEG group consisted of more complex patients (and therefore underwent MEG). However no differences in number

TABLE 1 | This table summarizes the outcome of studies focussing on the added value/effect of MSI on the decision making and/or management of patients in the presurgical evaluation.

Study	Inclusion level	N° PT	Change	Relevance	Remark
Sutherling et al. (62)	All consecutive surgical candidates with neocortical epilepsy*	69	23 (33%)	6/29 (20%) of patients who eventually underwent resective surgery	*All pt meeting the criteria for direct temporal lobectomy or lesionectomy are excluded
Knowlton et al. (55)	All patients planned for intracranial work-up	77	18 (23%) (extra electrode coverage)	7/18 (39%) (seizure onset on the extra electrodes)	
De Tiège et al. (64)	All consecutive surgical candidates*	70	15 (21%) (44% of eTL-cases)	9/11 (82%)	*Including the straight forward cases
Ito et al. (65)	pt studied for clinical diagnosis and preoperative evaluation*	73	17 (23%)		*Only pt with IED were included
Mohamed et al. (66)	Consecutive non-lesional surgical candidates*	31	21 (68%)	12? (could be an overestimation)	*All patients underwent MEG but this was not taken into account at the time of the decision making. Retrospectively the lack of this information was assessed
Duez et al. (12)	Consecutive included patients in whom **electromagnetic*** source imaging was part of the decision-making process (i.e., MRI negative or discordant other results)**	85	29 34%)	16/20 (with available results) 80%	*Simultaneous EEG and MEG source imaging **Potential overrepresentation of the more complex cases

of successful implantations could be found between both groups suggesting that MEG can contribute to identify the ideal implantation site when standard methods fail (71). Still, a randomized study would be the only way to proof this with more certainty, however the value of MEG in the work-up is already to established, making randomization unethical.

THE VALUE OF ICTAL MSI

Besides by IEDs, epilepsy is characterized by the occurrence of seizures and until today the seizure onset zone (SOZ) has always been considered the closest approximation of the EZ. During MEG acquisitions the recording of seizures is difficult because the sessions are generally rather short (mean of 90 min according to a recent European survey) (1) and movement can cause problems recording good signal quality. Moreover no consensus concerning the best way to process magnetic ictal data has been reached because of the low signal-to-noise ratio during ictal activity, the different ictal discharge presentations and the evolvement of these patterns over time (72). Nevertheless the value of magnetic seizure activity has been described by different authors using different ways to analyze the data.

Sometimes the recording of ictal activity is rather a coincidence but in some centers it is being planned or anticipated. In a recent retrospective study including 377 patients who underwent a standard 1 h MEG, ictal MEG by coincidence (or by using known triggers like sensory or music) was found in 11% of patients (72).

First ictal MEG studies were performed with only a limited number of channels (73) or with multichannel hemispherical MEG recordings in combination with foramen ovale electrodes (74). Further ictal MEG studies showed that signal-to-noise ratio (SNR) at seizure onset the may be to low for dipole analysis. Often the typical movement related artifacts will obscure the seizure onset, however occasionally it was demonstrated that the ictal source localization was superior to interictal MEG correlating very nicely to invasively recognized seizure onset (75, 76). Later in time continuous ictal head movement measurement allows movement correction artifacts (77). Here instead of dipole analysis short time Fourier transformation (STFT) rhythm analysis was performed. In 63% concordant lobar interictal and ictal source localizations existed, again it was shown that ictal source localization was closer than the interictal source when compared to the seizure onset zone defined by invasive recording. In addition ictal MEG provided clear source localizations even if interictal MEG spikes were bilateral or missing. If interictal spikes were recorded bilateral than ictal recordings showed unilateral seizure activity.

In the recent retrospective paper it was shown that the resection of areas containing a minimum-norm estimate of a narrow band at onset, rather than a single equivalent current dipole, was associated with sustained seizure freedom. They also showed that ictal MEG patterns were clear when this was not the case with EEG showing also here a complementarity (comparable to the interictal situation). Moreover in patients in whom intracranial data were available the SOZ identified by ictal MEG recording correlated with the lobe of onset as identified via intracranial data in 88% (72).

Another group introduced gradient magnetic-field topography (GMFT) for the analysis of ictal discharges in patients with neocortical epilepsy after finding a higher spatial resolution in this patient group compared to the standard equivalent current dipole method (78).

Badier et al. compared SEEG epileptogenicity index, source localization using dipoles, and linearly constrained minimum variance (LCMC) (a beamformer technique). They showed

that source imaging methods performed on rhythmic patterns were able to localize the EZ as validated by SEEG, but that LCMV was superior to ECD when concordance was compared (79).

The interictal MEG has a high sensitivity (0.95) and moderate specificity (0.75), ictal MEG has high sensitivity (0.96), and specificity (0.9) in predicting SOZ localization (80).

Finally it was shown that based on ictal-MEG, it was possible to change the management of patients initially considered unsuitable for surgery or planned for intracranial monitoring into candidates directly suitable for surgery with good postsurgical outcomes in those who were operated (81). A survey of comparisons of localizing accuracy using interictal and ictal MEG source localizations is provided by Stefan and Rampp (82).

OTHER FEATURES RECORDED WITH MEG AND OF VALUE IN THE PRESURGICAL EVALUATION

Because not all patients show seizures or even IED during an MEG acquisition, alternative "features" are more and more often being studied. Not only slow activity (83) but also fast activity (84–87) has recently gained attention as well as network-analysis. Based on the current results it has been shown that it is possible to non-invasively identify regional interictal epileptic networks and their pattern of connectivity with MEG (70).

CONCLUSION

Based on the review of the available literature patients who definitely need to be referred for magnetic source imaging are patients in whom a frontal, intrasylvian or insular focus is suspected, because MEG might be superior than EEG in localizing the irritative zone. Normal scalp EEG should not prevent patients from being referred for MSI and on the other hand neither should clear lesions on MRI prevent patients from being referred as MSI might help in the delineation of the resection needed beyond what is visible on imaging. It is clear that patients planned for an invasive video-EEG monitoring might benefit from MSI as it has been clearly shown that the implantation scheme can be optimized using the MSI-result.

In addition, in case of a focal MEG results in patients with normal imaging, MRI results need to be re-evaluated for subtle lesions guided by the focal MEG result. In case of patients with high seizure frequency it might be interesting to try to perform an ictal MEG as this can result in additional and accurate localizing information.

Besides these advantages specific limitations should be considered: Metal implants might cause problems, however specific filtering software might enable the interpretation of the signals. On the other hand the lack of IED (or seizures) during the MEG recording causes an inconclusive MEG result in up to 25% of patients undergoing MEG. Network-analysis like for example spike independent resting-state analysis might solve this problem in the future.

Just like all results within the presurgical evaluation, MEG should always be combined with the results of the other investigations and all results need to be interpreted with caution before the team can decide upon a next step. Today no unique presurgical tool is available to guide surgery and/or intracranial implantation on its own.

AUTHOR CONTRIBUTIONS

EC has written the review. HS has critically reviewed the drafts and added missing data.

REFERENCES

1. De Tiege X, Lundqvist D, Beniczky S, Seri S, Paetau R. Current clinical magnetoencephalography practice across Europe: are we closer to use MEG as an established clinical tool? *Seizure.* (2017) 50:53–9. doi: 10.1016/j.seizure.2017.06.002
2. Bagic A, Funke ME, Ebersole J. American Clinical MEG Society (ACMEGS) position statement: the value of magnetoencephalography (MEG)/magnetic source imaging (MSI) in noninvasive presurgical evaluation of patients with medically intractable localization-related epilepsy. *J Clin Neurophysiol.* (2009) 26:290–3. doi: 10.1097/WNP.0b013e3181b49d50
3. Stefan H, Hummel C, Scheler G, Genow A, Druschky K, Tilz C, et al. Magnetic brain source imaging of focal epileptic activity: a synopsis of 455 cases. *Brain.* (2003) *126(Pt* 11):2396–405. doi: 10.1093/brain/awg239
4. Pataraia E, Simos PG, Castillo EM, Billingsley RL, Sarkari S, Wheless JW, et al. Does magnetoencephalography add to scalp video-EEG as a diagnostic tool in epilepsy surgery? *Neurology.* (2004) 62:943–8. doi: 10.1212/01.WNL.0000115122.81621.FE
5. Paulini A, Fischer M, Rampp S, Scheler G, Hopfengartner R, Kaltenhauser M, et al. Lobar localization information in epilepsy patients: MEG–a useful tool in routine presurgical diagnosis. *Epilepsy Res.* (2007) 76:124–30. doi: 10.1016/j.eplepsyres.2007.07.006
6. Oishi M, Otsubo H, Kameyama S, Morota N, Masuda H, Kitayama M, et al. Epileptic spikes: magnetoencephalography versus simultaneous electrocorticography. *Epilepsia.* (2002) 43:1390–5. doi: 10.1046/j.1528-1157.2002.10702.x
7. Ebersole JS, Ebersole SM. Combining, M*EG and EEG source modeling in epilepsy evaluations. J Clin Neurophysiol.* (2010) 27:360–71. doi: 10.1097/WNP.0b013e318201ffc4
8. Iwasaki M, Pestana E, Burgess RC, Luders H O, Shamoto H, Nakasato N. *Detection of epileptiform activity by human interpreters: blinded comparison between electroencephalography and magnetoencephalography. Epilepsia.* (2005) 46:59–68. doi: 10.1111/j.0013-9580.2005.21104.x
9. Knake S, Halgren E, Shiraishi H, Hara K, Hamer HM, Grant PE, et al. The value of multichannel MEG and EEG in the presurgical evaluation of 70 epilepsy patients. *Epilepsy Res.* (2006) 69:80–6. doi: 10.1016/j.eplepsyres.2006.01.001
10. Heers M, Rampp S, Kaltenhauser M, Pauli E, Rauch C, Dolken MT, et al. *Detection of epileptic spikes by magnetoencephalography and electroencephalography after sleep deprivation. Seizure.* (2010) 19:397–403. doi: 10.1016/j.seizure.2010.06.004
11. Kharkar S, Knowlton R. Magnetoencephalography in the presurgical evaluation of epilepsy. *Epilepsy Behav.* (2015) 46:19–26. doi: 10.1016/j.yebeh.2014.11.029
12. Duez L, Tankisi HHPO, Sidenius P, Sabers A, Pinborg LH, Fabricius M, et al. Electromagnetic source imaging in presurgical workup of patients with epilepsy. *Neurology.* (2019) 92. doi: 10.1212/WNL.0000000000006877

13. Plummer C, Vogrin S, Woods W, Murphy M, Cook M, Liley D. Interictal and ictal source localisation for epilepsy surgery using high-density EEG with MEG: a prospective long-term study. *Brainl.* (2019) 142:932–51. doi: 10.1093/brain/awz015
14. Ebersole JS, Wagner M. *Relative yield of MEG and EEG spikes in simultaneous recordings. J Clin Neurophysiol.* (2018) 35:443–53. doi: 10.1097/WNP.0000000000000512
15. Ramantani G, Boor R, Paetau R, Ille N, Feneberg R, Rupp A, et al. MEG versus EEG: influence of background activity on interictal spike detection. *J Clin Neurophysiol.* (2006) 23:498–508. doi: 10.1097/01.wnp.0000240873.69759.cc
16. Ossenblok P, de Munck JC, Colon A, Drolsbach W, Boon, P. Magnetoencephalography is more successful for screening and localizing frontal lobe epilepsy than electroencephalography. *Epilepsia.* (2007) 48:2139–49. doi: 10.1111/j.1528-1167.2007.01223.x
17. Mikuni N, Nagamine T, Ikeda A, Terada K, Taki W, Kimura J, et al. Simultaneous recording of epileptiform discharges by MEG and subdural electrodes in temporal lobe epilepsy. *NeuroImage.* (1997) 5(4 Pt 1):298–306. doi: 10.1006/nimg.1997.0272
18. Tao JX, Ray A, Hawes-Ebersole S, Ebersole JS. Intracranial EEG substrates of scalp EEG interictal spikes. *Epilepsia.* (2005) 46:669–76. doi: 10.1111/j.1528-1167.2005.11404.x
19. Lin YY, Shih YH, Hsieh JC, Yu HY, Yiu CH, Wong TT, et al. Magnetoencephalographic yield of interictal spikes in temporal lobe epilepsy. Comparison with scalp EEG recordings. *NeuroImage.* (2003) 19:1115–26. doi: 10.1016/S1053-8119(03)00181-2
20. Vadera S, Burgess R, Gonzalez-Martinez J. Concomitant use of stereoelectroencephalography (SEEG) and magnetoencephalographic (MEG) in the surgical treatment of refractory focal epilepsy. *Clin Neurol Neurosurg.* (2014) 122:9–11. doi: 10.1016/j.clineuro.2014.04.002
21. Wu XT, Rampp S, Hopfengartner R, Buchfelder M, Zhou D, Stefan H. Complementary use of video-electroencephalography and magnetoencephalography in frontal lobe epilepsy. *Seizure.* (2012) 21:426–30. doi: 10.1016/j.seizure.2012.04.007
22. Mu J, Rampp S, Carrette E, Roessler K, Sommer B, Schmitt FC, et al. Clinical relevance of source location in frontal lobe epilepsy and prediction of postoperative long-term outcome. *Seizure.* (2014) 23:553–9. doi: 10.1016/j.seizure.2014.04.006
23. Wu X, Rampp S, Weigel D, Kasper B, Zhou D, Stefan H. The correlation between ictal semiology and magnetoencephalographic localization in frontal lobe epilepsy. *Epilepsy Behav.* (2011) 22:587–591. doi: 10.1016/j.yebeh.2011.08.009
24. Mohamed IS, Gibbs SA, Robert M, Bouthillier A, Leroux JM, Khoa Nguyen D. The utility of magnetoencephalography in the presurgical evaluation of refractory insular epilepsy *Epilepsia.* (2013) 54:1950–9. doi: 10.1111/epi.12376
25. Park HM, Nakasato N, Tominaga T. Localization of abnormal discharges causing insular epilepsy by magnetoencephalography. *Tohoku J Exp Med.* (2012) 226:207–11. doi: 10.1620/tjem.226.207
26. Ahmed R, Otsubo H, Snead C III, Donner E, Widjaja E, Ochi A, Drake JM, et al. Diagnostic evaluation and surgical management of pediatric insular epilepsy utilizing magnetoencephalography and invasive EEG monitoring. *Epilepsy Res.* (2018) 140:72–81. doi: 10.1016/j.eplepsyres.2017.12.011
27. Yu T, Ni D, Zhang X, Wang X, Qiao L, Zhou X, et al. The role of magnetoencephalography in the presurgical evaluation of patients with MRI-negative operculo-insular epilepsy. *Seizure.* (2018) 61:104–10. doi: 10.1016/j.seizure.2018.07.005
28. Yin C, Zhang X, Chen Z, Li X, Wu S, Lv P, et al. Detection and localization of interictal ripples with magnetoencephalography in the presurgical evaluation of drug-resistant insular epilepsy *Brain Res.* (2018) 1706:147–156. doi: 10.1016/j.brainres.2018.11.006
29. Kakisaka Y, Iwasaki M, Alexopoulos AV, Enatsu R, Jin K, Wang ZI, et al. Magnetoencephalography in fronto-parietal opercular epilepsy. *Epilepsy Res.* (2012) 102:71–7. doi: 10.1016/j.eplepsyres.2012.05.003
30. Gavaret M, Badier JM, Bartolomei F, Benar CG, Chauvel P. MEG and EEG sensitivity in a case of medial occipital epilepsy *Brain Topogr.* (2014) 27:192–6. doi: 10.1007/s10548-013-0317-7
31. Kaiboriboon K, Nagarajan S, Mantle M, Kirsch HE. Interictal MEG/MSI in intractable mesial temporal lobe epilepsy: spike yield and characterization. *Clin Neurophysiol.* (2010) 121:325–31. doi: 10.1016/j.clinph.2009.12.001
32. Tellez-Zenteno JF, Hernandez Ronquillo L, Moien-Afshari F, Wiebe S. Surgical outcomes in lesional and non-lesional epilepsy: a systematic review and meta-analysis. *Epilepsy Res.* (2010) 89:310–8. doi: 10.1016/j.eplepsyres.2010.02.007
33. Funke ME, Moore K, Orrison WW Jr, Lewine JD. The role of magnetoencephalography in "nonlesional" epilepsy *Epilepsia.* (2011) 52 (Suppl. 4):10–4. doi: 10.1111/j.1528-1167.2011.03144.x
34. Heers M, Rampp S, Stefan H, Urbach H, Elger CE, von Lehe M, et al. MEG-based identification of the epileptogenic zone in occult peri-insular epilepsy. *Seizure.* (2012) 21:128–33. doi: 10.1016/j.seizure.2011.10.005
35. Aydin U, Rampp S, Wollbrink A, Kugel H, Cho J, Knosche TR, et al. Zoomed MRI guided by combined EEG/MEG source analysis: a multimodal approach for optimizing presurgical epilepsy work-up and its application in a multi-focal epilepsy patient case study. *Brain Topogr.* (2017) 30:417–33. doi: 10.1007/s10548-017-0568-9
36. Jung J, Bouet R, Delpuech C, Ryvlin P, Isnard J, Guenot M, et al. The value of magnetoencephalography for seizure-onset zone localization in magnetic resonance imaging-negative partial epilepsy. *Brain*. (2013). 136(Pt 10):3176–86. doi: 10.1093/brain/awt213
37. Wu XT, Rampp S, Buchfelder M, Kuwert T, Blumcke I, Dorfler A, et al. Interictal magnetoencephalography used in magnetic resonance imaging-negative patients with epilepsy. *Acta Neurol Scand.* (2013) 127:274–80. doi: 10.1111/j.1600-0404.2012.01712.x
38. Jeong W, Chung CK, Kim JS. Localization value of magnetoencephalography interictal spikes in adult nonlesional neocortical epilepsy. *J Korean Med Sci.* (2012) 27:1391–7. doi: 10.3346/jkms.2012.27.11.1391
39. Itabashi H, Jin K, Iwasaki M, Okumura E, Kanno A, Kato K, et al. Electro- and magneto-encephalographic spike source localization of small focal cortical dysplasia in the dorsal peri-rolandic region. *Clin Neurophysiol.* (2014) 125:2358–63. doi: 10.1016/j.clinph.2014.02.028
40. Kim H, Kankirawatana P, Killen J, Harrison A, Oh A, Rozzelle C, et al. Magnetic source imaging (MSI) in children with neocortical epilepsy: surgical outcome association with 3D post-resection analysis. *Epilepsy Res.* (2013) 106:164–72. doi: 10.1016/j.eplepsyres.2013.04.004
41. Widjaja E, Otsubo H, Raybaud C, Ochi A, Chan D, Rutka JT, et al. Characteristics of MEG and MRI between Taylor's focal cortical dysplasia (type II) and other cortical dysplasia: surgical outcome after complete resection of MEG spike source and MR lesion in pediatric cortical dysplasia. *Epilepsy Res.* (2008) 82:147–55. doi: 10.1016/j.eplepsyres.2008.07.013
42. Wilenius J, Medvedovsky M, Gaily E, Metsahonkala L, Makela JP, Paetau A, et al. Interictal MEG reveals focal cortical dysplasias: special focus on patients with no visible MRI lesions. *Epilepsy Res.* (2013) 105:337–48. doi: 10.1016/j.eplepsyres.2013.02.023
43. Morioka T, Nishio S, Ishibashi H, Muraishi M, Hisada K, Shigeto H, et al. Intrinsic epileptogenicity of focal cortical dysplasia as revealed by magnetoencephalography and electrocorticography. *Epilepsy Res.* (1999) 33:177–87. doi: 10.1016/S0920-1211(98)00096-5
44. Bast T, Oezkan O, Rona S, Stippich C, Seitz A, Rupp A, et al. EEG and MEG source analysis of single and averaged interictal spikes reveals intrinsic epileptogenicity in focal cortical dysplasia. *Epilepsia.* (2004) 45:621–31. doi: 10.1111/j.0013-9580.2004.56503.x
45. Bouet R, Mauguiere F, Daligault S, Isnard J, Guenot M, Bertrand O, et al. The relationship between morphological lesion, magnetic source imaging, and intracranial stereo-electroencephalography in focal cortical dysplasia. *Neuroimage Clin.* (2017) 15:71–9. doi: 10.1016/j.nicl.2017.04.018
46. Heers M, Hirschmann J, Jacobs J, Dumpelmann M, Butz M, von Lehe M, et al. Frequency domain beamforming of magnetoencephalographic beta band activity in epilepsy patients with focal cortical dysplasia. *Epilepsy Res.* (2014) 108:1195–203. doi: 10.1016/j.eplepsyres.2014.05.003
47. Kasper BS, Rossler K, Hamer HM, Dorfler A, Blumcke I, Coras R, et al. Coregistrating magnetic source and magnetic resonance imaging for epilepsy surgery in focal cortical dysplasia. *Neuroimage Clin.* (2018) 19:487–96. doi: 10.1016/j.nicl.2018.04.034
48. Stefan H, Scheler G, Hummel C, Walter J, Romstock J, Buchfelder M, et al. Magnetoencephalography (MEG) predicts focal epileptogenicity in cavernomas. *J Neurol Neurosurg Psychiatry.* (2004) 75:1309–13. doi: 10.1136/jnnp.2003.021972
49. Jin K, Nakasato N, Shamoto H, Kanno A, Itoyama Y, Tominaga T. Neuromagnetic localization of spike sources in perilesional, contralateral

mirror, and ipsilateral remote areas in patients with cavernoma. *Epilepsia.* (2007) 48:2160–6. doi: 10.1111/j.1528-1167.2007.01228.x
50. El Tahry R, Wang ZI, Thandar A, Podkorytova I, Krishnan B, Tousseyn S, et al. Magnetoencephalography and ictal SPECT in patients with failed epilepsy surgery. *Clin Neurophysiol.* (2018) 129:1651–7. doi: 10.1016/j.clinph.2018.05.010
51. Lau M, Yam D, Burneo JG. A systematic review on MEG and its use in the presurgical evaluation of localization-related epilepsy. *Epilepsy Res.* (2008) 79:97–104. doi: 10.1016/j.eplepsyres.2008.01.004
52. Mouthaan B, Rados M, Boon P, Carrette E, Diehl B, Jung J, et al. Diagnostic accuracy of interictal source imaging in presurgical epilepsy evaluation: A systematic review from the E-PILEPSY consortium. *Clin Neurophysiol.* (2019) 130:845–55. doi: 10.1016/j.clinph.2018.12.016
53. Papanicolaou AC, Pataraia E, Billingsley-Marshall R, Castillo EM, Wheless JW, Swank P, et al. Toward the substitution of invasive electroencephalography in epilepsy surgery. *J Clin Neurophysiol.* (2005) 22:231–7. doi: 10.1097/01.WNP.0000172255.62072.E8
54. Knowlton RC. The role of FDG-PET, ictal SPECT, and MEG in the epilepsy surgery evaluation. *Epilepsy Behav.* (2006) 8:91–101. doi: 10.1016/j.yebeh.2005.10.015
55. Knowlton RC, Razdan SN, Limdi N, Elgavish RA, Killen J, Blount J, et al. Effect of epilepsy magnetic source imaging on intracranial electrode placement. *Ann Neurol.* (2009) 65:716–23. doi: 10.1002/ana.21660
56. Vadera S, Jehi L, Burgess RC, Shea K, Alexopoulos AV, Mosher J, et al. "Correlation between magnetoencephalography-based""clusterectomy and postoperative seizure freedom". *Neurosurg Focus.* (2013) 34:E9. doi: 10.3171/2013.4.FOCUS1357
57. Englot DJ, Nagarajan SS, Imber BS, Raygor KP, Honma SM, Mizuiri D, et al. Epileptogenic zone localization using magnetoencephalography predicts seizure freedom in epilepsy surgery. *Epilepsia.* (2015) 56:949–58. doi: 10.1111/epi.13002
58. Knowlton RC, Elgavish RA, Bartolucci A, Ojha B, Limdi N, Blount J, et al. Functional imaging: II. Prediction of epilepsy surgery outcome. *Ann Neurol.* (2008) 64:35–41. doi: 10.1002/ana.21419
59. Knowlton RC, Elgavish RA, Limdi N, Bartolucci A, Ojha B, Blount J, et al. Functional imaging: I. Relative predictive value of intracranial electroencephalography. *Ann Neurol.* (2008) 64:25–34. doi: 10.1002/ana.21389
60. Mamelak AN, Lopez N, Akhtari M, Sutherling WW. Magnetoencephalography-directed surgery in patients with neocortical epilepsy. *J Neurosurg.* (2002) 97:865–73. doi: 10.3171/jns.2002.97.4.0865
61. Minassian BA, Otsubo H, Weiss S, Elliott I, Rutka JT, Snead OC III. Magnetoencephalographic localization in pediatric epilepsy surgery: comparison with invasive intracranial electroencephalography. *Ann Neurol.* (1999) 46:627–33. doi: 10.1002/1531-8249(199910)46:4<627::AID-ANA11>3.0.CO;2-C
62. Sutherling WW, Mamelak AN, Thyerlei D, Maleeva T, Minazad Y, Philpott L, et al. Influence of magnetic source imaging for planning intracranial EEG in epilepsy. *Neurology.* (2008) 71:990–6. doi: 10.1212/01.wnl.0000326591.29858.1a
63. Stefan H, Rampp S, Knowlton RC. Magnetoencephalography adds to the surgical evaluation process. *Epilepsy Behav.* (2011) 20:172–7. doi: 10.1016/j.yebeh.2010.09.011
64. De Tiege X, Carrette E, Legros B, Vonck KM, de Beeck O, Bourguignon M, et al. Clinical added value of magnetic source imaging in the presurgical evaluation of refractory focal epilepsy. *J Neurol Neurosurg Psychiatry.* (2012) 83:417–23. doi: 10.1136/jnnp-2011-301166
65. Ito T, Otsubo H, Shiraishi H, Yagyu K, Takahashi Y, Ueda Y, et al. Advantageous information provided by magnetoencephalography for patients with neocortical epilepsy. *Brain Dev.* (2015) 37:237–42. doi: 10.1016/j.braindev.2014.04.006
66. Mohamed IS, Bouthillier A, Berube A, Cossette P, Finet P, Saint-Hilaire JM, et al. The clinical impact of integration of magnetoencephalography in the presurgical workup for refractory nonlesional epilepsy. *Epilepsy Behav.* (2018) 79:34–41. doi: 10.1016/j.yebeh.2017.10.036
67. Tanaka N, Hamalainen MS, Ahlfors SP, Liu H, Madsen JR, Bourgeois BF, et al. Propagation of epileptic spikes reconstructed from spatiotemporal magnetoencephalographic and electroencephalographic source analysis. *Neuroimage.* (2010) 50:217–22. doi: 10.1016/j.neuroimage.2009.12.033
68. Wang ZI, Jin K, Kakisaka Y, Mosher JC, Bingaman WE, Kotagal P, et al. Imag(in)ing seizure propagation: MEG-guided interpretation of epileptic activity from a deep source. *Hum Brain Mapp.* (2012) 33:2797–801. doi: 10.1002/hbm.21401
69. Kanamori Y, Shigeto H, Hironaga N, Hagiwara K, Uehara T, Chatani H, et al. Minimum norm estimates in MEG can delineate the onset of interictal epileptic discharges: a comparison with ECoG findings. *Neuroimage Clin.* (2013) 2:663–9. doi: 10.1016/j.nicl.2013.04.008
70. Malinowska U, Badier JM, Gavaret M, Bartolomei F, Chauvel P, Benar CG. Interictal networks in magnetoencephalography. *Hum Brain Mapp.* (2014) 35:2789–805. doi: 10.1002/hbm.22367
71. Agirre-Arrizubieta Z, Thai NJ, Valentin A, Furlong PL, Seri S, Selway RP, et al. The value of Magnetoencephalography to guide electrode implantation in epilepsy. *Brain Topogr.* (2014) 27:197–207. doi: 10.1007/s10548-013-0330-x
72. Alkawadri R, Burgess RC, Kakisaka Y, Mosher JC, Alexopoulos AVl. Assessment of the utility of ictal magnetoencephalography in the localization of the epileptic seizure onset zone. *JAMA Neurol.* (2018) 75:1264–72. doi: 10.1001/jamaneurol.2018.1430
73. Sutherling WW, Crandall PH, Engel JJr, Darcey TM, Cahan LD, Barth DS. The magnetic field of complex partial seizures agrees with intracranial localizations. *Ann Neurol.* (1987) 21:548–58. doi: 10.1002/ana.410210605
74. Stefan H, Schneider S, Feistel H, Pawlik G, Schuler P, Abraham-Fuchs K, et al. Ictal and interictal activity in partial epilepsy recorded with multichannel magnetoelectroencephalography: correlation of electroencephalography/electrocorticography, magnetic resonance imaging, single photon emission computed tomography, and positron emission tomography findings. *Epilepsia.* (1992) 33:874–87. doi: 10.1111/j.1528-1157.1992.tb02195.x
75. Eliashiv DS, Elsas SM, Squires K, Fried I, Engel J Jr. Ictal magnetic source imaging as a localizing tool in partial epilepsy. *Neurology.* (2002) 59:1600–10. doi: 10.1212/01.WNL.0000032493.83875.0B
76. Tilz C, Hummel C, Kettenmann B, Stefan H. Ictal onset localization of epileptic seizures by magnetoencephalography. *Acta Neurol Scand.* (2002) 106:190–5. doi: 10.1034/j.1600-0404.2002.02047.x
77. Fujiwara H, Greiner HM, Hemasilpin N, Lee KH, Holland-Bouley K, Arthur T, et al. Ictal MEG onset source localization compared to intracranial EEG and outcome: improved epilepsy presurgical evaluation in pediatrics. *Epilepsy Res.* (2012) 99:214–24. doi: 10.1016/j.eplepsyres.2011.11.007
78. Shirozu H, Hashizume A, Masuda H, Ito Y, Nakayama Y, Higashijima T, et al. Analysis of ictal magnetoencephalography using gradient magnetic-field topography (GMFT) in patients with neocortical epilepsy. *Clin Neurophysiol.* (2017) 128:1504–12. doi: 10.1016/j.clinph.2017.05.015
79. Badier JM, Benar CG, Woodman M, Cruto C, Chauvel P, Bartolomei F, et al. Ictal magnetic source imaging in presurgical assessment. *Brain Topogr.* (2016) 29:182–92. doi: 10.1007/s10548-015-0445-3
80. Medvedovsky M, Taulu S, Gaily E, Metsahonkala EL, Makela JP, Ekstein D, et al. Sensitivity and specificity of seizure-onset zone estimation by ictal magnetoencephalography. *Epilepsia.* (2012) 53:1649–57. doi: 10.1111/j.1528-1167.2012.03574.x
81. Ramanujam B, Bharti K, Viswanathan V, Garg A, Tripathi M, Bal C, et al. Can ictal-MEG obviate the need for phase II monitoring in people with drug-refractory epilepsy? A prospective observational study. *Seizure.* (2017) 45:17–23. doi: 10.1016/j.seizure.2016.10.013
82. Stefan H, Rampp S. Interictal and ictal magnetoencephalography in presurgical evaluation for epilepsy surgery. *Acta Epilepsy.* (2018) 1:65–71.
83. Bowyer SM, Shvarts V, Moran JE, Mason KM, Barkley GL, Tepley N. Slow brain activity (ISA/DC) detected by MEG. *J Clin Neurophysiol.* (2012) 29:320–6. doi: 10.1097/WNP.0b013e3182624342
84. Guggisberg AG, Kirsch HE, Mantle MM, Barbaro NM, Nagarajan SS. Fast oscillations associated with interictal spikes localize the epileptogenic zone in patients with partial epilepsy. *Neuroimage.* (2008) 39:661–8. doi: 10.1016/j.neuroimage.2007.09.036
85. Rampp S, Kaltenhauser M, Weigel D, Buchfelder M, Ingmar Blumcke I, Dorfler A, et al. MEG correlates of epileptic high

gamma oscillations in invasive EEG. *Epilepsia.* (2010) 51:1638–1642. doi: 10.1111/j.1528-1167.2010.02579.x

86. Jeong W, Kim JS, Chung CK. Localization of MEG pathologic gamma oscillations in adult epilepsy patients with focal cortical dysplasia. *Neuroimage Clin.* (2013) 3:507–14. doi: 10.1016/j.nicl.2013.09.009
87. Park CK, Hwang SJ, Jung NY, Chang WS, Jung HH, Chang JW. Magnetoencephalography as a prognostic method in patients with medically intractable temporal lobe epilepsy. *World Neurosurg.* (2018) 123:e753–9. doi: 10.1016/j.wneu.2018.12.024

Conflict of Interest Statement: EC has received refunding for travel and registration costs and HS has received honoraria and travel reimbursement for lectures.

frontiers in Neurology

SYSTEMATIC REVIEW
published: 03 December 2019
doi: 10.3389/fneur.2019.01250

Accuracy of Interictal and Ictal Electric and Magnetic Source Imaging: A Systematic Review and Meta-Analysis

Praveen Sharma[1,2], *Margitta Seeck*[3] *and Sándor Beniczky*[1,4]*

[1] Department of Clinical Neurophysiology, Danish Epilepsy Centre, Dianalund, Denmark, [2] Department of Neurology, King George's Medical University, Lucknow, India, [3] EEG & Epilepsy Unit, University Hospital of Geneva, Geneva, Switzerland, [4] Department of Clinical Neurophysiology, Aarhus University Hospital and Department of Clinical Medicine, Aarhus University, Aarhus, Denmark

Background: Electric and magnetic source imaging methods (ESI, MSI) estimate the location in the brain of the sources generating the interictal epileptiform discharges (II-ESI, II-MSI) and the ictal activity (IC-ESI, IC-MSI). These methods provide potentially valuable clinical information in the presurgical evaluation of patients with drug-resistant focal epilepsy, evaluated for surgical therapy. In spite of the significant technical advances in this field, and the numerous papers published on clinical validation of these methods, ESI and MSI are still underutilized in most epilepsy centers performing a presurgical evaluation. Our goal was to review and summarize the published evidence on the diagnostic accuracy of interictal and ictal ESI and MSI in epilepsy surgery.

Methods: We searched the literature for papers on ESI and MSI that specified the diagnostic reference standard as the site of resection and the postoperative outcome (seizure-freedom). We extracted data from the selected studies, to calculate the diagnostic accuracy measures.

Results: Our search resulted in 797 studies; 48 studies fulfilled the selection criteria (25 ESI and 23 MSI studies), providing data from 1,152 operated patients (515 for II-ESI, 440 for II-MSI, 159 for IC-ESI, and 38 for IC-MSI). The sensitivity of source imaging methods was between 74 and 90% (highest for IC-ESI). The specificity of the source imaging methods was between 20 and 54% (highest for II-MSI). The overall accuracy was between 50 and 75% (highest for IC-ESI). Diagnostic Odds Ratio was between 0.8 (IC-MSI) and 4.02–7.9 (II-ESI < II-MSI < IC-ESI).

Conclusions: Our systematic review and meta-analysis provides evidence for the accuracy of source imaging in presurgical evaluation of patients with drug-resistant focal epilepsy. These methods have high sensitivity (up to 90%) and diagnostic odds ratio (up to 7.9), but the specificity is lower (up to 54%). ESI and MSI should be included in the multimodal presurgical evaluation.

Keywords: EEG, epilepsy, ictal, interictal, MEG, presurgical evaluation, source imaging, source analysis

OPEN ACCESS

Edited by:
Yulin Ge,
Langone Medical Center, New York University, United States

Reviewed by:
Gabriel Gonzalez-Escamilla,
University Medical Centre, Johannes Gutenberg University Mainz, Germany
Jun Hua,
Johns Hopkins University, United States

****Correspondence:***
Sándor Beniczky
sbz@filadelfia.dk

Specialty section:
This article was submitted to Applied Neuroimaging, a section of the journal Frontiers in Neurology

Received: *25 March 2019*
Accepted: *11 November 2019*
Published: *03 December 2019*

Citation:
Sharma P, Seeck M and Beniczky S (2019) Accuracy of Interictal and Ictal Electric and Magnetic Source Imaging: A Systematic Review and Meta-Analysis. Front. Neurol. 10:1250. doi: 10.3389/fneur.2019.01250

INTRODUCTION

Rationale

In spite of the numerous published papers on the accuracy of electric source imaging (ESI) and magnetic source imaging (MSI) in localizing interictal epileptiform discharges and ictal activity, these methods have gained only partial acceptance in the presurgical evaluation of patients with drug-resistant focal epilepsy. A recently published survey by the E-PILEPSY consortium, comprising 25 European centers, showed that less than half of the centers used these methods for presurgical evaluation (1).

Interictal epileptiform discharges and ictal activity are typically recorded during long-term video EEG monitoring, which is part of the presurgical evaluation in almost all centers. However, signals are interpreted visually, without any post-processing or signal analysis. In the majority of centers, this is merely done by indicating the scalp region where the peak negativity of the discharges (phase reversal) is spotted. This can be misleading, since due to volume conduction, peak negativity can be recorded over a different lobe and even different side than the source. Interictal epileptiform discharges and ictal activity are essential components of the multimodal presurgical evaluation: they indicate the location of the irritative zone and the seizure-onset zone, respectively. Therefore, their accurate localization is extremely important for identifying the cortical area that needs to be surgically resected in order to render the patient seizure-free (2).

Source imaging methods estimate the location of the electric sources (ESI) and of the magnetic sources (MSI). Both methods can be applied for localizing interictal epileptiform discharges (II-ESI and II-MSI) and ictal activity (IC-ESI and IC-MSI). However, at present, MEG has the size of a scanner, and needs a shielded room together with special maintenance, requiring precisely scheduled recording times. Thus, restrictions in time (duration) and space (patient mobility) of the MEG recordings are inherent, so that IC-MSI is rarely performed.

Despite these limitations, during the last decades, these methods developed considerably. It is nowadays possible to record EEG and magnetoencephalographic (MEG) signals using high-density array, and individual head models are constructed using the patients' own MRI.

Objectives

Our goal was to review the published literature on ESI and MSI in presurgical evaluation of patients with drug-resistant focal epilepsy and to infer its accuracy, from the published results.

We wanted to include a wide spectrum of methods and modalities: low density (LD) EEG recordings, with $<$ 64 electrodes, high density (HD) EEG recordings (64–256 electrodes), MEG recordings, analysis of interictal epileptiform discharges as well as of the ictal activity.

Research Question

We have addressed the following question: What is the accuracy of electric and magnetic source imaging in the presurgical evaluation of patients with drug-resistant focal epilepsy?

METHODS

Study Design

This is a systematic review and meta-analysis of the accuracy of electric and magnetic source imaging in presurgical evaluation.

Participants, Interventions, Comparators

Participants: patients with drug-resistant focal epilepsy (3) who underwent presurgical evaluation for possible surgical treatment (resection).

Interventions: II-ESI (electric source imaging of interictal epileptiform discharges), IC-ESI (electric source imaging of ictal activity), II-MSI (magnetic source imaging of interictal epileptiform discharges) and IC-MSI (magnetic source imaging of ictal activity).

Comparators: The most widely accepted, clinically relevant gold standard (reference standard) for diagnostic methods in presurgical evaluation is the epileptogenic zone (EZ), inferred from the site of the resection and the postoperative outcome. Therefore, in this study we compared at sub-lobar level the location of the electric and magnetic sources with the resected area, and then the postoperative outcome ($\geq$1 year after surgery).

Systematic Review Protocol

Literature search was made for electric and magnetic source imaging studies in presurgical evaluation. We designed the review protocol, based on the PRISMA statement (Preferred reporting items for systematic reviews and meta-analyses) (4).

Search Strategy

We searched research studies published between January 1st 1991 and May 31st 2018. We restricted the search to human subjects that were published in English.

For ESI we used the following search string in PubMed and in EMBASE: (Epilepsy[Title/Abstract] AND Source imaging [Title/Abstract] AND Electric OR Electrical OR Electroencephalographic OR EEG [Title/Abstract]).

For MSI we used three different search strings in PubMed. String-1: (Epilepsy[Title] AND Magnetic [Title] OR MEG OR Magnetoencephalographic OR Electromagnetic OR[Title] AND Source Imaging[Title/Abstract]). String-2: (Ictal [Title] AND Magnetic Source Imaging [Title]). Sting-3: ((Magnetic source imaging[Title] OR Magnetoencephalography[Title]) AND Epilepsy[Title/Abstract] AND Interictal[Title/Abstract]).

Duplicate studies were eliminated.

Data Sources, Studies Selections, and Data Extraction

The studies were selected according to the following criteria: (1) Source Imaging compared with gold standard (as described in section Participants, Interventions, Comparators); (2) Studies with at least five subjects (up to four were included in case of ictal magnetic source imaging studies as there were very few studies); (3) follow up duration of minimum 1 year. First title and abstracts were screened, then the full text papers were screened and (for the selected papers) data were extracted, as detailed below.

The location of the epileptic focus indicated by the source imaging study was tested against gold standard to calculate

accuracy parameters. If more than one source were found then the dominant one was used. All included patients underwent respective surgery. Resection of the source and seizure-freedom (Engel-1 outcome) ≥1 year after surgery was considered as evidence for correct localization of the epileptogenic zone, by the source imaging methods.

The definitions for accuracy parameters were used as follows: (a) Source imaging focus within resected area and Engel-1 outcome = True positive (TP); (b) Source imaging focus within resected area and outcome other than Engel-1 = False positive (FP); (c) Source imaging focus outside resected area and outcome Engel-1 = False negative (FN); (d) Source imaging focus outside resected area and outcome other than Engel-1 = True negative (TN). These data (TP, TN, FP, FN) were extracted from the selected studies.

In addition, for ESI studies we extracted information on the electrode array (low density vs. high density array).

Data Analysis

Using the data extracted from the selected studies, we calculated the diagnostic accuracy measures, using the conventional formulae:

$$Sensitivity = \frac{TP}{TP + FN}$$

$$Specificity = \frac{TN}{TN + FP}$$

$$Accuracy = \frac{TP + TN}{TP + TN + FP + FN}$$

$$Diagnostic\ Odds\ Ratio = \frac{TP*TN}{FP*FN}$$

$$Positive\ Likelihood\ Ratio = \frac{sensitivity}{1 - specificity}$$

$$Negative\ Likelihood\ Ratio = \frac{1 - sensitivity}{specificity}$$

For all accuracy measures, we calculated 95% confidence intervals (CI). We compared the accuracy of the various source imaging methods (HD vs. LD recordings, interictal vs. ictal, ESI vs. MSI) using Chi square test, based on the numbers of TP, FP, TN, and FN. An open source software, OpenMeta[Analyst] was used to calculate accuracy parameters with statistical analysis (OpenMeta[Analyst] ([Windows],[CEBM@BROWN],[USA],[2018]).

RESULTS

Study Selection and Characteristics

Figures 1, **2** show the flow diagram of the studies on ESI and MSI, retrieved for the review.

Our search strategy resulted in 486 ESI studies and 311 MSI studies, after removal of duplicates (**Supplementary Material 1**). After screening the titles and the abstracts, 77 ESI studies and 53 MSI studies were selected for full text review. Forty-eight fulfilled all selection criteria. Twenty-five of them addressed ESI: 19 studies on II-ESI (5–23) and six on IC-ESI (24–29). Twenty-three studies addressed MSI: 19 on II-MSI (30–48) and four on IC-MSI (49–52). Data were extracted from these studies for the meta-analysis. These were cross-sectional cohort studies (**Supplementary Materials 2**, **3**).

From the studies selected for data extraction 15 ESI and eight MSI were prospective, including three IC-ESI and two IC-MSI studies, respectively. II-ESI studies included 11 studies with HD electrode array (64 or more electrodes, 64–256), four with LD electrode array (<64) and four with both. The studies with LD electrode array used 26 electrodes in one, 32 electrodes in other one and variable number of electrodes ranging from 19 to 29 and 27 to 32 in the rest. II-MSI studies mostly were with HD sensors except two with 37 sensor MEG and one study did not comment about the density of sensors.

There were three II-ESI and two II-MSI studies which included pediatric population of <18 years age. Other studies had mixed age group population with age ranging from 1 to 75 years from study to study.

There were very few studies on IC-MSI with fewer number of subjects fulfilling inclusion criteria. The sample size was very small, hence results should be interpreted in light of this bias. Study by Badier et al. (50) on IC-MSI used two methods of source analysis which resulted in two different results. These two methods were included as independent studies for the purpose of analysis. Both methods were correlated with epileptogenic zone mapped by intracranial EEG which in turn was used to calculate accuracy parameters. This introduces a methodical heterogeneity and reduces significance of results from this sub-group (IC-MSI).

Synthesized Findings

The pooled patient population for assessment of the accuracy of source imaging included 1,152 patients totally (**Table 1**).

Figures 3–14 show forest plots of the diagnostic outcome measures (sensitivity, specificity, diagnostic odds ratio, positive and negative likelihood rations) of the selected studies and the pooled data, for the source imaging methods: II-ESI, IC-ESI, II-MSI, IC-MSI. **Table 1** summarizes the diagnostic outcome measures, determined from the pooled data. **Table 2** summarizes comparisons of the outcome measures among the source imaging methods.

Sensitivity of the source imaging methods was between 73.8 and 89.9%, highest for IC-ESI and lowest for IC-MSI. Sensitivity was significantly higher for IC-ESI as compared with II-ESI ($p = 0.02$).

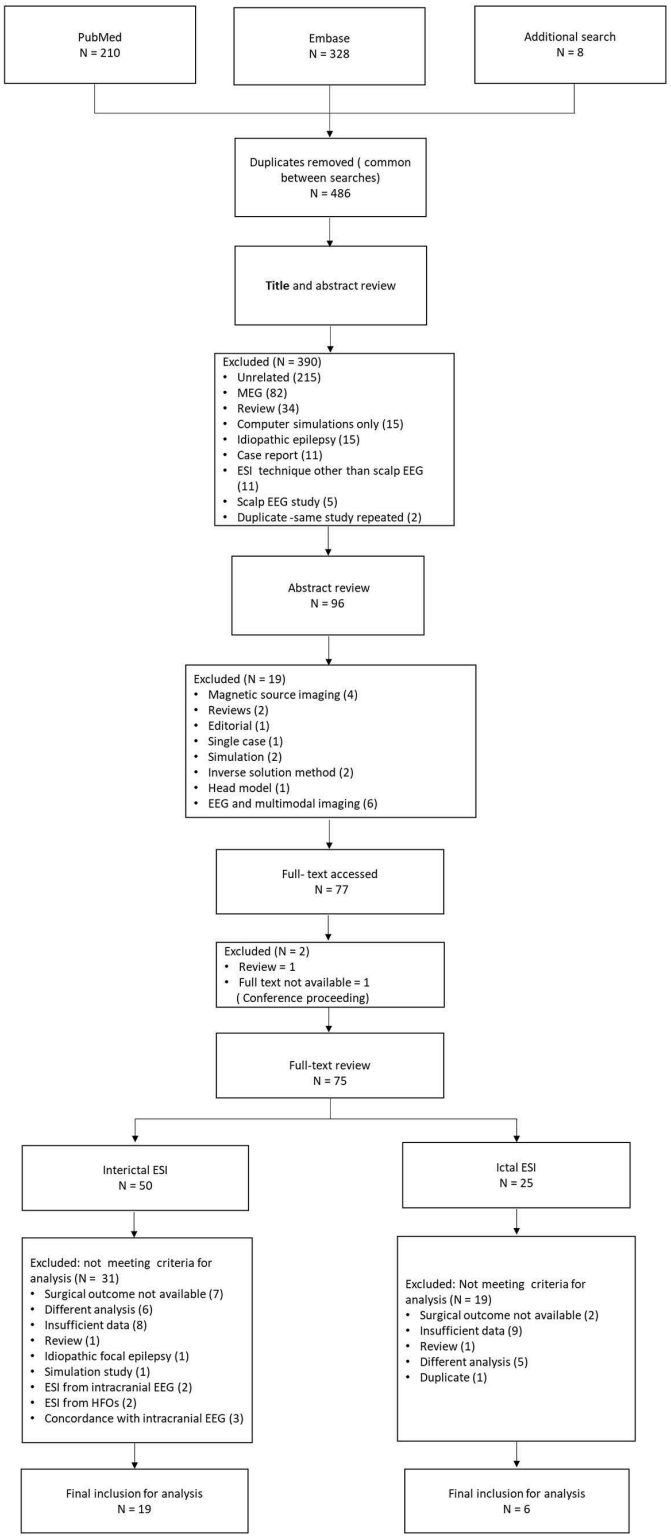

FIGURE 1 | Flow diagram of the studies on ESI, retrieved for the review.

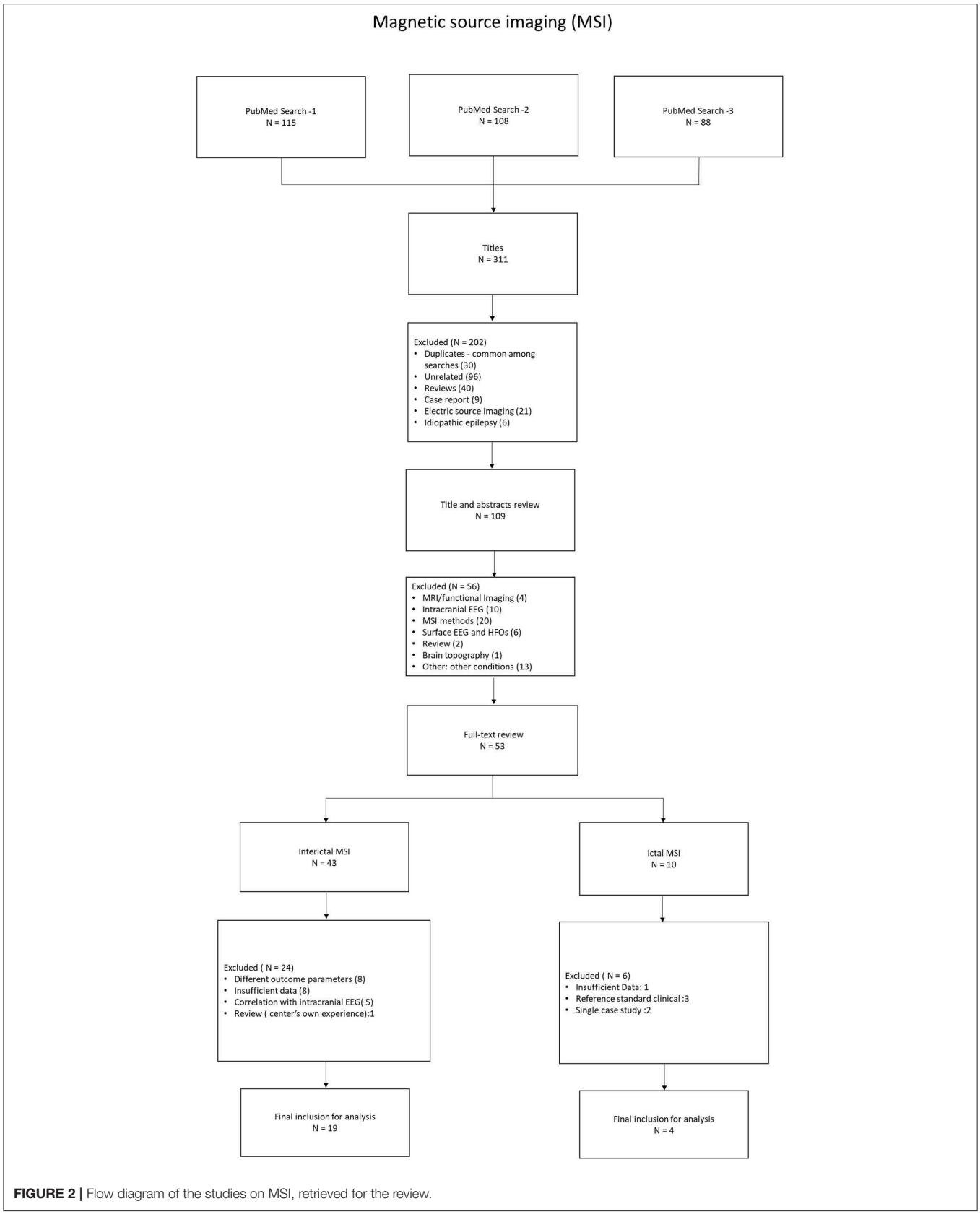

FIGURE 2 | Flow diagram of the studies on MSI, retrieved for the review.

TABLE 1 | Diagnostic outcome measures from pooled data (95% CIs in parenthesis).

	II-ESI	IC-ESI	II-MSI	IC-MSI
Number of patients	515	159	440	38
Sensitivity	81.1% (76.2–85.2%)	89.9% (81.8–94.6%)	77.4% (71.5–82.3%)	73.8% (48.4–89.4%)
Specificity	45.2% (36.0–54.7%)	46.9% (30.5–63.9%)	54.1% (46.2–61.9%)	20.5% (7.1–46.8%)
Accuracy	74.17% (70.39–77.95%)	74.84% (68.1−81.59%)	70.68% (66.43–74.94%)	50.00% (37.71–69.43%)
Diagnostic odds ratio	4.02 (2.31–6.98)	7.896 (3.117–20.004)	4.54 (2.81–7.32)	0.823 (0.16–4.229)
Positive likelihood ratio	1.31 (1.12–1.54)	1.47 (1.149–1.881)	1.42 (1.204–1.672)	0.98 (0.735–1.305)
Negative likelihood ratio	0.383 (0.263–0.557)	0.218 (0.169–0.281)	0.395 (0.282- 0.555)	1.04 (0.708–1.539)

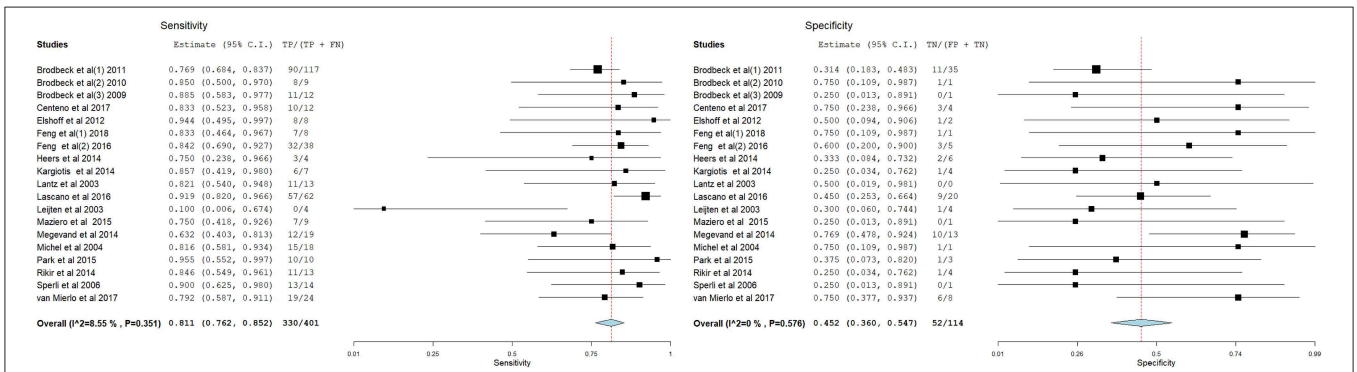

FIGURE 3 | Forest plot showing sensitivity and specificity of the II-ESI studies (individual studies: size of the squares are proportional to weights used in meta-analysis; the summary measure: center line of the diamond; associated 95% confidence intervals: lateral tips of the squares and the diamond).

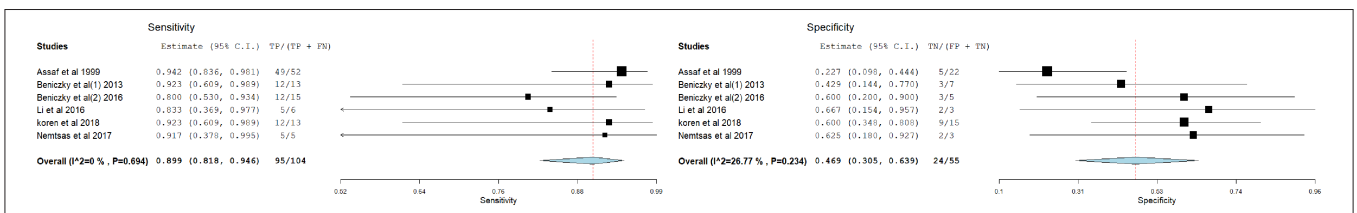

FIGURE 4 | Forest plot showing sensitivity and specificity of the IC-ESI studies (individual studies: size of the squares are proportional to weights used in meta-analysis; the summary measure: center line of the diamond; associated 95% confidence intervals: lateral tips of the squares and the diamond).

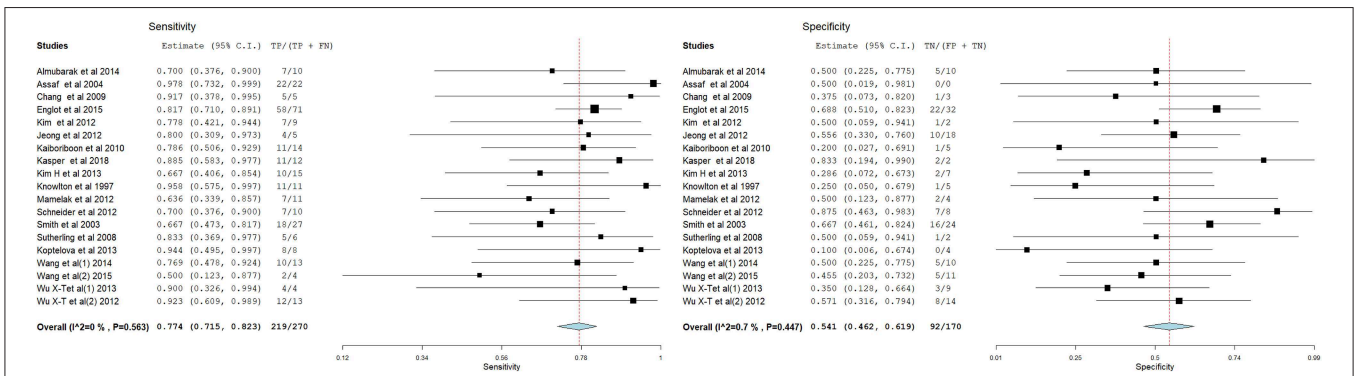

FIGURE 5 | Forest plot showing sensitivity and specificity of the II-MSI studies (individual studies: size of the squares are proportional to weights used in meta-analysis; the summary measure: center line of the diamond; associated 95% confidence intervals: lateral tips of the squares and the diamond).

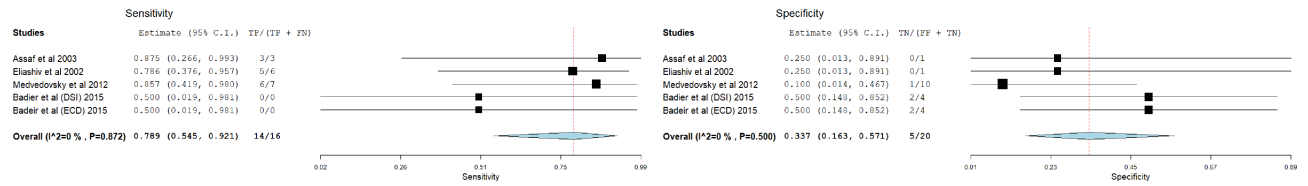

FIGURE 6 | Forest plot showing sensitivity and specificity of the IC-MSI studies (individual studies: size of the squares are proportional to weights used in meta-analysis; the summary measure: center line of the diamond; associated 95% confidence intervals: lateral tips of the squares and the diamond).

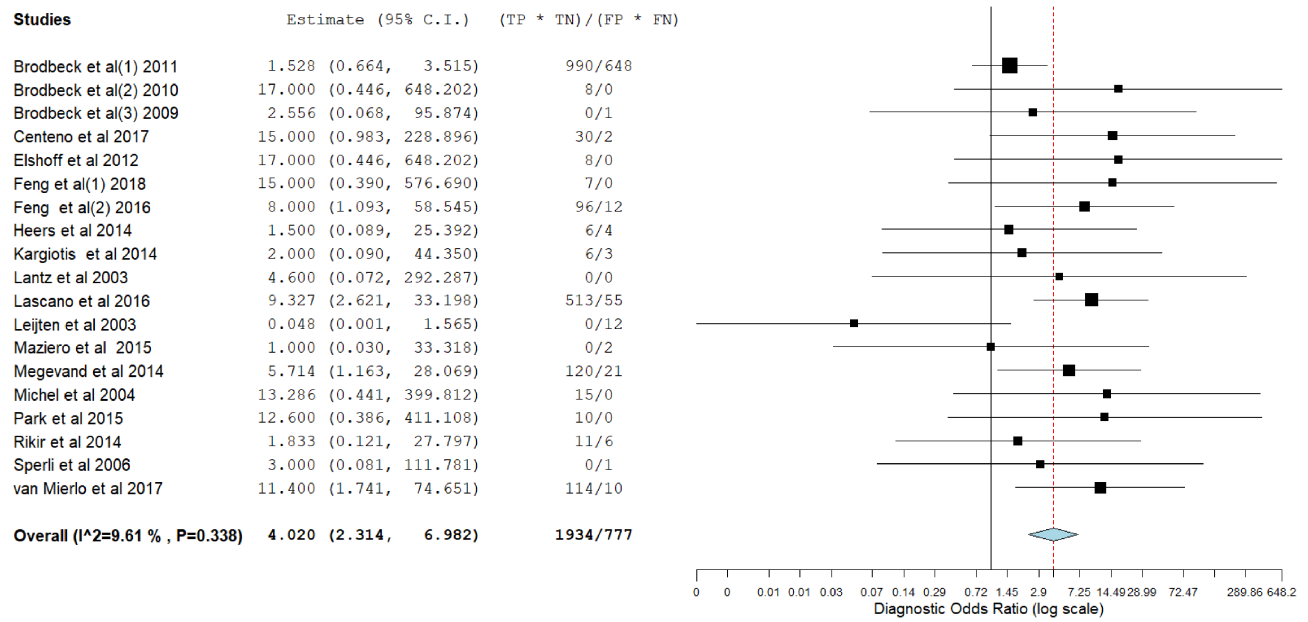

FIGURE 7 | Forest plot showing diagnostic odds ratio of the II-ESI studies (individual studies: size of the squares are proportional to weights used in meta-analysis; the summary measure: center line of the diamond; associated 95% confidence intervals: lateral tips of the squares and the diamond).

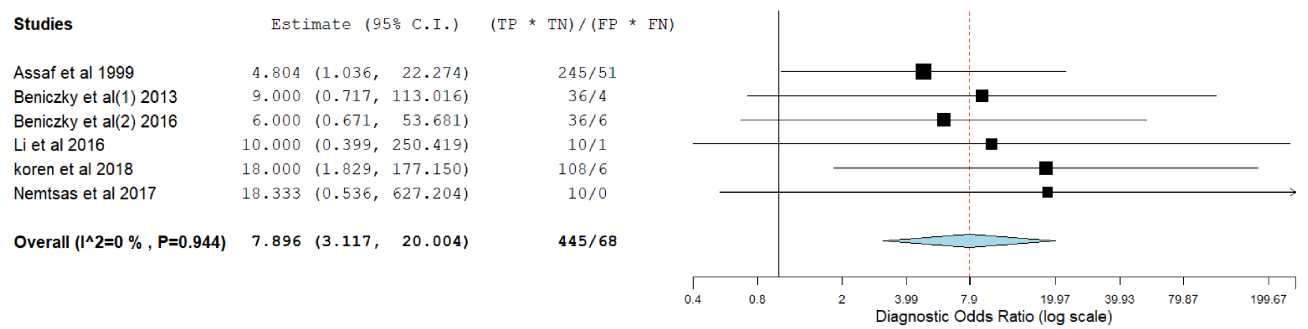

FIGURE 8 | Forest plot showing diagnostic odds ratio of the IC-ESI studies (individual studies: size of the squares are proportional to weights used in meta-analysis; the summary measure: center line of the diamond; associated 95% confidence intervals: lateral tips of the squares and the diamond).

Specificity of the source imaging methods was between 20.5 and 45.1%, highest for II-MSI and lowest for IC-MSI. Specificity of IC-MSI was significantly lower compare with II-MSI ($p = 0.007$) and IC-ESI ($p = 0.02$).

The overall accuracy of the source imaging methods was between 50 and 74.84%, highest for IC-ESI and lowest for IC-MSI. Accuracy of the IC-MSI was significantly lower compared to the other methods ($p < 0.002$). There was

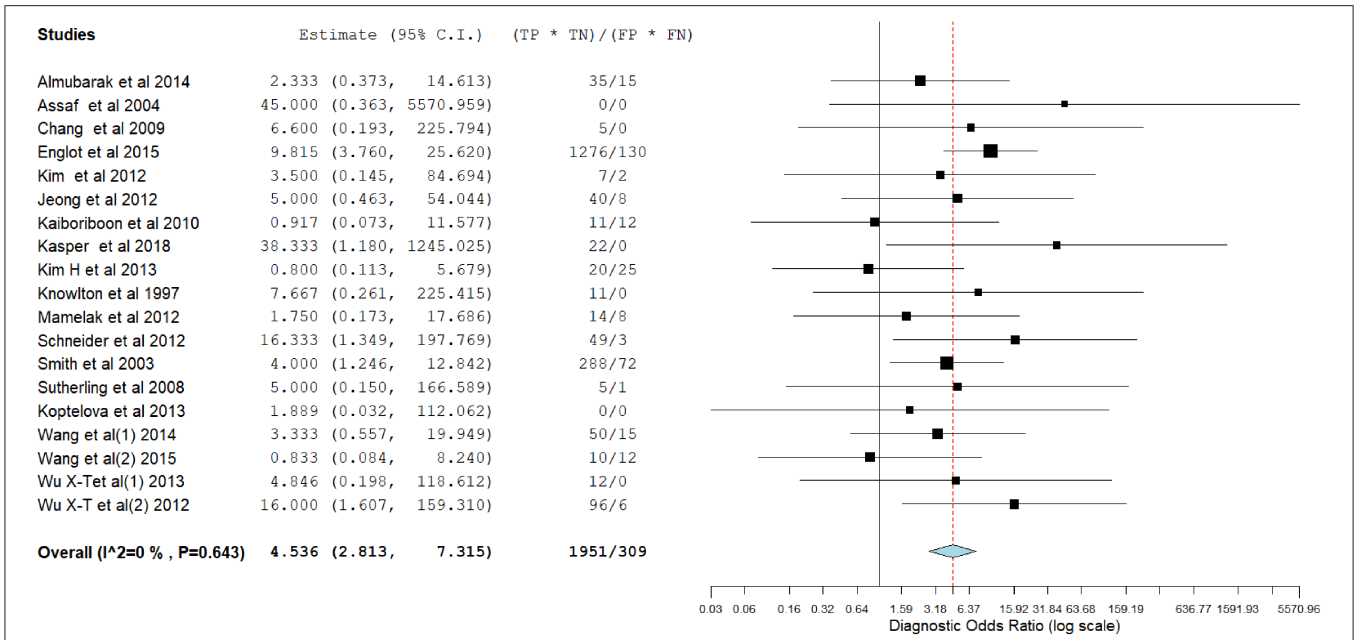

FIGURE 9 | Forest plot showing diagnostic odds ratio of the II-MSI studies (individual studies: size of the squares are proportional to weights used in meta-analysis; the summary measure: center line of the diamond; associated 95% confidence intervals: lateral tips of the squares and the diamond).

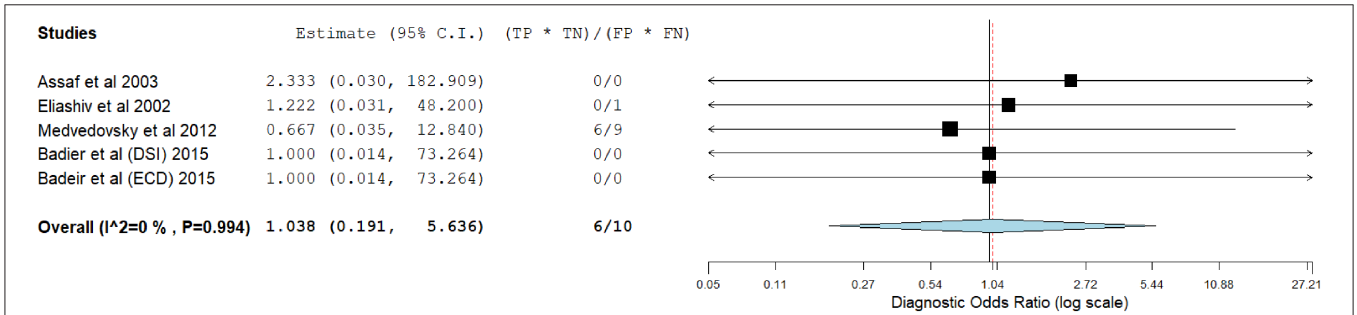

FIGURE 10 | Forest plot showing diagnostic odds ratio of the IC-MSI studies (individual studies: size of the squares are proportional to weights used in meta-analysis; the summary measure: center line of the diamond; associated 95% confidence intervals: lateral tips of the squares and the diamond).

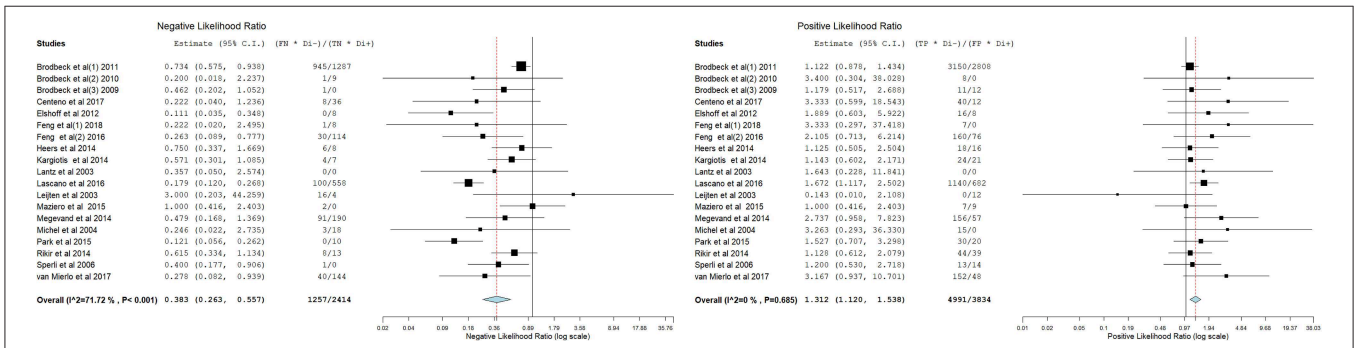

FIGURE 11 | Forest plot showing negative and positive likelihood ratios of the II-ESI studies (individual studies: size of the squares are proportional to weights used in meta-analysis; the summary measure: center line of the diamond; associated 95% confidence intervals: lateral tips of the squares and the diamond).

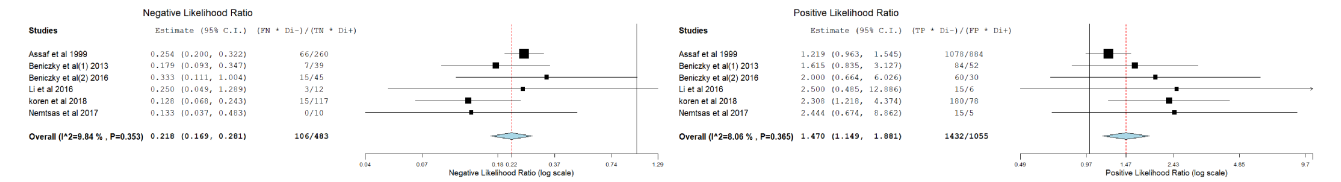

FIGURE 12 | Forest plot showing negative and positive likelihood ratios of the IC-ESI studies (individual studies: size of the squares are proportional to weights used in meta-analysis; the summary measure: center line of the diamond; associated 95% confidence intervals: lateral tips of the squares and the diamond).

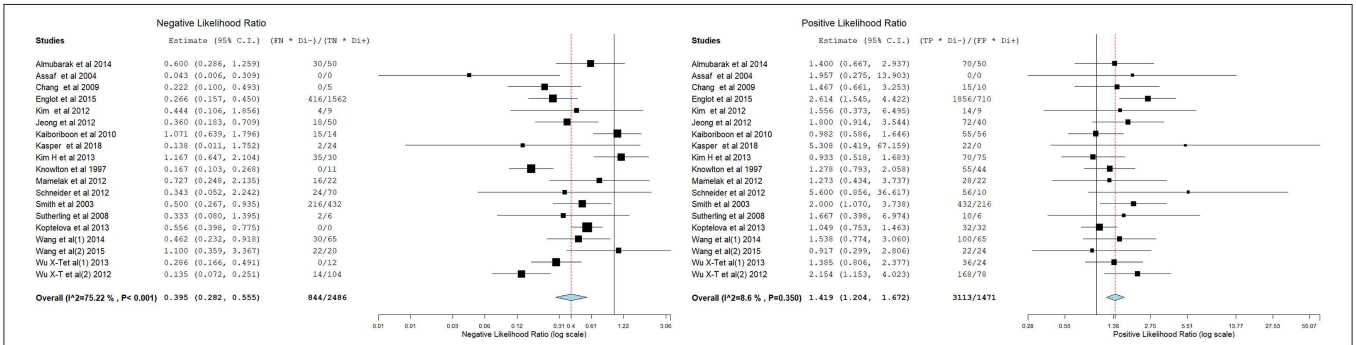

FIGURE 13 | Forest plot showing negative and positive likelihood ratios of the II-MSI studies (individual studies: size of the squares are proportional to weights used in meta-analysis; the summary measure: center line of the diamond; associated 95% confidence intervals: lateral tips of the squares and the diamond).

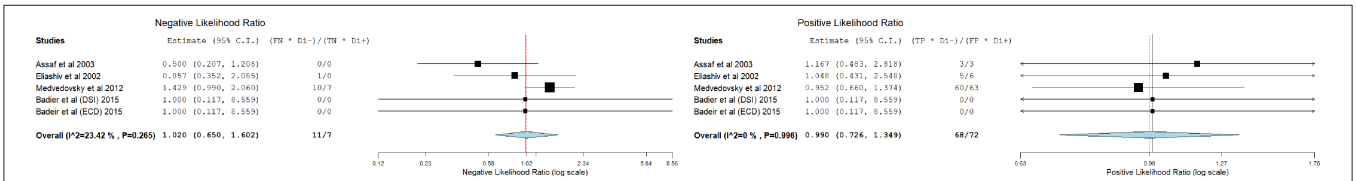

FIGURE 14 | Forest plot showing negative and positive likelihood ratios of the IC-MSI studies (individual studies: size of the squares are proportional to weights used in meta-analysis; the summary measure: center line of the diamond; associated 95% confidence intervals: lateral tips of the squares and the diamond).

no significant difference in accuracy between II-ESI, IC-ESI and II-MSI.

Diagnostic Odds Ratio was between 0.823 and 7.896, highest for IC-ESI and lowest for IC-MSI. The 95% CIs of all source imaging methods, except for IC-MSI, were >1.

Positive Likelihood Ratio was between 0.98 and 1.47, highest for IC-ESI and lowest for IC-MSI. Negative Likelihood Ratio was between 0.22 and 1.04, lowest for IC-ESI and highest for IC-MSI.

The sub-group analyses taking into account the spatial sampling, could not show significant difference in sensitivity, specificity or accuracy of II-ESI or IC-ESI, between HD and LD recordings (**Table 2**). However, the overall accuracy of II-ESI with HD recordings was significantly higher compared with II-MSI with HD recordings ($p = 0.0187$).

DISCUSSION

Based on a large number of operated patients ($n = 1{,}152$), the various EEG and MEG source imaging methods proved to have high accuracy in localizing the epileptic focus.

IC-MSI had the lowest performance, especially concerning its specificity. IC-ESI was done in a small number of patients ($n = 38$) due to its low feasibility (short recording time compared to EEG long term monitoring, and limited mobility of the patients with motor seizures in the MEG). These limitations might be overcome in future by the new generation of MEG equipment that allows room temperature measurements using optically-pumped magnetometers. Recently, EEG systems which allow EEG recordings of up to 256 electrodes for one or several days became commercially available. We hypothesize that there will be more studies on the yield of HD-EEG and HD-ESI with more widespread use of these systems, especially if electrode application and EEG analysis become easy to do.

Excluding the IC-MSI, the large pooled data showed high sensitivity of the source imaging methods, between 77 and 90%, highest for IC-ESI. However, their specificity was lower, between 45 and 54%, highest for II-MSI. The overall accuracy of the three methods was between 71 and 75% (highest for IC-ESI). Their Diagnostic Odds Ratio was between 4 and 7.9, highest for IC-ESI, demonstrating the diagnostic utility of these three source imaging methods.

TABLE 2 | Comparisons of the outcome measures among the source imaging methods.

	Sensitivity (95%CI)	*p*	Specificity (95%CI)	*p*	Accuracy (95%CI)	*p*
II-ESI	82.29% (78.56–86.03%)	**0.021**	45.61% (36.47–54.76%)	0.887	74.17% (70.39–77.95%)	0.865
IC-ESI	91.35% (85.94–96.05%)		43.64% (30.53–56.74%)		74.84% (68.10–81.95%)	
II-ESI	82.29% (78.56–86.03%)	0.697	45.61% (36.47–54.76%)	0.160	74.17% (70.39–77.95%)	0.22
II-MSI	81.11% (76.44–85.04%)		54.12% (46.63–45.61%)		70.68% (66.43–74.95%)	
IC-ESI	91.35% (85.94–96.05%)	0.056	43.64% (30.53–56.74%)	**0.023**	74.84% (68.10–81.95%)	**0.002**
IC-MSI	77.27% (59.76–94.17%)		12.50% (03.370–87.70%)		50.00% (34.10–65.95%)	
IC-MSI	77.27% (59.76–94.17%)	0.660	12.50% (03.370–87.70%)	**0.007**	50.00% (34.10–65.95%)	**0.0082**
II-MSI	81.11% (76.44–85.04%)		54.12% (46.63–45.61%)		70.68% (66.43–74.95%)	
II-ESI (HD)	84.21% (79.27–89.04%)	0.753	53.57% (40.51–46.63%)	0.964	77.74% (72.73–82.95%)	0.98
II-ESI (LD)	86.00% (76.38–95.09%)		52.94% (29.21–47.67%)		77.61% (67.63–87.95%)	
IC-ESI (HD)	85.00% (69.35–00.15%)	0.261	62.50% (28.95–37.05%)	0.245	78.57% (63.37–93.95%)	0.61
IC-ESI (LD)	92.86% (87.35–98.05%)		40.43% (26.40–59.46%)		74.05% (66.54–81.95%)	
II-ESI (HD)	84.21% (79.27–89.04%)	0.261	53.57% (40.51–46.63%)	0.962	77.74% (72.73–82.95%)	**0.0187**
II-MSI (HD)	80.00% (74.59–85.05%)		53.19% (44.96–46.43%)		69.23% (64.40–74.95%)	

Significant differences are highlighted in bold.

The pooled data showed a significantly higher sensitivity of IC-ESI compared with II-ESI. From a technical point of view, IC-ESI is more challenging, due to the lower signal-to-noise ratio, difficulties in delimiting the ictal onset epoch, rapid propagation, electrodecremental response. However, our data suggest that these difficulties can be overcome, and that the gain from imaging the SOZ exceeds the errors potentially induced by the technical difficulties.

When restricting the analyses to the sub-groups of patients with HD EEG and HD MEG recordings, II-ESI had a higher diagnostic accuracy compared to II-MSI. The pooled data could not confirm higher accuracy of HD compared to LD ESI. It is important to emphasize the limitations in comparing accuracy of the source imaging methods, based on data pooled from different studies. There was a high heterogeneity in terms of study design and included patient populations among the studies, which could have biased the results of comparisons among the source imaging methods. Ideally, these methods should have been compared on the same patients (cross-over design) which was not the case here. Furthermore, most LD-recordings were obtained with > 30 electrodes, which is not that low and might be sufficient for lesional epilepsy. Another important point is the underlying syndrome. Non-lesional extratemporal epilepsy may need HD-EEG/MEG to obtain correct localization, but this may be less relevant for tumoral temporal lobe epilepsy. Future studies may help to better stratify patients who need source localization with >64 electrodes or sensors

Our meta-analysis has several limitations. We did not limit our search strategy with any a priori assumption (for example, we did not exclude ictal studies or LD recordings). This rather inclusive strategy resulted in a high number of selected studies, but the drawback was the increased heterogeneity of study design, patient inclusion and source imaging methods, which potentially could have biased the results. Nevertheless, the large number of analyzed patients might have compensated for this, when inferring the main outcome results. The retrieval of published studies was limited to PubMed and EMBASE databases. We did not use Cochrane library. We restricted the studies that reported surgical standard as gold standard, thus excluding studies comparing source imaging with intracranial recordings. Strictly speaking, the best method of assessing the localization accuracy, *per se*, is comparing it with the intracranial recordings. However, the clinical relevance of this is questionable, since resecting the focus identified by intracranial recordings often does not lead to seizure-freedom. In addition, not all operated patients are implanted, which limits its use as a comparator for the whole group of operated patients. Furthermore, a systematic bias in all source imaging studies is the inclusion only of the operated patients. Although this is necessary for pragmatic reasons (need for gold standard), it potentially can lead to overestimation of the accuracy of the index test (source imaging). We grouped the methods according to the recorded modality (EEG vs. MEG) and the type of the analyzed EEG signals (interictal vs. ictal). This resulted in four categories, for which we calculated the accuracy measurements separately. Within each category, various types of inverse solutions were used for the analysis. However, recently published, large prospective and retrospective studies failed to prove significant difference I accuracy between the various inverse solutions (26, 53, 54).

Future studies need to address these limitations, with study design that overcome the issues listed above. There is a need for prospective, multi-center studies, with standardized electrode array and analysis pipeline (ideally as much automated as possible) and comparison of the various analysis methods within the same patients (cross-over design). Such a large, multi-center study has been recently initiated by European Reference Network (EpiCare), involving 20 epilepsy surgery centers.

Based on a large number of patients and studies, our results provide evidence for the accuracy of IC and II ESI and II MSI in localizing the epileptic focus. These methods should be included into the multimodal presurgical evaluation of patients with drug-resistant focal epilepsy.

DATA AVAILABILITY STATEMENT

The raw data supporting the conclusions of this manuscript will be made available by the authors, without undue reservation, to any qualified researcher.

AUTHOR CONTRIBUTIONS

PS, MS, and SB designed the study and contributed to editing the manuscript. PS and SB analyzed the data and drafted the manuscript.

FUNDING

This study was supported by the D. B. Gupta research fellowship, granted to PS by the European Academy of Neurology, and by a grant from Henry and Karla Hansen Foundation. MS was supported by SNF grants 163398 and 180365.

ACKNOWLEDGMENTS

We would like to express our gratitude to the authors of all studies selected into this meta-analysis.

SUPPLEMENTARY MATERIAL

The Supplementary Material for this article can be found online at: https://www.frontiersin.org/articles/10.3389/fneur.2019.01250/full#supplementary-material

Supplementary Material 1 | Results of the literature search.

Supplementary Material 2 | Design of the included studies.

Supplementary Material 3 | Characteristics of the included studies.

REFERENCES

1. Mouthaan BE, Rados M, Barsi P, Boon P, Carmichael DW, Carrette E, et al. Current use of imaging and electromagnetic source localization procedures in epilepsy surgery centers across Europe. *Epilepsia*. (2016) 57:770–6. doi: 10.1111/epi.13347
2. Rosenow F, Lüders H. Presurgical evaluation of epilepsy. *Brain*. (2001) 124:1683–700. doi: 10.1093/brain/124.9.1683
3. Kwan P, Arzimanoglou A, Berg AT, Brodie MJ, Allen Hauser W, Mathern G, et al. Definition of drug resistant epilepsy: consensus proposal by the ad hoc Task Force of the ILAE commission on therapeutic strategies. *Epilepsia*. (2010) 51:1069–77. doi: 10.1111/j.1528–1167.2009.02397.x
4. Moher D, Liberati A, Tetzlaff J, Altman DG, PRISMA Group. Preferred reporting items for systematic reviews and meta-analyses: the PRISMA statement. *PLoS Med*. (2009) 6:e1000097. doi: 10.1371/journal.pmed.1000097
5. Brodbeck V, Spinelli L, Lascano AM, Wissmeier M, Vargas MI, Vulliemoz S, et al. Electroencephalographic source imaging: a prospective study of 152 operated epileptic patients. *Brain*. (2011) 134:2887–97. doi: 10.1093/brain/awr243
6. Brodbeck V, Spinelli L, Lascano AM, Pollo C, Schaller K, Vargas MI, et al. Electrical source imaging for presurgical focus localization in epilepsy patients with normal MRI. *Epilepsia*. (2010) 51:583–91. doi: 10.1111/j.1528–1167.2010.02521.x
7. Brodbeck V, Lascano AM, Spinelli L, Seeck M, Michel CM. Accuracy of EEG source imaging of epileptic spikes in patients with large brain lesions. *Clin Neurophysiol*. (2009) 120:679–85. doi: 10.1016/j.clinph.2009.01.011
8. Centeno M, Tierney TM, Perani S, Shamshiri EA, St Pier K, Wilkinson C, et al. Combined electroencephalography-functional magnetic resonance imaging and electrical source imaging improves localization of pediatric focal epilepsy. *Ann Neurol*. (2017) 82:278–87. doi: 10.1002/ana.25003
9. Elshoff L, Groening K, Grouiller F, Wiegand G, Wolff S, Michel C, et al. The value of EEG-fMRI and EEG source analysis in the presurgical setup of children with refractory focal epilepsy. *Epilepsia*. (2012) 53:1597–606. doi: 10.1111/j.1528–1167.2012.03587.x
10. Feng R, Hu J, Wu J, Lang L, Ma C, Sun B, Gu X, Pan L. Accurate source imaging based on high resolution scalp electroencephalography and individualized finite difference head models in epilepsy pre-surgical workup. *Seizure*. (2018) 59:126–31. doi: 10.1016/j.seizure.2018.05.009
11. Feng R, Hu J, Pan L, Wu J, Lang L, Jiang S, et al. Application of 256-channel dense array electroencephalographic source imaging in presurgical workup of temporal lobe epilepsy. *Clin Neurophysiol*. (2016) 127:108–16. doi: 10.1016/j.clinph.2015.03.009
12. Heers M, Hedrich T, An D, Dubeau F, Gotman J, Grova C, et al. Spatial correlation of hemodynamic changes related to interictal epileptic discharges with electric and magnetic source imaging. *Hum Brain Mapp*. (2014) 35:4396–414. doi: 10.1002/hbm.22482
13. Kargiotis O, Lascano AM, Garibotto V, Spinelli L, Genetti M, Wissmeyer M, et al. Localization of the epileptogenic tuber with electric source imaging in patients with tuberous sclerosis. *Epilepsy Res*. (2014) 108:267–79. doi: 10.1016/j.eplepsyres.2013.11.003
14. Lantz G, Grave de Peralta R, Spinelli L, Seeck M, Michel CM. Epileptic source localization with high density EEG: how many electrodes are needed? *Clin Neurophysiol*. (2003) 114:63–9. doi: 10.1016/S1388–2457(02)00337–1
15. Lascano AM, Perneger T, Vulliemoz S, Spinelli L, Garibotto V, Korff CM, et al. Yield of MRI, high-density electric source imaging (HD-ESI), SPECT and PET in epilepsy surgery candidates. *Clin Neurophysiol*. (2016) 127:150–5. doi: 10.1016/j.clinph.2015.03.025
16. Leijten FS, Huiskamp GJ, Hilgersom I, Van Huffelen AC. High-resolution source imaging in mesiotemporal lobe epilepsy: a comparison between MEG and simultaneous EEG. *J Clin Neurophysiol*. (2003) 20:227–38. doi: 10.1097/00004691–200307000-00001
17. Maziero D, Sturzbecher M, Velasco TR, Rondinoni C, Castellanos AL, Carmichael DW, et al. A Comparison of Independent Component Analysis (ICA) of fMRI and Electrical Source Imaging (ESI) in Focal Epilepsy Reveals Misclassification Using a Classifier. *Brain Topogr*. (2015) 28:813–31. doi: 10.1007/s10548–015-0436–4
18. Mégevand P, Spinelli L, Genetti M, Brodbeck V, Momjian S, Schaller K, et al. Electric source imaging of interictal activity accurately localises the seizure onset zone. *J Neurol Neurosurg Psychiatry*. (2014) 85:38–43. doi: 10.1136/jnnp-2013–305515
19. Michel CM, Lantz G, Spinelli L, De Peralta RG, Landis T, Seeck M. 128-channel EEG source imaging in epilepsy: clinical yield and localization precision. *J Clin Neurophysiol*. (2004) 21:71–83. doi: 10.1097/00004691–200403000-00001
20. Park CJ, Seo JH, Kim D, Abibullaev B, Kwon H, Lee YH, et al. EEG source imaging in partial epilepsy in comparison with presurgical evaluation and magnetoencephalography. *J Clin Neurol*. (2015)11:319–30. doi: 10.3988/jcn.2015.11.4.319
21. Rikir E, Koessler L, Gavaret M, Bartolomei F, Colnat-Coulbois S, Vignal JP, et al. Electrical source imaging in cortical malformation-related epilepsy: a prospective EEG-SEEG concordance study. *Epilepsia*. (2014) 55:918–32. doi: 10.1111/epi.12591
22. Sperli F, Spinelli L, Seeck M, Kurian M, Michel CM, Lantz G. EEG source imaging in pediatric epilepsy surgery: a new perspective in presurgical workup. *Epilepsia*. (2006) 47:981–90. doi: 10.1111/j.1528–1167.2006.00550.x

23. van Mierlo P, Strobbe G, Keereman V, Birot G, Gadeyne S, Gschwind M, et al. Automated long-term EEG analysis to localize the epileptogenic zone. *Epilepsia Open*. (2017) 2:322–33. doi: 10.1002/epi4.12066
24. Assaf BA, Ebersole JS. Visual and quantitative ictal EEG predictors of outcome after temporal lobectomy. *Epilepsia*. (1999) 40:52–61. doi: 10.1111/j.1528–1157.1999.tb01988.x
25. Beniczky S, Lantz G, Rosenzweig I, Åkeson P, Pedersen B, Pinborg LH, et al. Source localization of rhythmic ictal EEG, activity: a study of diagnostic accuracy following STARD criteria. *Epilepsia*.. (2013) 54:1743–52. doi: 10.1111/epi.12339
26. Beniczky S, Rosenzweig I, Scherg M, Jordanov T, Lanfer B, Lantz G, et al. Ictal EEG source imaging in presurgical evaluation: high agreement between analysis methods. *Seizure*. (2016) 43:1–5. doi: 10.1016/j.seizure.2016.09.017
27. Li C, Jacobs D, Hilton T, Campo MD, Chinvarun Y, Carlen PL, et al. Epileptogenic Source Imaging Using Cross-Frequency Coupled Signals From Scalp EEG. *IEEE Trans Biomed Eng*. (2016) 63:2607–18. doi: 10.1109/TBME.2016.2613936
28. Koren J, Gritsch G, Pirker S, Herta J, Perko H, Kluge T, et al. Automatic ictal onset source localization in presurgical epilepsy evaluation. *Clin Neurophysiol*. (2018) 129:1291–9. doi: 10.1016/j.clinph.2018.03.020
29. Nemtsas P, Birot G, Pittau F, Michel CM, Schaller K, Vulliemoz S, et al. Source localization of ictal epileptic activity based on high-density scalp EEG data. *Epilepsia*. (2017) 58:1027–36. doi: 10.1111/epi.13749
30. Almubarak S, Alexopoulos A, Von-Podewils F, Wang ZI, Kakisaka Y, Mosher JC, et al. The correlation of magnetoencephalography to intracranial EEG in localizing the epileptogenic zone: a study of the surgical resection outcome. *Epilepsy Res*. (2014) 108:1581–90. doi: 10.1016/j.eplepsyres.2014.08.016
31. Assaf BA, Karkar KM, Laxer KD, Garcia PA, Austin EJ, Barbaro NM, et al. Magnetoencephalography source localization and surgical outcome in temporal lobe epilepsy. *Clin Neurophysiol*. (2004) 115:2066–76. doi: 10.1016/j.clinph.2004.04.020
32. Chang EF, Nagarajan SS, Mantle M, Barbaro NM, Kirsch HE. Magnetic source imaging for the surgical evaluation of electroencephalography-confirmed secondary bilateral synchrony in intractable epilepsy. *J Neurosurg*. (2009) 111:1248–56. doi: 10.3171/2009.6.JNS081376
33. Englot DJ, Nagarajan SS, Imber BS, Raygor KP, Honma SM, Mizuiri D, et al. Epileptogenic zone localization using magnetoencephalography predicts seizure freedom in epilepsy surgery. *Epilepsia*. (2015) 56:949–58. doi: 10.1111/epi.13002
34. Kim H, Kankirawatana P, Killen J, Harrison A, Oh A, Rozzelle C, Blount J, et al. Magnetic source imaging (MSI) in children with neocortical epilepsy: surgical outcome association with 3D post-resection analysis. *Epilepsy Res*. (2013) 106:164–72. doi: 10.1016/j.eplepsyres.2013.04.004
35. Jeong W, Chung CK, Kim JS. Localization value of magnetoencephalography interictal spikes in adult nonlesional neocortical epilepsy. *J Korean Med Sci*. (2012) 27:1391–7. doi: 10.3346/jkms.2012.27.11.1391
36. Kaiboriboon K, Nagarajan S, Mantle M, Kirsch HE. Interictal MEG/MSI in intractable mesial temporal lobe epilepsy: spike yield and characterization. *Clin Neurophysiol*. (2010) 121:325–31. doi: 10.1016/j.clinph.2009.12.001
37. Kasper BS, Rössler K, Hamer HM, Dörfler A, Blümcke I, Coras R, et al. Coregistrating magnetic source and magnetic resonanceimaging for epilepsy surgery in focal cortical dysplasia. *Neuroimage Clin*. (2018) 19:487–96. doi: 10.1016/j.nicl.2018.04.034
38. Kim H, Lim BC, Jeong W, Kim JS, Chae JH, Kim KJ, et al. Magnetoencephalography in pediatric lesional epilepsy surgery. *J Korean Med Sci*. (2012) 27:668–73. doi: 10.3346/jkms.2012.27.6.668
39. Knowlton RC, Laxer KD, Aminoff MJ, Roberts TP, Wong ST, Rowley HA. Magnetoencephalography in partial epilepsy: clinical yield and localization accuracy. *Ann Neurol*. (1997) 42:622–31. doi: 10.1002/ana.410420413
40. Mamelak AN, Lopez N, Akhtari M, Sutherling WW. Magnetoencephalography-directed surgery in patients with neocortical epilepsy. *J Neurosurg*. (2002) 97:865–73. doi: 10.3171/jns.2002.97.4.0865
41. Schneider F, Alexopoulos AV, Wang Z, Almubarak S, Kakisaka Y, Jin K, et al. Magnetic source imaging in non-lesional neocortical epilepsy: additional value and comparison with ICEEG. *Epilepsy Behav*. (2012) 24:234–40. doi: 10.1016/j.yebeh.2012.03.029
42. Smith JR, King DW, Park YD, Murro AM, Lee GP, Jenkins PD. A 10-year experience with magnetic source imaging in the guidance of epilepsy surgery. *Stereotact Funct Neurosurg*. (2003) 80:14–7. doi: 10.1159/000075153
43. Sutherling WW, Mamelak AN, Thyerlei D, Maleeva T, Minazad Y, Philpott L, et al. Influence of magnetic source imaging for planning intracranial EEG in epilepsy. *Neurology*. (2008) 71:990–6. doi: 10.1212/01.wnl.0000326591.29858.1a
44. Koptelova AM, Arkhipova NA, Golovteev AL, Chadaev VA, Grinenko OA, Kozlova AB, et al. [Magnetoencephalography in the presurgical evaluation of patients with drug-resistant epilepsy]. *Zh Vopr Neirokhir Im N N Burdenko*. (2013) 77:14–21.
45. Wang ZI, Alexopoulos AV, Jones SE, Najm IM, Ristic A, Wong C, et al. Linking MRI postprocessing with magnetic source imaging in MRI-negative epilepsy. *Ann Neurol*. (2014) 75:759–70. doi: 10.1002/ana.24169
46. Wang Y, Liu B, Fu L, Cui Z. Use of interictal (18)F-fluorodeoxyglucose (FDG)-PET and magnetoencephalography (MEG) to localize epileptogenic foci in non-lesional epilepsy in a cohort of 16 patients. *J Neurol Sci*. (2015) 355:120–4. doi: 10.1016/j.jns.2015.05.039
47. Wu XT, Rampp S, Buchfelder M, Kuwert T, Blümcke I, Dörfler A, et al. Interictal magnetoencephalography used in magnetic resonance imaging-negative patients with epilepsy. *Acta Neurol Scand*. (2013) 127:274–80. doi: 10.1111/j.1600–0404.2012.01712.x
48. Wu XT, Rampp S, Hopfengärtner R, Buchfelder M, Zhou D, Stefan H. Complementary use of video-electroencephalography and magnetoencephalography in frontal lobe epilepsy. *Seizure*. (2012) 21:426–30. doi: 10.1016/j.seizure.2012.04.007
49. Assaf BA, Karkar KM, Laxer KD, Garcia PA, Austin EJ, Barbaro NM, et al. Ictal magnetoencephalography in temporal and extratemporal lobe epilepsy. *Epilepsia*. (2003) 44:1320–7. doi: 10.1046/j.1528–1157.2003.14303.x
50. Badier JM, Bénar CG, Woodman M, Cruto C, Chauvel P, Bartolomei F, et al. Ictal magnetic source imaging in presurgical assessment. *Brain Topogr*. (2016) 29:182–92. doi: 10.1007/s10548–015-0445–3
51. Eliashiv DS, Elsas SM, Squires K, Fried I, Engel J Jr. Ictal magnetic source imaging as a localizing tool in partial epilepsy. *Neurology*. (2002) 59:1600–10. doi: 10.1212/01.WNL.0000032493.83875.0B
52. Medvedovsky M, Taulu S, Gaily E, Metsähonkala EL, Makela JP, Ekstein D, et al. Sensitivity and specificity of seizure-onset zone estimation by ictal magnetoencephalography. *Epilepsia*. (2012) 53:1649–57. doi: 10.1111/j.1528–1167.2012.03574.x
53. Sharma P, Scherg M, Pinborg LH, Fabricius M, Rubboli G, Pedersen B, et al. Ictal and interictal electric source imaging in pre-surgical evaluation: a prospective study. *Eur J Neurol*. (2018) 25:1154–60. doi: 10.1111/ene.13676
54. Duez L, Tankisi H, Hansen PO, Sidenius P, Sabers A, Pinborg LH, et al. Electromagnetic source imaging in presurgical workup of patients with epilepsy: a prospective study. *Neurology*. (2019) 92:e576–86. doi: 10.1212/WNL.0000000000006877

Conflict of Interest: MS has shares in Epilog, and received speaker fees by Philips.

The remaining authors declare that the research was conducted in the absence of any commercial or financial relationships that could be construed as a potential conflict of interest.

Advantages of publishing in Frontiers

OPEN ACCESS
Articles are free to read for greatest visibility and readership

FAST PUBLICATION
Around 90 days from submission to decision

HIGH QUALITY PEER-REVIEW
Rigorous, collaborative, and constructive peer-review

TRANSPARENT PEER-REVIEW
Editors and reviewers acknowledged by name on published articles

Frontiers
Avenue du Tribunal-Fédéral 34
1005 Lausanne | Switzerland

Visit us: www.frontiersin.org
Contact us: info@frontiersin.org | +41 21 510 17 00

REPRODUCIBILITY OF RESEARCH
Support open data and methods to enhance research reproducibility

DIGITAL PUBLISHING
Articles designed for optimal readership across devices

FOLLOW US
@frontiersin

IMPACT METRICS
Advanced article metrics track visibility across digital media

EXTENSIVE PROMOTION
Marketing and promotion of impactful research

LOOP RESEARCH NETWORK
Our network increases your article's readership